THE UNIVERSITY *of* EDINBURGH

Using Satellite Remote Sensing to Quantify Woody Cover & Biomass across Africa

Edward T. A. Mitchard

DOCTOR OF PHILOSOPHY

The University of Edinburgh

School of GeoSciences

2011

Declaration

I confirm that this work is my own, except where indicated otherwise. No part of this thesis has been submitted for any other degree or qualification.

Signed: .....

Edward T. A. Mitchard

Date: .....

Dedicated to my parents,

Helen & James,

and to my wife, Kirsty.

Abstract

The goal of quantifying the woody cover and biomass of tropical savannas, woodlands and forests using satellite data is becoming increasingly important, but limitations in current scientific understanding reduce the utility of the considerable quantity of satellite data currently being collected. The work contained in this thesis reduces this knowledge-gap, using new field data and analysis methods to quantify changes using optical, radar and LiDAR data.

The first paper shows that high-resolution optical data (Landsat & ASTER) can be used to track changes in woody vegetation in the Mbam Djerem National Park in Cameroon. The method correlates a satellite-derived vegetation index with field-measured canopy cover, and the paper concludes that forest encroached rapidly into savanna in the region from 1986-2006. Using the same study area, but with radar remote sensing data from 1996 and 2007 (ALOS PALSAR & JERS-1), the second paper shows that radar backscatter correlates well with field-measured aboveground biomass (AGB). This dataset confirms the woody encroachment within the park; however, in a larger area around the park, deforestation dominates.

The AGB-radar relationships described above are expanded in the next paper to include field plots from Budongo Forest (Uganda), the Niassa Reserve (north Mozambique), and the Nhambita Community Project (central Mozambique). A consistent AGB-radar relationship is found in the combined dataset, with the RMSE for predicted AGB values for a site increasing by <30 %, compared with a site-specific equation, when using an AGB-radar equation derived from the three other sites. The study of the Nhambita site is extended in the following paper to assess the ability of radar to detect change over short time periods in this environment, as will be needed for REDD (Reducing Emissions from Deforestation and Degradation). Using radar mosaics from 2007 and 2009, areas known (from detailed ground data) to have been degraded decreased in AGB in the radar change detection, whereas areas of agroforestry and forest protection showed small increases.

The AGB-radar relationships described above saturate at ~150 Mg ha^{-1}, limiting the ability of radar to map AGB in tropical forest regions, which typically have much high AGB values. Spaceborne LiDAR data does not saturate, but does not provide continuous coverage, instead sampling a small percentage of the landscape with 0.25 ha footprints. A new methodology was therefore devised, that fused ground data, radar and spaceborne LiDAR (ICESat GLAS) to create a biomass map for the high-biomass and persistently cloudy Lopé National Park in Gabon. In this method, radar was used to classify the landscape and LiDAR (calibrated with ground data) was used to provide biomass values for the classes.

Errors and uncertainties in remote sensing estimations are discussed throughout the thesis. Such errors are often not fully considered in remote sensing studies, and this becomes particularly important when spatially-limited field dataset used train parameter-estimation over a much wider extent than the original field data. The large potential errors of this approach are illustrated in a Comment paper, which uses an independent ground dataset of 1154 field plots from 16 African countries, and the ICESat GLAS LiDAR dataset, to test the accuracy of a continental-scale1-km resolution biomass map of Africa developed by other authors in 2008.

The thesis concludes with a discussion of the potential of satellite data to monitor woody vegetation, with known accuracies and uncertainties. It is stated that in order to produce valid conclusions, uncertainties must be quantified and propagated with care, analyses need to be performed at an appropriate resolution, and recent field data is essential for calibration and validation.

Acknowledgements

I owe a huge debt of gratitude to the vast number of people and organisations who made it possible for me to complete this PhD. I list below those that were key throughout the whole process, and there are additional sections following each research chapter listing additional people and organisations who facilitated that particular area of the project.

Professor Patrick Meir, my principal supervisor, was instrumental in designing the project, and has supported and directed all aspects of my research over the past four years. I owe him many thanks for his constant insights, analyses and support. Additionally I was lucky to have three assistant supervisors: Dr Sassan Saatchi (NASA-JPL and UCLA), Dr Iain Woodhouse (Univeristy of Edinburgh), and Dr France Gerard (CEH Wallingford). Sassan Saatchi taught me much of what I have learnt of remote sensing, and assisted in the analyses involved in all my papers, as well as introducing me to numerous collaborators, and hosting me in UCLA and JPL for 6 months. Iain Woodhouse provided help and support on field data design and radar remote sensing analysis, and proved a valuable check on my sometimes overly-enthusiastic interpretation of my data! France Gerard provided training and expertise in using optical remote sensing data, and advice on change detection, and first introduced me to the true scale of the challenges presented by image resolution; additionally she kindly hosted me during three visits to CEH.

Though not part of my formal supervisory team, the input of the following people have contributed markedly to my development as a scientist, and to the production of this thesis: Simon Lewis (University of Leeds); Ted Feldpausch (University of Leeds); Tim Malthus (CSIRO); Richard Tipper (Ecometrica); Jon Lloyd (James Cook University, Australia); Wolfgang Buermann (UCLA); Mat Williams (University of Edinburgh); Casey Ryan (University of Edinburgh); and Danae Maniatis (FAO). Many thanks for sharing your time and knowledge.

I owe great thanks to the Gatsby Charitable Foundation, which awarded me the Sainsbury's PhD which funded this research. This funding was ultimately provided by Lord David Sainsbury, for whose generosity I am exceedingly grateful. I also benefited greatly from the support of the Gatsby Plants Network, which provided training and support throughout the PhD. Jane Langdale, my Gatsby mentor while at Oxford, and member of the Gatsby Plants Scientific Advisory board, encouraged me to apply for this PhD, and has been an excellent source of advice throughout this process.

Additional funding, and field support, for my field trip to Cameroon in 2007 came from the Tropical Biomes in Transition (TROBIT) NERC Consortium project. The Remote Sensing and Photogrammetry Society and the Elizabeth Sinclair Irvine Fund kindly provided funds for me to attend various international conferences.

My friends and family have supported me throughout the last four years, providing useful sounding boards for ideas and proof-reading drafts. Thank you!

I would like to thank my wife, Kirsty, for her support, assistance and patience throughout the last four years. Also she admirably put up with my long hours and long trips abroad, and somehow manages to still look interested when I talk about Africa or satellites.

Finally, many thanks to all the other people not listed here who have assisted me in producing this thesis: I am sorry there is not room to list you all here, but your help is greatly appreciated.

Table of Contents

Abbreviations

AGB:	Aboveground Biomass
ASTER:	Advanced Spaceborne Thermal Emission and Reflection Radiometer
ALOS:	Advanced Land Observing Satellite
BFR:	Budongo Forest Reserve (Uganda)
DBH:	Diameter at Breast Height (1.3 m)
ETM+:	Enhanced Thematic Mapper + (Sensor on Landsat 7)
EVI:	Enhanced Vegetation Index
CAI:	Canopy Area Index
FPC:	Foliage Projected Cover
JERS-1:	Japanese Earth Resource Satellite - 1
LAI:	Leaf Area Index
LNP:	Lopé National Park (Gabon)
MDNP:	Mbam Djerem National Park (Cameroon)
MODIS:	MODerate-resolution Imaging Spectroradiometer
MSS:	Multi-Spectral Scanner (sensor on Landsat 1-5)
NDVI:	Normalised Difference Vegetation Index
NNR:	Niassa National Reserve (Mozambique)
NCCP:	Nhambita Community Carbon Project (Mozambique)
OLS:	Ordinary Least Squares (regression)
PALSAR:	Phased Array L-band Synthetic Aperture Radar (sensor on ALOS)
PPC:	Plant Project Cover
RFDI:	Radar Forest Degradation Index
RMA:	Reduced Major Axis (regression)
RMSE:	Root Mean Square Error
SAR:	Synthetic Aperture Radar
TM:	Thematic Mapper (sensor on Landsat 4/5)

1. Introduction

1.1 Overview

This thesis presents the results of research into how satellite remote sensing data can be used to map woody cover and aboveground biomass (AGB) in Africa. This research spans a variety of different sensor types (optical, radar and LiDAR), study sites (primarily in Cameroon, Uganda, and Mozambique), and scales (from sub-meter up to 8 km pixels), and the results are arranged into six distinct research papers. These papers, when taken together, assist with the process of developing a framework describing how woody vegetation should be mapped and monitored, and with what accuracy and limitations this can be done using different satellite remote sensing platforms.

This chapter provides a general overview of the context of this research. The chapter ends with a summary of the content of, and interactions among, the subsequent chapters, and is immediately followed in Chapter 2 by a more technical introduction into the remote sensing techniques that can be used to monitor certain parameters of vegetation. Chapters 3-8 are research papers, either published in the peer-reviewed literature or currently going through the peer-review process. A final concluding chapter synthesises these results and looks towards the future.

1.2 Why map Africa's woody cover and biomass?

1.2.1 Unique ecosystems and relationship with mankind

The vast majority of sub-Saharan Africa's[1] surface is not agriculture or other artificial vegetation (86 %, Mayaux *et al.* (2004)), despite its rapidly growing population of 863 million people (2010 estimate, with annual population increase since 1950 estimated at 2.6 % (UN 2008)). However, the 86 % of Africa's surface that is not agriculture is not truly natural: there is a unique and pervasive anthropogenic influence on almost all ecosystems in the continent. Humankind

[1] The Sahara is such a vast barrier to species dispersal, and the countries to the north of it so different from sub-Saharan Africa socially and economically as well as ecologically, that this thesis will concentrate solely on sub-Saharan Africa. Indeed, when the term 'Africa' is used, it should be assumed that 'Sub-Saharan Africa' is meant unless it is specifically stated otherwise.

evolved in Africa, and thus humanoid species have been influencing its ecosystems for millions of years. This influence is particularly evident in the prevalence of ecosystems influenced by fire (Bird & Cali 1998; Bond *et al.* 2005), which accounts for more than 55 % of the total surface of the continent, a total of 13.4 million square kilometres (Mayaux *et al.* 2004).

The majority of fire in Africa is anthropogenic in origin (Furley 2010), and has been since at least the early Holocene (Bird & Cali 1998). This has (and has had) a substantial effect on the nature of the vegetation of Africa, greatly suppressing woody biomass (Bond *et al.* 2005; Sankaran *et al.* 2005). Africa has two thirds of the world's woodlands and savannas (Olson *et al.* 1985), but in the absence of human influence over 70 % of Africa's open canopy systems could become closed-canopy forests (Bond *et al.* 2005). The woody cover of these biomes is also influenced by many other factors, including, for example, rainfall (both in terms of an annual average and the frequency of exteme droughts), wild herbivore density, the prevalence of domesticated grazing animals, and other human activities (Sankaran *et al.* 2005). Fire is associated with many of these factors, and is very important in regulating and changing woody cover. The importance of fire is such that the landcover state of this 55 % of Africa's surface could rapidly increase or decrease its woody cover were anthropogenic influences to change (in Figures 1 & 2, mosaic forest, woodlands, shrublands and grasslands all have their woody cover influenced to a lesser or greater extent by humankind).

Figure 1 – Landcover of sub-Saharan Africa in 2000

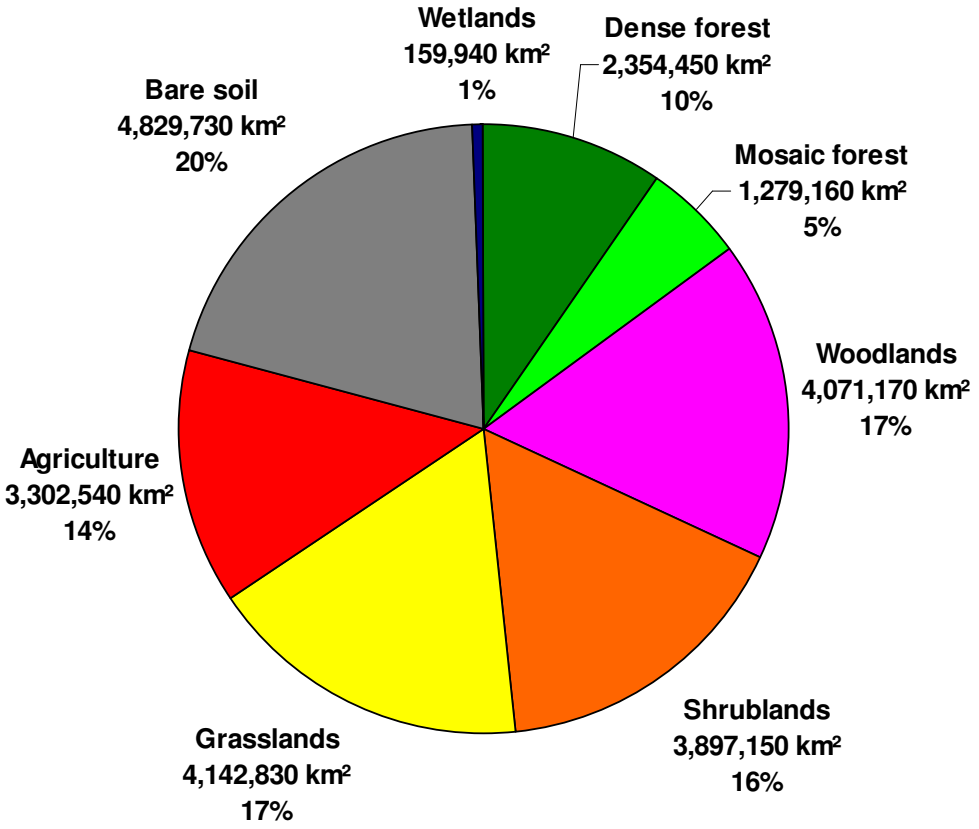

Figure 1 shows the distribution of broad landcover types across Africa, as classified by the Global Land Cover 2000 project (Mayaux *et al.* 2004). Figure 2 shows the same data displayed on a map.

Figure 2 – Landcover of sub-Saharan Africa in 2000

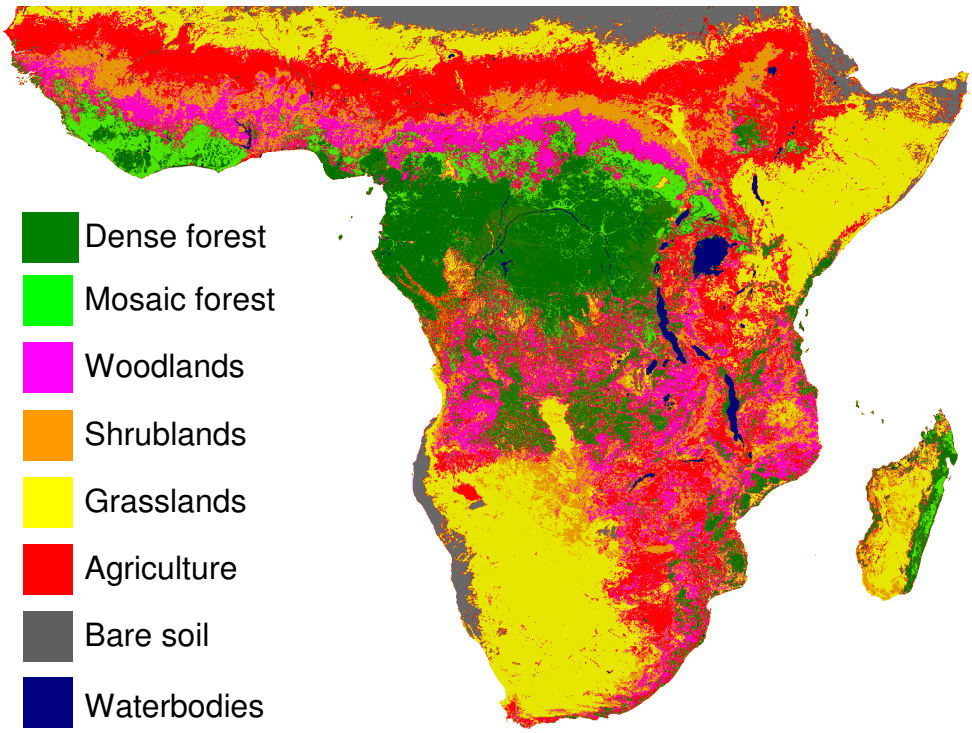

The savannas and woodlands of Africa are also unique because of their abundant large herbivorous mammals, which are largely absent from the rest of the world. It has been suggested that animals may have remained here while becoming extinct elsewhere because they were present throughout human evolution and thus adapted to the presence of humans (Martin 1984), though there are other potential explanations (Owen-Smith 1987; Gill *et al.* 2009). Whatever the reason, Africa currently has vast areas of globally unique ecosystems.

The exact distribution of woody vegetation types in Africa is relatively poorly defined (Mayaux *et al.* 2004). Broad-category landcover maps exist, for example the Mayaux *et al.* (2004) map mentioned above (which was part of the Global Land Cover 2000 project), and the European Space Agency's GLOBCOVER product, which is a 300 m resolution global landcover classification for the years 2005 and 2009. However, none divided the vegetation types into sufficiently narrow categories

to properly characterise Africa's landscape. The authoritative vegetation-type map that does go to a deeper layer of classification was one produced by Dr Frank White in 1983 (White 1983), which is still widely cited, though it is in all likelihood quite inaccurate in many areas due partly to the lack of consistent data used in its creation (it is largely based on broad-scale climatic map layers and field experience), and due to significant land-cover changes that have occurred over the past thirty years.

As so much of Africa's landcover is dependent on the influence of non-climatic factors such as humans, fire and grazing (Bond *et al.* 2005; Sankaran *et al.* 2005), the use of computer modelling to predict landcover type is especially difficult. Most Dynamic Global Vegetation Models perform poorly for Africa, over-predicting forest area and thus Net Primary Productivity (NPP, the total net assimilation of carbon into vegetation for a given area and time) (Scheiter & Higgins 2009). This greatly reduces the accuracy of local and global model performance and thus future climate predictions (Scheiter & Higgins 2009). Producing accurate landcover maps is therefore a scientific imperative, to allow for improvements in these models and more accurate predictions of climate change and feedbacks between climate change and vegetation.

1.2.2 Africa's development and population growth

Africa has undergone very rapid population growth over the past sixty years, from 183.5 million in 1950 to 863.3 million in 2010, an increase of 2.6 % per year (UN 2008). Though the rate of growth is expected to slow over the next half-century, the population is still expected to increase at an average annual rate of 1.8 % until 2050, almost doubling the current population to 1.75 billion (UN, 2008, Medium variant prediction). The rapid growth in population has already caused significant changes to Africa's natural environment, with much woodland and forest being cleared for agriculture or degraded by cattle, sheep and goats (Lambin *et al.* 2001). As the population doubles over the next 40 years, this pressure on the natural environment will only increase. It is hard to see how food supply will keep up with this growing population, and the risk of famine is likely to increase. The additional population will dramatically increase the land area influenced by humanity, with the most likely

consequence being that forest cover will decrease. The majority of the populations of most African countries currently use locally collected wood (in the countryside) or charcoal (in cities) for their fuel needs, so again this increase in population will cause an increase in the rate of deforestation, which is already at unsustainable levels due merely to fuel demand in some countries (for example, Kenya (Bailis 2009)). In addition to the impacts on wood fuel availability and terrestrial emissions of CO_2 to the atmosphere, anticipated changes in landcover away from forest cover have the potential to increase the incidence of both flooding and droughts (Milton *et al.* 1994), and the potential for humanitarian disasters.

There are attempts being made to help increase the efficiency of agriculture in Africa, which currently reports yields far below those in South East Asia, Europe or North America (Evenson & Gollin 2003). These low yields are caused by a combination of small-scale, non-mechanised farming, a lack of fertiliser and pesticide use, and the lack of prevalence of modern high-yielding crop varieties (Evenson & Gollin 2003). Additionally plantations of fast-growing coppiced trees can provide a sustainable source of wood fuel (Namaalwa *et al.* 2009). Such a transition from extensive to intensive agriculture could allow Africa to feed its growing population without increasing farmed land area dramatically. Indeed, research in Amazonia suggests that if extensive deforestation for agriculture does not cease, then an ecological 'tipping-point' could be crossed, causing wide-scale loss of rainfall and a transition of forests into savanna-like vegetation (Nepstad *et al.* 2008).

The precise land-cover of Africa, and how it has changed over the last century, is poorly quantified (Section 1.2.1). In order to be able to assess and assist in the prevention of the loss of natural ecosystems and their associated ecosystem services, and the optimisation of agriculture, it is necessary to increase the certainty in landcover mapping.

1.2.3 Climate change

The uncertainty in the magnitude and extent of changes in temperature and rainfall associated with anthropogenic climate change is larger for Africa than all other

continents except Antarctica (IPCC 2007). However, there is consistency in predictions that the magnitude of such changes in Africa are likely to be larger, and the effects start earlier, than in most other continents (Delire *et al.* 2008). Additionally, the naturally high climate variability of many areas of Africa is likely to increase over the coming century, with droughts and floods becoming more frequent and widespread (IPCC 2007). Part of this uncertainty links back to uncertainties in modelling the current landcover of Africa, and how the land surface will interact with the climate. Indeed, globally the uncertainty in 21st century atmospheric CO_2 emissions estimated using current earth system models results more from uncertainty in the land surface components of these models than any other, except for variability in the anthropogenic drivers relating to different economic development scenarios (Meir *et al.* 2006).

What is certain is that forest and woodland cover reduces the impact of climate change and helps to mitigate against extreme weather events (Delire *et al.* 2008): areas where forest has been cleared suffer from high soil erosion and run-off after heavy rainfall, and the reduction in the transpiration and water storage capacity of the surface increases peak temperatures and reduces cloud formation and rainfall. Developing methods to allow the quantification and monitoring of forest cover will assist in assessing the vulnerability of different areas within Africa to climate change, and finding the most effective and efficient policies and incentives to reduce this vulnerability.

1.2.4 REDD+

Reducing Emissions from Deforestation and forest Degradation (REDD+) is a protocol first suggested in the mid-2000s as a component of a future agreement of the parties subject to the UN Framework Convention on Climate Change (UNFCCC). It was formally adopted by the Conference of Parties in Cancun, Mexico, in December 2010 (UNFCCC 2010), though many of the details remain to be developed and legally formalised.

Essentially, REDD+ aims to provide payments to countries in return for lowering their deforestation rates, and indeed for increasing their forest cover. Under the Kyoto Protocol's Clean Development Mechanism (CDM), carbon credits could be earned for reforesting land that was classified as not forest on 31st December 1989 (UN 1998). However, credits cannot be created under the CDM for the reforestation of more recently deforested land, nor for avoiding deforestation, and thus the CDM could not be used to directly reduce the rate of tropical deforestation. The new REDD+ policy proposals aim to fill this gap and achieve the globally-important goal of reducing deforestation.

REDD+ has the potential to reduce poverty and the loss of ecosystems in Africa, by providing an income for maintaining forest cover. However, currently Africa is in danger of missing out on many of these potential opportunities to wealthier tropical regions, in part because these countries have a better capacity for monitoring current and future deforestation rates. This issue of designing robust monitoring systems for REDD+ is discussed in detail in Chapters 6 and 7.

1.2.5 The need for better understanding and monitoring

Research into monitoring Africa's aboveground biomass and woody vegetation is quite limited in most countries in the continent, and is even more limited at the scale of the whole continent. Unlike South America (and in particular Brazil), which has a good forest monitoring system designed to track deforestation (Hansen *et al.* 2008), landcover and especially landcover change is poorly monitored in Africa. Partly this is due to a lack of political will, government resources, and cooperation among the 34 countries of sub-Saharan Africa. However, there is also an element that is caused by limited scientific capacity: mapping changes in forest cover from ground data and remote sensing data, and linking that to changes in carbon stocks, is technically difficult and requires extensive training and timely access to satellite data, sophisticated computing equipment, and proprietary software.

This situation is changing, for three main reasons. First, the scientific capacity of the continent in increasing as it develops, and as universities and research organisations

from developed countries increasingly work with African institutions to build their capacity for research (Barrett *et al.* 2011). South Africa, in particular, has excellent resources, universities, and the capacity for accurate land cover mapping and monitoring. Secondly, investment in conservation and tourism has led to better monitoring around and within the continent's many national parks. Thirdly, the awareness of the importance of forest cover in climate change has led to initiatives that aim to introduce economic incentives for reforesting land or avoiding deforestation (e.g. CDM and REDD+); this has increased the economic incentives of countries to monitor their landcover and woody biomass.

There remains, however, a need for increased scientific understanding of the issues involved in mapping and monitoring woody cover and biomass in the continent. Mapping these variables consistently over such a large area with limited ground data is not simple. This thesis aims to partially fill this gap in understanding and expertise, by developing satellite remote sensing methods that can be used for this purpose.

1.3 Aims:

Following from the knowledge gaps identified above, the aims of this research can be summarised as:

1) Collate existing field data on woody cover and above-ground biomass (AGB) over a range of ecosystems in Africa, and collect new field data, in order to provide ground-truth datasets over a range of sites to test remote sensing methodologies.
2) Use these ground data to explore relationships between remote sensing variables (using radar, optical and LiDAR sensors) and woody cover/AGB in a range of test sites across Africa.
3) Use the above relationships to create maps of woody cover and AGB, and investigate how these parameters have changed with time using appropriate change-detection techniques.

4) Compare the accuracies, uncertainties and limitations associated with mapping these variables with different sensor types, and test how consistent the relationships are in time and space.
5) Attempt to quantify all the errors and uncertainties involved in the above maps, and appropriately propagate these errors through the analyses.
6) Make recommendations on how different remote sensing data should be used and combined to optimise the monitoring of woody cover and biomass in different ecosystems in Africa.

1.4 Overview of the thesis

This chapter has presented an introduction to the subject area and the urgency of this research, as well as an overview of the structure of the thesis. Chapter 2 is a more technical literature review, introducing the field of the remote sensing of woody vegetation and change detection, and discussing the parameters of woody vegetation that can be measured.

The next six chapters are each stand-alone papers, which have either been published or are at the time of writing going through the peer-review process. For the five that have been published the as-published versions, along with their supplementary information, can be found in the Appendices. Though these chapters are arranged in a linear fashion they interact and develop from each other in a more complex manner, summarised in Figure 3:

Figure 3 – Diagram showing the interactions of the chapters

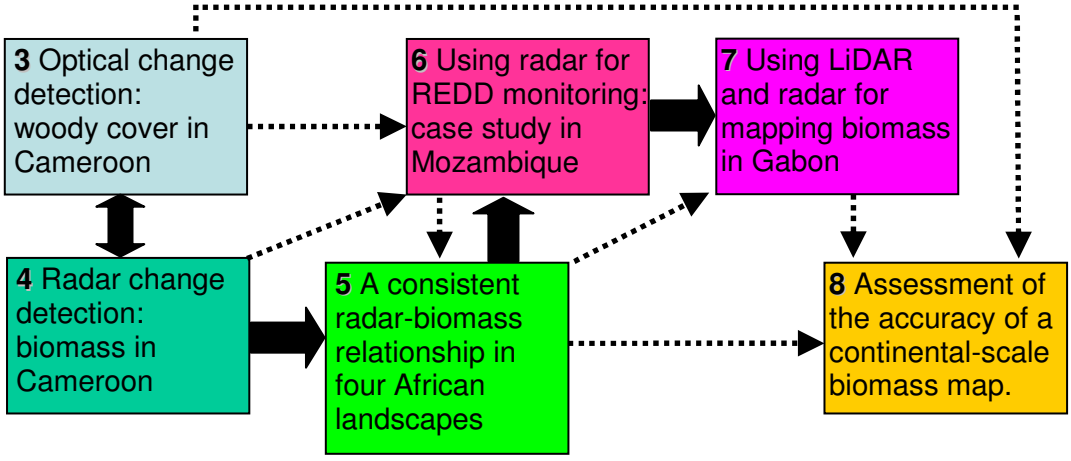

Chapters 3 and 4 consider changes in woody cover (Chapter 3) and AGB (Chapter 4) in and around the Mbam Djerem National Park in Cameroon, using field data collected in 2007 as part of the Tropical Biomes in Transition (TROBIT) expedition to the area. Chapter 3 uses exclusively optical data whereas Chapter 4 uses radar data, which is found to be more sensitive to AGB than optical data. Chapter 5 then extends this radar-AGB analysis across Africa, again finding a strong and consistent relationship between AGB and radar backscatter in lower biomass areas. This latter analysis incudes new field data collected during a field campaign in Budongo Forest in Uganda (2008), and additional field data collected by other researchers from two separate sites in Mozambique.

In addition to mapping AGB, the finding reported in Chapter 5 has important implications for monitoring deforestation and degradation, a topic explored in Chapter 6, using the *Miombo* forests of the Gorongosa Community Carbon Project in Mozambique as a case study. This study finds that repeat imagery from a radar satellite can detect degradation, and that even increases in AGB due to agroforestry/afforestation/reforestation should be quantifiable over a number of years of observation. Chapter 7 extends some of the earlier work on mapping AGB to a more challenging environment, the persistently cloudy, mountainous and high-biomass forests of Lopé National Park in Gabon. Here again, a map with defined

accuracy is produced, but the radar data are used only for classifying the landscape, with satellite LiDAR data (calibrated and verified by extensive field plots) providing the AGBestimates for each class.

In Chapter 8 there is a step change in terms of scale – this chapter is a 'Comment' on a previously published AGB map of much of sub-Saharan Africa (Baccini *et al.* (2008)). During this PhD a database of 1154 field plots from 16 countries was collated, involving newly collected plot data, and published and unpublished data collected by other scientists; additionally the complete ICESat GLAS LiDAR dataset for Africa was processed. These field plots and LiDAR data were used to test the accuracy of the Baccini *et al.* map, and attempts are made to examine the reasons behind the differences detected.

Finally, Chapter 9 synthesises the findings of the preceding chapters, and presents a vision for using these results to both map woody biomass and to monitor changes at a variety of scales.

1.5 References

Baccini, A., Laporte, N., Goetz, S.J., Sun, M., & Dong, M. (2008) A first map of tropical Africa's above-ground biomass derived from satellite imagery. *Environmental Research Letters, 3*, 045011

Bailis R. (2009) Modeling climate change mitigation from alternative methods of charcoal production in Kenya. *Biomass and Bioenergy*, 33, 1491-1502

Barrett A.M., Crossley M. & Dachi H.A. (2011) International collaboration and research capacity building: learning from the EdQual experience. *Comparative Education*, 47, 25-43

Bird M.I. & Cali J.A. (1998) A million-year record of fire in sub-Saharan Africa. 394, 767-769

Bond W.J., Woodward F.I. & Midgley G.F. (2005) The global distribution of ecosystems in a world without fire. *New Phytologist*, 165, 525-538

Delire C., Ngomanda A. & Jolly D. (2008) Possible impacts of 21st century climate on vegetation in Central and West Africa. *Global and Planetary Change*, 64, 3-15

Evenson R.E. & Gollin D. (2003) Assessing the Impact of the Green Revolution, 1960 to 2000. *Science*, 300, 758-762

Furley P. (2010) Tropical savannas: Biomass, plant ecology, and the role of fire and soil on vegetation. *Progress in Physical Geography*, 34, 563-585

Gill J.L., Williams J.W., Jackson S.T., Lininger K.B. & Robinson G.S. (2009) Pleistocene Megafaunal Collapse, Novel Plant Communities, and Enhanced Fire Regimes in North America. *Science*, 326, 1100-1103

Hansen M.C., Shimabukuro Y.E., Potapov P. & Pittman K. (2008) Comparing annual MODIS and PRODES forest cover change data for advancing monitoring of Brazilian forest cover. *Remote Sensing of Environment*, 112, 3784-3793

IPCC (2007) *Contribution of Working Group I to the Fourth Assessment Report of the Intergovernmental Panel on Climate Change*. Cambridge University Press, Cambridge.

Lambin E.F., Turner B.L., Geist H.J., Agbola S.B., Angelsen A., Bruce J.W., Coomes O.T., Dirzo R., Fischer G., Folke C., George P.S., Homewood K., Imbernon J., Leemans R., Li X., Moran E.F., Mortimore M., Ramakrishnan P.S., Richards J.F., Skånes H., Steffen W., Stone G.D., Svedin U., Veldkamp T.A., Vogel C. & Xu J. (2001) The causes of land-use and land-cover change: moving beyond the myths. *Global Environmental Change*, 11, 261-269

Martin P.S. (1984) Prehistoric Overkill. In: *Quaternary Extinctions* (eds. Martin PS & Klein RG). University of Arizona Press, Tuscan

Mayaux P., Bartholome E., Fritz S. & Belward A. (2004) A new land-cover map of Africa for the year 2000. *Journal of Biogeography*, 31, 861-877

Meir P., Cox P. & Grace J. (2006) The influence of terrestrial ecosystems on climate. *Trends in Ecology & Evolution*, 21, 254-260

Milton S.J., Dean W.R.J., Plessis M.A.d. & Siegfried W.R. (1994) A Conceptual Model of Arid Rangeland Degradation. *Bioscience*, 44, 70-76

Namaalwa J., Hofstad O. & Sankhayan P.L. (2009) Achieving sustainable charcoal supply from woodlands to urban consumers in Kampala, Uganda. *International Forestry Review*, 11, 64-78

Nepstad D.C., Stickler C.M., Filho B.S.-. & Merry F. (2008) Interactions among Amazon land use, forests and climate: prospects for a near-term forest tipping point. *Philosophical Transactions of the Royal Society B: Biological Sciences*, 363, 1737-1746

Olson J.S., Watts J.A. & Allison L. (1985) Major World Ecosystem Complexes Ranked by Carbon in Live Vegetation: A Database. In, Oak Ridge National Laboratory, Tennessee

Owen-Smith N. (1987) Pleistocene Extinctions: The Pivotal Role of Megaherbivores. *Paleobiology*, 13, 351-362

Sankaran M., Hanan N.P., Scholes R.J., Ratnam J., Augustine D.J., Cade B.S., Gignoux J., Higgins S.I., Le Roux X., Ludwig F., Ardo J., Banyikwa F., Bronn A., Bucini G., Caylor K.K., Coughenour M.B., Diouf A., Ekaya W., Feral C.J., February E.C., Frost P.G.H., Hiernaux P., Hrabar H., Metzger K.L., Prins H.H.T., Ringrose S., Sea W., Tews J., Worden J. & Zambatis N. (2005) Determinants of woody cover in African savannas. *Nature*, 438, 846-849

Scheiter S. & Higgins S.I. (2009) Impacts of climate change on the vegetation of Africa: an adaptive dynamic vegetation modelling approach. *Global Change Biology*, 15, 2224-2246

UN (1998) The Kyoto Protocol to the United Nations Framework Convention on Climate Change. In, http://unfccc.int/resource/docs/convkp/kpeng.pdf#page=12

UN (2008) Population Division of the Department of Economic and Social Affairs of the United Nations Secretariat, World Population Prospects: The 2008 Revision. In, http://esa.un.org/unpp

UNFCCC (2010) Decision CP16 Section III C. In, p. Section III C, http://unfccc.int/files/meetings/cop_16/application/pdf/cop16_lca.pdf

White F. (1983) *The vegetation of Africa : a descriptive memoir to accompany the Unesco/AETFAT/UNSO vegetation map of Africa*. UNESCO, Paris.

2. Introduction to the Remote Sensing of Woody Cover and Biomass

This chapter provides a general introduction to the research field for non-specialists, and introduces and explains many of the concepts and terms used in later chapters. In particular, it provides an overview of the characteristics of woody vegetation measured in the field, and an introduction to the satellite sensors used here to attempt to map these variables across the landscape. This chapter finishes with a discussion of change detection techniques.

2.1 Quantifying Characteristics of Woody Vegetation

Before discussing the satellite sensors and methodologies used to estimate parameters of woody vegetation remotely, it is important to correctly define the ecological variables we are interested in, and how they are measured on the ground. Most of this thesis is concerned with aboveground biomass (AGB), but Chapter 3 discusses woody cover, and the concepts of height, basal area and below-ground biomass are also relevant to other chapters. Here these concepts, and the techniques used to measure them in the field, are defined.

2.1.1 Canopy Cover

Canopy cover is normally defined as the percentage cover (or proportion) of a unit area that is covered by a vertical projection of tree crowns, where the crowns are considered opaque objects (McElhinny *et al.* 2005). Thus the value is normally 70-100 % (or 0.7 – 1.0) for closed-canopy tropical forest, ranges widely for woodlands, and is 0 % for grasslands. It is often used slightly imprecisely, with the height of vegetation included as canopy, and the radius of canopy observed from a ground point, poorly defined. The methods used to estimate this parameter also vary, with the the more accurate being hemispherical photos (Potapov *et al.* 2009) or vertical point-based measurements (Emlen, 1967), and the less accurate (though more commonly used) being curved mirrors with an embossed grid, through which an observer views a section of canopy and estimates the ‘gap fraction’ by eye.

A much better defined related concept is the Leaf Area Index, or LAI, which is the area of one-sided leaf surfaces that cover each 1 m^2 of ground (m^2 m^{-2}). Estimating this is more difficult than for canopy cover, but the issues involved are better understood (Weiss *et al.* 2004). The destructive sampling of all leaves in an area is also possible, if rarely undertaken. This provides data to allow the calibration and verification of less time-consuming methods (McWilliam *et al.* 1993). LAI is of less relevance to this thesis than canopy cover, as leaf area is not well correlated to biomass (as leaves are present on both woody and non-woody vegetation), and varies significantly during the annual cycle.

In both cases the definitions become very scale-dependent when transitioning from a constant land-cover class (e.g. forest or grassland), to mixed tree-grass systems (woodlands and savannas). Savanna and woodland systems are by their nature highly heterogeneous at all scales (Scholes & Archer 1997; Chave *et al.* 2004; Ryan *et al.* in press), and therefore the exact radius of observation and the point chosen to measure from can greatly affect the estimated woody cover/LAI. The inaccuracies resulting from this heterogeneity can be reduced by extensive sampling. In general, however, estimating the woody cover of savannas and woodlands using methods intended for forestry can lead to significant errors and biases (Walker, 1980).

The concept of point-based sampling in field ecology led to two related concepts to assist with robust measurements of canopy cover in mixed tree-grass systems. These include Foliage Projected Cover (FPC, Armston *et al.* 2009) and Plant Projected Cover (PPC), and were derived in a number of studies in South Africa and Australia (Lucas *et al.* 2011). In this case of PPC this is the percentage horizontal cover of a landscape with plant material, and for FPC the percentage horizontal cover with photosynthetically active material (in both cases often only vegetation above an arbitrary height cut-off, e.g. 2 m, is considered). PPC is similar to canopy cover as defined at the start of this section, though the method of estimation is often different. FPC is related to LAI, but because it does not allow for overlapping leaves. LAI cannot be calculated from FPC, though it can be estimated if the distribution of leaf angles and the degree of clumping within a forest type are known. In both cases estimation is often performed through the use of a vertical-pointing periscope, with

the observer following transect lines and recording the presence or absence of vegetation every meter (or similar fixed distance).

The concepts FPC and PPC are very useful measures of canopy cover, but for the study in Chapter 3, the only chapter of the thesis where woody cover is the principle parameter investigated, their suitability was questioned because a continuous and short transition between forest and savanna landcover types were being investigated. It was therefore desired that a maps of the crown dimensions of every tree was known, so this transition could be investigated in a variety of ways. The absolute diameter of the canopy of every tree was measured (the extent of branches in the north, south, east and west dimensions were determined), and the position of the tree stem recorded to a sub-meter accuracy. In order to convert these measurements into a measure of canopy cover, a measurements called the Canopy Area Index, CAI, was defined. The CAI is, however, not directly comparable to conventionally-defined canopy cover or PPC, as like LAI it can (and does) rise considerably beyond 1, due to the overlapping canopies of individual trees. However, unlike LAI it does not vary seasonally, as it is based on branches not leaves. Also, it produces a consistent estimate for savanna/woodland plots, being much less sensitive to the collector and resilient to the heterogeneity of mixed tree-grass systems.

In woodlands and savannas, canopy cover is often easier to determine from high-resolution optical remote sensing imagery. Providing the resolution is sufficiently fine such that all the crowns can be clearly determined (a resolution <3 m is therefore ideal, though the minimum resolution depends on the minimum size of the tree crowns to be distinguished), the ratio of visible ground to canopy can be used to estimate canopy cover (e.g. Wang *et al.* 2005). An alternative method, that tends to be less sensitive to the user and exact methodology chosen, is to overlay a fine grid on the imagery (for example 5 m x 5 m), and at every vertex make the decision as to whether the point is covering ground or canopy (Nowak *et al.* 1996). The canopy cover is then the proportion of points that covered tree canopy divided by the total number of points sampled; this is a very similar measurement in principle to FPC. In both cases a robust and useful measure of canopy cover can be given; however one

should be aware that this will not necessarily be directly comparable to measurements from the ground.

2.1.2 Basal area

Basal area is also sometimes used to compare different wooded areas, especially by forest managers but also by ecologists. Unlike canopy cover, basal area tends to correlate well with aboveground biomass (especially within a forest type), and is defined as the area of a vertically-projected forest that would be tree-stem if the forest was sectioned at 1.3 m above the ground. Normally only stems with a diameter greater than 10 cm are considered, as in most forests stems smaller than 10 cm represent only a small fraction of the basal area (Chave *et al.* 2003). It can be easily calculated by using the standard primary measurement collected in field forestry, that is the Diameter at Breast Height (DBH, diameter at 1.3 m). From this, basal area can be calculated using the Equation 1, where basal area is B_a (m^2/ha), DBH is D_{BH} (cm), and the plot area is A (ha):

$$B_a = \frac{\sum\left[\pi\left(\frac{1}{2}D_{BH}\right)^2\right]}{A} \quad (1)$$

Basal area estimates can be biased easily by incorrect DBH measurement methodologies. For example, not correctly treating multiple stems, or measuring over buttresses and other stem irregularities, can cause large errors. For this reason strict guidelines should be followed, for example those laid out in the RAINFOR field manual (Phillips *et al.* 2009); these were followed for all the field data in this thesis.

In order to correctly estimate basal area in some savanna woodlands, the case has been made that diameter measurements should be taken nearer to the ground level, for example at 30 cm above the ground (Burrows *et al.* 2000). While this may be appropriate in some circumstances, we do not advocate it here as standard DBH measurements at 1.3 m (following standard conventions to measure above buttresses and other stem irregularities) are such widely collected data that they allow for ready comparison between sites and time periods.

2.1.3 Tree height, dominant height, Lorey's height

Tree height is defined as the distance from the ground to the topmost leaf. It can be hard to measure, especially in dense forest, but as long as the top and bottom of the tree is visible it can be determined relatively accurately with a vertex hypsometer or clinometer (Phillips *et al.* 2009).

Tree height is largely used in this thesis in combination with DBH and wood density in order to estimate the AGB of a tree. However, it can also be used as a parameter in its own right to characterise a forest. Simply describing the average height of a stand is of limited value, as all trees, from saplings to emergents, have an equal weight in the averaging (and an arbitrary minimum diameter or height cut-off has to be made). Instead therefore, three metrics are often used to summarise tree height data within a plot; these are:

a) Maximum height: the height of the tallest tree in a plot;
b) Dominant height: the average height of the 20 % of tallest stems
c) Lorey's height: the average height where each stem is weighted by its basal area (see Chapter 7).

The latter two of these three metrics can be estimated with relative accuracy from LiDAR data. Since both dominant height and Lorey's height are usually well correlated to AGB within a given landscape, this provides a useful means to produce estimates of AGB from LiDAR data.

2.1.4 Aboveground Biomass (AGB)

AGB is the principle parameter of interest throughout this thesis, and it is defined as the mass of aboveground living material per unit area, expressed in tonnes biomass per hectare (Mg ha^{-1}). While living aboveground biomass is by no means the only carbon in a hectare of forest or savanna, it is normally the principle pool, and often correlates well with other pools such as below-ground biomass and necromass (Brown 1997) (though it is often poorly correlated with the soil carbon pool, see Section 2.1.5 and Ryan, 2009).

AGB is very time-consuming and destructive to measure directly: doing so for a whole 1 ha plot would involve cutting down and weighing at least several hundred trees. In practice therefore AGB is normally estimated by measuring a few parameters of each tree: ideally DBH, height, and species, and using an allometric equation to convert these measurements to AGB. Allometric equations are equations relating the sizes and volumes of an organism, and in the case of trees are normally produced not from first principles, but from destructively harvesting a tree.

DBH is the most useful parameter to include in an allometric equation for estimating AGB, as DBH correlates well with AGB in every environment, and is comparatively easy, quick and accurate to measure. Height is of secondary importance, helping to refine the accuracy of the estimate derived from DBH. Height is especially important when using allometric equations not specifically derived at the same location and with the same species being studied, as much of the error between different allometric equations involving DBH alone can be explained by changes in DBH-height relationships across different areas (Chave *et al.* 2005). Finally, knowing the species is important because it allows the inclusion of a species-specific wood specific gravity (also known as wood density) measurement. Wood specific gravity is defined as the over-dry mass of a sample of wood (in grams) divided by its green volume (in cm^3). Height and diameter essentially just allow the estimation of a tree's volume: wood specific gravity allows this to be accurately converted to biomass, again increasing accuracy.

The importance of the choice of allometric equation cannot be overstated. Different allometric equations can produce very different AGB estimates using the same measurements, especially for large trees (e.g. >50 cm DBH) (Keller *et al.* 2001; Williams *et al.* 2008). For the vast majority of tropical tree species insufficient destructive harvesting measurements have been made to allow for species-specific relationships to be derived (Cole & Ewel 2006). Even if such relationships did exist, some would argue that using them could introduce errors if used in a different site, or if the equation was derived from relatively few trees (Henry *et al.* 2010).

Given the impossibility of using species-specific equations in most circumstances in the tropics, it is normal to use pan-tropical equations, which collate thousands of individual measurements in order to derive generally-applicable equations, with known uncertainties. The equation most widely used in the tropics was derived by Jerome Chave (Chave *et al.* 2005), who collated 2,410 individual tree measurements to derive equations (involving either DBH and wood density, or DBH, height and wood density) for dry, moist, wet and mangrove tropical forests. These equations are widely trusted and used, and are thought to be relatively accurate (~ ±10 %), especially in the form including site-specific height measurements. However, this is an area where uncertainty for Africa is especially high, as the equations of Chave et al. (2005) do not include data from Africa. However, a recent analysis using 74 destructively harvested trees from Cameroon concluded that the Chave et al. (2005) equations had lower errors for Africa than for other continents (Djomo *et al.* 2010). That study was however for tropical forests, and the problem is greatest in woodland and savanna vegetation, as the 'dry forest' equation from Chave et al. (2005) is derived from data from dry forests in Australia, India and the Yucatan Peninsula in Mexico, where the vegetation structure is significantly different from Africa's savannas and woodlands. This error is currently hard to assess, but in this thesis locally-derived allometrics have been used for savannas and woodlands where available, and otherwise the Chave *et al.* (2005) equations have been used, with site-specific DBH-height equations incorporated to reduce errors.

2.1.5 Below-ground carbon

Carbon is stored below-ground in two major pools – the below-ground biomass held in living plant material (Below Ground Plant Biomass, BGPB), and the organic carbon stored in the soil, both in decaying plant material and in other organisms, for example bacteria, fungi and animals (Below Ground Organic Carbon, BGOC). Often significant quantities of inorganic carbon are also found in soil. These pools vary greatly, and are only determinable by laboratory analysis of soil samples: the remote sensing of below-ground carbon is not currently possible.

PGPB is often estimated using standard root:shoot ratios for a particular species or ecosystem type. This relies on the theory that a larger tree will tend to have a large

root system, as the root system is needed to supply the stem with water and nutrients, and provide structural support, so the size of the root system should scale with the size of the tree (Ågren & Ingestad, 1987). This appears to be relatively accurate within a geographic area and particular set of environmental conditions, but the root:shoot ratio does vary greatly with factors such as altitude (Leuschner *et al.* 2007), so site-specific measurements remain important.

While the AGB of a site relates directly to the root biomass (and thus knowing AGB can allow a good estimate of this carbon pool), the non-plant store of carbon in soils also varies greatly depending on the soil type, location, temperature and slope (Aragao *et al.* 2009; Gibbon *et al.* 2010; Zimmermann *et al.* 2010a; Zimmermann *et al.* 2010b). Estimating this pool must rely on collecting and analysing soil samples from across a site; several soil pits are normally dug, as soil carbon can be highly heterogeneous even at a very local scale. Soil carbon stores can be very large, and in savannas is often considerably larger than the aboveground pool (Grace *et al.* 2006; Ryan *et al.* in press).

2.2 Sensor types

Optical, radar and LiDAR sensors are the three broad categories of sensor that can be used for retrieving the biophysical properties of vegetation. Optical sensors are detect reflected sunlight, and at longer wavelengths the direct emissions of electromagnetic waves from the Earth surface. Radar and LiDAR sensors are both ‘active’ sensors (whereas optical sensors are passive). Active sensors transmit pulses of radiation and detect returns: in the case of radar these returns are the ‘backscatter’ from transmitted microwave pulses, and for LiDAR sensors the pulses are of laser light. Figure 1 summarises the mechanism each uses.

The very different mechanisms used by the three sensor types listed above results in an ability to detect different characteristics of vegetation. Each type is also sensitive to other potentially confounding surface characteristics, and has its own particular error sources and potential artefacts. The major characteristics of each system are

summarised below in turn, in addition to an introduction to the principle sensors of each type used in the thesis.

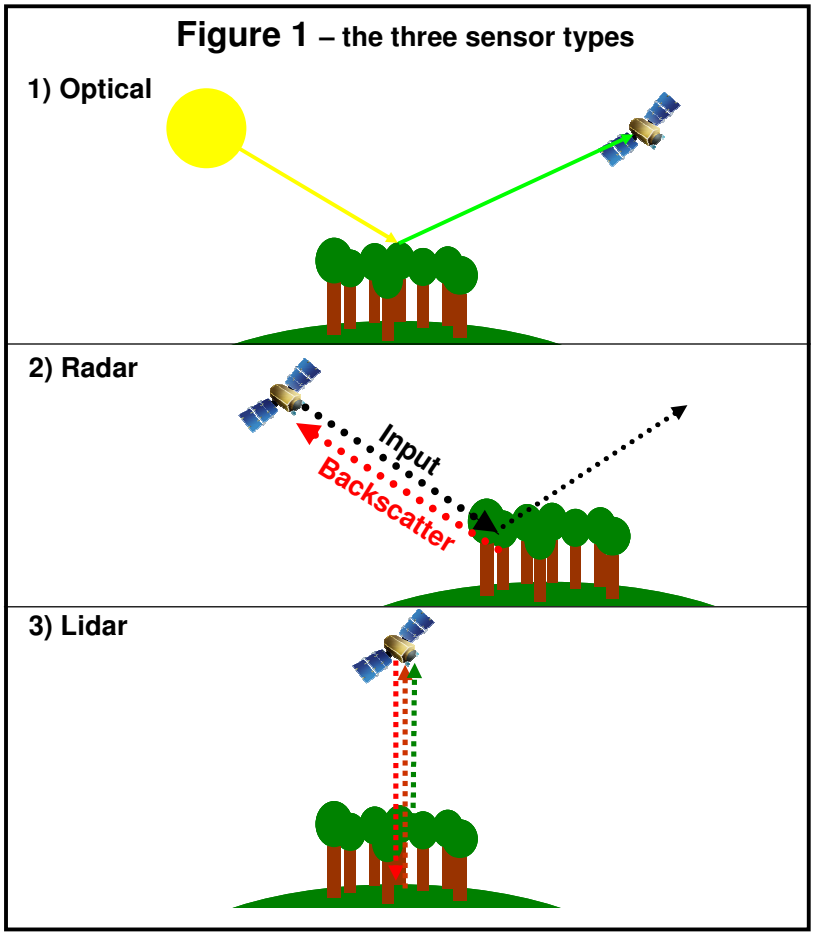

2.2.1 Optical sensors

'Optical sensor' is the term used throughout this thesis to refer to multispectral passive sensors detecting in the visible-light, infrared and thermal portions of the electromagnetic spectrum (with the wavelength detected between approximately 0.4 - 15 µm). This spectrum is split into four regions in terms of wavelength: visible light (0.4 – 0.75 µm, near-infrared (NIR, 0.75 – 1.4 µm), short-wave infrared (SWIR, 1.4 – 3 µm), and thermal infrared (3-15 µm) (Figure 2). For visible, NIR and SWIR such sensors use the sun as an illumination source, detecting the magnitude of reflected radiation in a number of different 'bands', narrow portions of the spectrum. For thermal infrared the emission of the objects themselves is detected, which allows such sensors to directly estimate the temperature of objects (Jacob *et al.* 2004).

By comparing reflection values in different bands, characteristics of the landcover can be elucidated: for example green plants absorb red light strongly, but reflect infrared, whereas soils tend to reflect both approximately equally (Figure 3). The bands for three major optical sensors (the principle optical sensors used in this thesis), Landsat TM/ETM+, ASTER and MODIS, are shown in Figure 2.

Figure 2 – wavelengths of the bands of three optical satellite sensors

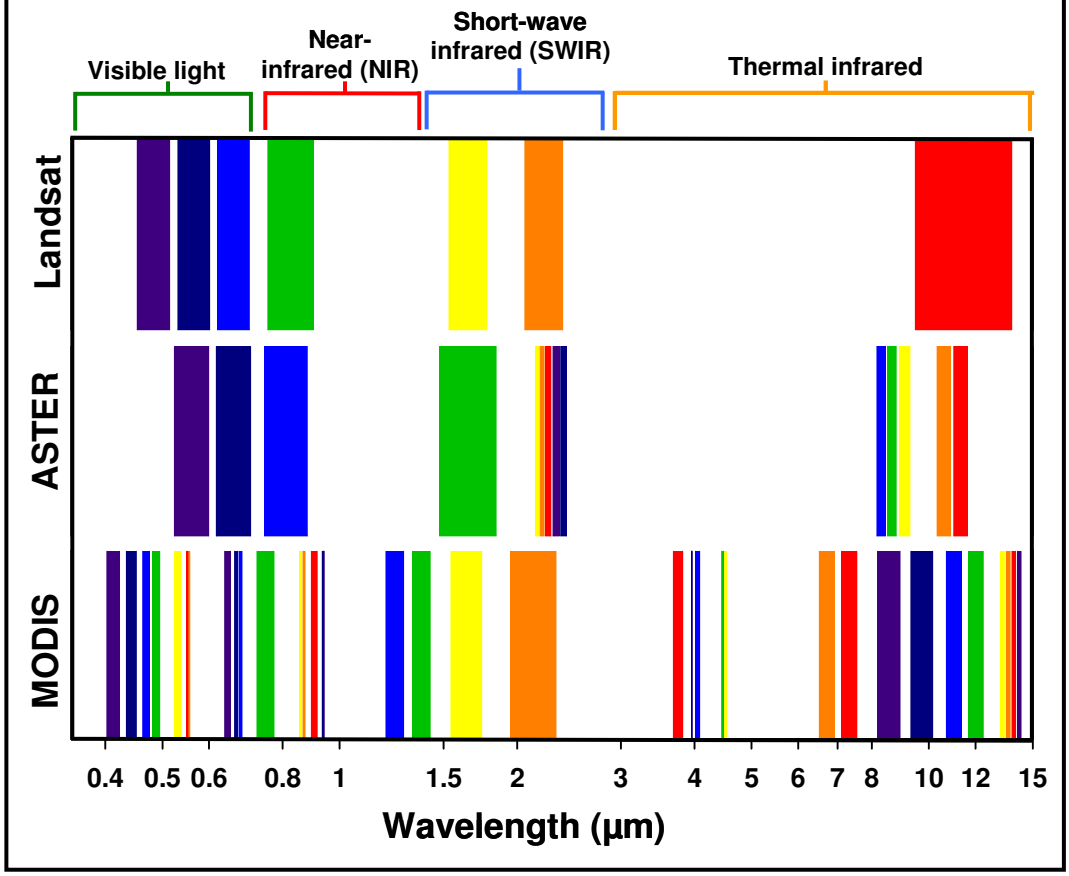

Figure 3 - Reflectance spectra of green vegetation, dry vegetation and soil

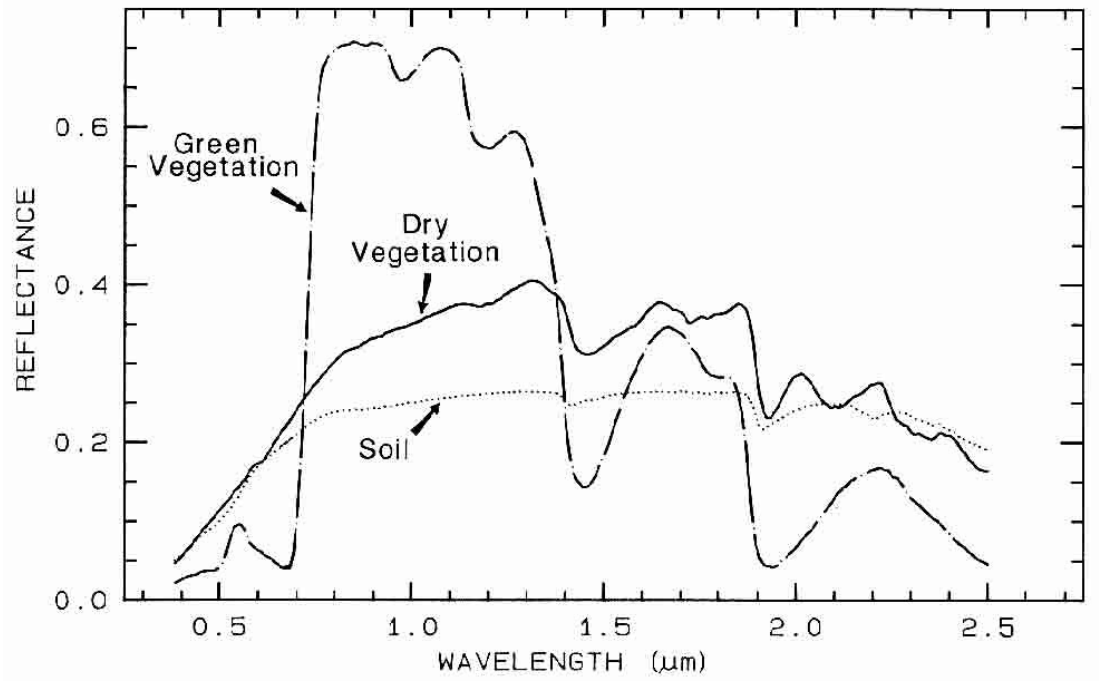

This figure is taken from Clark (1999), and shows idealised reflectance spectra for green vegetation, dry vegetation and soil in response to sunlight.

The narrowness of the bands increases from Landsat to ASTER, and again from ASTER to MODIS (Figure 2). Over approximately the same range of wavelengths, Landsat has 7 bands, ASTER 14, and MODIS 36. The narrower the bands, the greater the capacity of the sensor to differentiate between different landcover classes/states using spectral information. Taking this to an extreme are hyperspectral sensors, such as NASA's satellite sensor Hyperion, that can elucidate full reflectance signatures using hundreds of narrow bands (220 bands for Hyperion). However, no current or planned hyperspectral satellite sensor achieves coverage of a significant portion of the Earth's surface at a useful spatial resolution, therefore such data cannot yet be used for mapping and monitoring woody cover at a regional scale. Only optical satellite sensors with multi-spectral capabilities are therefore considered here.

Different bands are often combined into metrics that give more information on the landcover than either band individually. In the context of woody vegetation, such metrics are often called 'vegetation indices'. The most well-known is the Normalised

Difference Vegetation Index (NDVI), a ratio of red (b_n) and infra-red (b_r) light that responds strongly to the quantity of green vegetation within a pixel:

$$NDVI = \frac{b_n - b_r}{b_n + b_r} \quad (1)$$

Different vegetation indices are discussed in more detail in Chapter 3.

The large number of optical sensors currently in orbit differ greatly not just to the spectral bands to which they are sensitive, but also in their spatial resolution. For non-military satellite, this varies between 46 cm pixels (WorldView 2) to tens of kilometres (weather satellites). In general, there is a trade-off between resolution and repeat time: the Meteosat series of weather satellites are geostationary satellites that take an image of a constant large portion (almost a hemisphere) of the Earth every 15 minutes at a ~2.5 km resolution; MODIS, a NASA sensor found on two satellites that collects data at a 250 m resolution, and images the whole surface of the Earth 2-4 times daily; Landsat, at a 30 m resolution, images the whole Earth a few times per year; and WorldView 2, at a 46 cm resolution, can at most image 0.5 % of the Earth's surface in a year.

There is no ideal position along the resolution/repeat-time trade-off continuum; instead the sensor chosen will depend greatly on the task at hand. For example for weather monitoring a coarse resolution with a very high repeat time s idea; whereas for monitoring urban development a very high resolution will be necessary, but images once per year are sufficient. Other factors are also important, such as the cost of the imagery (which generally increases with resolution, with most coarse-resolution data being distributed free of charge), and the availability of comparable historical data (with very high resolution data typically not being available historically, as it normally needs to be ordered on demand; however in some cases aerial photography and/or satellite imagery do allow historical analyses).

For mapping and monitoring vegetation characteristics, in general resolutions of 10 m – 500 m present the best balance between being able to differentiate the relevant landscape units and repeat time. As already mentioned, three satellite sensors from

this range are principally used for this thesis, and these will be discussed in more detail below.

2.2.1.1 Landsat

The Landsat satellite series is a set of six satellites built and controlled by the USGS and NASA (numbered 1-5 & 7, as 6 was lost at launch) that have been monitoring the surface of the Earth from 1972 to present. Landsats 1-3 featured (among others) the MultiSpectral Scanner sensor (MSS), a ~60 m resolution sensor with 5 spectral bands. Landsat 4 & 5, in addition to carrying an MSS sensor for data continuality reasons, carrry a 30 m resolution[1] Thematic Mapper (TM) sensor, with seven bands (Figure 2). This sensor features much better radiometric calibration and consistency than the MSS sensor, in addition to a higher resolution, and led to it becoming the standard tool of landscape change detection. Finally, Landsat 7, launched in 1999, features a sensor called the Enhanced Thematic Mapper-plus, ETM+. This is essentially identical to the TM sensor, but adds a 15 meter resolution panchromatic (black-and-white) band, which, while not giving additional spectral information, can be used to 'pan-sharpen' the other bands, effectively increasing the resolution to 15 m.

All Landsat data are now freely available, presenting a resource that has been very widely used. However, no sensor has been launched since 1999, creating a potential data gap as the Landsat Data Continuity Mission (LDCM) is not planned to be launched until December 2012. Two of the satellites in orbit are currently still partially operational: Landsat 5 and Landsat 7. Landsat 5 has had problems with its battery and solar panels, meaning that it can no longer capture and transmit imagery for the whole globe as it orbits; however it still provides a significant quantity of useful data, 23 years beyond its expected mission life (it was launched in 1984 with a three-year design life, Williams *et al.* 2006). In 2003, Landsat 7 developed a fault in its scanline-corrector. Despit this fault imagery is still being captured, but lines of data are missing, equating to a loss of about a third of the image. A central portion of

[1] With TM, as with all the sensors mentioned here, the longer-wavelength infra-red bands operate at a lower resolution than the figure given, which is for the short-wavelength bands.

each scene is largely unaffected, but data loss becomes more apparent towards the edge of each scene, greatly reducing the utility of the imagery.

2.2.1.2 ASTER

The Advanced Spaceborne Thermal Emission and Reflection Radiometer (ASTER) sensor is positioned on the TERRA satellite, which was launched in 1999, and has been collecting imagery from February 2000 until the present day. ASTER has a multispectral spatial resolution four-times higher than Landsat TM/ETM+, with 15 m pixels, and still captures images over the whole of the Earth's surface several times a year. It also features a higher number of narrower spectral bands, especially in the infrared region (Figure 2). However, despite problems with the Landsat statellites over the past decade, ASTER is still less widely used for landcover characterisation and change detection than Landsat 5/7, for three reasons:

a) The spectral bands differ, hindering comparisons with historical Landsat imagery
b) It lacks a blue band, which hinders atmospheric correction, and data from this portion of the spectrum is essential for some analyses
c) The relatively small scene sizes compared to Landsat (ASTER: 60 km x 60 km; Landsat:170 km x 183 km) makes it considerably harder to make seamless mosaics over large areas.

There are a number of other satellites with similar characteristics to Landsat and ASTER. For example the SPOT satellite series (France), CBERS (China/Brazil), and AVNIR-2 (Japan), all observe in the optical region and have been successfully used for landcover mapping.

2.2.1.3 MODIS

The MODerate-resolution Imaging Spectroradiometer (MODIS) instrument is associated with two NASA satellites: Terra (launched in December 1999) and Aqua (launched in May 2002). MODIS has 36 bands (Figure 2), with two (green and near-infra red, used specifically for vegetation monitoring) at a nominal resolution of 250 m, with the remainder at 500 m or 1 km resolution. The resolution is therefore an order of magnitude lower than Landsat or ASTER, greatly reducing its ability to resolve features in the landscape and detect detailed change, and because of the prevalence of pixels containing multiple landcover classes at this resolution ('mixed pixels'). However, between the two sensors, the majority of the tropical and sub-tropical belt is imaged four times per day. Cloud-free mosaics can thus be produced over the majority of the Earth's surface multiple times per year, something that is not possible with higher resolution imagery. MODIS is widely used not only because of its high number of observations and excellent geolocation and radiometric accuracy (Wu *et al.*, 2011), but also because all the data collected, in the form of a wide range of high-level products, are freely available and easily accessible online.

2.2.1.4 Artefacts, cloud and calibration

One further factor with optical imagery is the influence of the atmosphere, sun-angle, haze and cloud cover. The spectral make-up of light from the sun is relatively constant, but the composition and state of the atmosphere is not. For optical satellite sensors the light from the sun has to pass through the atmosphere twice, once *en route* to the surface, and then once it has interacted with the object on the surface going back up to the satellite. Sensors differ in how well they are post-processed automatically to reduce atmospheric effects, producing scenes where differences are attributed to changes in the landcover not in the atmosphere. MODIS does particularly well here, with its frequent observations and range of bands allowing very sophisticated correction. Landsat and ASTER scenes can be corrected for atmospheric effects by the user, but this becomes harder with historic imagery (pre-2000), when real-time measurements of the characteristics of the atmosphere were not performed to the same degree as they are now. Often absolute atmospheric correction is not possible for these older images, but as shown in Chapter 3, relative

atmospheric correction (i.e. cross-calibrating one scene to another) can be sufficient to enable the detection of landcover change with high confidence.

Most optical Earth-observation satellites we are interested in follow sun-synchronous near-polar orbits, meaning they image a particular latitude at the same time every day. Thus, images captured over a number of years in the same season should have the same sun-angle, creating comparable data. However, this is not necessarily the case if different sensors are being compared or if imagery captured at a different time of year is used. Again, sun-angle can be corrected to a certain extent at a processing stage, but ideally its effect on change-detection can be avoided by considering imagery only from the same season. As long as it is not extreme, modelling studies suggest differing sun angles should not bias change detection results unduly, especially in tropical latitudes (Gerard 2003).

Haze and cloud-cover are extremes along a spectrum of problems, where the transparency of the atmosphere is reduced by the condensation of atmospheric water vapour into droplets. The surface of the Earth can still be seen through haze, but the spectral characteristics are often changed and in effect haze can render imagery unusable. Nothing can be seen in our wavelengths of interest through cloud cover, and cloudy portions of imagery have to be discarded. Some areas of the tropics can be cloud-covered almost all the time, making finding high resolution optical imagery very difficult; although, due to its daily repeats, some cloud-free MODIS imagery can normally be guaranteed.

2.2.2 Radar

Radar sensors use an entirely different type of technology to passive optical sensors, and thus are sensitive to very different characteristics of the Earth's surface. The wavelength used is in the microwave portion of the spectrum, with the wavelengths used for mapping vegetation typically varying from 1 cm to about 1 m (300 MHz - 30 GHz). These sensors are 'active', as they send a pulse of radiation at the surface and then detect the returns. Spaceborne radar sensors send the pulse at an oblique angle, normally between 20° and 40°; the majority of the signal will reflect in the opposite direction, but some radiation interacts with the surface and is scattered back

to the sensor (Figure 1). This detected radiation is called 'backscatter', and is often reported in terms of the dimensionless log-scaled "sigma-naught" (σ^0), defined as the normalised radar cross-section, scaled to dB.

Radar data is transmitted 'polarised', that is with all the electro-magnetic waves orientated into the same plane. When the signal interacts with the surface this polarisation can be changed, so sensors are often designed to detect incoming radiation both in the original polarisation, and at 90° to this in order to detect the cross-polarised backscatter. There are up to four different polarisation combinations used: Horizontal-send/Horizontal-receive (HH); Horizontal-send/Vertical-receive (HV); Vertical-send/Vertical-receive (VV); and Vertical-send/Horizontal-receive (VH). Ideally all four combinations would be collected, giving fully polarimetric data and the maximum possible information on the characteristics of scatterers on the surface; however, from satellite sensors only a subset of possible polarisations are normally collected.

The details of how radar interacts with the surface, and how backscatter information is collected and processed, is considerably more technically involved than for optical data, but detailed models of the surface can be derived through inverse-modelling of the backscatter signal returned (Oliver & Quegan 2004). Equally it is possible to use two radar images from different angles to build up interferograms, giving information on surface structure and scatterers. Interferometry is not used in this thesis, nor is it necessary to understand the more technical aspects of radar data in detail for the purposes of the analyses presented here; more details can however be found in Woodhouse (2005).

Radar sensors typically only collect data in one wavelength band, and, as with optical data, the choice of wavelength for the band changes greatly what is detected. The radar spectrum is divided into sections named using single-letters, which were so-named during the military development of the technology. The bands that have been used for determining vegetation characteristics are, in increasing order of wavelength, X, C, L and P. Their characteristics are given in Table 1, along with the major satellites that operate in each band.

Table 1 – Radar bands and satellites

Band	Wavelength	Frequency	Typical maximum resolution from satellites	Satellites
X-band	2.5-3.75 cm	8-12 GHz	~1 m	TerraSAR-X (2007-) TanDEM-X (2010-)
C-band	3.75-7.5 cm	4-8 GHz	~3 m	ERS-1 (1991-2000) ERS-2 (1994-) ENVISAT (2002-) RADARSAT 1 (1994-) RADARSAT 2 (2007-)
L-band	15-30 cm	1-2 GHz	~20 m	JERS-1 (1992-1998) ALOS PALSAR (2007-) *DESDynI (2016)*
P-band	70-130 cm	230-430 MHz	~50 m	*?BIOMASS (2016)*

The wavelength of the radar determines with what features it will interact, and its ability to penetrate into surface features. In general shorter wavelengths will interact with smaller target features and penetrate less far through a complex surface (Imhoff, 1995; Woodhouse, 2005). For example, when the target is a forest, X- and C- bands will principally be scattered by the leaves and twigs near the top of the canopy, as these are of a similar size to the wavelength, and will not penetrate more than a meter into the forest canopy (Imhoff, 1995). L-band, being a considerably longer wavelength, will not interact much with leaves, but instead will be scattered branches and stems, penetrating through the canopy and potentially interacting to a limited extent with stems (trunks) and ground. P-band is a longer wavelength still, and will be almost exclusively influenced by the stems and the ground surface (Imhoff, 1995). Thus, while all bands should be able to differentiate forest from non-forest because of changes in backscatter from the very different surface characteristics, the ability to detect and quantify AGB will increase with wavelength, as the canopy is penetrated and the objects that contain the biomass (stems and branches) interact more strongly with the microwave radiation.

As this thesis is concerned with sensing changes in woody biomass, only L-band data are used, as this wavelength is the most sensitive to biomass available (there are currently no P-band satellites). The only exception to this is the C-band data from the Shuttle Radar Topography Mission (SRTM), which was collected in 11-days in February 2000, which is used throughout the thesis to provide a Digital Elevation Model (DEM).

There have been two L-band satellites launched, both by the Japanese Aerospace Exploration Agency (JAXA). The Japanese Earth Resource Satellite (JERS-1) was launched in 1992 and operated until 1998; and the Phased Array L-band Synthetic Aperture Radar (PALSAR) sensor on the Advanced Land Observing Satellite (ALOS), which was launched in 2006 and collected data until April 2011. JERS-1 collected data only in the HH polarisation, at around a 40 meter resolution. PALSAR principally collected data in Fine-Beam Dual-polarisation (FBD) mode, giving HH and HV data at around a 20 m resolution (Rosenqvist *et al.*, 2007). However it also had the capacity to collect fully-polarimetric data, though in this mode resolution is reduced to ~30 m, and only a small quantity of data was collected in this experimental mode.

2.2.3 LiDAR data

LiDAR is an active sensor, and thus superficially similar to radar, involving the sending of a pulse of electromagnetic radiation and detecting the return. However, unlike radar's microwaves, pulses of laser data in the visible or short-wave infrared portions of the spectrum are used. Unlike radar, the sensor normally looks down at the surface from a vertical or near-vertical angle, rather than looking sideways (Figure 1). When imaging a forest canopy some laser light is reflected from the top of the trees, and some penetrates through to the ground before reflecting. The difference in time between these returns allows an estimate of canopy and ground height. Modern sensors can detect the 'full waveform' reflected; in the context of the tree canopy, this means that the relative reflective power of different parts of the canopy can be elucidated, allowing for an estimation of the depth of the canopy (Ni-Meister *et al.*, 2001). LiDAR therefore has a far greater potential to characterise the 3-D structure of a forest than optical or radar data.

Collecting LiDAR data from space is still a developing technology. ICESat (launched 2003, retired 2009) is the only satellite that has so far successfully collected data useful for retrieving information on forest characteristics. ICESat-2 is planned to be launched in 2016, so there will be no spaceborne lidar data collected for at least the period 2010-2015. However, the use of plane-mounted sensors is rapidly increasing, and significant areas of the forest are now being surveyed by such instruments. For example 4.3 million hectares of the Peruvian Amazon was recently inventoried in this way (Asner *et al.* 2010).

Spaceborne LiDAR data take the form of large, widely separated elliptical footprints (e.g. for ICESat, at the equator, these footprints are ellipses approximately 0.25 ha in size, separated by several hundred meters along a track, separated from the next track by several kilometres). Though these footprints will be more numerous and smaller for ICESat-2, spaceborne LiDAR data will still be used largely as a sampling tool for calibrating and validating other remote sensing data (as used in Chapter 7). However, from aircraft, many tens of footprints can be retrieved for every square meter, allowing very detailed 3-dimensional models of forest structure to be developed: in this capacity LiDAR is a useful tool for well-resourced forest projects, but for general wide-scale monitoring such data are too expensive and time-consuming to collect.

2.3 Change detection

The previous section described the different remote sensing datasets that can be used to map landcover and retrieve estimates of woody cover and AGB. The precise details of methods used will be discussed in more detail in later chapters, but this section provides a brief introduction to the field of change detection.

The method used for change detection can greatly affect the observed change, even between identical datasets (Lu *et al.* 2005; Lu 2006). However, before any change detection methodology can be applied, the datasets must first be made comparable in order for accurate results to be obtained. There are two main components here:

1) **Calibration:** the same vegetation-type on the ground must produce an identical response in all the satellite images compared. That is to say that an AGB of 100 Mg ha^{-1}, or a canopy cover of 60 %, or a degraded forest, must produce the same observed spectral response, backscatter, or landcover type in the end products to be compared. This can be very hard to directly confirm (Lu 2006; Mitchard *et al.* 2009; Mitchard *et al.* 2011), but is nevertheless a highly desirable ideal. One approach is to ensure that the ground conditions, atmospheric conditions and sensor properties are identical at all time points: for example choosing images from the same season, with the same sensor, and then checking that rainfall in the previous few months, and atmospheric conditions on the day, are identical across the time points. However, especially at higher resolutions, or when looking back far into the past, it is not normally possible to come close to this ideal. Therefore, another approach is to calibrate the images separately to ensure they are identical. This can either involve calibration to some independent standard (*e.g.* adjusting all reflectances so they correspond to standard reference-spectra), or the images can be cross-calibrated to each other using invariant features. These latter techniques are useful; but fundamentally when comparing images from different seasons or sensors, or with different sun-angles or atmospheric conditions, there is always a possibility that some observed changes are artefacts, even after calibration procedures.

2) **Geolocation:** when comparing two (or more) images it is essential that every pixel overlays exactly, or else spurious change will be detected. This can be very difficult, as the geolocation information that comes with satellite data is often only accurate to 50 – 100 m, and is never exactly identical between two images. In general, in my experience, the accuracy for MODIS and Landsat is high, without much correction needed, whereas the accuracy for radar satellites such as ALOS PALSAR and JERS-1 is generally lower (often 2-4 pixels different from Landsat). In order for good, accurate change detection it is normally necessary to manually 'warp' one image to the other, by finding invariant features (such as road junctions and bridges) and using a software

package such as ENVI (ITT Systems) to warp one image to another using these user-defined points. In areas without many features this process can be very time-consuming, and high accuracies are not always possible.

Once comparable datasets are produced, a large number of change-detection methodologies can be applied (Rignot & Vanzyl 1993; Lu 2004; Lu *et al.* 2005). The method chosen depends greatly on the data type being analysed, and often more than one method is applied to allow comparisons between the results.

The datasets being compared in this research are continuous distributions, (e.g. maps of woody cover or AGB). This in many ways simplifies the whole procedure, as one map can simply be subtracted from the other, giving a change map with a continuous distribution (with accuracy related to the accuracy of the two original input datasets – see discussion in Chapter 6). Ideally such a continuous change map would be accompanied with a map of predicted uncertainty, e.g. Saatchi *et al.* (2007), however in practice this is often not possible, as the relevant data to produce a spatially-explicit map of uncertainty is not available.

However, often an output change map containing a continuous variable is not appropriate, e.g. when trying to assess changes in forest area. In such cases the output variable needs to be a categorical variable; in the forest change example pixels need to be given classes such as 'forest in both images', 'non-forest in both images', 'deforested', or 'afforested'. This is also the case with comparing continuous distributions where considerable uncertainty exists on each axis, and so change maps will show positive or negative values for many pixels where no change has actually happened. Producing categorical change maps in such circumstances either involves artificially thresholding a continuous change-map, or using a more complex change algorithm (Lu 2004). More discussion of this issue is given in Chapter 3, but it remains a contentious issue with more research needed, as results can be very dependent on the researchers' choice of algorithm (Lu, 2004).

2.4 References

Ågren G.I., & Ingestad, T. (1987). Root: shoot ratio as a balance between nitrogen productivity and photosynthesis. *Plant, Cell, and Environment* 10, 579-586.

Aragao L., Malhi Y., Metcalfe D.B., Silva-Espejo J.E., Jimenez E., Navarrete D., Almeida S., Costa A.C.L., Salinas N., Phillips O.L., Anderson L.O., Alvarez E., Baker T.R., Goncalvez P.H., Huaman-Ovalle J., Mamani-Solorzano M., Meir P., Monteagudo A., Patino S., Penuela M.C., Prieto A., Quesada C.A., Rozas-Davila A., Rudas A., Silva J.A. & Vasquez R. (2009) Above- and below-ground net primary productivity across ten Amazonian forests on contrasting soils. *Biogeosciences*, 6, 2759-2778

Armston J.D., Denham R.J., Danaher T.J., Scarth P.F. & Moffiet T.N. (2009) Prediction and validation of foliage projective cover from Landsat-5 TM and Landsat-7 ETM+ imagery", *Journal of Applied Remote Sensing,* 3, 033540

Asner G.P., Powell G.V.N., Mascaro J., Knapp D.E., Clark J.K., Jacobson J., Kennedy-Bowdoin T., Balaji A., Paez-Acosta G., Victoria E., Secada L., Valqui M. & Hughes R.F. (2010) High-resolution forest carbon stocks and emissions in the Amazon. *Proceedings of the National Academy of Sciences of the United States of America*, 107, 16738-16742

Brown S. (1997) Estimating Biomass and Biomass Change of Tropical Forests. FAO Forest Paper 134, Rome.

Burrows W.H., Hoffman M.B., Compton J.F., Back P.V. & Tait L.J. (2002) Allometric relationships and community biomass estimates for some dominant eucalypts in Central Queensland woodlands. *Australian Journal of Botany*, 48, 707–714.

Chave, J., Condit R., Lao S., Caspersen J.P., Foster R.B., & Hubbell S.P. (2003) Spatial and temporal variation in biomass of a tropical forest: results from a large census plot in Panama. *Journal of Ecology*, 91, 240-252.

Chave J., Andalo C., Brown S., Cairns M.A., Chambers J.Q., Eamus D., Folster H., Fromard F., Higuchi N., Kira T., Lescure J.P., Nelson B.W., Ogawa H., Puig H., Riera B. & Yamakura T. (2005) Tree allometry and improved estimation of carbon stocks and balance in tropical forests. Oecologia, 145, 87-99

Chave J., Condit R., Aguilar S., Hernandez A., Lao S. & Perez R. (2004) Error propagation and scaling for tropical forest biomass estimates. *Philosophical Transactions of the Royal Society of London Series B-Biological Sciences*, 359, 409-420

Clark, R.N. (1999) *Manual of Remote Sensing*, ed. A. Rencz, J. Wiley and Sons, New York

Cole T.G. & Ewel J.J. (2006) Allometric equations for four valuable tropical tree species. *Forest Ecology and Management*, 229, 351-360

Djomo A.N., Ibrahima A., Saborowski J. & Gravenhorst G. (2010) Allometric equations for biomass estimations in Cameroon and pan moist tropical equations including biomass data from Africa. *Forest Ecology and Management*, 260, 1873-1885

Emlen, J.T. (1967). A Rapid Method for Estimating Arboreal Canopy Cover. *Ecology*, 48, 158-160

Gerard F. (2003) Single angle, dual angle and multi-temporal viewing: assessing through modelling the implications for forest structure variable extraction. *International Journal of Remote Sensing*, 24, 1317-1334

Gibbon A., Silman M.R., Malhi Y., Fisher J.B., Meir P., Zimmermann M., Dargie G.C., Farfan W.R. & Garcia K.C. (2010) Ecosystem Carbon Storage Across the Grassland-Forest Transition in the High Andes of Manu National Park, Peru. *Ecosystems*, 13, 1097-1111

Grace J., San Jose J., Meir P., Miranda H.S. & Montes R.A. (2006) Productivity and carbon fluxes of tropical savannas. *Journal of Biogeography*, 33, 387-400

Henry M., Besnard A., Asante W.A., Eshun J., Adu-Bredu S., Valentini R., Bernoux M. & Saint-Andre L. (2010) Wood density, phytomass variations within and among trees, and allometric equations in a tropical rainforest of Africa. *Forest Ecology and Management*, 260, 1375-1388

Imhoff, M.l. (1995). A theoretical analysis of the effect of forest structure on synthetic aperture radar backscatter and the remote sensing of biomass. *IEEE Transactions on Geosciences and Remote Sensing,* 33, 341-352.

Jacob F., Petitcolin F., Schmugge T., Vermote E., French A. & Ogawa K. (2004) Comparison of land surface emissivity and radiometric temperature derived from MODIS and ASTER sensors. *Remote Sensing of Environment*, 90, 137-152

Keller M., Palace M. & Hurtt G. (2001) Biomass estimation in the Tapajos National Forest, Brazil: Examination of sampling and allometric uncertainties. *Forest Ecology and Managemen* 154, 371-382

Leuschner C., Moser G., Bertsch C., Roderstein M. & Hertel D. (2007) Large altitudinal increase in tree root/shoot ratio in tropical mountain forests of Ecuador. *Basic and Applied Ecology*, 8, 219-230

Lu D., Mausel P., Batistella M. & Moran E. (2005) Land-cover binary change detection methods for use in the moist tropical region of the Amazon: a comparative study. *International Journal of Remote Sensing*, 26, 101-114

Lu D.S. (2004) Change detection techniques. *International Journal of Remote Sensing*, 25, 2365-2401

Lu D.S. (2006) The potential and challenge of remote sensing-based biomass estimation. *International Journal of Remote Sensing*, 27, 1297-1328

Lucas R.M. Lee A.C., Armston J., Carreiras M.B., Viergever K., Bunting P., Clewley D., Moghaddam M., Siqueira P. & Woodhouse I. 2011. The Role of Active Sensors in Measurements of Tree Structure and Biomass. In: *Ecosystem Function in Savannas; Measurement and Modeling at Landscape to Global Scales.* Editors: Hill M.J. & Hanan N.P. CRC Press, FL, USA.

McElhinny C., Gibbons P., Brack C. & Bauhus J. (2005) Forest and woodland stand structural complexity: Its definition and measurement. *Forest Ecology and Management*, 218, 1-24

McWilliam A.-L.C., Roberts J.M., Cabral O.M.R., Leitao M.V.B.R., Costa A.C.L.d., Maitelli G.T. & Zamparoni C.A.G.P. (1993) Leaf Area Index and Above-Ground Biomass of terra firme Rain Forest and Adjacent Clearings in Amazonia. *Functional Ecology*, 7, 310-317

Mitchard E.T.A., Saatchi S., Woodhouse I., Feldpausch T., Lewis S., Sonké B., Rowland C. & Meir P. (2011) Measuring biomass changes due to woody encroachment and deforestation/degradation in a forest-savanna boundary region of central Africa using multi-temporal L-band radar backscatter. *Remote Sensing of Environment*

Mitchard E.T.A., Saatchi S.S., Gerard F.F., Lewis S.L. & Meir P. (2009) Measuring Woody Encroachment along a Forest-Savanna Boundary in Central Africa. *Earth Interactions*, 13, 1-29

Ni-Meister, W., Jupp, D.L.B., & Dubayah, R. 2001. Modeling lidar waveforms in heterogeneous and discrete canopies. *IEEE Transactions on Geoscience and Remote Sensing*, 39, 1943-1958.

Nowak D.J., Rowntree R.A., McPherson E.G., Sisinni S.M., Kerkmann E.R. & Stevens J.C. (1996) Measuring and analyzing urban tree cover. *Landscape and Urban Planning*, 36, 49-57

Oliver C. & Quegan S. (2004) Understanding synthetic aperture radar images. SciTech Publishing, Raleigh, NC.

Phillips O.L., Baker T.R., Feldpausch T.R. & Brienen R. (2009) Field manual for plot establishment and remeasurement, http://www.geog.leeds.ac.uk/projects/rainfor/

Potapov P., Laestadius L., Yaroshenko A., Turubanova S. (2009) Global mapping and monitoring the extent of forest alteration: the intact forest landscapes method. FAO, Forest Resources Assessment Working Papers, 166. Rome.

Rignot E.J.M. & Vanzyl J.J. (1993) Change Detection Techniques for ERS-1 Sar Data. *IEEE Transactions on Geoscience and Remote Sensing*, 31, 896-906

Rosenqvist, A., Shimada, M., Ito, N., & Watanabe, M. (2007). ALOS PALSAR: A pathfinder mission for global-scale monitoring of the environment. *IEEE Transactions on Geoscience and Remote Sensing*. 45, 3307-3316.

Ryan C.M. (2009) Carbon cycling, fire and phenology in a tropical savanna woodland in Nhambita, Mozambique. PhD Thesis, University of Edinburgh.

Ryan C.M., Williams M. & Grace J. (In press) Above- and Belowground Carbon Stocks in a Miombo Woodland Landscape of Mozambique. *Biotropica*

Saatchi S.S., Houghton R.A., Alvala R., Soares J.V. & Yu Y. (2007) Distribution of aboveground live biomass in the Amazon basin. *Global Change Biology*, 13, 816-837

Scholes R.J. & Archer S.R. (1997) Tree-grass interactions in savannas. *Annual Review of Ecology and Systematics*, 28, 517-544

Walker BH. 1980. Bush encroachment in southern Africa: an ecological overview. In: *Proceedings of a Workshop on Bush Encroachment*. Dept. of Agriculture and Technical Services. Pretoria, South Africa.

Wang C.Z., Qi J.G. & Cochrane M. (2005) Assessment of tropical forest degradation with canopy fractional cover from landsat ETM plus and IKONOS imagery. *Earth Interactions*, 9.

Weiss M., Baret F., Smith G.J., Jonckheere I. & Coppin P. (2004) Review of methods for in situ leaf area index (LAI) determination Part II. Estimation of LAI, errors and sampling. *Agricultural and Forest Meteorology*, 121, 37-53

Williams D.L., Goward S. & Arvidson T. (2006) Landsat: Yesterday, today, and tomorrow. *Photogrammetric Engineering and Remote Sensing*, 72, 1171-1178

Williams M., Ryan C.M., Rees R.M., Sarnbane E., Femando J. & Grace J. (2008) Carbon sequestration and biodiversity of re-growing miombo woodlands in Mozambique. *Forest Ecology and Management*, 254, 145-155

Woodhouse I.H. (2005) Introduction to Microwave Remote Sensing. CRC Press.

Wu, A.S., Xiong, X.X., Angal, A., Barnes, W. (2011) Evaluation of detector-to-detector and mirror side differences for Terra MODIS reflective solar bands using simultaneous MISR observations. *International Journal of Remote Sensing*, 32, 299-312.

Zimmermann M., Meir P., Bird M.I., Malhi Y. & Ccahuana A.J.Q. (2010a) Temporal variation and climate dependence of soil respiration and its components along a 3000 m altitudinal tropical forest gradient. *Global Biogeochemical Cycles*, 24, GB4012

Zimmermann M., Meir P., Silman M.R., Fedders A., Gibbon A., Malhi Y., Urrego D.H., Bush M.B., Feeley K.J., Garcia K.C., Dargie G.C., Farfan W.R., Goetz B.P., Johnson W.T., Kline K.M., Modi A.T., Rurau N.M.Q., Staudt B.T. & Zamora F. (2010b) No differences in soil carbon stocks across the tree line in the Peruvian Andes. *Ecosystems*, 13, 62-74

3. Measuring Woody Encroachment along a Forest–Savanna Boundary in Central Africa

Authors: E.T.A. Mitchard[a], S.S. Saatchi[b], F.F. Gerard[c], S.L. Lewis[d], & P. Meir[a]

a *School of GeoSciences, University of Edinburgh, EH8 9XP, UK*

b *Jet Propulsion Laboratory, California Institute of Technology, Pasadena, CA 91109, USA*

c *Centre for Ecology and Hydrology, Maclean Building, Benson Lane, Crowmarsh Gifford, Wallingford, Oxfordshire, OX10 8BB, UK*

d *Earth and Biosphere Institute, School of Geography, University of Leeds, LS2 9JT , UK*

As published in *Earth Interactions*, May 2009[1]

Author contributions: ETAM, SSS, & PM devised the research; ETAM collected the field data; ETAM conducted the analysis after training from SSS and with assistance from all other authors; ETAM wrote the paper with assistance and revisions from all other authors.

[1] *Earth Interactions*, Vol. 13, Paper No. 8, DOI: 10.1175/2009EI278.1. See Appendix 1.

Abstract

Changes in net area of tropical forest are the sum of several processes: deforestation, regeneration of previously deforested areas, and the changing spatial location of the forest-savanna boundary. We conducted a long-term (1986-2006) quantification of vegetation change in a 5400 km^2 forest-savanna boundary area in central Cameroon. We used a cross-calibrated NDVI change detection method to compare three high-resolution images, from 1986, 2000 and 2006. We measured the canopy dimensions and locations of over 1000 trees in the study area, finding a very strong relationship between Canopy Area Index (CAI) and NDVI. Across 5400 km^2 12.6 % of the area showed significant positive change in canopy cover from 1986 – 2000 (0.9 % yr^{-1}), and 7.8 % from 2000 – 2006 (1.29 % yr^{-1}), whereas < 0.4 % of the image showed a significant decrease in either period. The largest changes were in the lower canopy cover classes: the area with < 0.2 m^2/m^2 CAI decreased by 43 % in 20 years. One cause may be a recent reduction in fire frequency, as documented by ATSR-2/AATSR data on fire frequency over the study area from 1996-2006. We suggest this is due to a reduction in human pressure caused by urbanisation, as rainfall did not alter significantly over the study period. An alternative hypothesis is that increasing atmospheric CO_2 concentrations are altering the competitive balance between grasses and trees. Our data add to a growing weight of evidence that forest encroachment into savanna is an important process, occurring in forest-savanna boundary regions across tropical Africa.

3.1 Introduction

It has long been appreciated that the woody cover of large areas of tropical Africa has undergone rapid changes in the recent past, with forest having retreated to a small fraction of its present area due to an arid period from c. 4000 to 1300 years before present, and having expanded to its present extent by around 900 years before present despite increasing human pressure (Maley, 1996; Salzmann and Hoelzmann, 2005). Many factors interact to control the woody cover of an area, including rainfall, soil characteristics, seasonality, temperature, and the level and history of disturbance (Sankaran *et al.*, 2005; Buccini & Hanan, 2007). The majority of the woody savannas of Africa would, in the absence of disturbance, become forest: Sankaran *et al.* (2005) show that if mean annual precipitation (MAP) is > 650 mm, then only disturbance (fire, herbivory, timber extraction) prevents canopy closure. This has been confirmed by the observation of rapid woody encroachment in long-term fire exclusion experiments in Ghana (Swaine *et al.* 1992), Burkina Faso (Menaut, 1977), and Ivory Coast (Vauttoux, 1976).

Assessing the dynamics of the rainforest-savanna boundary is important, as change will have large influences on people, ecosystems, and human populations. Changes in tree cover in the wide ecotone between rainforest and dry savannas in Africa depend on the relative strengths of many processes, the most important of which are: forest clearance for agriculture and pasture; forest degradation for timber and fuel; changes in fire frequency; and climate change (which includes increasing atmospheric CO_2 concentrations, increasing air temperature, and changes in precipitation, Malhi & Wright, 2004). Climate change excepted, increased human presence increases the first three of these, reducing the tree cover of an area, whereas reduced human impact will result in a reduction in these factors, and both an expansion of forest into savannas and a general increase in the woody cover of those savannas (Bucini & Hanan, 2007). The importance of fire frequency cannot be overstated here: almost all fires in African savannas are anthropogenic in origin, and given the ability of fires to spread widely from where they are set they have the potential to influence the vegetation across large areas, even far from human settlements (Favier *et al.*, 2004). The impact of anthropogenic climate change on

these ecosystems is still uncertain: although increasing temperatures are likely to reduce the competitiveness of trees over C4 grasses, increasing CO_2 concentrations do the reverse, reducing the advantage C4 grasses have over C3 trees (Lloyd & Farquhar, 2008). Increased atmospheric CO_2 concentrations have also been hypothesised to lead to increased success of trees in savannas due to a reduced transpiration rate leading to increased water percolation and reduced seedling mortality (Polley *et al.*, 2007), and by increasing the ability of saplings to re-sprout successfully following fire damage, thus making it more likely that they will escape the flame zone (Bond & Midgley, 2000). While it is appreciated that increased rainfall would over the long-term increase tree cover, provided the effect is not negated by increasing temperature (Hély *et al.*, 2006), significant uncertainties exist as to the long-term precipitation trends in the region (IPCC, 2007). These uncertainties are exacerbated because changes in vegetation in this sensitive region will result in strong feedbacks with climate (Zeng & Neelin, 2000).

There is a large body of evidence that woody encroachment (involving both trees and shrubs) into semi-arid savannas and grasslands is occurring (Archer *et al.*, 2000; Eamus & Palmer, 2007); Archer *et al.* (2000) found 28 studies showing increases in woody vegetation in Africa, and 202 studies finding such changes worldwide. There are fewer studies finding such an increase in tropical savannas, but some do exist. For example, in Northern Australia (Hopkins *et al.*, 1996; Bowman *et al.*, 2001; Russel-Smith *et al.*, 2004; Brook & Bowman, 2006), the Western Ghats of India (Puyravaud *et al.*, 2003), and South America (Duarte *et al.*, 2006; Durigan & Ratter, 2006; Marimon *et al.*, 2006; Roitman *et al.*, 2008). In Africa, just four studies showing increasing tree cover in tropical rainforest-savanna boundary regions have been reported. Boulvert (1990) drew on anecdotal evidence to suggest that woody expansion was occurring in the forest-savanna ecotones of central Africa due to the urbanization of the population, but provided little concrete evidence. Happi (1998) compared a high resolution aerial photograph from 1950 with Landsat TM data from 1990 to find gallery forest encroachment into surrounding savannas at a rate of 0.6 – 2 meters a year in central Cameroon. Guillet *et al.* (2001) used field studies and soil carbon isotopes ($^{13}C/^{12}C$, ^{14}C) along two transects in Eastern Cameroon to show both

significant expansion of the forest, and that increased woody cover of the savanna has occurred over the past century. Nangendo *et al.* (2005) used a combination of field studies and vegetation index based satellite change detection to find a 14 % increase in woody vegetation over a 14 year period in the woodlands of the Budongo Forest Reserve, Uganda. However, all the African studies are small in scale, and reliant on detailed local field data for success. As such, their methods are not easily applicable to a larger spatial scale, which is necessary to assess whether this forest encroachment is indeed widespread. No studies showing the opposite process (i.e. woody regression) were found for Africa apart from in areas where there has been an increase in anthropogenic activity, e.g. around cities and in areas of agricultural encroachment.

Mapping woody cover from remote sensing data can follow a wide range of different methods. Manual interpretation is best suited to hyperspatial satellite data and aerial photographs (Couteron *et al.*, 2001; Xiao & Moody, 2005), where the human brain can better recognise complex features and account for shadows than many automatic features. At a coarser resolution, classification-based methodologies can be effective (Sedano *et al.*, 2005; Su *et al.*, 2007). However the imposition of artificial classes can result in a tendency towards subjectivity, and lead to an overestimation of dominant classes and underestimation of rare classes (*e.g.* Couteron *et al.*, 2001). A classification-based approach was thought especially unsuitable for this study as deteting changes in woody cover within a class (e.g. 'woody savanna') is not possible. Empirical regressions between vegetation indices or red reflectance can be successful, often finding strong relationships (Leprieur *et al.*, 2000; Lu *et al.*, 2003; Ferreira *et al.*, 2004; Ferreira & Huete, 2004), though problems of soil reflectance (Chen *et al.*, 1998; Leprieur *et al.*, 2000), and the influence of the herbaceous vegetation (Fuller *et al.*, 1997; Qin & Gerstl, 2000), must be considered. More sophisticated techniques that can consider more bands (e.g. spectral mixture analysis or neural networks), or metrics that include image texture in addition to spectral information, are becoming increasingly accepted; they are however very sensitive to differing environmental conditions, sensor type and calibration, solar-target geometry, and atmospheric conditions, and as such are not appropriate for change

detection unless there is useable ground data for all dates (Coppin *et al.* 2004; Lu, 2004; Lu, 2006).

Numerous techniques have been developed for bi-temporal change detection, but they can be broadly classed into three categories: post-classification comparisons, image differencing/ratioing, and more sophisticated multi-band algorithms (such as change vector analysis or cross calibration analysis) (Coppin *et al.* 2004, Lu *et al.* 2004). Which methodology is chosen depends on the types of data being used, both remotely sensed and ground data, as well as the aims of the change detection. In general, when changes in clear categories of land-cover are being assessed, classification-based methodologies are appropriate; where the variable being assessed is relatively simple and different sensors or exact atmospheric correction is not possible, image differencing is preferred; and where identical sensors are used and atmospheric and field data are available, more sophisticated change algorithms may be appropriate, though in most cases they do not give superior results to image differencing-based methodologies (Coppin *et al.* 2004).

In this paper, we examine changes in woody cover in a large study area in central Cameroon. The Normalised Difference Vegetation Index (NDVI) derived from Landsat and ASTER remote sensing platforms is used in combination with field studies, coarse spatial resolution data (AVHRR), and very high spatial resolution satellite imagery (Quickbird) to identify and characterise, with great confidence, the changes in woody cover from 1986 to 2006. The methods presented here, due to their relative simplicity and the ready availability of historical NDVI data, allow the possibility of scaling up to a regional level using data at a coarser spatial resolution.

3.2 Study area

The study area is a 5 400 km^2 region in central Cameroon, centered around 6° 1' 22" N, 12° 48' 40" E, and encompasses the northern two-thirds of the Mbam Djerem National Park and the area to the north of the park, including the town of Tibati and lake Mbakauo. This region was chosen as it includes a complete range of regional vegetation types, from forest in the south contiguous with the Congo Basin rainforest

belt, through a forest-savanna matrix in the north of the park, to savanna with narrow gallery forests in the north of the study area (Figure 1). The area experiences an annual rainfall of 1650 mm, with a pronounced dry season (average 4 mm/month) from December to March (CRU TS 2.1 dataset, Mitchell & Jones, 2005, and TRMM 3B43 V6 satellite data, Kummerow *et al.*, 2001).

Figure 1

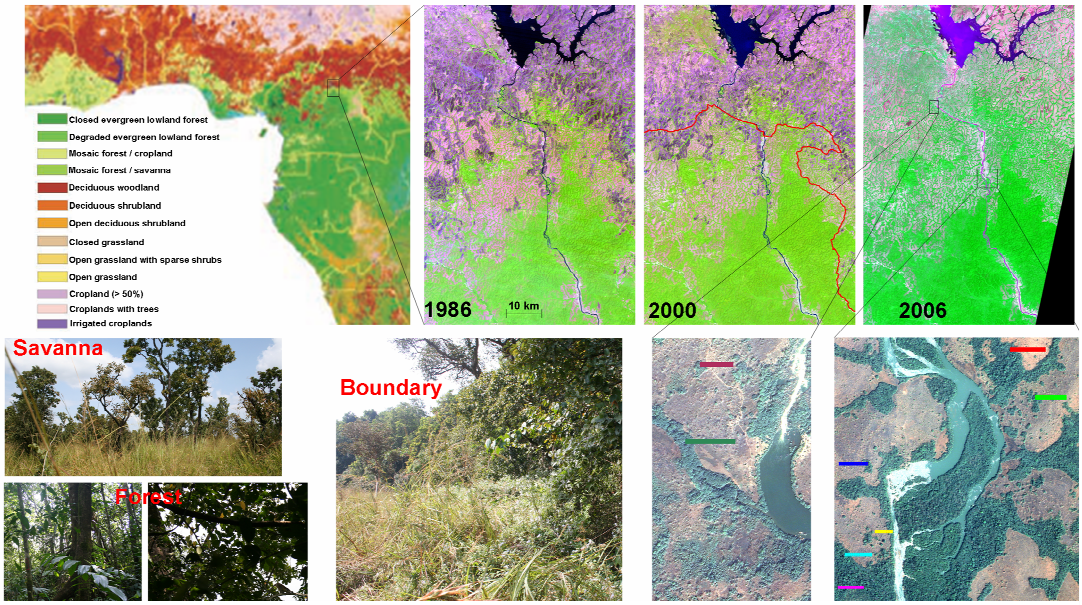

Top row: vegetation map taken from Mayaux *et al.* 2004, showing the location of the study area within Cameroon, with the three satellite images compared in this study: Landsat TM from 1986, Landsat ETM+ from 2000, and ASTER mosaic from 2006. The north and east borders of the Mbam Djerem National Park are shown in red on the 2000 image. Bottom row: pictures taken from the study area in 2007, showing typical forest and savanna biomes, as well as the sharp transition between the two; portions of Quickbird images showing the location of the eight transects where canopy cover was measured.

The human population of the southern part of the study area is very small, and has decreased over the study period due to the formation first of the Reserve de Faune de Pangar et Djerem in 1982, which encompasses 2 400 km^2, and then the Mbam Djerem National Park in 2000 which expanded this to 4 165 km^2. The population density in the northern half of the study area is higher than within the National Park, but still low, with the only major population centre being the town of Tibati, which has increased in population by almost 90 % over the study period, from 15 522 in the 1987 census to an estimated 28 981 by 2007 (CIESIN *et al.*, 2004). Small-scale agriculture occurs around settlements, and there is a limited amount of nomadic

cattle herding passing through the area; local people believe this has decreased significantly over the past 20-30 years. The other major local source of income is fishing (Anon, 2007).

3.3 Methods

3.3.1. Field data

The study area was visited October-December 2007 as part of the Tropical Biomes in Transition field campaign (TROBIT; www.geog.leeds.ac.uk/research/trobit). Eight transects 20 m wide and 100 – 200 m long were established, positioned in three different areas near the Djerem River in the north to middle of the Mbam Djerem National Park (Figure 1). Seven of these transects were in the transition from forest to savanna, with one entirely in forest. All trees with a diameter at 1.3 m (DBH) greater than 5 cm were measured for DBH, height, canopy dimensions (distance from trunk to outermost leaf measured for all four compass points) and identified to species. A total of 1009 trees, representing 79 species from 33 families, were measured (see Appendix 1A for species list). Each tree was located using a handheld differential GPS (Trimble GeoHX, Trimble, USA); these positions were later corrected using data from the SOPAC N'Koltang ground station in Libreville, Gabon, using the H-STAR differential correction facility in the software GPS Pathfinder Office 3.10 (Trimble, USA), resulting in accuracies of < 0.5 m in the horizontal direction and < 1 m in the vertical dimension. The transects were divided into 30 m sections, and the canopy dimensions used to calculate the vertically projected canopy area for each region of the transects (an elliptic canopy shape was assumed), which we have defined as the Canopy Area Index (CAI); this is similar to Plant Project Cover (Chapter 2, Section 2.1.1). We calculated CAI as m^2 canopy divided by m^2 ground area. The changes in species composition in the different portions of the eight transects are detailed in Appendix 1A.

3.3.2. Remote sensing data

A Landsat Thematic Mapper (TM) image captured on 30th December 1986 and a Landsat Enhanced Thematic Mapper Plus (ETM+) image captured on 12th December 2000, both for Path 156 Row 56, were downloaded from the Global Land Cover

Facility. Both were provided at a pixel size of 28.5 m. Two Advanced Spaceborne Thermal Emission and Reflection Radiometer (ASTER) scenes, between them covering almost the whole study area, captured 4th December 2006, were acquired from the NASA Land Processes Distributed Active Archive Center. Of the ASTER scene only the visible and near infrared bands were used in further analysis, which were provided at a 15 m pixel size. Two 0.6 m resolution Quickbird images were acquired from Eurimage covering all the field sites, by a combination of a 12 x 8 km archive image from 19th February 2004 covering the northern field sites, and a 10 x 10 km new acquisition, captured 23rd January 2008, covering the southern field sites.

To remove atmospheric effects from the TM, ETM+, and ASTER data, atmospheric correction was performed using ATCOR-2 (ReSe, Switzerland). This model used the post-launch offsets and gains and a tropical atmospheric model to produce reflectance images. The software package ENVI IDL (ITT, USA) was used for all subsequent remote sensing analysis. The two ASTER scenes were mosaicked together, and visual analysis of the join showed it to be seamless. No sharp changes in the reflectance values of any bands were apparent in 20 transects placed across the join of the two images, so no further correction of the individual scenes was considered necessary. This outcome was expected given that the scenes were captured with the same sensor within 10 seconds of each other.

The 60 x 90 km study area was subsetted from the 2000 ETM+ image, and the 1986 TM image was georeferenced to this using a network of 40 visually-selected ground control points taken from features such as road junctions, islands, small clumps of trees and branching points of gallery forests, with a resulting root mean square error (RMSE) of 0.37 pixels (10.5 m). Similarly the 2006 ASTER mosaic was georeferenced to the 2000 ETM+ image, with a network of 38 ground control points resulting in a RMSE of 0.35 pixels (10 m). The ASTER image was subsequently resampled to 28.5 m pixels using the pixel aggregate method.

Given the difficulties of calibrating images captured by different sensors under different, unknown, atmospheric conditions, it was decided to analyse the changes

using normalised univariate image differencing, implemented on cross-calibrated Vegetation Indices. Univariate image differencing essentially subtracts one date of imagery from another date, and is often chosen as the preferred change detection approach for tropical environments (Coppin *et al.*, 2004; Lu *et al.*, 2004), with Coppin *et al.* (2004) stating in their conclusions summary that 'image differencing and linear transformations appear to perform generally better than other bi-temporal change detection methods.' More sophisticated change detection techniques were thought to be unsuitable for this analysis, as the sensor used at each time point is different, and absolute atmospheric correction of the earlier scenes is not possible.

Using vegetation indices, which are in effect a ratio between two spectral bands, reduces the errors inherent in univariate change detection analyses because ratios between bands are affected to a smaller degree by different atmospheric conditions and different sensor characteristics than raw reflectance values (Coppin *et al.*, 2004; Pettorelli *et al.*, 2005). These indices are developed from the red and near infrared bands, and their response to vegetation cover is widely acknowledged (e.g. Huete *et al.*, 2002). The visible red wavelengths are absorbed by chlorophyll in vegetation and near infrared wavelengths are strongly reflected by the plant cuticle and cell wall, giving higher values for vegetation than for non-vegetated surfaces. As all three images were captured in the early dry season, when the grass layer is dead and dry, containing no chlorophyll, but leaves are still present on most trees, it is to be expected that the value of a vegetation index in a pixel will correspond directly to the CAI of that pixel (Fuller *et al.*, 1997; Qin & Gerstl, 2000, Archibold & Scholes, 2007). Vegetation indices have been shown to be strongly related to woody cover in savanna environments on a number of occasions (e.g. Lu *et al.*, 2003; Ferreira *et al.*, 2004; Ferreira & Huete, 2004). Typical problems with using these indices, such as topography and soil reflectance, were minimised in this study as the study area has little relief, and is insufficient in area to have much heterogeneity in the CAI to vegetation index relationship.

We investigated the use of three vegetation indices: the Normalised Difference Vegetation Index (NDVI), the Modified Soil Adjusted Vegetation Index (MSAVI)

(Qi *et al.*, 1994) and the Enhanced Vegetation Index (EVI) (Huete *et al.*, 1994). The EVI, though it appeared to be very sensitive to vegetation and as such was useful for comparing the two Landsat scenes, was abandoned because of the necessity of a blue band (450-515 nm), which is not present in ASTER data. MSAVI, designed to minimise the influence of soil reflectance, produced a small dynamic range for this ecosystem, and though it did differentiate forest from savanna well, it was less successful than the NDVI. NDVI was therefore the vegetation index chosen for all subsequent analysis. Its formula is:

$$NDVI = \frac{b_n - b_r}{b_n + b_r} \quad (1)$$

where b_n is the near-infrared band (750-900 nm), and b_r is the red band (630 – 690 nm).

Figure 2

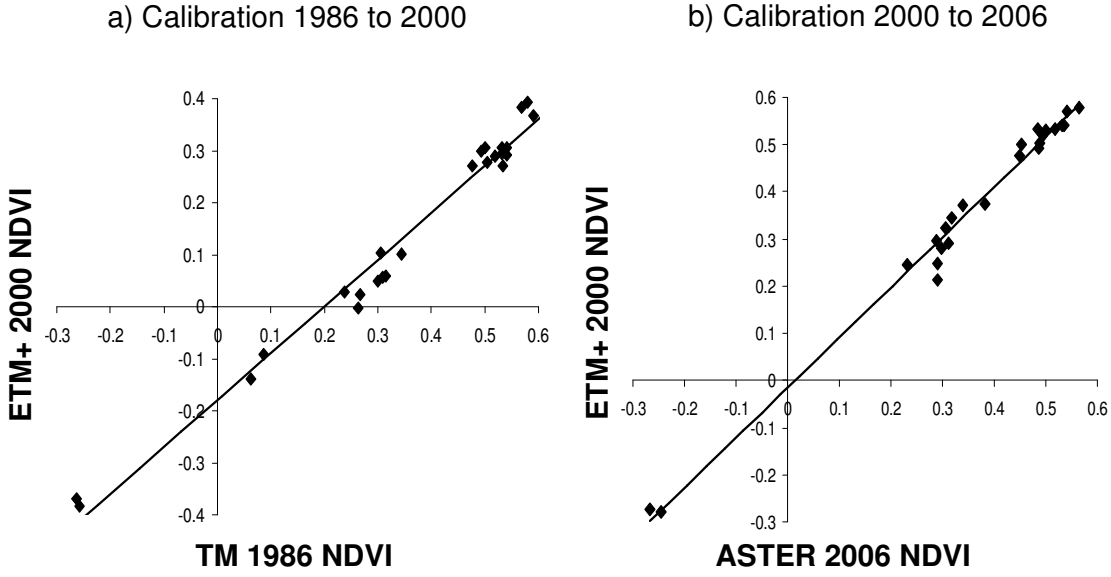

NDVI cross-calibration points, drawn from suspected unchanged areas such as water bodies, grasslands, and dense tropical forest, plotted for a) ETM+ 2000 against TM 1986, and b) ETM+ 2000 against ASTER 2006.

The NDVIs from the 1986 TM and 2006 ASTER images were then calibrated to the 2000 ETM+ image using linear regression models derived from 25 known invariant targets (i.e. their land cover type and appearance did not appear to change in any of the three images). These targets were drawn from water bodies, grasslands, and dense tropical forest (1986 to 2000, $NDVI_{adj} = -0.1804 + 0.9009(NDVI_{86})$, $r^2 = 0.98$; 2006 to 2000, $NDVI_{adj} = -0.0226 + 1.069(NDVI_{06})$, $r^2 = 0.98$, Figure 2). This process

should have removed most remaining calibration problems between the different sensors and atmospheres, and is as successful as absolute radiative correction (Songh *et al.*, 2001; Coppin *et al.* 2004), which is not possible here due to the lack of accurate atmospheric data for the 1986 image.

To test that the NDVI is correlated with woody cover, the NDVI values extracted from the ASTER 2006 pixels covering each 30 m section of the eight transects were regressed against the CAI measured *in situ*. A different georeferencing was used here, involving two 10 x 10 km sections taken from the 15 m adjusted-NDVI ASTER image, and performing a very detailed tie-point matching process with the ground control point corrected Quickbird data (which is estimated to be geocorrected to < 2 m). RMSE values were always less than 0.3 ASTER pixels (< 4.5 m), based on at least 50 tie-points, giving high confidence that the NDVI values extracted correspond to the portions of the transects measured on the ground.

To examine whether precipitation was similar during November-December 1986, 2000 and 2006, a combination of weather station and modeling-derived CRU TS 2.1 dataset, (1901-2002, Mitchell & Jones 2005) and the Tropical Rainfall Measuring Mission (TRMM) TRMM Microwave Imager (TMI) 3B43 V6 satellite data (1998-2007, Kummerow *et al.*, 2001) were used to estimate the rainfall in these months. The monthly precipitation data at a 0.5° resolution was used in both cases, making these two data sources readily comparable. These datasets were also analysed for long-term rainfall and temperature trends over the study area (1901-2007).

To confirm trends observed at individual time slices are representative of a genuine trend and not merely caused by problems with calibration or different environmental conditions, NDVI values from the GIMMS AVHRR 8-km dataset (Pinzon *et al.* 2005, Tucker *et al.* 2005) were extracted over the study area. These data were examined for trends in the annual average NDVI, as well as the annual average NDVIs for the dry and wet seasons.

As fire frequency is considered an important factor in controlling woody cover, an estimate of the changes in fire frequency over the study area was also desirable. No data of sufficient sensitivity exists for the whole study period (AVHRR fire data detected just six hotspots in the study area from 1986 – 2006), so data were acquired from the ATSR-2 and AATSR World Fire Atlas from 1996 to 2006. Fires detected from within the study area were extracted, and the number of fires counted for each year. This thermal anomaly dataset is known to be accurate, having very good geolocation and low commission errors (Arino *et al.*, 2005; George *et al.*, 2006), but it is also acknowledged that it underestimates the total fire number, due both to a lack of sensitivity to low intensity fires, and the night-time detection missing day-time fires. However, this is not of concern here, as we are interested in the trend in fire frequency, not the absolute rate of fire occurrence.

3.3.3. Change detection

Image comparisons were performed between 1986 and 2000, and 2000 and 2006. However, before any comparisons, water bodies and urban areas were masked from all images by excluding any pixels with a negative NDVI. A proportion of savanna areas were identified as burn scars (due to a characteristic blue/purple colour on 5-4-3 composite images, on areas where were green in the other images), and found to have an NDVI between 0.05 and 0.16. Leaving these areas in the analysis with their raw NDVI values would bias the analysis, as the same area changing from burnt grassland to unburnt grassland would appear to have increased in woody cover, whereas, in fact, no change would have occurred. Rather than exclude these areas from the analysis, which would reduce the area available to detect changes, the value of all unmasked pixels with an NDVI < 0.2 was adjusted to 0.2. This in effect converted all the burnt areas in the images to areas with the same NDVI as savanna with a CAI of 0 – 0.2 m^2/m^2, as it is assumed that areas that burn in this way, early in the dry season, will have a low CAI (Lambin *et al.*, 2003; Felderhof & Gillieson, 2006). The validity of this procedure was confirmed by the observation that the majority of burnt patches in the 1986 image have similar NDVI values to their surrounding, unburnt, areas after this procedure is applied. In order to confirm that this procedure is not driving the observed results, an identical analysis was

performed without this process, instead using a supervised classification to remove all the burnt areas (see Appendix 1B).

Rather than comparing the simple differences in NDVI between the various time points (as recommended by Singh (1989) and used by for example Nangendo *et al.* (2005)), the changes by comparing the difference ratioed by the sum of the pixels, as this further increases confidence in the results of vegetation index differencing change detection (Coppin *et al.* 2004). This is because difference values of the same absolute magnitude vary in significance depending on the size of the original NDVI values: an increase from 0.25 to 0.35 is much more significant than an increase from 0.45 to 0.55 (Figure 3), but a simple differencing method will predict the same magnitude of change for both.

Figure 3

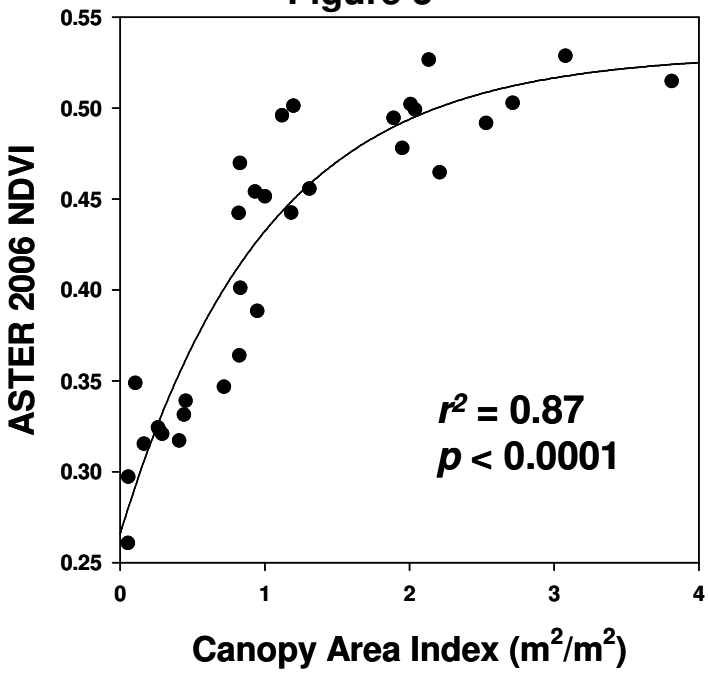

Adjusted ASTER 2006 NDVI regressed against field-measured Canopy Area Index (CAI) (m^2 canopy per m^2 area) for 30 m sections of field transects.

The formula used for the change detection was therefore:

$$Change = \frac{NDVI_{new} - NDVI_{old}}{NDVI_{new} + NDVI_{old}} \quad (2)$$

This produces change images, with every pixel having a value from -1 to +1, where zero indicates no change, positive values positive change (i.e. an increase in woody cover), and negative values negative change (i.e. a decrease in woody cover). The

resulting distribution of points was tested for normality using a Shapiro-Wilk normality test, and then the standard deviation of the distribution calculated, allowing an assessment of how much of a deviation from zero indicates a significant change in woody cover. The pixels were therefore grouped into classes according to the number of standard deviations each pixel deviated from zero, with < ±1 standard deviation considered no change, > ±1 standard deviation considered marginally significant change, and > ±2 standard deviations considered significant change at approximately the 95 % confidence level.

By using the relationship between the *in situ* measured CAI and ASTER NDVI, absolute changes in the extent of woody cover over the study area were quantified. The relationship between NDVI and projected CAI was applied to the NDVI image in each of the three time points, and the ground area in five cover-classes quantified (water bodies, urban areas, and areas not present in the 2006 mosaic were not included).

3.4 Results

3.4.1. Sensitivity of NDVI to CAI

NDVI is shown to be strongly correlated with field-measured CAI in this environment ($r^2 = 0.87$, $p < 0.0001$, $n = 32$, Figure 3). CAI is directly proportional to the density and size of trees per unit area, and believed therefore to be a good measure of woody cover. The fitted line is:

$$NDVI = 0.27 + 0.26(1 - e^{-CAI}) \quad (3)$$

Which can be rearranged to:

$$CAI = -\ln\left(\frac{0.53 - NDVI}{0.26}\right) \quad (4)$$

Sensitivity decreases rapidly above a CAI of 2 m^2/m^2, but NDVI is undoubtedly a very good metric for detecting changes in the woodiness of savannas and the position of the rainforest-savanna boundary, giving confidence that the change detection shown below relates to genuine changes in woody vegetation.

3.4.2. Change detection

Both normalised image differencing analyses produced normal distributions centered on 0, with a positive skew, suggesting respectively that the cross-calibration process was effective, and that increases in NDVI were observed (Figure 4).

Figure 4

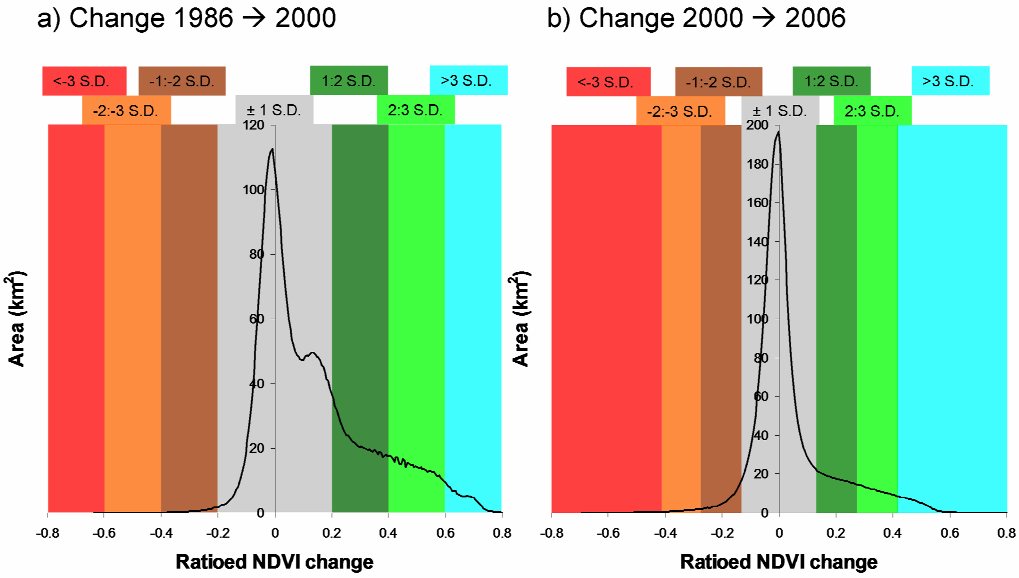

Adjusted ASTER 2006 NDVI regressed against field-measured Canopy Area Index (CAI) (m^2/m^2) for 30 m sections of field transects.

When thresholded according to standard deviations, very significant increases in NDVI over savanna regions are found both between 1986 and 2000, and 2000 and 2006, as displayed in Figure 5 and Table 1. 12.6 % of the study area showed a significant positive increase in NDVI (>2 standard deviations, approximately equivalent to a 95 % confidence level) from 1986 to 2000, and 7.8 % from 2000 to 2006. There is evidence from this that the rate of woody encroachment has risen over the 20 year period, as the percentage increase divided by the number of years of comparison is 0.9 % yr^{-1} from 1986 to 2000, but 1.3 % yr^{-1} from 2000 to 2006. In contrast, the number of pixels showing significant negative trends is negligible in both comparisons.

Figure 5

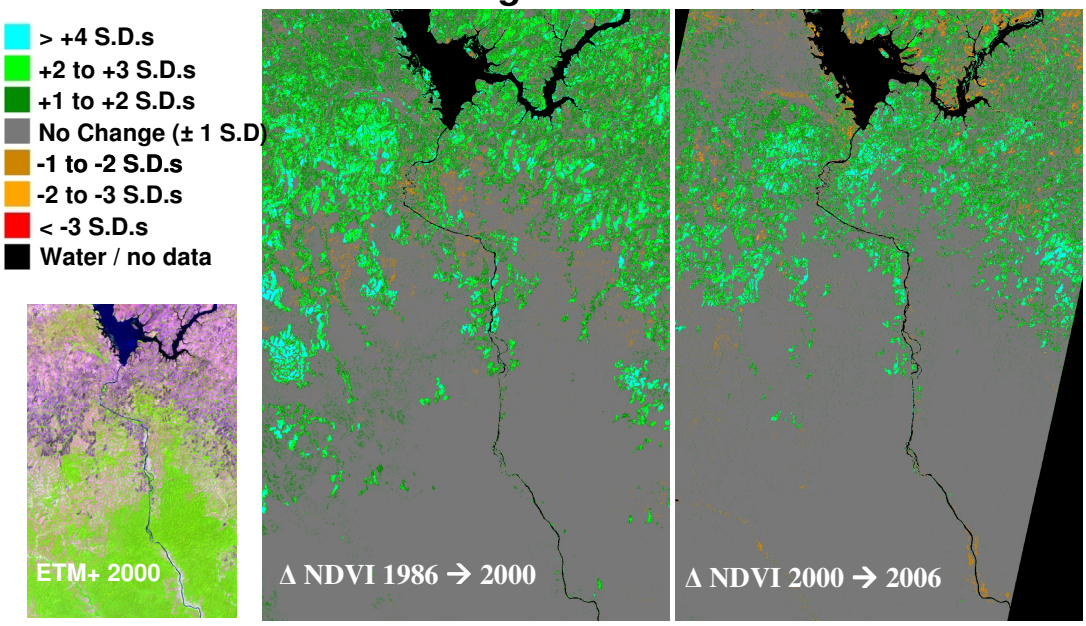

Two images showing the change in NDVI between 1986 and 2000, and 2000 to 2006, in standard deviations (see text). Changes > ±2 standard deviations should be considered significant at the 95 % level. The 5-4-3 composite image from 2000 is also included to show that the increases in NDVI occurred in the savannas, consistent with an increase in woody vegetation.

Applying Equation 4 to the NDVI images allowed an assessment of how the area covered by each vegetation type has changed over the study period (Figure 6). While less sensitive than the change detection analysis, due to inaccuracies in the CAI – NDVI relationship and the necessity to categorise the vegetation into distinct classes, this analysis is useful in that it can quantify which cover classes experienced the most rapid change. The largest changes occur in the low CAI classes, with the area of grassland (CAI < 0.2 m^2) decreasing by 43 % over the twenty years, from 2132 km^2 in 1986 to 1214 km^2 in 2006. All the other classes increase over the study period, with the largest increase in the 0.2-0.4 m^2/m^2 CAI class, and the smallest in the > 1 m^2/m^2 CAI class.

Table 1

Class	1986-2000		2000-2006	
	%	Area (km^2)	%	Area (km^2)
Significant positive change (>+2 S.D.s)	**12.57**	**679.2**	**7.76**	**419.1**
Marginally significant positive change (>1 S.D.s)	12.46	673	8.02	433
No change (-1 to +1 S.D.s)	70.28	3795.1	73.35	3960.7
Marginally significant negative change (<-1 S.D.s)	1.32	71.2	1.68	90.7
Significant negative change (<-2 S.D.s)	**0.08**	**4.3**	**0.38**	**20.4**
Masked (water/urban areas/areas not present in 2006 mosaic)	3.28	177.1	8.82	476.0
% Significant positive change per year	***0.9 % yr^{-1}***		***1.29 % yr^{-1}***	

Percentage and area of change images falling into each change class in the two comparisons, TM 1986 with ETM+ 2000, and ETM+ 2000 with ASTER 2006. The percentage significant positive change divided by the number of years of comparison is also included.

Figure 6

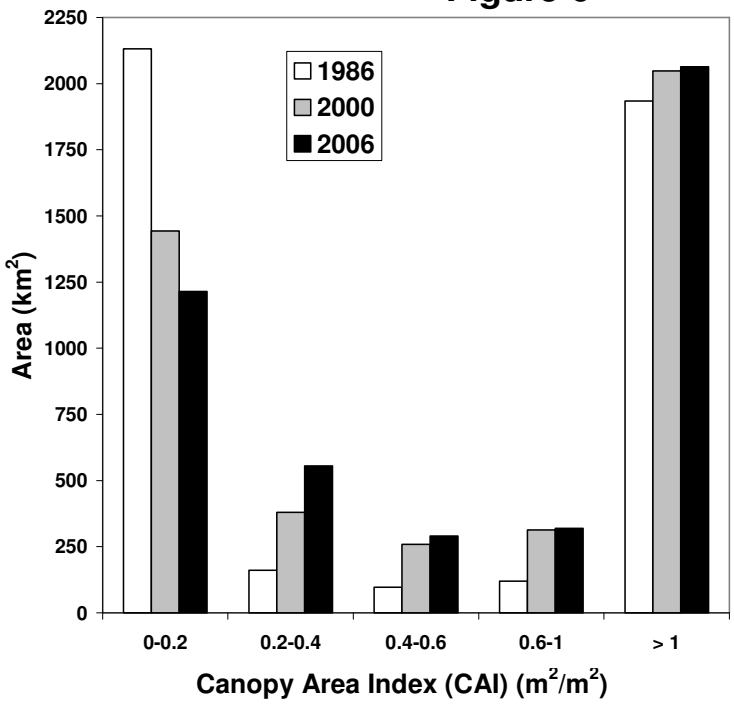

Changes in the total area of vegetation found in different canopy projected cover classes in 1986, 2000, and 2006.

Similar trends were found in the analysis where burnt areas where removed prior to the change analysis (see Appendix 1A). The trends found were approximately half the magnitude of the changes above, as would be expected given the large areas of savanna that were removed. However this provides evidence that the above results are not an artifact of the thresholding methodology used to enable to inclusion of burnt areas.

3.4.3. High temporal resolution NDVI record

Figure 7

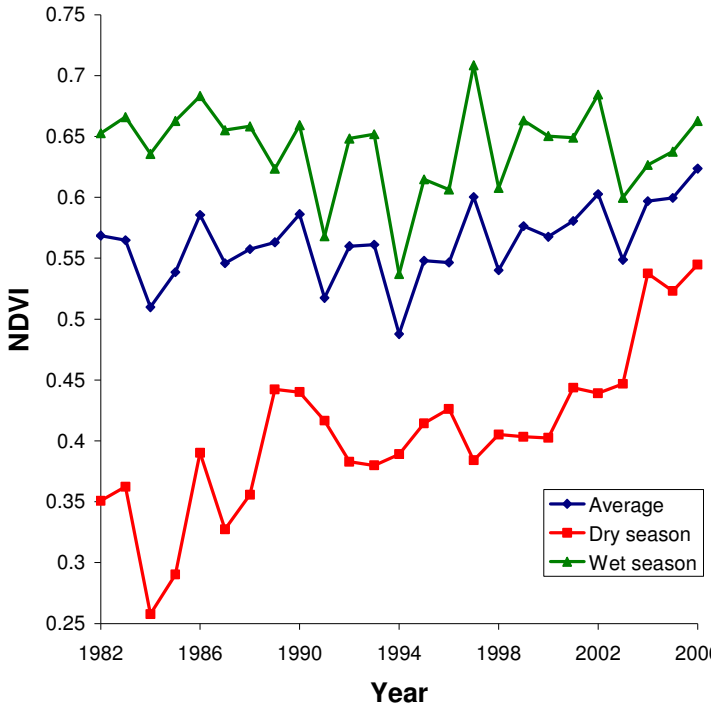

Trends in AVHRR average NDVI for the study area, derived from GIMMS data (Pinzon *et al.* 2005, Tucker *et al.* 2005). Red points show the average dry season NDVI (December to March), green points the average wet season NDVI (April to November), and blue the annual average NDVI.

The AVHRR GIMMS NDVI record shows no significant trend in the annual average nor the wet season average from 1982 to 2006. However there is a very clear increasing trend in the dry season NDVI (Figure 7), showing that the trends found in the high spatial but low temporal resolution dry-season analysis are part of a larger trend.

3.4.4. Rainfall, temperature, and fire frequency

No significant long term trends were found in the rainfall or temperature data for the study site. Average annual temperature fluctuated from just 22.5 to 23.6 degrees

Celsius, with no obvious trends, and while annual rainfall was more variable, most of the variation was due to fluctuations in the wettest months, and still no trends were apparent (Figure 8).

Figure 8

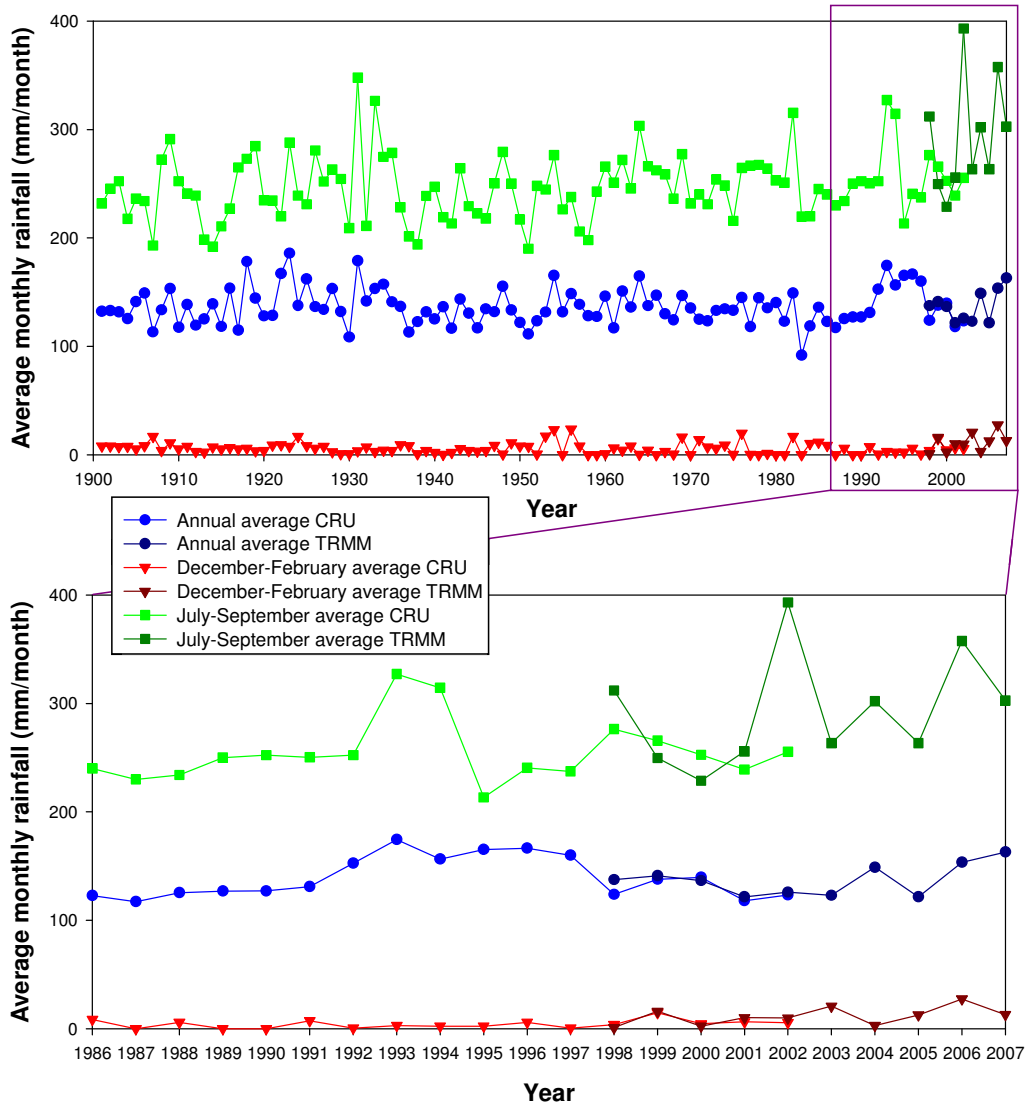

Trends in AVHRR average NDVI for the study area, derived from GIMMS data (Pinzon *et al.* 2005, Tucker *et al.* 2005). Red points show the average dry season NDVI (December to March), green points the average wet season NDVI (April to November), and blue the annual average NDVI.

For the above remote sensing-based change detection to be valid, it is essential that precipitation in the months preceding the image capture are identical, otherwise the results could be due to changes in the greenness of the vegetation (especially grasses), not due to changes in CAI. A comparison was made of precipitation in the month of image capture, three months before image capture, and six months before

image capture; no differences are apparent between years in the month of image capture nor the average of the previous three months (Figure 9). However there does appear to have been greater average rainfall in 2006 than in the other two years when the 6 month average is compared. This should not interfere with the results as the grass layer should still have been dead in 2006. However, it should be considered when interpreting the results of the second period of change detection.

Figure 9

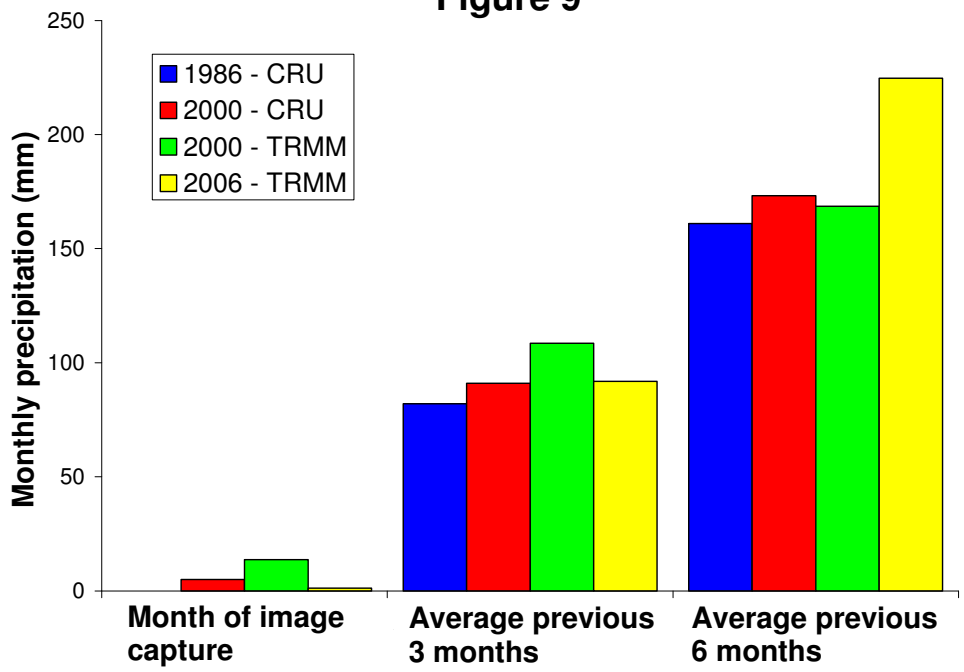

Trends in AVHRR average NDVI for the study area, derived from GIMMS data (Pinzon *et al.* 2005, Tucker *et al.* 2005). Red points show the average dry season NDVI (December to March), green points the average wet season NDVI (April to November), and blue the annual average NDVI.

Analysis of the ATSR-2 and AATSR data provides some evidence that fire occurrence in the study area decreased over the second half of the study period (from 1996 to present); unfortunately there are no suitable data for the first half, as AVHRR data has too coarse a resolution and is not sufficiently sensitive to detect these small-scale fires. Figure 10 displays the result, with linear regression finding a significant negative trend in fire frequency against time (gradient = -1.08 fires yr^{-1}, $r^2 = 0.57$, $p < 0.01$, $n = 11$).

Figure 10

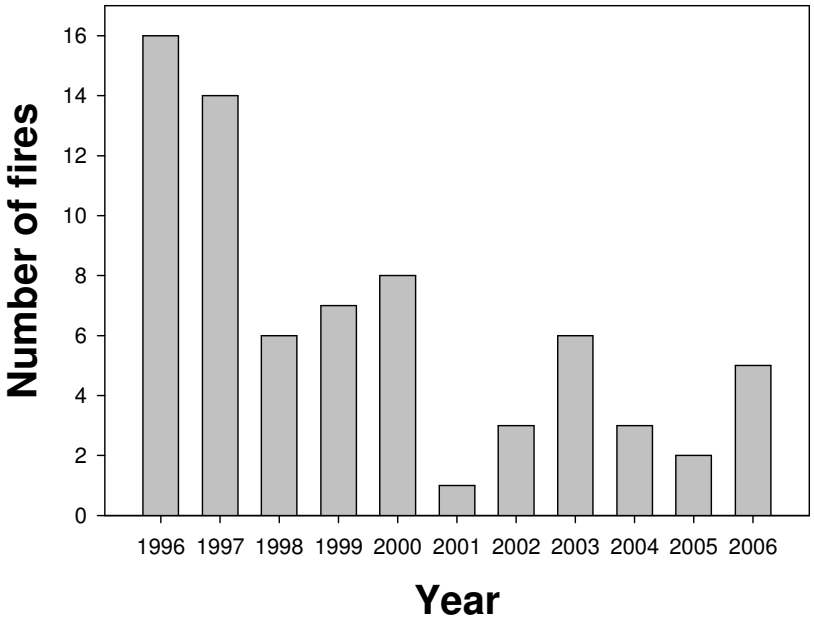

Annual fire count for the study area from 1996 to 2006 derived from ATSR-2 and AATSR World Fire Atlas, using the more sensitive algorithm 2.

3.5. Discussion

3.5.1. Woody encroachment

Woody encroachment is occurring rapidly in the Mbam Djerem National Park, corroborating smaller-scale (40 – 600 km^2) studies showing woody expansion in the forest-savanna ecotones of Africa. This also confirms observations within the study area in Nov 2007, where forest edges were dominated by young pioneer trees, with dead and dying savanna trees prevalent, strong evidence that this constituted young encroaching forests (*pers. obs.* ETAM & SLL; and also the presence of savanna trees in the forest sections of all transects, see Appendix 1A.) When looking at the change maps, it is possible to see changes along some gallery forests, suggesting they have increased in width. However, the resolution of the comparisons, 28.5 m, means that even relatively rapid increases in the size of forests are unlikely to be detected by this method: the forest advance rate of 2 m yr^{-1} found in a nearby region by Happi (1998)

would equate to a movement of 28 m (one pixel) in the 1986 – 2000 comparison, and 12 m (under half a pixel) in the 2000 – 2006 comparison, both of which could be missed due to slight inaccuracies in the georeferencing. The majority of the increases detected are thus an increase in the woodiness of the savannas, rather than an increase in forest area, as can be seen in Figure 6. We note that though we are confident the changes we observe genuinely represent an increase in woody cover, the lack of historical field data and local rainfall data results in us not being able to reject the possibility that some or all of these changes are artifacts caused by increases in dry-season rainfall causing greener grasses. We believe the data presented in Figures 7, 8 and 9 show that this is unlikely to be the case, but without historical field data we cannot be entirely certain, especially for the second period of change detection (2000 – 2006), where though the rainfall for the preceding 3 months is similar to that in the other two years, the preceding wet season had higher rainfall (though it is possible this could be an artifact of using TRMM data, which appears to produce much more variable results in the wet season than the CRU 2.1 dataset, Figure 8).

While the legal formation of the Mbam Djerem National Park is responsible for some of this gain, slightly over half of the significant positive change in both comparisons occurred outside the park. The likely cause of these changes are hard to determine with confidence, but local people considered the changes due to reductions in human population density, caused by urbanization, resulting in decreased burning of the savannas and thus an increase in the number and size of trees (*pers. obs.* ETAM & SLL). They also observe that nomadic cattle herding has moved to other more profitable areas, so burning to produce a flush of grass for cattle is also less widespread. The establishment of the Chad-Cameroon Petroleum Development and Pipeline Project by the World Bank in 2000 may also be an important factor. This project brought the prospect of jobs and consequently caused a shift in the labour force from the mid 1990s (Guyer, 2002). The Mbam Djerem National Park also owes its creation in 2000 to this project, which was initially funded by the World Bank with the aim of offsetting some of the environmental damage caused by the project. There is a low-frequency trend distinguishable in the increase in dry season GIMMS

NDVI data (Figure 7), with rapid increases in the 1980s and 2000s, but a stagnation in the 1990s. The increase from 2000 is easy to explain as it coincides both with the creation of the Mbam Djerem National Park and the Chad-Cameroon Pipeline, as discussed above. The change in the 1980s may be concurrent with urbanization and a reduction in cattle herding, though it is harder to explain why this increase disappears in the 1990s without better local demographic data.

Our analysis of the ATSR-2/AATSR World Fire Map data for the study area from 1996 – 2006 goes some way towards confirming the reduction in fire activity in the area, putitively caused by a reduction in human impact. Although this satellite sensor is not able to detect low-intensity fires, which represent the majority of fires in the study area, the data are unbiased and as such general trends are thought likely to correspond to genuine changes in fire frequency in an area (Arino *et al.*, 2005). The approximate halving in fire frequency over a ten year period we see here therefore provides some evidence that a reduction in fire frequency has occurred. Unfortunately it is impossible to know what the fire frequency was in the mid 1980s over this area as the only satellite data available is not sensitive enough to detect the small-scale fires typical of this ecosystem, but we hypothesise that it was considerably higher than present.

There are no reliable population data available at a sufficient resolution to ascertain whether population levels have genuinely fallen in the study area over the time period considered here. Data for the whole of Cameroon show that, while the urban population has risen at an average 4.44 % per year from 1986 – 2006, rural population has only increased by only 0.69 % per year over the same period (World Bank, 2007). It is therefore possible that the rural population could have fallen in this small area, as local people suggest, especially given that the population density is already very low (excluding the towns of Tibati and Yoko, the Global Rural-Urban Mapping Project estimates the population density of the area to be just 2 people per km^2, CIESIN *et al.*, 2004).

Analysis of the rainfall and temperature data suggests that this woody encroachment is not environmentally driven. However, it is possible that part of the increase could be due to slight increases in average rainfall. In particular the years 1992 – 1997 stand out as six consecutive years where the average annual rainfall is consistently above the long-term average (Figure 8). There is no increase in the average dry season rainfall period however, where an increase in rainfall would be most likely to influence the survival of woody vegetation both through reduced water stress and a reduction in fire intensity and area (Hély *et al.*, 2006), and equally this increase in precipitation occurs in a period where no increase in dry season NDVI is detected in the coarse resolution GIMMS dataset (Figure 7). It has also been suggested that while rainfall may not have increased, there is evidence of a global reduction in pan evaporation, putatively caused by decreased wind speed and decreased receipt of solar radiation, due to increased cloud cover and atmospheric aerosol content (Eamus & Palmer, 2007). Such a reduction would have the same effect as an increase in rainfall, increasing soil moisture, which in combination with the potential reduction in stomatal conductance caused by an increase in the CO_2 concentration (Lloyd & Farquhar, 2008) could explain woody encroachment. Though Eamus & Palmer's (2007) model is more suited to arid and semi-arid systems than the more mesic environment studied here, the intense dry season makes this a possible causal factor.

3.5.2. Potential of methodology

The finding that NDVI is very well correlated with CAI in forest-savanna ecotones opens a realm of possibilities for change detection and monitoring of tropical woody vegetation. NDVI can be calculated from numerous sensors at a full range of resolutions, and is easily available in products such as the GIMMS AVHRR data, which has global coverage at an 8 km resolution from 1982 to present. In this study the trend of increasing CAI detected at a high resolution is clearly matched by an increase in NDVI in the dry season GIMMS dataset. This provides potential for using dry season coarse resolution NDVI data to examine changes both at a continental scale (*e.g.* using AVHRR or MODIS), in order to assess large scale changes in woody vegetation, and at a more localised scale (*e.g.* using Landsat and ASTER), for example to monitor the success of avoided deforestation or carbon

sequestration forestry projects. However, heterogeneity of climate and soil may introduce difficulties when using this methodology at a larger scale, though these could potentially be overcome with high-quality and extensive ground data; and potentially further reduced by analysis of the annual NDVI cycle made possible by the daily revisits of coarser resolution satellite sensors. Such data must always be analysed with reference to a precipitation dataset.

3.6 Acknowledgements

Two anonymous reviewers provided helpful and detailed comments on an earlier draft of the manuscript. Jon Lloyd, TROBIT P.I., provided useful advice and expertise. Jeanette Sonké, Wildlife Conservation Society-Cameroon (WCS-Cameroon), The University of Yaounde I, and 14 canoeists from Mbakaou provided invaluable support in Cameroon. Adam Freedman provided useful advice on the sources of accurate population data, and Thijs vanden Bergh helped collate the fire data. Remote sensing data was provided by the USGS Global Landcover Facility (Landsat and ASTER), Eurimage (Quickbird), ESA ATSR World Fire Atlas (ATSR-2/AATSR hotspot data), and the NASA Giovanni Rainfall Archive (TRMM rainfall data). The CRU TS 2.1 dataset was downloaded from the University of East Anglia's Climate Research Unit at www.cru.uea.ac.uk/~timm/grid/CRU_TS_2_1 .html.

3.7 References

Anon (2007) *Park National du Mbam et Djerem, Plan d'Aménagement 2007-2011*, Le Ministère des Forêts et de la Faune, Cameroun.

Archer, S., Boutton, T.W. & Hibbard, K.A. (2001) Trees in grasslands: biogeochemical consequences of woody plant expansion. *Global biogeochemical cycles in the climate system* (ed. by Schulze, E.-D., Harrison, S., Heimann, M., Holland, E., Lloyd, J., Prentice, I. & Schimel, D.), pp. 115-133. Academic Press, San Diego.

Archibold, S., & Scholes, R.J. (2007) Leaf green-up in a semi-arid African savanna – separating tree and grass responses to environmental cues. *Journal of Vegetation Science*, 18, 583-594.

Arino, O., S. Plummer & Defrenne, D. (2005) Fire disturbance: the ten years time series of the ATSR world fire atlas. *Proceedings of the MERIS-AATSR workshop 2005*, Frascati, Italy.

Bond, W.J. & Midgley, G.F. (2000) A proposed CO_2-controlled mechanism of woody plant invasion in grasslands and savannas. *Global Change Biology,* 6, 865-869.

Boulvert, Y. (1990) Avancée ou recul de la forêt centroafricaine. Changements climatiques, influence de l'homme et notamment de feux. *Paysages Quaternaries de l'Afrique Central Atlantique* (ed. by Lanfranchi, R. & Schwartz, D.), pp. 353-366. Initiations et Didactiques ORSTROM, Paris.

Bowman, D.M.J.S., Walsh, A. & Milne, D.J. (2001) Forest expansion and grassland contraction within a Eucalyptus savanna matrix between 1941 and 1994 at Litchfield National Park in the Australian monsoon tropics. *Global Ecology and Biogeography,* 10, 535-548.

Brook, B.W. & Bowman, D. (2006) Postcards from the past: charting the landscape-scale conversion of tropical Australian savanna to closed forest during the 20th century. *Landscape Ecology*, 21, 1253-66.

Bucini, G. & Hanan, N.P. (2007) A continental-scale analysis of tree cover in African savannas. *Global Ecology and Biogeography,* 16, 593-605.

Center for International Earth Science Information Network (CIESIN), Columbia University; International Food Policy Research Institute (IPFRI); the World Bank; and Centro Internacional de Agricultura Tropical (CIAT). (2004) Global Rural-Urban Mapping Project (GRUMP): Urban/Rural Population grids. Downloaded from http://sedac.ciesin.columbia.edu/gpw/

Chen, Z., Elvidge, C.D. & Groeneveld, D.P. (1998) Monitoring Seasonal Dynamics of Arid Land Vegetation Using AVIRIS Data. *Remote Sensing of Environment,* 65, 255-266.

Coppin, P., Jonckheere, I., Nackaerts, K., Mys, B., & Lambin, E. (2004) Digital change detection methods in ecosystem monitoring: a review. *International Journal of Remote Sensing,* 25, 1565-1569.

Couteron, P., Deshayes, M. & Roches, C. (2001) A flexible approach for woody cover assessment from SPOT HRV XS data in semi-arid West Africa. Application in northern Burkina Faso. *International Journal of Remote Sensing,* 22, 1029-1051.

Duarte, L.D.S., Machado, R.E., Hartz, S.M. & Pillar, V.D. (2006) What saplings can tell us about forest expansion over natural grasslands. *Journal of Vegetation Science,* 17, 799-808.

Durigan, G. & Ratter, J.A. (2006) Successional changes in cerrado and cerrado/forest ecotonal vegetation in western Sao Paulo State, Brazil, 1962 - 2000. *Edinburgh Journal of Botany*, 63, 119-130.

Eamus, D., & Palmer, A.R. (2007) Is climate change a possible explanation for woody thickening in arid and semi-arid regions? *Research Letters in Ecology,* Volume 2007, Article ID 37364.

Favier, C., Chave, J., Fabing, A., Schwartz, D., & Dubois, M.A. (2004) Modelling forest-savanna mosaic dynamics in man-influenced environments: effects of fire, climate and soil heterogeneity. *Ecological Modelling,* 171, 85-102

Felderhof, L., & Gillieson, D. (2006) Comparison of fire patterns and fire frequency in two tropical savanna bioregions. *Austral Ecology,* 31, 736-746.

Ferreira, L.G., & Huete, A.R. (2004) Assessing the seasonal dynamics of the Brazilian Cerrado vegetation through the use of spectral vegetation indices. *International Journal of Remote Sensing,* 25, 1837-1860.

Ferreira, L.G., Yoshioka, H., Huete, A., & Sano, E.E. (2004) Optical characterization of the Brazilian Savanna phyiognomies for improved land cover monitoring of the cerrado biome: preliminary assessments from an airborne campaign over an LBA core site. *Journal of Arid Environments,* 56, 425-447.

Fuller, D. O., Prince, S. D. & Astle, W. L. (1997) The influence of canopy strata on remotely sensed observations of savanna-woodlands. *International Journal of Remote Sensing,* 18, 2985-3009.

George, C., Rowland, C., Gerard, F., & Balzter, H. (2006) Retrospective mapping of burnt areas in Central Siberia using a modification of the normalised difference water index. *Remote Sensing of Environment,* 104, 346-359.

Guillet, B., Achoundong, G., Happi, J.Y., Beyala, V.K.K., Bonvallot, J., Riera, B., Mariotti, A., & Schwartz, D. (2001) Agreement between floristic and soil organic carbon isotope ($^{13}C/^{12}C$, ^{14}C)

indicators of forest invasion of savannas during the last century in Cameroon. *Journal of Tropical Ecology,* 17, 809-832.

Guyer, J.I. (2002) Briefing: The Chad-Cameroon petroleum and pipeline development project. *African Affairs,* 101, 109-115.

Happi, J.Y. (1998) *Arbres contre graminees: la lenta invasion de la savane par la foret au center-Cameroun*. Doctoral thesis, Université de Paris Sorbonne.

Hély, C., Bremond, L., Alleaume, S., Smith, B., Sykes, M.T. & Guiot, J. (2006) Sensitivity of African biomes to changes in precipitation regime. *Global Ecology and Biogeography,* 15, 258-70.

Hopkins, M.S., Head, J., Ash, J.E., Hewett, R.K., & Graham, A.W. (1996) Evidence of a Holocene and continuing recent expansion of lowland rain forest in humid, tropical North Queensland. *Journal of Biogeography,* 6, 737-745.

Hostert, P., Roder, A. & Hill, J. (2003) Coupling spectral unmixing and trend analysis for monitoring of long-term vegetation dynamics in Mediterranean rangelands. *Remote Sensing of Environment,* 87, 183-197.

Huete, A., Justice, C., & Liu, H. (1994) Development of vegetation and soil indices for MODIS EOS. *Remote Sensing of Environment,* 49, 224–234.

Huete, A., Didan, K., Miura, T., Rodriguez, E. P., Gao, X., & Ferreira, L. G. (2002) Overview of the radiometric and biophysical performance of the MODIS vegetation indices. *Remote Sensing of Environment,* 83, 195-213.

IPCC. (2007) *Climate Change 2007: Synthesis Report. Contribution of Working Groups I, II and III to the Fourth Assessment Report of the Intergovernmental Panel on Climate Change* (ed. by Core Writing Team, Pachauri, R.K and Reisinger, A.) IPCC, Geneva, Switzerland.

Kummerow, C., Hong, Y., Olson, W.S., Adler, R.F., McCollum, J., Ferraro, R., Petty, G., Shin, B.-B., & Wilheit, T.T. (2001) The evolution of the Goddard profiling algorithm (GPROF) for rainfall estimation from passive microwave sensors. *Journal of Applied Metrology,* 39, 1801–1820.

Lambin, E.F., Goyvaerts, K., & Petit, C. (2003) Remotely-sensed indicators of burning efficiency of savannah and forest fires. *International Journal of Remote Sensing,* 24, 3105–3118.

Leprieur, C., Kerr, Y. H., Mastorchio, S. & Meunier, J. C. (2000) Monitoring vegetation cover across semi-arid regions: comparison of remote observations from various scales. *International Journal of Remote Sensing,* 21, 281 - 300.

Lloyd, J. & Farquhar, G.D. (2008) Effects of rising temperatures and [CO_2] on the physiology of tropical forest trees. *Philosophical Transactions of the Royal Society of London B,* 363, 1811-1817.

Lu, H., Raupach, M. R., McVicar, T. R. & Barrett, D. J. (2003) Decomposition of vegetation cover into woody and herbaceous components using AVHRR NDVI time series. *Remote Sensing of Environment,* 86, 1-18.

Lu, D., Mausel, P., Brondizio, E., & Moran, E. (2004) Change detection techniques. *International Journal of Remote Sensing,* 25, 2365-2401.

Lu, D. (2006) The potential and challenge of remote sensing-based biomass estimation, *International Journal of Remote Sensing*, 27, 1297-1328.

Maley, J. (1996) The African rain-forest – main characteristics of changes in vegetation and climate from the Upper Cretaceous to the Quaternary. *Proceedings of the Royal Society of Edinburgh B,* 104, 31-73.

Malhi, Y., & Wright, J. (2004) Spatial patterns and recent trends in the climate of tropical rainforest regions. *Philosophical Transactions of the Royal Society of London B*, 359, 311-329.

Marimon, B. S., Lima, E.S., Duarte, T.G., Chieregatto, L.C. & Ratter, J.A. (2006) Observations on the vegatation of northeastern Mato Grosso, Brazil. IV. An analysis of the cerrado-Amazonian forest ecotone. *Edinburgh Journal of Botany*, 63, 323-341.

Mayaux, P., Batholomé, E., Fritz, S., & Belward, A. (2004) A new land-cover map of Africa for the year 2000. *Journal of Biogeography*, 31, 861-877.

Menaut, J.C. (1977) Evolution of plots protected from fire since 13 years in a Guinea savanna of Ivory Coast. *Actas IV Simposium Internacional Ecología Tropical*, pp. 541-481. Impresora Nación, LNAC, Panama.

Mitchell, T.D. & Jones, P.D. (2005) An improved method of constructing a database of monthly climate observations and associated high-resolution grids. *International Journal of Climatology,* 25, 693-712.

Nangendo, G., van Straaten, O., & de Gier, A. (2005) Biodiversity conservation through burning: a case study of woodlands in Budongo Forest Reserve, NW Uganda. *African forests between nature and livelihood resources: interdisciplinary studies in conservation and forest management* (ed. by Ros-Tonen, M.A.F. & Dietz, T.), pp. 113-128. The Edin Mellen Press, Lewiston NY.

Pettorelli, N., Vik, J.O., Mysterud, A., Gaillard, J.M., Tucker, C.J.,& Stenseth, N.C. (2005) Using the satellite-derived NDVI to assess ecological responses to environmental change. *Trends in Ecology & Evolution,* 20, 503-510.

Pinzon, J., Brown, M.E., & Tucker, C.J. (2005) Satellite time series correction of orbital drift artifacts using empirical mode decomposition. *Hilbert-Huang Transform: Introduction and Applications* (ed. by N. Huang), pp. 167-186. World Scientific, Hackensack, NJ.

Polley, H.W., Mayeux, H.S., Johnson, H.B., Tischler, C.R. (1997) Viewpoint: atmospheric CO_2, soil water and shrub/grass ratios on rangelands. *Journal of Range Management,* 50, 278-284.

Puyravaud, J.P., Dufour, C., & Aravajy, S. (2003) Rain forest expansion mediated by successional processes in vegetation thickets in the Western Ghats of India. *Journal of Biogeography,* 30, 1067-1080.

Qi J, Chehbouni A, Huete A.R., & Kerr Y.H. (1994) A modified soil adjusted vegetation index. *Remote Sensing of Environment*, 48, 119-126.

Qin, W. & Gerstl, S.A.W. (2000) 3-D Scene modeling of semidesert vegetation cover and its radiation regime. *Remote Sensing of Environment,* 74, 145-162.

Roder, A., Hill, J., Duguy, B., Alloza, J. A. & Vallejo, R. (2008) Using long time series of Landsat data to monitor fire events and post-fire dynamics and identify driving factors. A case study in the Ayora region (eastern Spain). *Remote Sensing of Environment,* 112, 259-273.

Roitman, I., Felfili, J.M., & Rezende, A.V. (2008) Tree dynamics of a fire-protected *cerrado sensu stricto* surrounded by forest plantation, over a 13-year period (1991-2004) in Bahia, Brazil. *Plant Ecology,* 197, 255-267.

Russell-Smith, J., Stanton, P.J., Edwards, A.C. & Whitehead, P.J. (2004) Rain forest invasion of eucalypt-dominated woodland savanna, Iron Range, north-eastern Australia: II. Rates of landscape change. *Journal of Biogeography,* 31, 1305-16

Salzmann, U. & Hoelzmann, P. (2005) The Dahomey Gap: an abrupt climatically induced rain forest fragmentation in West Africa during the late Holocene. *Holocene,* 15, 190-199.

Sankaran, M., Hana, N.P., Scholes, R.J., Ratnam, J., Augustine, D.J., Cade, B.S., Gignoux, J., Higgins, S.I., le Roux, X. , Ludwig, F., Ardo, J., Banyikwa, F., Bronn, A., Bicini, G., Caylor, K.K., Coughenour, M.B., Diouf, A., Ekaya, W., Feral, C.J., February, E.C., Frost, P.G.H., Hiernaux, P., Hrabar, H., Metzger, K.L., Prins, H.H.T., Ringrose, S., Sea, W., Tews, J., Worden, J., & Zambatis, N. (2005) Determinants of woody cover in African savannas. *Nature,* 438, 846-849.

Sedano, F., Gong, P. & Ferrao, M. (2005) Land cover assessment with MODIS imagery in southern African Miombo ecosystems. *Remote Sensing of Environment,* 98, 429-441.

Singh, A. (1989) Review article: digital change detection techniques using remotely-sensed data. *International Journal of Remote Sensing,* 10, 989-1003.

Sonnentag, O., Chen, J.M., Roberts, D.A., Talbot, J., Halligan, K.Q. & Govind, A. (2007) Mapping tree and shrub leaf area indices in an ombrotrophic peatland through multiple endmember spectral unmixing. *Remote Sensing of Environment,* 109, 342-360.

Songh, C., Woodcock, C. E., Seto, K. C., Lenney, M. P., & Macomber, S. A. (2001) Classification and change detection using Landsat TM data: when and how to correct atmospheric effects? *Remote Sensing of Environment*, 75, 230–244.

Su, L., Chopping, M.J., Rango, A., Martonchik, J.V. & Peters, D.P.C. (2007) Support vector machines for recognition of semi-arid vegetation types using MISR multi-angle imagery. *Remote Sensing of Environment,* 107, 299-311.

The World Bank. (2007) World Bank Development Indicators Database, March 2007. World Bank, Washington DC. Accessed online at http://www.worldbank.org/data/onlinedatabases/wdi

Tucker, C.J., Pinzon, J.E., Brown, M.E., Slayback, D., Pak, E.W., Mahoney, R., Vermote, E., & El Saleous, N. (2005) An Extended AVHRR 8-km NDVI Data Set Compatible with MODIS and SPOT Vegetation NDVI Data. *International Journal of Remote Sensing*, 26, 4485-5598.

Vauttoux, R. (1976) Contribution a l'etude de l'evolution des strates arboree et arbustive dans la savane de Lamto (Cote-d'Ivore). *Annals de l'Universite Abdjan C,* 13, 35-63.

Xiao, J. & Moody, A. (2005) A comparison of methods for estimating fractional green vegetation cover within a desert-to-upland transition zone in central New Mexico, USA. *Remote Sensing of Environment,* 98, 237-250.

Zeng, N. & Neelin, D. (2000) The role of vegetation-climate interaction and interannual variability in shaping the African savanna. *Journal of Climate,* 13, 2665-2670.

4. Measuring Biomass Changes due to Woody Encroachment and Deforestation/Degradation in a Forest-Savanna Boundary Region of Central Africa using Multi-Temporal L-band Radar Backscatter

Authors: E.T.A. Mitchard[a], S.S. Saatchi[b], I.H. Woodhouse[a], S.L. Lewis[c], T.R. Feldpausch[c], B. Sonké[d], C. Rowland[e], & P. Meir[a]

a *School of GeoSciences, University of Edinburgh, EH8 9XP, UK*

b *Jet Propulsion Laboratory, California Institute of Technology, Pasadena, CA 91109, USA*

c *Earth and Biosphere Institute, School of Geography, University of Leeds, LS2 9JT, UK*

d *Department of Biology, University of Yaoundé 1, P.O. Box 047, Yaoundé, Cameroon*

e *Centre for Ecology and Hydrology, Maclean Building, Benson Lane, Crowmarsh Gifford, Wallingford, Oxfordshire, OX10 8BB, UK*

As published in Remote Sensing of Environment[1], *May 2011*

Author contributions: ETAM, SSS, & PM devised the research; ETAM, SLL, TRF & BS collected the field data; ETAM conducted the analysis after training from SSS and with assistance from all other authors; ETAM wrote the paper with assistance and revisions from all other authors.

[1]*Remote Sensing of Environment*, 115, 2861-2873, DOI:. 10.1016/j.rse.2010.02.022. See Appendix 2.

Abstract

Satellite L-band synthetic aperture radar backscatter data from 1996 and 2007 (from JERS-1 and ALOS PALSAR respectively) were used with field data collected in 2007 and a back-calibration method to produce biomass maps of a 15 000 km^2 forest-savanna ecotone region of central Cameroon. The relationship between the radar backscatter and aboveground biomass (AGB) was strong (r^2 = 0.86 for ALOS HV to biomass plots, r^2 = 0.95 relating ALOS-derived biomass for 40 suspected unchanged regions to JERS-1 HH). The root mean square error (RMSE) associated with AGB estimation varied from ~25% for AGB < 100 Mg ha^{-1} to ~40% for AGB > 100 Mg ha^{-1} for the ALOS HV data. Change detection showed a significant loss of AGB over high biomass forests, due to suspected deforestation and degradation, and significant biomass gains along the forest-savanna boundary, particularly in areas of low population density. Analysis of the errors involved showed that radar data can detect changes in broad AGB class in forest-savanna transition areas with an accuracy >95%. However, quantitative assessment of changes in AGB in Mg ha^{-1} at a pixel level will require radar images from sensors with similar characteristics collecting data from the same season over multiple years.

4.1 Introduction

The interface between tropical forest and savanna in west and central Africa is a wide, structurally and floristically diverse mosaic of vegetation types, with forest penetrating deeply into the savanna biome as gallery forests along river banks, and also as forest patches on plateaus and in between rivers (Dai *et al*. 2004; Hely *et al*. 2006; Menaut 1983). The savannas in this region are not maintained by precipitation, there being enough rainfall to support full canopy closure except in the poorest or inundated soils. Instead they are maintained largely by anthropogenic disturbance such as fire and clearance for grazing, agriculture and timber (Bucini & Hanan 2007; Sankaran *et al*. 2005). Changes in these disturbance regimes can therefore result in rapid changes in the woody cover of this region. Due to the large extent of the tropical forest-savanna ecotone in Africa (1.28 million km^2 is forest-savanna mosaic, compared with 2.36 million km^2 forest and 4.12 million km^2 woodland (Mayaux *et al*. 2004)), any changes in the woody vegetation cover and the resulting feedbacks could have significant implications for biodiversity and the carbon cycle (Lewis 2006). Such ecotones are also important as they are transitional habitats that appear to be areas of evolutionary dynamism, storing genetic diversity and acting as an important locus for the generation of new species (Smith *et al*. 1997, 2001).

Dynamics of woody vegetation in this ecotone are the result of the integration of a variety of different competing processes, each of largely unknown magnitude and spatial distribution. Forest is being cleared for agriculture, and woody savannas are often burnt to assist agriculture and cattle grazing (FAO 2007; Zhang *et al*. 2006). Forest and woody savannas are also undergoing degradation, especially around settlements, for timber (legal logging concessions and illegal extraction), wood fuel and charcoal (Goetze *et al*. 2006; Mertens & Lambin 2000). Changes in climate also have the potential to alter the area of forest and savanna, for example increases in dry season length will favor savanna, as would rising temperatures (Dai *et al*. 2004; Hely *et al*. 2006; Zeng & Neelin 2000). In contrast, there are also processes that could cause forest to expand into savanna and savannas to increase in woodiness: reduced anthropogenic fire, caused by reduced human activity in an area; increased CO_2

concentration, which has the potential to increase tree growth in forests and therefore biomass (Lewis *et al*. 2004, 2009) by favouring the growth of trees with a C3 photosynthetic pathway, over grasses that have a C4 pathway[2] (Lloyd & Farquhar 1996, 2008); and if rainfall increased, which would again favor trees over grasses (Hely *et al*. 2006).

It has been suggested that forest is expanding into savannas in central Africa because of urban-migration and a consequent reduction in fire frequency (Boulvert 1990). Indeed, this forest encroachment has been found to be occurring in other tropical forest-savanna ecotones, including northern Australia (Bowman *et al*. 2001; Brook & Bowman 2006; Hopkins *et al*. 1996), the Western Ghats of India (Puyravaud *et al*. 2003), and South America (Duarte *et al*. 2006; Durigan and Ratter 2006; Marimon *et al*. 2006). However, little quantitative analysis followed Boulvert's initial observations in Africa: a literature search found only three studies reporting woody expansion in African tropical forest-savanna transitions, though there is much evidence of woody encroachment in semi-arid environments in Africa (Archer *et al*. 2001; Eamus and Palmer 2007). In an ecotonal region of central Cameroon, optical remote sensing data and field measurements were used to show that over a period of 40 years (1950-1990), gallery forests encroached into the savanna landscape at a rate of 0.6 to 2 meters a year (Happi 1998). In eastern Cameroon, analysis of soil carbon isotopes ($^{13}C/^{12}C$, ^{14}C) along two transects showed both significant expansion of the forest, and that increased woody cover of the savanna has occurred over the past century (Guillet *et al*. 2001). In a forest-woodland-savanna mosaic north of the Budongo Forest Reserve, Uganda, a combination of field studies and vegetation index-based satellite change detection were used to demonstrate a 14 % increase in the area of forest in 17 years, an increase of nearly 4000 hectares (Nangendo, 2005).

[2] C3 photosynthesis is the photosynthetic pathway that occurs in most plants including all trees. C4 photosynthesis is an alternative used by some grasses, including the majority found in this area, that gives increased efficiency of photosynthesis with respect to water 'use' (i.e. water loss through transpiration), and is therefore beneficial in drier and hotter environments (Taiz & Zeiger 2006). However, the advantage which C4 plants have over C3 plants is reduced as the concentration of CO_2 in the atmosphere increases (energetically costly adaptations that increase the concentration of CO_2 in leaf cells becomes less advantageous (Lloyd & Farquhar 2008)). Thus increasing CO_2 concentrations could be responsible for woody encroachment by reducing the competitiveness of C4 grasses compared with C3 plants. However, increasing temperatures or a reduction in rainfall, that may occur concurrently with an increase in CO_2 concentration, could negate this effect by increasing the competitive advantage of C4 grasses over C3 trees.

In combination, these studies provide some evidence that forest expansion is occurring, but none used a method that can be extrapolated to larger areas without a huge investment of resources: all involved extensive field studies or the manual interpretation of high-resolution remotely sensed images.

The use of space-borne radar backscatter data is becoming increasingly accepted as a useful method for measuring woody biomass over much larger areas in the tropics because of the capability of radar to penetrate through the forest canopy, and its capacity for all-weather acquisition (Lu 2006; Ribeiro *et al*. 2008; Sano *et al*. 2005; Santos *et al*. 2002). Radar data are likely to be particularly applicable to forest-savanna boundary regions, as theory suggests there will be a substantial increase in backscatter as both the density and size of trees increase (Podest & Saatchi 2002; Woodhouse 2006), and biomass changes from savanna to forest are in the lower biomass ranges, where radar is most sensitive. As radar backscatter responds to the density, size, orientation, and water content of scattering elements on the surface (Rosenqvist *et al*. 2007), rather than just the color and density of leaves, it has the potential to be more sensitive to changes in the woodiness of savanna than spectral data. This is especially true because the radar signal will be much less sensitive to grasses than spectral data, especially when longer radar wavelengths are used. The spectral vegetation signal from trees can be very hard to distinguish from that of grasses unless hyperspatial data, capable of resolving individual trees (Lu 2006), or multi-temporal data which enables the phenology of different landcover types to be separated (Loveland *et al*. 2000), are used.

The successful launch of the Advanced Land Observing Sattelite's Phased Array-type L-band Synthetic Aperture Radar (ALOS PALSAR) in 2006 has increased the potential to use radar to measure biomass, as this is the first long-wavelength (L-band, 23-cm wavelength) synthetic aperture radar (SAR) satellite sensor to have the capability of collecting cross-polarized (HV, horizontal-send, vertical receive) data in addition to horizontal-send, horizontal-receive (HH) data. This is an advantage for detecting biomass because for HV only scattering elements that change the polarization of the incoming electromagnetic radiation will be detected, so complex

three-dimensional structures such as trees will produce a strong response, but soil moisture, which does not change the polarization of the incoming radiation, will not be detected.

Radar has been used only rarely to quantify biomass in forest-savanna transition regions, though when used it has been with considerable success (Lucas *et al*. 2000; Ribeiro *et al*. 2008; Sano *et al*. 2005; Santos *et al*. 2002). It has to our knowledge never previously been used for long-term biomass change detection in forest-savanna transition regions, despite the availability and potential of the data. Here, we compare satellite L-band radar data from 1996 and 2007 over a large ecotonal region of central Cameroon, both to assess changes in aboveground woody biomass (AGB) in this region, and as a proof of concept for its application for large scale monitoring of changes in biomass from space.

4.2 Study area

The study area covers a 15 000 km^2 region in central Cameroon, centered around 6°4'18" N, 12°53'18" E, encompassing the Mbam Djerem National Park and the surrounding area to the north and east (Figure 1).

Figure 1

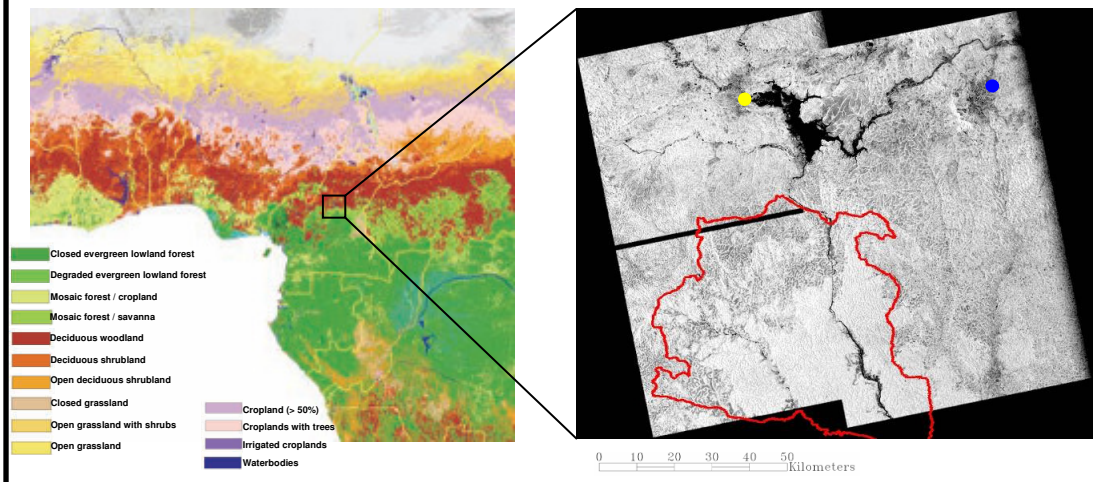

A section of a vegetation map of Africa taken from Mayaux *et al.* 2004, showing the location of the study area within Cameroon, with the ALOS HV 2007 mosaic showing the Mbam Djerem National Park outlined in red, Tibati in yellow and Ngaoundal in blue.

This region was chosen as it extends across a range of tropical vegetation types, from humid forests contiguous with the Congo Basin tropical forest belt in the south to savanna with narrow gallery forests in the north. It experiences an annual rainfall of 1720 mm, with a standard deviation of 213 mm (derived from Tropical Rainfall Measuring Mission (TRMM) 3B43 V6 data from January 1998 to December 2008). There is a pronounced dry season from December to March, with an average rainfall of 20 mm per month. The Mbam Djerem National park was established in the year 2000 as an expanded version of the longer-standing Pangare Djerém reserve with funds from Chad-Cameroon Pipeline Project, and is currently maintained by the Wildlife Conservation Society. It has a high species diversity, containing over 360 bird and 50 mammal species (Anon 2007), and is regarded as having critical importance for the preservation of Central African biodiversity (Doumenge *et al.* 2003). The park itself has a very low human population density, with almost no permanent residents. Major anthropogenic disturbances in the park are fishing, bushmeat hunting in the southern forests, and grazing accompanied by burning in areas along the northern forest-savanna boundary. The regions surrounding the park are more populated, especially on the eastern side, with the two major towns being Tibati on the western side of Lake Mbakaou, and Ngaoundal in the northeast of the study area. The population of both towns has increased by approximately 85 % in the past twenty years, from 15 522 and 11 382 respectively in 1987 to 28 981 and 21 239 in 2006 (CIESIN 2004; PNUD 1999).

4.3. Methods

4.3.1. Field data

The study area was visited in October-December 2007 as part of the Tropical Biomes in Transition project (TROBIT, www.geog.leeds.ac.uk/research/trobit). Vegetation was sampled in four regions from the top to the middle of the Mbam Djerem National Park. In all, data were collected from four one-hectare savanna plots, four one-hectare forest plots, a pair of 0.4 hectare plots (one in transitional forest, one savanna), and eight 20 by 200 meter transects (8 x 100 m x 100 m; 2 x 40 m x 100 m; 8 x 20 m x 200 m). Seven transects ran from forest into savanna, and as the transition from forest to savanna was very sharp (typically occurring in under five

meters), they were each split into a forest and a savanna portion, hence each giving two data points. We did not sub-divide these transects further (nor divide the ten larger plots), in order to remove any problems of autocorrelation: all data-points are sufficiently separated in space or vegetation type to be considered independent. One transect was solely located in forest, and for this AGB was averaged across its whole length. So, in total, 25 biomass plots were used in this study, 13 from forest and transitional forest, and 12 from savanna.

Within these 18 sampling locations data were collected for every tree with a diameter ≥10 cm at 1.3 m along the stem, or above buttresses or stem deformities, a forestry convention called 'diameter at breast height' (DBH). The variables used in this study were the species, DBH, and height (the latter measured for only a subset of trees). Height was estimated using vertex hypsometers (Laser Vertex Hypsometer/Vertex Hypsometer III, Haglöf, Sweden). The height of every tree was measured for the 8 transects and for the remaining 10 plots height was collected for only a random subsample of trees, and site-specific power-law regression equations used to estimate height from diameter for the remaining trees (average n = 56 trees for each plot, average RMSE < 1.6 m, $p < 0.001$ in all cases). The field sites were located using a handheld differential GPS (Trimble GeoHX, Trimble, USA). The GPS positions were later corrected using data from the SOPAC N'Koltang ground station in Libreville, Gabon, using the H-STAR differential correction facility in the software GPS Pathfinder Office 3.10 (Trimble, USA), resulting in accuracies of < 0.5 m in the horizontal direction and < 1 m in the vertical.

The aboveground biomass (AGB) in kilograms of each tree was estimated using the optimal pan-tropical allometric equations as derived by Chave *et al*. (2005). For the savanna species the dry forest equation (Equation 1) was used, for forest species the moist forest equation (Equation 2) was used:

$$\mathrm{AGB} = \exp\left[-2.187 + 0.916 \ln(\rho D^2 H)\right] \quad (1)$$

$$\mathrm{AGB} = \exp\left[-2.977 + \ln(\rho D^2 H)\right] \quad (2)$$

where ρ is the wood mass density (oven-dry wood mass divided by green volume, g/cm^3), D is the DBH in cm at 1.3 m, and H is the tree height in meters. Species were differentiated into forest and savanna species based on knowledge of the ecology of the species from BS & SLL, and in which environment they were predominantly found. Wood mass density (also known as wood specific gravity) data were collated from the Global Wood Density Database (Chave *et al*. 2009, Zanne *et al*. 2009), in which wood density values measured at 12% or 18% moisture were converted to wood mass density. We also calculated biomass for the forest species using the dry forest allometric equation (Equation 1). Though this reduced the biomass of the forest plots by 5-10 %, this did not change any of the conclusions reported in the paper so the results are not shown.

The biomass values produced using the allometric equations and all three tree-specific variables were then summed and normalized by the area of the plots to produce estimates of woody AGB in Mg ha^{-1}. Stems with a DBH < 10 cm were not measured for all plots, so the term AGB for the remainder of this paper refers to the dry biomass of stems with a DBH ≥10 cm, which are likely to comprise > 95% of the woody biomass in these ecosystems (based on the 8 transects which were measured to a 5 cm minimum diameter, and pan-African estimates from Lewis *et al*. 2009). These larger trees will be the component to which L-band radar responds most strongly.

4.3.2. Remote sensing data

JERS-1 HH L-band SAR data were collated from the Global Rainforest Mapping Project (GRMP) (De Grandi *et al*. 2000), for the study area from the beginning and end of the dry season (November and March) of 1996. The scenes had been geometrically corrected, radiometrically calibrated, mosaicked into one image, and resampled from the original 12.5 m pixel spacing to 100 m pixels using wavelet decomposition, maintaining as much of the true signal as possible while greatly reducing speckle and noise (De Grandi *et al*. 2000). These data were converted from digital number (DN) to sigma^0 values using the equation and calibration coefficients

provided by the GRMP (see http://southport.jpl.nasa.gov/GRFM/), using ENVI 4.4 (ITT, USA):

$$\text{sigma}^0\ [\text{dB}] = 20.\log_{10}(6.\text{DN} + 250) - 68.2 \quad (3)$$

The 2007 data comprised four ALOS PALSAR scenes collected in the FBD (Fine Beam Double-polarization) mode were acquired from the Alaska Satellite Facility, having been provided to them by JAXA. Two were captured on the 26th July 2007, and the other two on the 12th of August 2007. These are, like the JERS data, L-band, but are polarimetric, including HH and HV polarizations, and were provided at the original 12.5 m pixel spacing.

Quickbird data (60 cm panchromatic resolution and 2.4 m multispectral resolution) were acquired from Eurimage for all the sites by purchasing an archive image from 19th February 2004 for the southern sites and requesting a new acquisition, captured on 30th January 2008, for the northern sites. These ground-point corrected Quickbird data are estimated to be geo-correct to < 2 m. In order to reduce speckle noise, the ALOS image was resampled by averaging blocks of 2 x 2 pixels to produce an image at 25 m resolution. Areas of the ALOS scenes covering the field data plots were georeferenced by eye to the Quickbird data, by using 30 ground control points taken from features such as islands, small clumps of trees and branching points of gallery forests, with resulting RMSE < 0.4 ALOS pixels (10 m).

The ALOS scenes were converted to sigma^0 values using the following equation and data-specific calibration factors, identical for all scenes:

$$\text{sigma}^0\ [\text{dB}] = 10(\log_{10} \text{DN}^2) + CF \quad (4)$$

where *CF* is the calibration factor, set at -80.2 for the HV polarization and -83.2 for the HH polarization for scenes generated before 1st January 2009 (Shimada *et al.* 2009).

4.3.3. Radar sensitivity to structure and biomass

The sigma^0 values for pixels covering the plots were converted to the power domain before averaging, to ensure the use of the arithmetic, not geometric, means. Eighteen of the twenty-five biomass plots fell on the overlap between the two scenes captured

seventeen days apart. A regression analysis between the two sets of backscatter values found that they were very well correlated (dB_{SE} = 1.0074(dB_{SW}), r^2=0.88, p < 0.00001, where dB_{SE} and dB_{SW} are the sigma^0 HV backscatter values for the 18 sites found in both the south-east and south-west images respectively), and were not significantly different from each other (paired t-test of difference not equal to zero, p = 0.384), therefore the mean of the two raw power averages for each site was used in all presented analyses. The sigma^0 values for both polarizations were then regressed against structural features of the plots (basal area, average height, stem density and average DBH), and then against the AGB values for each site. Best fit empirical relationships were then calculated comparing backscatter with these variables, as no consensus has yet been reached as to what functional form *a priori* best describes these relationships. These comparisons with structural features are important as the majority of previous studies relating such data to backscatter are from temperate plantation forests (Lu 2006; Woodhouse 2005), and as such there is little data from natural heterogeneous tropical savanna-forest mosaics. All regression analyses were performed with the software SigmaPlot 10.0 (Systat Software, USA).

4.3.4. Biomass change detection

To allow comparison with the JERS data, the ALOS data were mosaicked and subsequently resampled to 100 m pixels. The JERS data were then georeferenced to the ALOS data using a network of 40 ground control points, selected by eye, which resulted in an RMSE of 0.48 pixels (48 m); areas in the JERS image not present in the ALOS mosaic were then masked.

As there were no field data available for this area from 1996, and the field data collected in 2007 is from areas near the forest edges that are suspected to have increased in biomass over the preceding eleven years (Chapter 3, Mitchard *et al.* 2009), it was necessary to back-calibrate the JERS HH data to the ALOS-derived AGB values from areas that were unlikely to have changed over the time period. This methodology relies on the fact that there are identifiable areas where AGB is relatively stable in forest-savanna transition regions and the impacts of environmental variables on the radar backscatter such as soil and canopy moisture

are relatively small (Hovestadt *et al*. 1999; Jeltsch *et al*. 1999; Ratter 1992; Santos *et al*. 2002). Pixels were randomly selected from the image, and when they were judged to have fallen in an area that was unlikely to have changed (*e.g.* dense forest, or known grassland, confirmed by visual analysis of a Landsat ETM+ scene from 2000 compared with ASTER images from 2006/7), pixel values were extracted and averaged for a homogeneous area of 5 x 5 pixels around this pixel from both images (25 ha). These larger areas were used in order to limit errors caused by speckle and geolocation problems, with this averaging across homogeneous areas greatly increasing the confidence in the relationship produced. A regression between the ALOS-derived AGB values and the sigma^0 values from the JERS image was then performed, using the same relationship as with ALOS HH to ensure that the biomass of young and regenerating forests was calibrated correctly, and the derived relationship used to create a biomass map for the JERS image. Although there is evidence for a general increase in AGB across higher biomass tropical African forests (Lewis *et al*. 2009), at most this increase would be a small fraction of the total biomass of these sites (< 4 %), too small to be detectable by the radar backscatter data at these high biomass values. Hence we assumed that no detectable change had occurred in the AGB of the selected high biomass sites.

The accuracy of the derived relationship between JERS HH and AGB was evaluated by examining the relationship between ALOS HH and AGB, as both sensors have similar characteristics and incidence angles. We did not use the HH channel from both sensors to perform the change detection directly (using differences in dB value after a cross-calibration procedure) because the ALOS HH data were acquired in the wet season and as such were not comparable, as the HH channel responds strongly to soil moisture as well as to AGB.

The biomass class widths were chosen to be approximately equal to the RMSE of the biomass estimation at that level, and thus the classes increase in width as biomass increases, with the highest class taking as its lowest value the point where there is no evidence of a significant positive relationship between biomass and backscatter above that point. The area covered by the different classes at the two time points was

compared, and a change map was produced showing the changes in average biomass at a 500 m (25 ha) resolution. Subsequently, an assessment of the sources and likely magnitude of uncertainties was performed.

4.4. Results

4.4.1 Field data

Figure 2

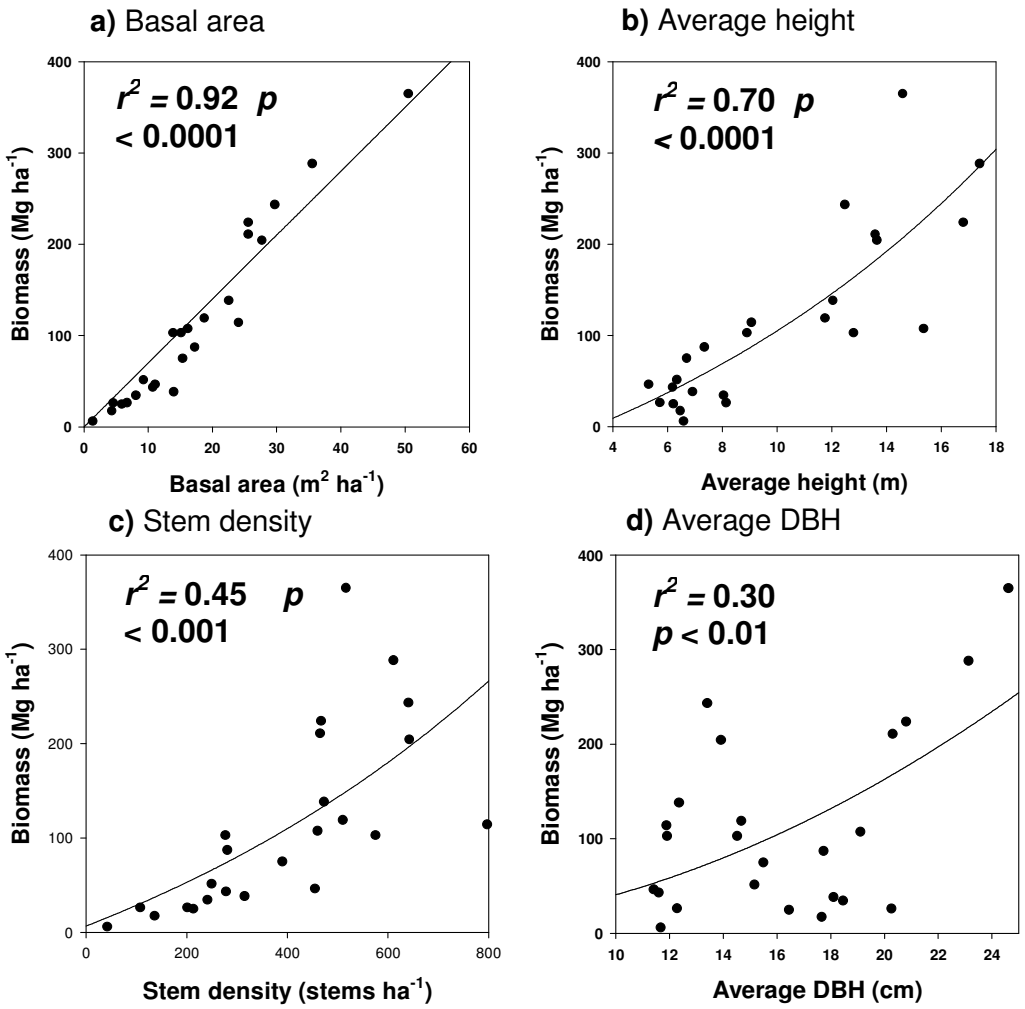

Biomass values for the field plots against a) basal area, b) average height, c) stem density, and d) average DBH. The fit for a) is linear, for b), c) and d) quadratic.

In total 4368 trees were measured, representing 205 species from 142 genera and 58 families. AGB measurements for the 25 data points ranged from 6 to 424 Mg ha^{-1}. Table 1 gives the full plot data combined with the ALOS HH and HV backscatter data. As expected biomass values were strongly related to basal area, with a fitted

linear relationship giving an r^2 of 0.92 (Figure 2). However the influence of height and wood density values on the biomass estimates using these equations can be seen here, as if an allometric equation that used only DBH values had been used this relationship would have an r^2 of 1. Biomass was also significantly related to average height (r^2 = 0.70) and to stem density (r^2 = 0.45), though in both cases the quadratic terms were significant in the regression, suggesting a reduction in the strength of the relationship at higher biomass values. There was a weaker but still significant correlation between biomass and the average DBH for each plot when a quadratic relationship was fitted (r^2 = 0.30, $p < 0.01$).

Table 1 – Plot data

Biomass *Mg ha^{-1}*	Stem density *stems ha^{-1}*	Average height *m*	Average DBH *cm*	Basal area *m^2 ha^{-1}*	ALOS HH sigma^0 *dB*	ALOS HV sigma^0 *dB*
6.1	42	6.6	11.7	1.4	-9.42	-15.72
17.4	136	6.5	17.7	4.3	-10.26	-16.37
24.9	213	6.2	16.4	5.9	-9.35	-15.54
26.3	108	8.1	20.3	4.5	-9.01	-14.69
26.4	201	5.7	12.3	6.7	-10.33	-15.19
34.5	241	8.0	18.5	8.1	-7.93	-14.28
38.4	315	6.9	18.1	14.0	-7.58	-13.8
43.2	278	6.2	11.6	10.7	-8.27	-14.22
46.3	455	5.3	11.4	11.1	-7.98	-14.77
51.4	249	6.3	15.2	9.3	-9.28	-15.6
75.1	390	6.7	15.5	15.4	-7.92	-13.78
87.2	281	7.3	17.7	17.3	-7.1	-14.15
102.9	575	12.8	11.9	13.9	-7.48	-12.59
103.1	277	8.9	14.5	15.1	-6.86	-12.34
107.8	460	15.4	19.1	16.2	-7.16	-12.35
114.7	797	9.1	11.9	24.1	-7.67	-12.73
119.7	510	11.8	14.7	18.7	-7.02	-13.2
141.2	473	12.0	12.4	22.6	-7.29	-12.65
204.4	642	13.6	13.9	27.7	-6.45	-11.99
212.3	465	13.6	20.3	25.6	-7.34	-12.26
240.5	467	16.8	20.8	25.6	-7.94	-11.98
247.1	641	12.5	13.4	29.7	-7.34	-12.33
306.97	*611*	*17.4*	*23.1*	*35.6*	*-8.36*	*-13.22*
456.13	516	14.6	24.6	50.5	-6.25	-12.02

Biomass (Mg ha^{-1}), stem density (stems ha^{-1}), average height (m), basal area (m^2 ha^{-1}), and ALOS 2007 HH and HV sigma^0 (dB) are given for all the field plots. The plot in italics was not used in the biomass regression analysis because it was on a steep slope facing away from the sensor, and thus in radar shadow, whereas the other plots were all from relatively flat ground.

Figure 3

a) HV against basal area

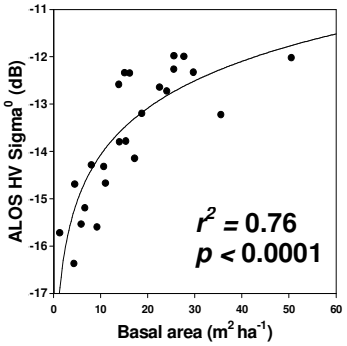

b) HH against basal area

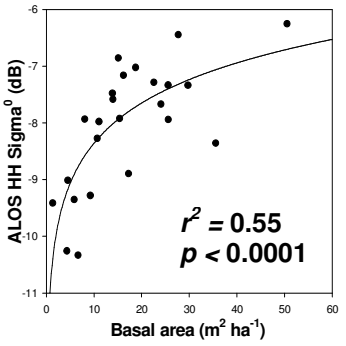

c) HV against average height

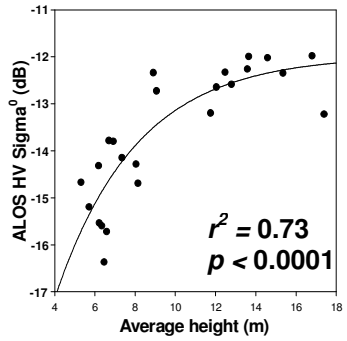

d) HH against average height

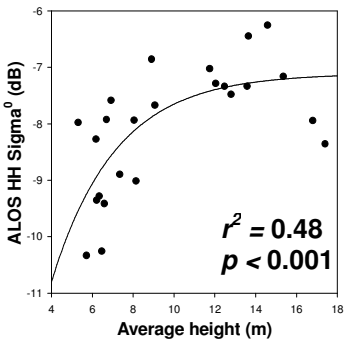

e) HV against stem density

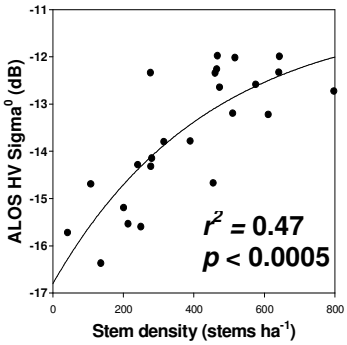

f) HH against stem density

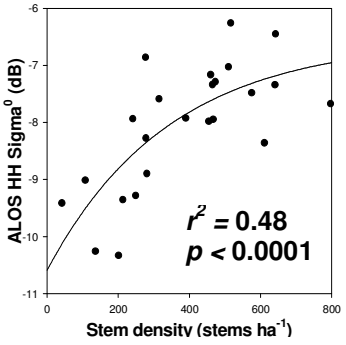

g) HV against average DBH

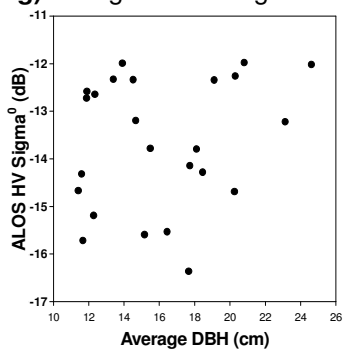

h) HH against average DBH

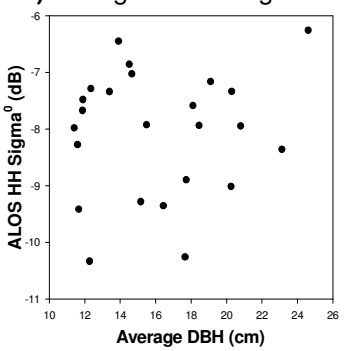

ALOS 2007 HV and HH sigma^0 plotted against basal area, average height, stem density and average DBH (stem diameter at 1.3 m). Best fit log relationships were fitted for a – f; no significant relationships were found for g) and h).

4.4.2. ALOS backscatter sensitivity to vegetation structure

Significant log relationships were found between ALOS HV and HH sigma^0 backscatter and basal area, average height, and stem density (Figure 3). No significant relationship was found between average DBH for the plot and either polarization. As expected, both polarizations responded most strongly to basal area (HV: r^2 = 0.76, HH: r^2 = 0.55), with HV having the smaller residuals. HV backscatter responded almost as strongly to average height (r^2 = 0.73), though HH responded less strongly to this variable (r^2 = 0.48). A loss of sensitivity appeared to occur quite early in both cases, with a strong relationship with height up to about 9 meters and little evidence of a predictive relationship above this point. There was a significant response to stem density in both polarizations (HV r^2 = 0.47, $p < 0.0005$, HH r^2 = 0.48, $p < 0.0001$); interestingly in this case, HH is more strongly correlated than HV, even if only marginally and insignificantly so. This is possibly due to the influence of ground-trunk scattering, which should increase with stem density, and is a more influential component of the HH than HV backscatter (Woodhouse 2005).

4.4.3. ALOS to biomass regression

One biomass plot was on a significant slope (*c*. 25°), in radar shadow, and consequently had an anomalously low radar return (Woodhouse 2005). It was therefore thought most appropriate to remove this point from subsequent analyses, as all other plots were located on comparatively flat ground (0°–7° slope), and therefore were unsuitable for developing and testing a slope-correction procedure to apply to the anomalous plot. Attempts were made to fit a relationship between AGB and a combination of HH and HV polarizations, however the strongest relationship was found between ALOS HV sigma^0 alone and AGB, using an exponential rise-to-maximum model, as this best fitted the backscatter data, with the loss of sensitivity at approximately 150 - 200 Mg ha^{-1} well modeled (see Figure 4a). This fitted model happens to be equivalent to the simple Water Cloud Model (Attema & Ulaby 1978), but the equation was chosen because it it had a higher r^2 than any other relationship that was tested, rather than for theoretical reasons. For this analysis, data points were weighted according to the square root of their area (Zar 2007), to correct for the differences between the sizes of the sample plots. The fitted relationship was:

$$ALOS\ HV_{sigma^0} = a + b\left[1 - e^{-c.AGB}\right] \quad (5)$$

where a = -16.59 ±*0.46*, b = 4.63 ±*0.44*, and c = 0.014 ±*0.004* (uncertainties in parameter estimation are standard errors). The r^2 for the fitted regression was 0.86, an F-test for the regression found it to be highly significant ($F_{2,22}$ = 63.23, p < 0.0001), and the data passed a Shapiro-Wilk normality test (p = 0.47).

Figure 4

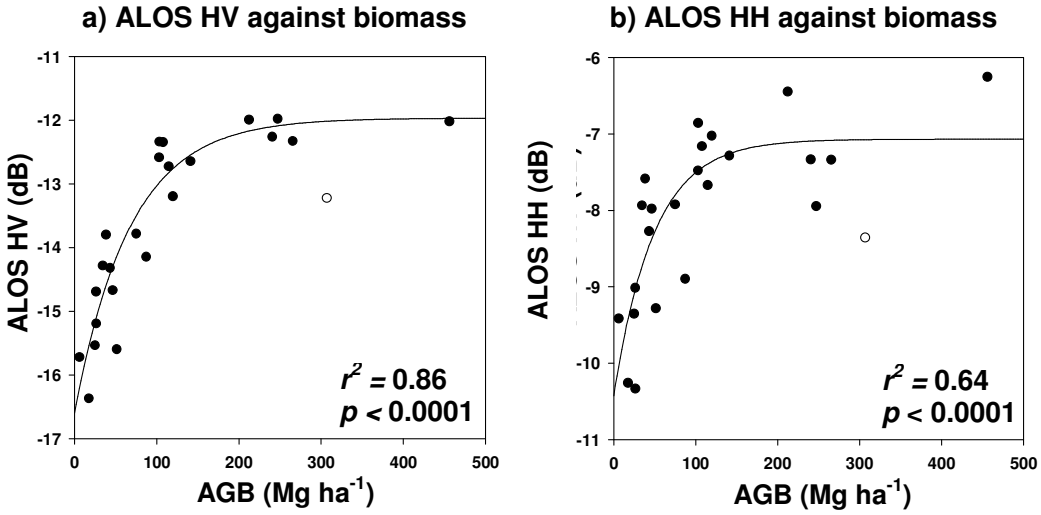

a) ALOS HV sigma^0 (dB) and b) ALOS HH sigma^0 (dB) plotted against field-measured AGB (Mg ha^{-1}), with area-weighted negative exponential relationships fitted. The point in white is from a steep slope and for this reason was excluded from the regression calculations.

To create a biomass map from the ALOS HV backscatter data Equation 5 was rearranged to:

$$AGB = \frac{1}{c} \times -\ln\left[1 - \frac{ALOSHV_{sigma^0} - a}{b}\right] \quad (6)$$

There was also a good, but weaker, relationship with the ALOS HH polarization alone, which gives as estimate of the accuracy of the relationship between JERS HH data from 1996 and AGB (r^2 = 0.64, $F_{2,22}$ = 17.96, p < 0.0001, Figure 4b).

4.4.4. Accuracy of ALOS-biomass regression

The accuracy of the ALOS HV AGB predictions decrease as biomass increases (Figure 5). The overall root mean square error (RMSE) for these data is 49 Mg ha^{-1}; however this decreases to 29 Mg ha^{-1} if only values below 150 Mg ha^{-1} are

considered, and to 24 Mg ha^{-1} using only data points < 100 Mg ha^{-1}. These results led us to map AGB in classes chosen to be similar in size to the RMSE at each level: 0-25, 25-50, 50-75, 75-100, 100-150, 150-200, and > 200 Mg ha^{-1}. The large degree of scatter and possible bias observable in Figure 5 for values > 200 Mg ha^{-1} suggests that no subdivision of biomass classes above this point is appropriate.

Figure 5

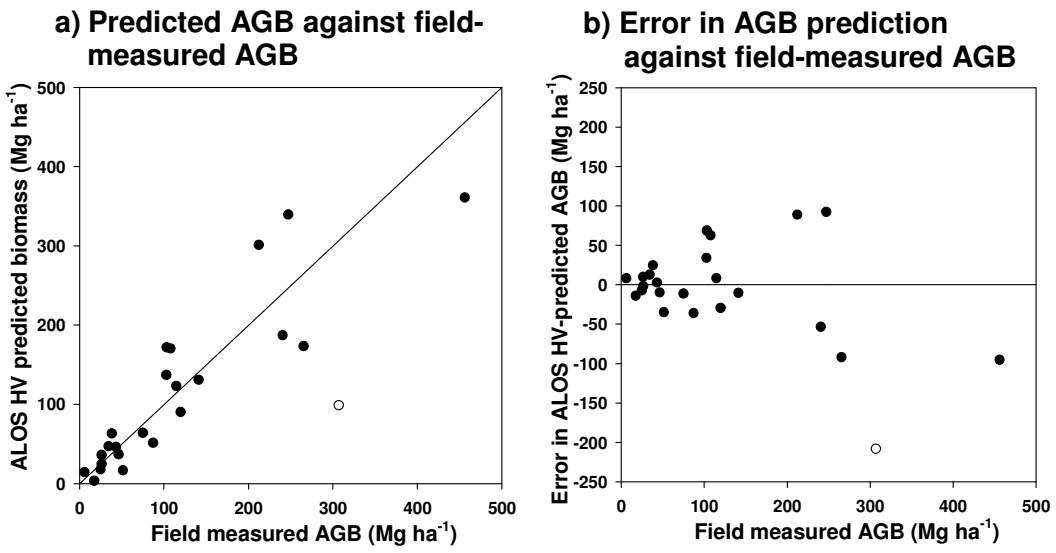

Errors in predicting biomass from the ALOS HV relationship are shown by a) ALOS HV-predicted AGB plotted against field-measured AGB (Mg ha^{-1}), with an x = y line shown, and b) the error in ALOS HV biomass prediction plotted against field-measured biomass.

The relationship between ALOS HH and biomass is clearly noisier, with a loss of sensitivity occurring earlier than for the HV data, at around 100-150 Mg ha^{-1} (Figure 4b). The RMSE values are consequently higher: 65 Mg ha^{-1} for the whole dataset, 52 Mg ha^{-1} for points < 150 Mg ha^{-1}, and 39 Mg ha^{-1} for values < 100 Mg ha^{-1}. Note the acquisition of these ALOS data was in the wet season, where the HH polarization would be expected to be responding to soil moisture as well as to biomass, and this perhaps explains the poorer than expected performance at lower biomass values. The JERS HH data were captured in the dry season and would therefore be expected to considerably outperform the ALOS HH backscatter. However, to be conservative, it was assumed that the dry season JERS HH is only as accurate as the wet season ALOS HH. Thus much broader biomass classes were used for the JERS data (and thus also the change detection): 0 – 50, 50 – 100, 100 – 150, and > 150.

4.4.5. JERS to ALOS-derived biomass regression

Figure 6

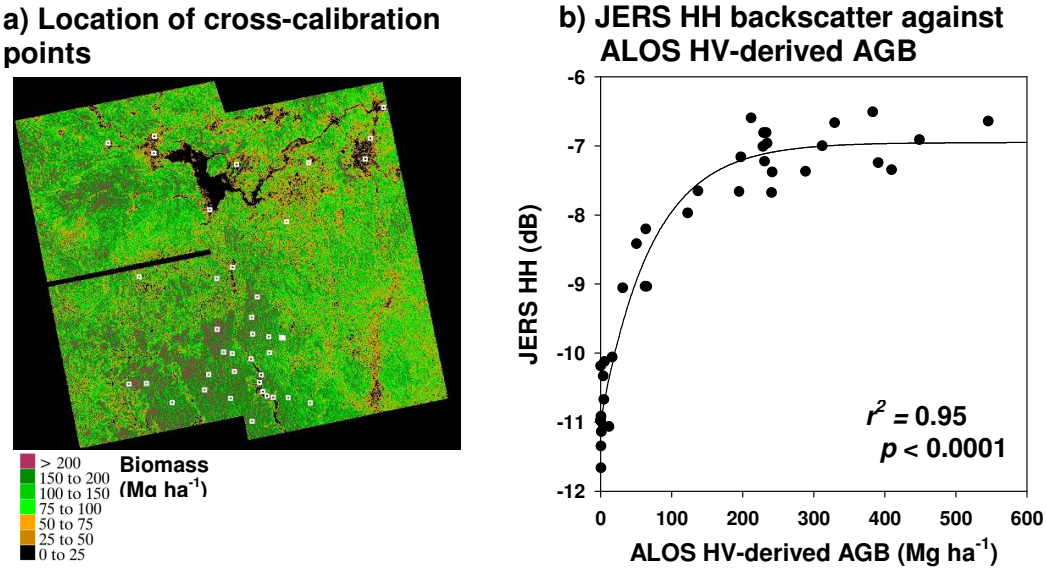

a) Location of 40 x 500 m x 500 m suspected unchanged areas used to back-calibrate JERS HH data to ALOS HV-derived AGB, and b) JERS HH sigma^0 from 1996 (dB) plotted against ALOS HV-derived AGB (Mg ha^{-1}) from 2007 for these 40 suspected unchanged 25 ha areas.

A strong relationship was found between the 40 suspected unchanged areas in the JERS HH sigma^0 data from March 1996 (dry season) with the ALOS HV biomass data (r^2 = 0.95, $F_{2,48}$ = 341.1, p < 0.0001; Figure 6). The equation used was identical to Equation 5, but with coefficients: a = -10.98 *±0.12*, b = 4.03 *±0.16*, and c = 0.014 *±0.002*. The relationship with the JERS HH sigma^0 data from November 1996 (wet season) was less strong (r^2 = 0.72, data not shown), confirming that radar data are more sensitive to biomass in the dry season. The reason the r^2 is higher here than with the ALOS HV data is because of the large areas used to calibrate the relationship (25 ha each), greatly reducing the geolocation errors and noise apparent when a relationship is derived from comparatively small field plots, as in the ALOS to biomass regression. This higher r^2 value should not be taken to show that JERS HH is more sensitive to biomass than ALOS HV, as in general its accuracy is likely to be similar to that for ALOS HH (though in all likelihood better as the drier conditions should result in less soil moisture influence). The relationship was used to estimate AGB from JERS HH imagery and a map was produced by classifying AGB into 4 classes with 50 Mg ha^{-1} intervals, chosen to capture the estimation

uncertainties predicted using the ALOS HH data (Figure 7a), the training data is put in the correct class with a 94% accuracy using these classes. For comparison the ALOS HV map with its seven classes is included as Figure 7b.

Figure 7

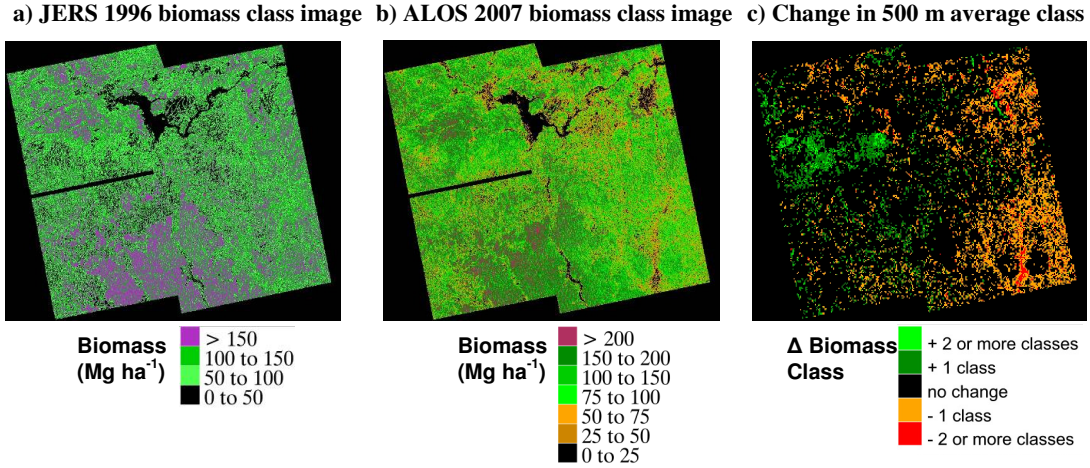

Biomass class images produced using a) JERS HH 1996 data and b) ALOS HV 2007 data, using scales with the size of biomass classes based on RMSE error values, with broader classes for the JERS HH 1996 data than the ALOS HV 2007 data; and c) change in 500 m average class (JERS class image subtracted from ALOS class image) for the two images (using the broader JERS classes).

4.4.6. Change detection

Figure 8

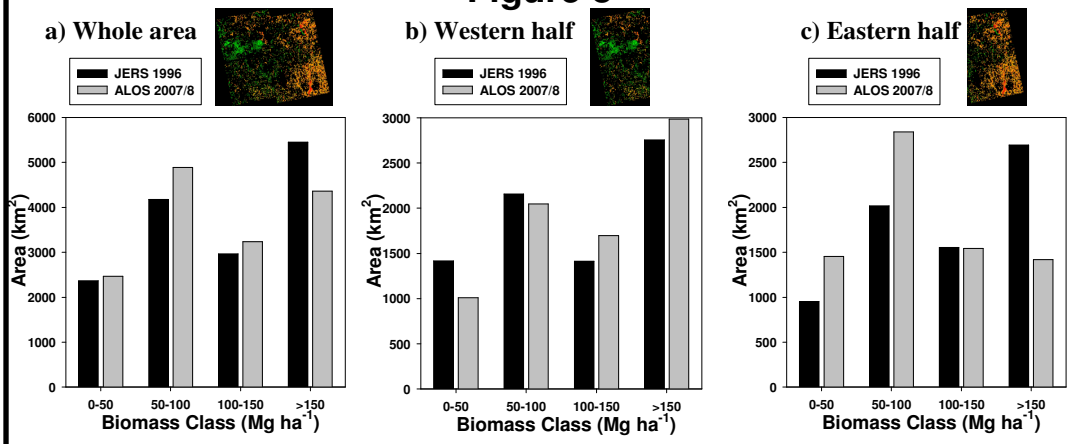

The total area in km^2 against biomass class (Mg ha^{-1}) for the two biomass maps from 1996 and 2007 for: a) the whole data set; b) the less-populated western half of the study region; and c) the more-populated right hand half.

The biomass change map was produced by tracing the number of biomass classes each 500 m pixel changed between the two periods (Figure 7c). Although the ALOS

biomass map has smaller intervals and a larger biomass range, we produced the change map by using 50 Mg ha^{-1} as the class interval and 150 Mg ha^{-1} as the upper limit, as these are the best that can be confidently predicted using the JERS data. The resulting map shows biomass losses and gains dominating in different parts of the study area, with losses of higher biomass classes in the eastern side, and gains on the western side. Changes in the absolute area covered by each biomass class are also shown in Figure 8, both for the whole study area, and for the eastern and western sides individually. A loss of the high biomass classes dominates the east of the study area, which appears to be concentrated around the major population centres and along the railway line (Figure 9).

Figure 9

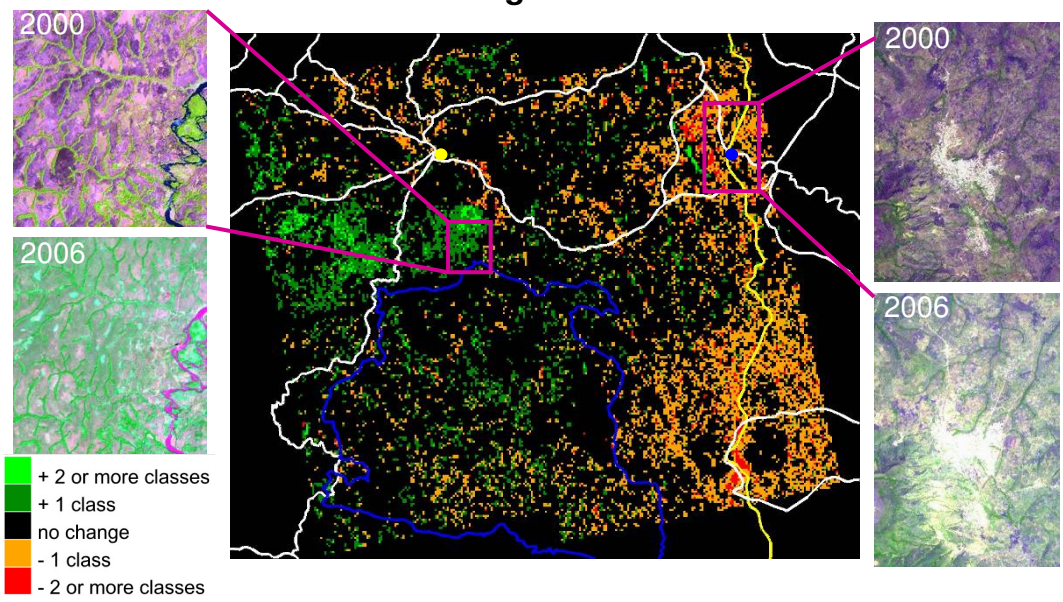

Change in class image using the same method as for Figure 6 c. The major towns of Tibati and Ngaundal are shown as yellow and blue circles respectively, Mbam Djerem National Park is outlined in blue, roads are shown in white, and the railway line in yellow. Optical close-up images are Landsat ETM+ from 2000 (bands 5-4-3) and ASTER from 2006 (bands 3n, 2, 1), showing the widening of gallery forests and increased woody vegetation on the left-hand pair, and the rapid clearing of woody vegetation around the town of Ngaundal on the right-hand pair.

Here the area covered by forest > 150 Mg ha^{-1} has declined almost by half, from 2700 km^2 in 1996 to 1400 km^2 in 2007. However, there are also areas of positive change (*i.e.* biomass gain), concentrated in the western side of the study area, particularly in the savanna areas of the Mbam Djerem National Park and the area north of it. Increases in biomass appear to occur in all the woodland-savanna areas without a high human population density. These increases are shown by a reduction

in the area of biomass classes < 100 Mg ha^{-1}, and an increase in area for both cover classes > 100 Mg ha^{-1}.

4.5. Uncertainty analysis

There are two major sources of uncertainty in this analysis: uncertainties in calculating biomass values from field data, and uncertainties in using radar remote sensing data to estimate biomass. Uncertainties in the first case seem unlikely to affect the results of the change detection, so increases and decreases should be correctly located, but the magnitude of the biomass classes could be incorrect. Uncertainties inherent in using radar remote sensing data to estimate biomass across an area may, however, affect the results of the change detection, and these errors are particularly uncertain for the JERS data from 1996 as there are no field data, making an assessment of the accuracy of that classification difficult. Here we will subdivide these uncertainties into their major sources, and estimate the likely contribution from each.

4.5.1. Errors in field data to AGB estimation

1. ***Uncertainties in diameter, height and species measurements*****.** Diameter measurements are considered very accurate (Alder & Synnott 1992), and though height measurements are less precise, an in-field assessment, involving re-measuring 10 trees across the full height range at least 8 times from different angles and on different days, suggested our methods were accurate to greater than ±10 %. All species were identified in the field by expert local botanists, and as such mis-identifications are likely to be relatively few, and given the similarities of wood density within a genus, unlikely to have a major effect on the biomass estimation (Chave *et al*. 2006, 2009).

2. ***Uncertainties in the allometric equation*****.** It is not possible to use species-specific, or even region-specific, allometric equations for most tropical ecosystems, as the species diversity is too large and the relevant data have not been collected. However using a pan-tropical equation including height, diameter and species-specific wood density minimizes overall uncertainty in biomass estimates to an estimated ±10 %

(though Chave *et al*. (2005) optimistically estimate ±5 % for the equation we used). This error could be considerably higher for larger trees, where accurate biomass data are very scarce.

We therefore estimate that the biomass classes used could be inaccurate by at worst ±20 %, assuming a consistent 10 % error in height estimation combined with the allometric equation used that poorly predicts tree biomass and consistently over- or under- estimating by a further 10 %. The consequence of this is that, for example, the 100 – 150 Mg ha^{-1} biomass class could in fact at worst be 80 – 120 Mg ha^{-1} or 120 - 180 Mg ha^{-1}.

4.5.2. Uncertainties in radar to biomass estimation

We now consider the errors involved in putting a pixel into the correct biomass class. This was estimated using the RMSE values from the original biomass estimation, as discussed in Section 4.5, though these RMSE values are likely to overestimate the true error value because of their small plot size. The biomass class sizes were chosen to be approximately equal to the RMSE values at the respective biomass level. Assuming errors are normally distributed, this should result in approximately 68 % of data points being placed in the correct class, and approximately 95 % in the correct class or a neighbouring class (Zar 2007). These are indeed approximated in the field data, with 65 % of the data points being correctly classified for the ALOS HV data, and 96 % being placed in the correct or neighbouring class; for ALOS HH (with the wider biomass classes) these values are 57 % and 96 % respectively.

These errors in classifying pixels should, unlike those for the biomass estimation, be randomly distributed, with no bias (*i.e.* there is assumed to be an equal chance of over- and under- estimation for every point). Thus, while the chances of a randomly chosen pixel being correctly classified is just 66 %, the large number of pixels considered in all the classes suggests the overall accuracy in estimating the total area of this class is much higher. This assumption would not be valid if the number of pixels varied considerably between classes, as rare classes would be overestimated due to mis-estimation from neighbouring classes; however as all the classes are of a

similar magnitude this is unlikely to be a serious problem. Equally, 25 pixels are averaged to produce each average class at a 500 m resolution before the change detection routine is performed. Therefore the total area covered by each class in Figure 8, and the changes in average biomass class at a 500 m resolution in Figure 7, are thought accurate to at least a 95 % (based on a simple statistical simulation model assuming a random distribution of biomass classes at a 100 m resolution aggregated to 500 m, implemented in R, data not shown), and possibly higher, suggesting that the changes observed are robust. However, using this methodology to track changes in individual 100 m pixels is likely to give poor estimates, so we produced a biomass change map at a 500 m resolution, as the averaging of the class of 25 pixels gives a level of confidence in the results (> 95 %) which could not be achieved with a higher resolution (Figure 7c).

4.6. Discussion

4.6.1. Using radar data to detect changes in forest-savanna ecotones

We detected forest expansion over a large, less-populated western part of our study area, and rapid forest loss in the eastern side. This strongly suggests that satellite L-band SAR data can be used to detect biomass changes in forest-savanna transition regions. While a reduction in signal sensitivity at higher biomasses makes the accurate estimation of forest biomass difficult, detecting changes in the woodiness of savannas, and detecting deforestation and degradation, is possible using a combination of JERS and ALOS PALSAR, and in future with two PALSAR images. The errors in the analysis have been assessed, and shown to be small compared to the signal in the data, increasing our confidence in results derived from L-band SAR data combined with on-the-ground field measurements.

The lack of field data corresponding to the 1996 satellite data increases the error in the results, but apparently not dramatically so; although this error is impossible to quantify precisely, we can be confident in the results given the conservative methodology and broad biomass classes used. These broad classes mean that only pixels that have undergone rapid biomass change will be detected, thus providing

confidence that any observed changes are genuine and not caused by noise or mis-calibration of the datasets.

The ALOS data were captured in the wet season, and the HH signal is therefore likely to be less sensitive to differences in biomass than if the imagery had been obtained during the dry season with lower soil moisture influences. Consequently, the HH data from JERS captured in the dry season is likely to have considerably smaller errors than suggested by the ALOS HH data. The benefits of using HV over HH can be seen clearly, with a relationship found with $r^2 = 0.86$ for the ALOS HV data, despite the wet season image capture. This is due to the minimal impact of soil moisture on L-band HV, which has been shown elsewhere (Dubois *et al*. 1995; Oh *et al*. 1992).

4.6.2. Forest expansion

The smaller-scale (40 – 300 km^2) reports of Boulvert (1990), Happi (1998) and Guillet *et al*. (2001) showing woody expansion in Cameroon are consistent with our larger scale (15 000 km^2) study: woody expansion is indeed occurring in some forest-savanna transition regions, and it is occurring rapidly, with many pixels increasing by two biomass classes over the eleven year study period, equivalent to at least a doubling in biomass. While this increase is rapid, it is not necessarily unrealistic: increases of 1.4-2.0 Mg ha^{-1} yr^{-1} have been observed in the drier Miombo woodlands (Chidumayo 1997, Williams *et al.* 2008), and increases > 10 Mg ha^{-1} yr^{-1} have been found for secondary forest growth in Amazonia (Gehring *et al.* 2005, Feldpausch *et al.* 2004, Houghton *et al.* 2000), in wetter, less seasonal conditions. We therefore estimate that increases in the order of 5 Mg ha^{-1} yr^{-1} would be possible in this area, which is sufficient to produce the observed increases over the eleven years.

This also corroborates a recent study using high resolution spectral vegetation index data over a 5000 km^2 region equivalent to the central-west section of this study area from 1986 – 2006, which found significant increases in the woody cover of the savanna regions (Chapter 3, Mitchard *et al*. 2009). Equally, this finding agrees with informal independent field observations in the Mbam Djerem National Park: the first

30 meters or so of most gallery forests were dominated by young pioneer trees, with a scattering of older dead and dying savanna trees being shaded by the arrival of faster growing and ultimately taller forest biome species (Chapter 3, Mitchard *et al*. 2009 & personal observation by ETAM, TRF, SLL & BS).

It is likely that the expansion of forest is caused by a reduction in human disturbance, especially fire, which may have resulted from a combination of urban migration, changes in lifestyle away from cattle herding, and the formation of the Mbam Djerem National Park. These factors have previously been shown to be the cause of woody encroachment in a number of semi-arid environments in Africa (Dalle *et al*. 2006; Ward 2005). Although it is difficult to quantify the total positive effect of the designation of the area as a National Park on biomass gain, the study does show the potential for national parks in forest-savanna ecotone regions to be managed to sequester carbon. It is possible that adopting a policy of limiting savanna burning and exploitation might enable such parks to earn valuable funds, either in the voluntary carbon market or the proposed Reduced Emissions from Deforestation and Degradation (REDD) scheme. By contrast, it demonstrates that a policy of savanna burning may need to be implemented in Mbam Djerem National Park in order to maintain the unique diversity of ecosystem types present.

This study also demonstrates that a combination of satellite radar data with field studies can provide sufficiently robust evidence to claim and validate carbon stocks (though robust baseline field data will also be needed to enable calculations of carbon credits). Ideally however a still-more robust analysis would be performed, using L- or P-band data from the same sensor in the same season under similar ground moisture conditions, in combination with field data collected in the same year as each radar scene. This would increase the accuracy and confidence in the results, removing any need for back calibration, and allowing direct estimation of biomass changes per pixel, without the need for broad biomass classes. It would also reduce the influence of soil moisture. The impact of soil moisture in this study cannot be ruled out entirely, although we believe it could not explain the biomass increases observed in this study, because (a) forest-savanna boundaries and gallery forests in

the ALOS HV image are clearly visible, (b) these boundaries correspond well with the Quickbird data, and (c) we used a large number of biomass plots and calibration points around the area which showed the largest biomass increase.

4.6.3. Forest loss

Despite the significant gains shown in the west, the overall biomass trend for the study area is negative, with a net loss of 20 % (1090 km^2) of high biomass forest (> 150 Mg ha^{-1}) over the 11 year study period. The losses along the railway line and paved road on the eastern side of the study area are very obvious, and similarly around the town of Ngaoundal in the north-east (Figure 9). We suspect strongly that this change is due to human-driven deforestation and degradation (SLL personal observation), but cannot rule out the possibility that it is due to forest die-back following a localized drought (Dai *et al*. 2004). The population density there is higher, and as well as farming and timber extraction for fuel (both woodfuel for local use and charcoal for transport to towns and cities), there are logging operations in the forest areas outside the park. Clearly, the fate of woody vegetation in this region is currently largely in the hands of humans, and without intervention it seems likely that rapid net forest biomass losses will continue; biomass gains in protected areas are very unlikely to be large enough to offset losses of forest and biomass elsewhere. However, recent population trends leave some room for cautious optimism regarding biomass stocks: although the urban population of Cameroon grew by 3.61 % per year from 2002 till 2006, the rural population actually fell slightly, at an average rate of -0.023 % per year (World Bank 2007). Yet, the growing urban population will, of course, have larger demands for fuel, food and timber, so while remote or protected areas may have the potential for an increase in biomass, areas of forest and woody savanna near settlements and access routes are likely to continue to decrease in biomass unless affordable alternatives are available to local biomass-based products. The Mbam Djerem National Park is relatively well protected and the savannas are not currently systematically burned, and as such the land in the park may continue sequestering carbon into the future. Given the rate of loss outside the park, perhaps community projects in this area attempting to reduce deforestation and promote the planting of trees may be more successful at carbon sequestration than relying on

natural regeneration within undisturbed savannas (Williams *et al*. 2008). However, as Geist and Lambin (2002) showed in a meta-analysis of 152 sub-regional deforestation studies, the principal causes of deforestation is demand from remote foreign markets, so local intervention may not alone provide a solution. In addition to local action large-scale, concerted international solutions such as REDD, involving making performance-based payments to reduce deforestation and degradation rates alongside demand management for wood products, may be necessary.

4.6.4. Implications for future radar satellites

While the methods used in this study are sufficient to accurately find areas of large-magnitude biomass change, using these data we cannot be very exact in assessing the precise magnitude of such changes, nor of absolute carbon stocks. However, in the future it is likely to be possible to produce quantitative estimates of biomass change using radar backscatter images captured during the same season over different years from identical or similar L- or P-band polarimetric sensors. The similar geometric configuration and radiometric accuracy of the sensors will allow the use of established radar change detection algorithms which directly compare backscatter values (Carincotte *et al*. 2006; Rignot & Vanzyl 1993; Touzi *et al*. 1999). This will be possible using ALOS PALSAR data (which will be continued by ALOS-2), but also with more informative data including information about tree heights from new satellites such as NASA's interferometric L-band SAR and LiDAR DESDynI, and ESA's planned interferometric P-band BIOMASS. Such data should allow for accurate large-scale, high resolution and long-term monitoring of forest degradation and regeneration.

It is also possible that the accuracy of the biomass maps produced at each time point could be improved by the addition of optical data and digital elevation models (DEMs) to the radar data, using multivariate analysis techniques. Optical data, such as vegetation indices, provide a different suite of information about forest structure in these ecosystems (for example canopy cover; Chapter 3, Mitchard *et al*. 2009) that might be beneficial in producing more robust biomass maps, and DEMs could be used to correct for the influence of slope on radar backscatter. This technique of

incorporating many different layers to produce biomass maps has been conducted at a coarse resolution in Amazonia (e.g. Saatchi *et al*. 2007), but would suffer from the difficulties of acquiring comparable, high resolution and cloud-free images captured at a similar time to the radar images for each year for this kind of high resolution change detection. In general, however, more information should provide greater constraints on potential errors and improve accuracy, so this type of combined-data approach should be investigated.

4.7 Acknowledgements

Jon Lloyd, TROBIT P.I., provided useful advice and expertise. Three anonymous referees provided helpful suggestions and comments on an earlier version of the manuscript that were instrumental in improving the study. Adam Freedman provided advice on the sources of accurate population data. Jeanette Sonké, Wildlife Conservation Society-Cameroon (WCS-Cameroon), The University of Yaounde I, and 14 canoeists from Mbakaou provided invaluable support in Cameroon. Remote sensing data were provided by the Alaska Satellite Facility, the Global Rainforest Mapping Project, NASA and Eurimage; Landsat and ASTER images were provided free of charge by Terralook, courtesy of USGS EROS and NASA's Jet Propulsion Laboratory; TRMM 3B43 data was downloaded from the Giovanni online data system, developed and maintained by the NASA Goddard Earth Sciences (GES) Data and Information Services Center (DISC).

4.8 References

Alder, D., & Synnott, T.J. (1992). Permanent sample plot techniques for mixed tropical forest. *Oxford Forestry Institute Tropical Forestry Papers,* 25

Anon (2007). *Park National du Mbam et Djerem, Plan d'Aménagement 2007-2011*. Cameroun: Le Ministère des Forêts et de la Faune

Archer, S., Boutton, T.W., & Hibbard, K.A. (2001). Trees in grasslands: biogeochemical consequences of woody plant expansion. In E.-D. Schulze, S. Harrison, M. Heimann, E. Holland, J. Lloyd, I. Prentice & D. Schimel (Eds.), *Global biogeochemical cycles in the climate system* (pp. 115-133). San Diego: Academic Press

Attema, E.P.W., & Ulaby, F.T. (1978). Vegetation Modeled as a Water Cloud. *Radio Science,* 13, 357-364

Boulvert, Y. (1990). Avancée ou recul de la forêt centroafricaine. Changements climatiques, influence de l'homme et notamment de feux. In R. Lanfranchi & D. Schwartz (Eds.), *Paysages Quaternaries de l'Afrique Central Atlantique* (pp. 353-366). Paris: Initiations et Didactiques ORSTROM

Bowman, D., Walsh, A., & Milne, D.J. (2001). Forest expansion and grassland contraction within a Eucalyptus savanna matrix between 1941 and 1994 at Litchfield National Park in the Australian monsoon tropics. *Global Ecology and Biogeography,* 10, 535-548

Brook, B.W., & Bowman, D. (2006). Postcards from the past: charting the landscape-scale conversion of tropical Australian savanna to closed forest during the 20th century. *Landscape Ecology,* 21, 1253-1266

Bucini, G., & Hanan, N.P. (2007). A continental-scale analysis of tree cover in African savannas. *Global Ecology and Biogeography,* 16, 593-605

Carincotte, C., Derrode, S., & Bourennane, S. (2006). Unsupervised change detection on SAR images using fuzzy hidden Markov chains. *IEEE Transactions on Geoscience and Remote Sensing,* 44, 432-441

Chave, J., Andalo, C., Brown, S., Cairns, M.A., Chambers, J.Q., Eamus, D., Folster, H., Fromard, F., Higuchi, N., Kira, T., Lescure, J.P., Nelson, B.W., Ogawa, H., Puig, H., Riera, B., & Yamakura, T. (2005). Tree allometry and improved estimation of carbon stocks and balance in tropical forests. *Oecologia,* 145, 87-99

Chave, J,, Coomes, D., Jansen, S., Lewis, S.L., Gwenson, N.G., & Zanne, A.E. (2009). Towards a worldwide wood economics spectrum. *Ecology Letters,* 12, 351-366

Chave, J., Muller-Landau, H.C., Baker, T.R., Easdale, T.A., Ter Steege, H., & Webb, C.O. (2006). Regional and phylogenetic variation of wood density across 2456 neotropical tree species. *Ecological Applications,* 16, 2356-2367

Chidumayo, E.N. (1997). *Miombo Ecology and Management: An Introduction*. London: IT Publications in association with the Stockholm Environment Institute

Center for International Earth Science Information Network (CIESIN) Columbia University; International Food Policy Research Institute (IPFRI); World Bank; Centro Internacional de Agricultura Tropical (CIAT). (2004). *Global Rural-Urban Mapping Project (GRUMP): Urban/Rural Population grids*. Palisades, NY: CIESIN, Columbia University. Downloaded from http://sedac.ciesin.columbia.edu/gpw/

Dai, A.G., Trenberth, K.E., & Qian, T.T. (2004). A global dataset of Palmer Drought Severity Index for 1870-2002: Relationship with soil moisture and effects of surface warming. *Journal of Hydrometeorology,* 5, 1117-1130

Dalle, G., Maass, B.L., & Isselstein, J. (2006). Encroachment of woody plants and its impact on pastoral livestock production in the Borana lowlands, southern Oromia, Ethiopia. *African Journal of Ecology,* 44, 237-246

De Grandi, G., Mayaux, P., Rauste, Y., Rosenqvist, A., Simard, M., & Saatchi, S.S. (2000). The Global Rain Forest Mapping Project JERS-1 radar mosaic of tropical Africa: Development and product characterization aspects. *IEEE Transactions on Geoscience and Remote Sensing,* 38, 2218-2233

Doumenge, C., Ndinga, A., Nembot, T.F., Tchanou, Z., Ondo, V.M., Nze, N.O., Bourobou, H.B., & Ngoye, A. (2003). Forest biodiversity conservation in Atlantic regions of central Africa: II. Identifying a network of critical sites. *Bois et Forest des Tropiques,* 296, 43-58

Duarte, L.D.S., Machado, R.E., Hartz, S.M., & Pillar, V.D. (2006). What saplings can tell us about forest expansion over natural grasslands. *Journal of Vegetation Science,* 17, 799-808

Dubois, P.C., Vanzyl, J., & Engman, T. (1995). Measuring Soil-Moisture with Imaging Radars. *IEEE Transactions on Geoscience and Remote Sensing,* 33, 915-926

Durigan, G., & Ratter, J.A. (2006). Successional changes in cerrado and cerrado/forest ecotonal vegetation in western Sao Paulo State, Brazil, 1962 - 2000. *Edinburgh Journal of Botany,* 63, 119-130

Eamus, D., & Palmer, A. (2007). Is Climate Change a Possible Explanation for Woody Thickening in Arid and Semi-Arid Regions? *Research Letters in Ecology*, 2007, Article ID 37364.

FAO (2007). *State of the World's Forests 2007*. Rome: Food and Agriculture Organization of the United Nations

Feldpausch, T.R., M.A. Rondon, E.C.M. Fernandes, S.J. Riha, & Wandelli, E. (2004). Carbon and nutrient accumulation in secondary forests regenerating on pastures in central Amazonia. *Ecological Applications,* 14S, S164-S176

Geist, H.J., & Lambin, E.F. (2002). Proximate causes and underlying driving forces of tropical deforestation. *Bioscience,* 52, 143-150

Gehring, C., Denich, M., & Vlek, P.L.G. (2005). Resilience of secondary forest regrowth after slash-and-burn agriculture in central Amazonia. *Journal of Tropical Ecology,* 21, 519-527

Goetze, D., Horsch, B., & Porembski, S. (2006). Dynamics of forest-savanna mosaics in north-eastern Ivory Coast from 1954 to 2002. *Journal of Biogeography,* 33, 653-664

Guillet, B., Achoundong, G., Happi, J.Y., Beyala, V.K.K., Bonvallot, J., Riera, B., Mariotti, A., & Schwartz, D. (2001). Agreement between floristic and soil organic carbon isotope (C-13/C-12, C-14) indicators of forest invasion of savannas during the last century in Cameroon. *Journal of Tropical Ecology,* 17, 809-832

Happi, J.Y. (1998). Arbres contre graminees: la lenta invasion de la savane par la foret au center-Cameroun. Doctoral Thesis: Université de Paris Sorbonne

Hely, C., Bremond, L., Alleaume, S., Smith, B., Sykes, M.T., & Guiot, J. (2006). Sensitivity of African biomes to changes in the precipitation regime. *Global Ecology and Biogeography,* 15, 258-270

Hopkins, M.S., Head, J., Ash, J.E., Hewett, R.K., & Graham, A.W. (1996). Evidence of a Holocene and continuing recent expansion of lowland rain forest in humid, tropical North Queensland. *Journal of Biogeography,* 23, 737-745

Houghton, R.A., D.L. Skole, C.A. Nobre, J.L. Hackler, K.T. Lawrence, & Chomentowski, W.H. (2000). Annual fluxes of carbon from deforestation and regrowth in the Brazilian Amazon. *Nature,* 403, 301-304

Hovestadt, T., Yao, P., & Linsenmair, K.E. (1999). Seed dispersal mechanisms and the vegetation of forest islands in a West African forest-savanna mosaic (Comoe National Park, Ivory Coast). *Plant Ecology,* 144, 1-25

Jeltsch, F., Moloney, K., & Milton, S.J. (1999). Detecting process from snapshot pattern: lessons from tree spacing in the southern Kalahari. *Oikos,* 85, 451-466

Lewis, S.L., Malhi, Y., & Phillips, O.L. (2004). Fingerprinting the impacts of global change on tropical forests. *Philosophical Transactions of the Royal Society of London Series B-Biological Sciences,* 359, 437-462

Lewis, S.L. (2006). Tropical forests and the changing Earth system. *Philosophical Transactions of the Royal Society of London Series B-Biological Sciences,* 361, 195-210

Lewis, S.L., Lopez-Gonzalez, G., Sonke, B., Affum-Baffoe, K., Baker, T.R., Ojo, L.O., Phillips, O.L., Reitsma, J.M., White, L., Comiskey, J.A., Djuikouo, M.N., Ewango, C.E.N., Feldpausch, T.R., Hamilton, A.C., Gloor, M., Hart, T., Hladik, A., Lloyd, J., Lovett, J.C., Makana, J.R., Malhi, Y., Mbago, F.M., Ndangalasi, H.J., Peacock, J., Peh, K.S.H., Sheil, D., Sunderland, T., Swaine, M.D., Taplin, J., Taylor, D., Thomas, S.C., Votere, R., & Woll, H. (2009). Increasing carbon storage in intact African tropical forests. *Nature,* 457, 1003-U1003

Lloyd, J., & Farquhar, G.D. (1996). The CO2 dependence of photosynthesis, plant growth responses to elevated atmospheric CO2 concentrations and their interaction with soil nutrient status .1. General principles and forest ecosystems. *Functional Ecology,* 10, 4-32

Lloyd, J., & Farquhar, G.D. (2008). Effects of rising temperatures and [CO2] on the physiology of tropical forest trees. *Philosophical Transactions of the Royal Society B-Biological Sciences,* 363, 1811-1817

Loveland, T.R., Reed, B.C., Brown, J.F., Ohlen, D.O., Zhu, Z., Yang, L., & Merchant, J.W. (2000). Development of a global land cover characteristics database and IGBP DISCover from 1 km AVHRR data. *International Journal of Remote Sensing,* 21, 1303-1330

Lu, D.S. (2006). The potential and challenge of remote sensing-based biomass estimation. *International Journal of Remote Sensing,* 27, 1297-1328

Lucas, R.M., Milne, A.K., Cronin, N., Witte, C., & Denham, R. (2000). The potential of synthetic aperture radar (SAR) for quantifying the biomass of Australia's woodlands. *Rangeland Journal,* 22, 124-140

Marimon, B.S., Lima, E.S., Duarte, T.G., Chieregatto, L.C., & Ratter, J.A. (2006). Observations on the vegetation of northeastern Mato Grosso, Brazil. IV. An analysis of the cerrado-Amazonian forest ecotone. *Edinburgh Journal of Botany,* 63, 323-341

Mayaux, P., Bartholome, E., Fritz, S., & Belward, A. (2004). A new land-cover map of Africa for the year 2000. *Journal of Biogeography,* 31, 861-877

Menaut, J.C. (1983). The vegetation of African savanna. In F. Bourliere (Ed.), *Ecosystems of the World: Tropical Savannas*. Amsterdam: Elsevier

Mertens, B., & Lambin, E.F. (2000). Land-cover-change trajectories in southern Cameroon. *Annals of the Association of American Geographers,* 90, 467-494

Mitchard, E.T.A., Saatchi, S.S., Gerard, F.F., Lewis, S.L., & Meir, P. (2009). Measuring woody encroachment along a forest-savanna boundary in central Africa. *Earth Interactions,* 13, 8.

Nangendo, G.v.S.O.d.G.A. (2005). Biodiversity conservation through burning: a case study of woodlands in Budongo Forest Reserve, NW Uganda. In M.A.F.D.T. Ros-Tonen (Ed.), *African forests between nature and livelihood resources: interdisciplinary studies in conservation and forest management* (pp. 113-128). New York: The Edin Mellen Press

Oh, Y., Sarabandi, K., & Ulaby, F.T. (1992). An Empirical-Model and an Inversion Technique for Radar Scattering from Bare Soil Surfaces. *IEEE Transactions on Geoscience and Remote Sensing,* 30, 370-381

PNUD (UNDP, United Nations Development Program) (1999). *Rapport sur le pauvreté rurale au Cameroun*. Yaoundé: PNUD

Podest, E., & Saatchi, S. (2002). Application of multiscale texture in classifying JERS-1 radar data over tropical vegetation. *International Journal of Remote Sensing,* 23, 1487-1506

Puyravaud, J.P., Dufour, C., & Aravajy, S. (2003). Rain forest expansion mediated by successional processes in vegetation thickets in the Western Ghats of India. *Journal of Biogeography,* 30, 1067-1080

Ratter, J.A. (1992). Transitions between cerrado and forest vegetation in Brazil. In P.A. Furley, J. Proctor & J.A. Ratter (Eds.), *Nature and Dynamics of Forest-Savanna Boundaries*. London: Chapman and Hall

Ribeiro, N.S., Saatchi, S.S., Shugart, H.H., & Washington-Allen, R.A. (2008). Aboveground biomass and Leaf Area Index (LAI) mapping for Niassa Reserve, northern Mozambique. *Journal of Geophysical Research-Biogeosciences,* 113¸ G02S02

Rignot, E.J.M., & Vanzyl, J.J. (1993). Change Detection Techniques for Ers-1 Sar Data. *IEEE Transactions on Geoscience and Remote Sensing,* 31, 896-906

Rosenqvist, A., Shimada, M., & Milne, A.K. (2007). The ALOS Kyoto & Carbon Initiative. In: *Geoscience and Remote Sensing Symposium, 2007.* IEEE International. pp. 3614-3617

Saatchi, S.S., Houghton, R.A., Alvala, R., Soares, J.V., & Yu, Y. (2007). Distribution of aboveground live biomass in the Amazon basin. *Global Change Biology,* 13, 816-837

Sankaran, M., Hanan, N.P., Scholes, R.J., Ratnam, J., Augustine, D.J., Cade, B.S., Gignoux, J., Higgins, S.I., Le Roux, X., Ludwig, F., Ardo, J., Banyikwa, F., Bronn, A., Bucini, G., Caylor, K.K., Coughenour, M.B., Diouf, A., Ekaya, W., Feral, C.J., February, E.C., Frost, P.G.H., Hiernaux, P.,

Hrabar, H., Metzger, K.L., Prins, H.H.T., Ringrose, S., Sea, W., Tews, J., Worden, J., & Zambatis, N. (2005). Determinants of woody cover in African savannas. *Nature,* 438, 846-849

Sano, E.E., Ferreira, L.G., & Huete, A.R. (2005). Synthetic aperture radar (L band) and optical vegetation indices for discriminating the Brazilian savanna physiognomies: A comparative analysis. *Earth Interactions,* 9, 1-15

Santos, J.R., Lacruz, M.S.P., Araujo, L.S., & Keil, M. (2002). Savanna and tropical rainforest biomass estimation and spatialization using JERS-1 data. *International Journal of Remote Sensing,* 23, 1217-1229

Shimada, M., Isoguchi, O., Tadono, T., & Isono, K. (2009). PALSAR radiometric calibration and geometric calibration. *IEEE Transactions on Geoscience and Remote Sensing,* 47, 3915 - 3932

Smith, T.B., Kark, S., Schneider, J., Wayne, R.K., & Moritz, C. (2001). Biodiversity hotspots and beyond: the need for preserving environmental transitions. *Trends in Ecology and Evolution,* 16, 431

Smith, T.B., Wayne, R.K., Girman, D.J., & Bruford, M.W. (1997). A role for ecotones in generating rainforest biodiversity. *Science,* 276, 1855-1857

Taiz, L., & Zeiger, E. (2006). *Plant Physiology 4th Edition*. Sunderland, MA: Sinauer Associates

Touzi, R., Lopes, A., Bruniquel, J., & Vachon, P.W. (1999). Coherence estimation for SAR imagery. *IEEE Transactions on Geoscience and Remote Sensing,* 37, 135-149

Ward (2005). Do we understand the causes of bush encroachment in African savannas? *African Journal of Range and Forage Science,* 22, 101-105

Williams, M., Ryan, C.M., Rees, R.M., Sarnbane, E., Femando, J., & Grace, J. (2008). Carbon sequestration and biodiversity of re-growing Miombo woodlands in Mozambique. *Forest Ecology and Management,* 254, 145-155

Woodhouse, I.H. (2005). *Introduction to Microwave Remote Sensing*. Taylor & Francis.

Woodhouse, I.H. (2006). Predicting backscatter-biomass and height-biomass trends using a macroecology model. *IEEE Transactions on Geoscience and Remote Sensing,* 44, 871-877

Zanne, A.E., Lopez-Gonzalez, G., Coomes, D.A., Ilic, J., Jansen, S., Lewis, S.L., Miller, R.B., Swenson, N.G., Wiemann, M.C., & Chave, J. (2009). Global wood density database. Dryad. http://hdl.handle.net/10255/dryad.235

World Bank (2007). World Bank Development Indicators Database, March 2007. World Bank, Washington DC. Accessed online at http://www.worldbank.org/data/onlinedatabases/wdi

Zar, J.H. (2007). *Biostatistical Analysis. 5th Edition*. USA: Prentice-Hall.

Zeng, N., & Neelin, J.D. (2000). The role of vegetation-climate interaction and interannual variability in shaping the African savanna. *Journal of Climate,* 13, 2665-2670

Zhang, Q.F., Justice, C.O., Jiang, M.X., Brunner, J., & Wilkie, D.S. (2006). A GIS-based assessment on the vulnerability and future extent of the tropical forests of the Congo Basin. *Environmental Monitoring and Assessment,* 114, 107-121

5. Using Satellite Radar Backscatter to Predict Above-ground Woody Biomass: a Consistent Relationship Across Four Different African Landscapes

Authors: E.T.A. Mitchard[a], S.S. Saatchi[b], I.H. Woodhouse[a], G. Nangendo[c], N.S. Ribeiro[d], M. Williams[a], C.M. Ryan[a], S.L. Lewis[e], T.R. Feldpausch[e], & P. Meir[a]

a *School of GeoSciences, University of Edinburgh, EH8 9XP, UK*

b *Jet Propulsion Laboratory, California Institute of Technology, Pasadena, CA 91109, USA*

c *Wildlife Conservation Society, Uganda Office, P.O.Box 7487, Uganda*

d *Faculdade de Agronomia e Engenharia Florestal, Universidade Eduardo Mondlane, P.O.Box 257, Maputo, Mozambique*

e *Earth and Biosphere Institute, School of Geography, University of Leeds, LS2 9JT , UK*

This is a slightly expanded version of a paper with the same title and authors published in *Geophysical Research Letters*, December 2009[1]. The original paper can be found in Appendix 3.

Author contributions: ETAM, SSS, & PM devised the research; ETAM, SLL & TRF collected the field data from Cameroon; ETAM and GN collected the field data from Uganda; NSR collected the field data from the Niassa Reserve, Mozambique; and MW & CMR collected the data from the Nhambita Community Carbon Project, Mozambique; ETAM conducted the analysis with assistance from SSS, PM, IHW & SLL; ETAM wrote the paper with assistance and revisions from all other authors.

[1]*Geophysical Research Letters*, Vol. 36, L23401, doi:10.1029/2009GL040692. See Appendix 3

Abstract

Regional-scale above-ground biomass (AGB) estimates of tropical savannas and woodlands are highly uncertain, despite their global importance for ecosystems services and as carbon stores. In response, we collated field inventory data from 253 plots at four study sites in Cameroon, Uganda and Mozambique, and examined the relationship between field-measured AGB and cross-polarized radar backscatter values derived from ALOS PALSAR, an L-band satellite sensor. The relationships were highly significant, similar among sites, and displayed high prediction accuracies up to 150 Mg ha^{-1} (± ~20%). AGB predictions for any given site obtained using equations derived from data from only the other three sites generated only small increases in error. The results suggest that a widely applicable general relationship exists between AGB and L-band backscatter for lower-biomass tropical woody vegetation. This relationship allows regional-scale AGB estimation, required for example by planned REDD (Reducing Emissions from Deforestation and Degradation) schemes.

5.1 Introduction

There is no universally accepted methodology for assessing the aboveground woody biomass (AGB) of woody tropical landscapes. While there is a degree of consensus on the best methods of collecting ground-based inventory data (Brown, 1997; Chave *et al.*, 2009; Phillips *et al.*, 2009), and a general agreement that remote sensing data provides the best methodology for both scaling-up ground-based measurements and monitoring changes over large scales, there is a plethora of different sensors and analytical procedures available for scaling-up AGB estimates (Lu, 2006).

Tropical savanna and woodland ecosystems provide substantial ecosystem services at local to global scales: the provision of timber, fuel and other products, the regulation of soil and water, biodiversity retention, atmospheric services and eco-tourism. However, attempts to mitigate rising atmospheric CO_2 levels have led to projects aiming to preserve these ecosystems based solely on their carbon stocks. To be successful, whether in voluntary carbon markets or via a post-Kyoto climate change agreement under one of the Reducing Emissions from Deforestation and Degradation (REDD) frameworks, a universal, low-cost and robust way to measure and monitor carbon stocks over large regions is needed (Grassi *et al.*, 2008).

An ideal large-scale AGB measurement system would be one that could sense AGB directly, and as such would have no upper biomass limit, and do so independently of cloud cover. Currently no such system exists, although future satellite platforms which will combine fully polarimetric radar with measurements of vegetation height may come closer to this goal (Donnellan *et al.*, 2008; Le Toan *et al.*, 2008). However, for areas with an AGB < ~150 Mg ha^{-1}, which incorporates the savanna and woodland biomes, and drier tropical forest formations, the L-band radar sensor ALOS PALSAR may go some way towards providing a system for measuring AGB that meets observational requirements. In this paper we set out evidence supporting this claim.

Synthetic Aperture Radar (SAR) sensors are active instruments, sending a pulse of microwave radiation and detecting the radiation scattered back (backscatter, referred to as sigma0 (σ^0)) by the surface and the 3-dimensional structures on it. When longer wavelength microwaves are used (>20cm) the detected radiation is mostly due to backscattering from the branching elements and stems of the trees, and thus radar

should respond in a characteristic way to forest volume and biomass (Saatchi & Moghaddam, 2000). As a result, long wavelength SAR has a stronger and more universal relationships than optical or short wavelength microwave sensors which are sensitive to leaf characteristics, where relationships with the woody component of vegetation are indirect and thus highly site- and season- specific. The radar backscatter response saturates at higher biomass values in savanna ecosystems, at a variable point (>60 Mg ha^{-1} (Santos *et al.*, 2002), >80 Mg ha^{-1} (Lucas *et al.*, 2000), and >150 Mg ha^{-1} (Chapter 4, Mitchard *et al.*, 2011), all using different L-band systems). This saturation point is due to the competing mechanisms of scattering and attenuation (absorption) of microwave energy in the canopy of the vegetation, and is highly dependent on the canopy density, stems density, tree species, and vegetation and soil moisture conditions, as well as the characteristics of the radar data used. Nevertheless, this point is high enough that useful biomass estimates are possible for mixed tree-grass systems (savannas and woodlands), as these typically have maximum AGB values <100 Mg ha^{-1}, though higher values can exist in gallery forests (Brown, 1997).

Advanced Land Observing Satellite (ALOS) Phased Array L-band Synthetic Aperture Radar (PALSAR) was launched in January 2006. It operates at a 23.6 cm wavelength in a number of modes, but the Fine-Beam Dual-polarization (FBD) mode, which provides HH (horizontal transmit and horizontal receive) and HV (horizontal transmit and vertical receive) data at a 34.3° incidence angle, shows the greatest potential for these purposes. This is because of its high signal:noise ratio, high resolution (~20 m), provision of cross-polarized data, and because it is being systematically collected across the tropics with the aim of forming a freely-available 50 m resolution mosaic (http://www.eorc.jaxa.jp/ALOS/en/kc_mosaic/kc_mosaic.htm).

PALSAR, and other L-band systems, have previously been shown to respond to the AGB of tropical savannas and woodlands with varying degrees of accuracy (Lucas *et al.*, 2000; Chapter 4, Mitchard *et al.*, 2011; Podest & Saatchi, 2002; Santos *et al.*, 2002). However, in these studies the field datasets were small and from one geographic area. Here we examine the PALSAR response to AGB at four different intensively sampled locations across tropical Africa to test the consistency of the relationship between backscatter and AGB. We then examine the efficacy of models

derived from three sites to predict the AGB of measured plots in a forth site, thus providing a much better test of the utility of such data for assessing AGB than has previously been performed.

5.2 Data and Methods

5.2.1 Field data

The field sites were located in Cameroon, Uganda and Mozambique (Figure 1); in all cases standardized forestry methodologies were employed. Diameters of all stems >10 cm diameter at breast height (DBH) were measured and their species recorded; height was also measured for ~30 % of stems in the Cameroon and Uganda sites using vertex hypsometers (Haglöf, Sweden). None of the study areas exhibit steeply dissected topography.

Mbam Djerem National Park (MDNP), Cameroon

MDNP encompasses the transition between savanna and forest contiguous with the Congo Basin. Eight 1 ha square plots and ten 0.4 ha transects (8 x 20 m x 200 m & 2 x 40 m x 100 m) in forest and savanna regions in three areas of the park near 6°9'N, 12°50'E were sampled in 2007, with AGB ranging from 6 – 418 Mg ha^{-1} (Chapter 4, Mitchard *et al.,* 2011). Transects that occurred in both the forest and savanna were split into two data-points, giving 24 points in total.

Budongo Forest Reserve (BFR), Uganda

BFR is a remnant patch of tropical forest surrounded by farmland to the south and east, and savanna to the west and north. One 1.86 ha square plot and eleven 0.5 ha transects (20 m x 250 m) were measured in 2008 by E Mitchard, and 261 x 0.04 ha & 335 x 0.05 ha circular plots in the savannas and woodlands to the north of the reserve were measured in 2001 (Nangendo *et al.*, 2005); these latter plots are small and highly clustered, and as such were averaged in groups of 5-6 within 100 m x 100 m areas, giving a total of 118 data points (0.2 – 0.3 ha). AGB ranged from 6 – 876 Mg ha^{-1}, with the plots near 1°52'N, 31°39'E.

Figure 1

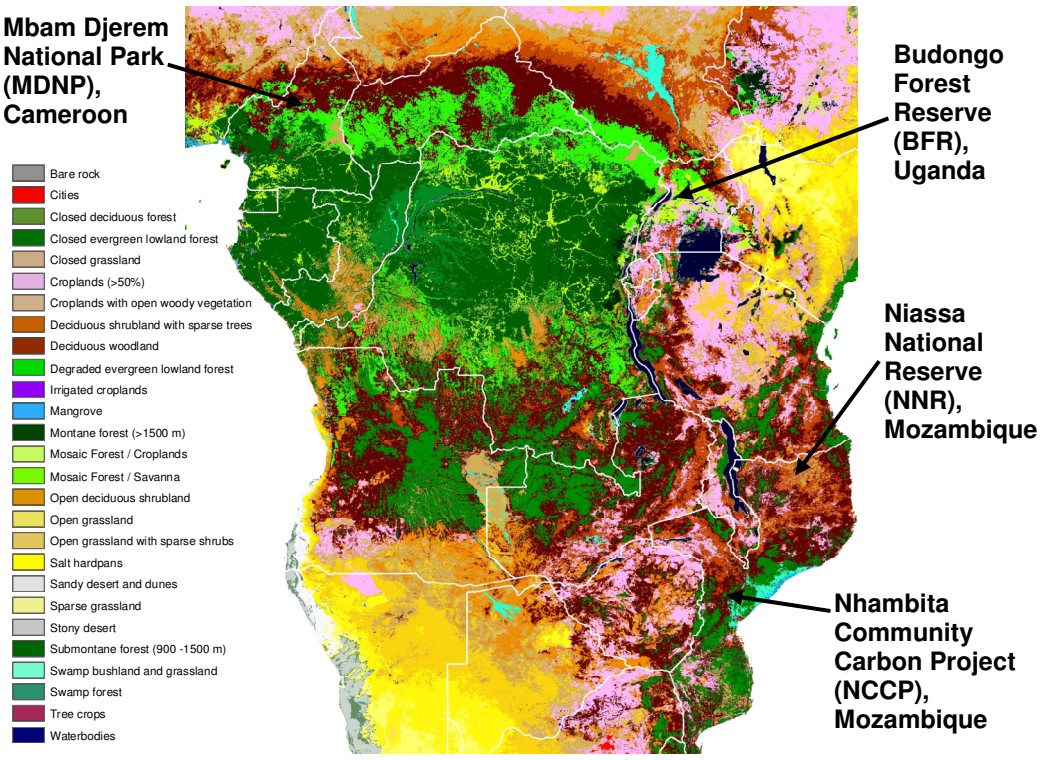

The location of the field sites is shown on a landcover map for the year 2000 produced by Mayaux *et al.* (2004).

Niassa National Reserve (NNR), Mozambique

NNR is a 23 000 km^2 protected area in the north of Mozambique, dominated by Miombo woodland, with the woody fraction of vegetation increasing in density from East to West due to a rainfall and disturbance gradient. Fifty 0.07 ha circular plots distributed across the park were measured in 2004 (Ribeiro *et al.*, 2008) around 12°2'S, 37°15'E. ALOS PALSAR scenes were available for 42, ranging in AGB from 2 – 41 Mg ha^{-1}.

Nhambita Community Carbon Project (NCCP), Mozambique

NCCP is an area of Miombo woodland in central Mozambique. It has more influence from humans and is more regularly burnt than NNR, and has different dominant species. Data were collected for thirteen 1 ha square plots, five 0.5 ha circular plots, and thirty-eight 0.25 ha square plots in 2004-7, with an AGB of 3 – 120 Mg ha^{-1}, near 18°57'S, 34°9'E (Williams *et al.*, 2008).

5.2.2 Conversion to AGB

Field plot data were converted to AGB using the best available methods for each vegetation type. For MDNP and BFR no local allometry data exist, so the Chave *et al.* (2005) pan-tropical optimum allometric equations were used, using wood density, height and DBH. The moist tropical forest equation was used for forest species, and the dry forest equation for savanna species. Height data were measured for ~30 % of the stems and used to develop site-specific height-DBH relationships to obtain AGB (Chapter 4, Mitchard *et al.*, 2011). Wood density data were taken from the Global Wood Density Database (Chave *et al.*, 2009); where species-specific data was not present, the average value for African members of the same genus were used. For NNR an allometric equation involving DBH alone was used, derived from similar vegetation and climatic conditions nearby in Tanzania, taken from Mugasha & Chamshama (2002). For NCCP destructive sampling was performed to produce a site-specific allometric relationship (Ryan, 2009). All plot AGB values were then converted to Mg ha^{-1}; it should be noted that these values are dry AGB, not carbon content, and exclude woody stems < 10 cm, shrubs, grasses, below-ground sources and necromass. This exclusion of other aboveground vegetation will cause an underestimate of AGB of ~5 % for forest and dense woody savanna plots (Chapter 4, Mitchard *et al.,* 2011), and the size of this error will increase for lower biomass plots (it is 12 % for NCCP (Ryan, 2009)). However, the derivation from field data of a local correction factor should be sufficient to correct for this, as L-band radar will respond mostly to larger stems (Collins *et al.*, 2009).

5.2.3 SAR data

L-band dual-polarization (HH/HV) satellite radar data from the ALOS PALSAR sensor in the FBD mode were acquired over all field sites from 2007 (see Table 1 for scene IDs and dates). The data were provided at a 12.5 m pixel spacing (4 looks per pixel), and were converted from digital number to sigma0 using the revised calibration coefficients (Shimada *et al.*, 2009). The scenes were warped to Landsat ETM+ data covering the areas of the field sites, using observable common features such as islands, road junctions, and permanent vegetation features, with a Root Mean Square Error (RMSE) always < 0.6 Landsat pixels (18 m), and the backscatter values for pixels covering each field site extracted, with pixels avearged in the power domain so the arithmetic not geometric means were used. This type of warping is only

possible because all the study areas have little significant topography, so the problem of layover (where topographic features are distorted, bending towards the sensor) is minimized. After averaging, power values were converted back to sigma0 before being regressed against AGB. All remote sensing analyses were performed using ENVI 4.6 (ITT, Boulder, USA), and all regression analyses with Sigmaplot 11.0 (Systat, Chicago, USA).

Table 1 – Scene ID's and dates for all ALOS PALSAR scenes

Site	Scene ID	Date
MDNP, Cameroon	ALPSRP080060100	26 July 2007
MDNP, Cameroon	ALPSRP082540100	12 August 2007
BFR, Uganda	ALPSRP078740020	17 July 2007
NNR, Mozambique	ALPSRP086466940	8 September 2007
NNR, Mozambique	ALPSRP088946940	25 September 2007
NNR, Mozambique	ALPSRP088946930	25 September 2007
NNR, Mozambique	ALPSRP090696940	7 October 2007
NCCP, Mozambique	ALPSRP075236800	23 June 2007
NCCP, Mozambique	ALPSRP077716800	10 July 2007

5.3. Results

5.3.1 Plot level AGB-backscatter relationships

Strong relationships between AGB and HV backscatter were found at each of the four landscapes (r^2 0.61 – 0.76, $p < 0.0001$), with a clear reduction in sensitivity (saturation) obvious between 150 and 200 Mg ha^{-1}; relationships with the HH polarization were less consistent, though significant positive relationships were still observable in all cases (Figure 2, Table 2). The fitted models were of the form:

$$\sigma^0 = a + b.\ln(B_{AG}) \quad (1)$$

$$\sigma^0 = a + b.\ln(B_{AG}) + c.(\ln(B_{AG}))^2 \quad (2)$$

Where σ^0 is the sigma0 in decibels, B_{AG} is the AGB in Mg ha^{-1}, and a, b and c are constants. Both models were fitted to the observed data, with Equation 2 being preferred if the log-squared term was significantly different from zero. These models were chosen as they produced the highest r^2 and lowest RMSE values of a number of simple models tested. Coefficients and uncertainties are shown in Table 2.

Figure 2

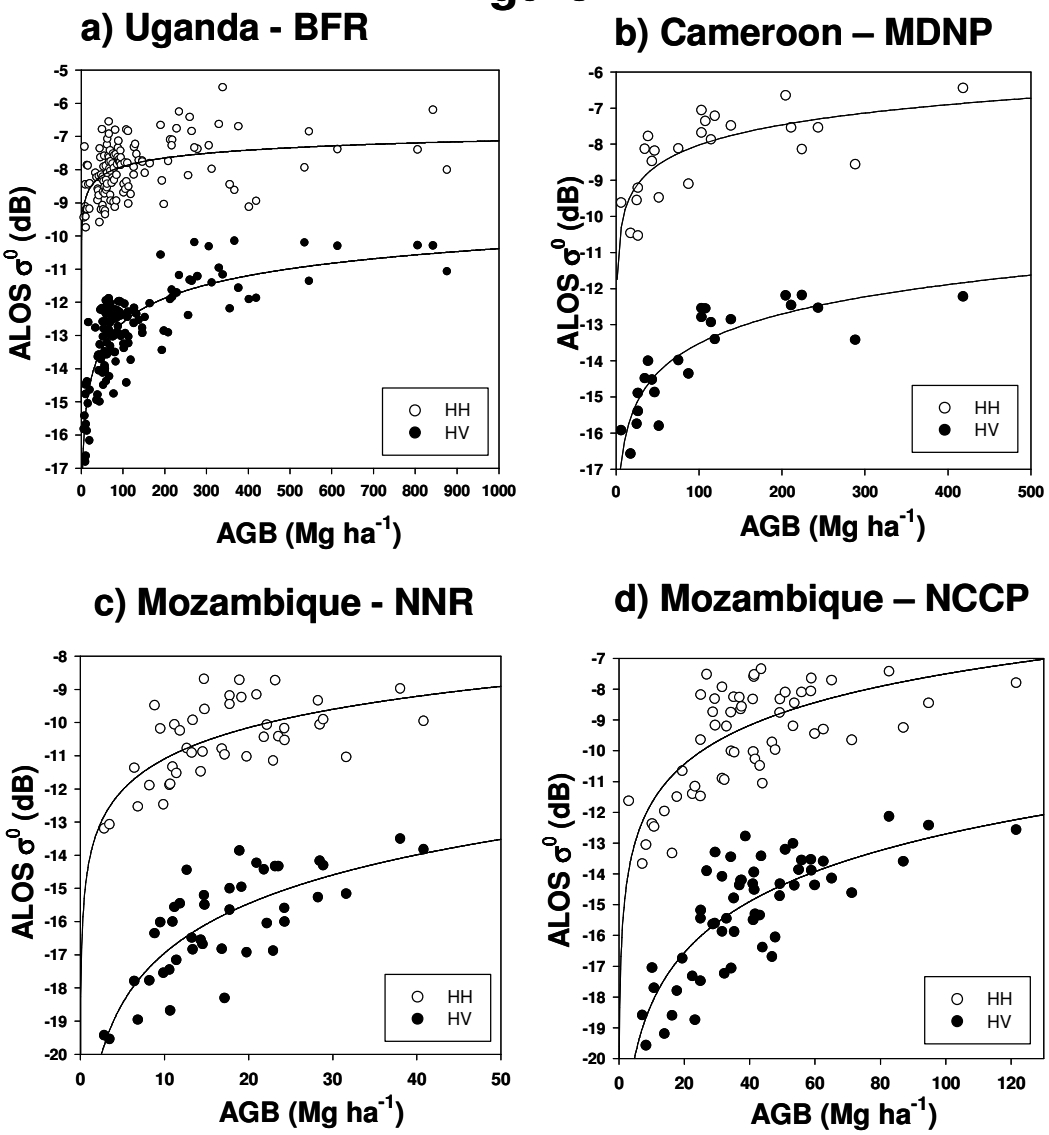

ALOS PALSAR HH and HV backscatter (dB) is plotted against field-measured AGB (Mg ha^{-1}) for a) Budongo Forest Reserve, Uganda, b) Mbam Djerem National Park, Cameroon, c) Niassa Reserve, Mozambique, and d) Nhambita Community Project, Mozambique. Log regressions are also shown.

Table 2 – Table showing the coefficients of the different radar-biomass models

	HH 2-parameter				HV 2-parameter				
Site	**a**	**b**	r^2	***p***	**a**	**b**	r^2	***p***	***N***
MDNP, Cameroon	-11.7 ± 0.7	0.81 ± 0.15	0.55	< 0.0001	-18.9 ± 0.6	1.18 ± 0.14	0.76	< 0.0001	24
BFR, Uganda	-9.7 ± 0.3	0.39 ± 0.07	0.22	< 0.0001	-17.8 ± 0.3	1.12 ± 0.07	0.67	< 0.0001	129
NNR, Mozambique	-14.2 ± 0.7	1.36 ± 0.24	0.44	< 0.0001	-21.9 ± 0.8	2.16 ± 0.27	0.61	< 0.0001	58
NCCP, Mozambique	-15.8 ± 0.9	1.82 ± 0.25	0.49	< 0.0001	-23.7 ± 0.8	2.39 ± 0.23	0.67	< 0.0001	42
Combined	*- 12.7 ± 0.3*	*1.00 ± 0.06*	*0.51*	*< 0.0001*	*-20.3 ± 0.25*	*1.59 ± 0.06*	*0.72*	*< 0.0001*	*253*

	HH 3-parameter					HV 3-parameter				
Site	**a**	**b**	**c**	r^2	***p***	**a**	**b**	**c**	r^2	***p***
MDNP, Cameroon	*log-squared term not significant*					*log-squared term not significant*				
BFR, Uganda	*log-squared term not significant*					-18.9 ± 0.9	1.62 ± 0.41	-0.06 ± 0.02	0.68	< 0.0001
NNR, Mozambique	*log-squared term not significant*					*log-squared term not significant*				
NCCP, Mozambique	*log-squared term not significant*					*log-squared term not significant*				
Combined	*-15.5 ± 0.6*	*2.53 ± 0.32*	*-0.19 ± 0.04*	*0.55*	*< 0.0001*	*-22.4 ± 0.6*	*2.74 ± 0.32*	*-0.15 ± 0.04*	*0.73*	*< 0.0001*

Table showing the coefficients (± standard errors), r-squared and p-values estimated for each of the sites independently, and for the combined dataset. The two models are:

Two parameter model: $\sigma^0 = a + b.\ln(B_{AG})$

Three parameter model: $\sigma^0 = a + b.\ln(B_{AG}) + c.(\ln(B_{AG}))^2$

where σ^0 is the sigma0 in decibels and B_{AG} is the AGB in Mg ha^{-1}. Coefficients for the three-parameter model are not shown for the majority of the individual datasets as the 'c' terms were not significantly different to zero at the 5 % significance level.

Figure 3

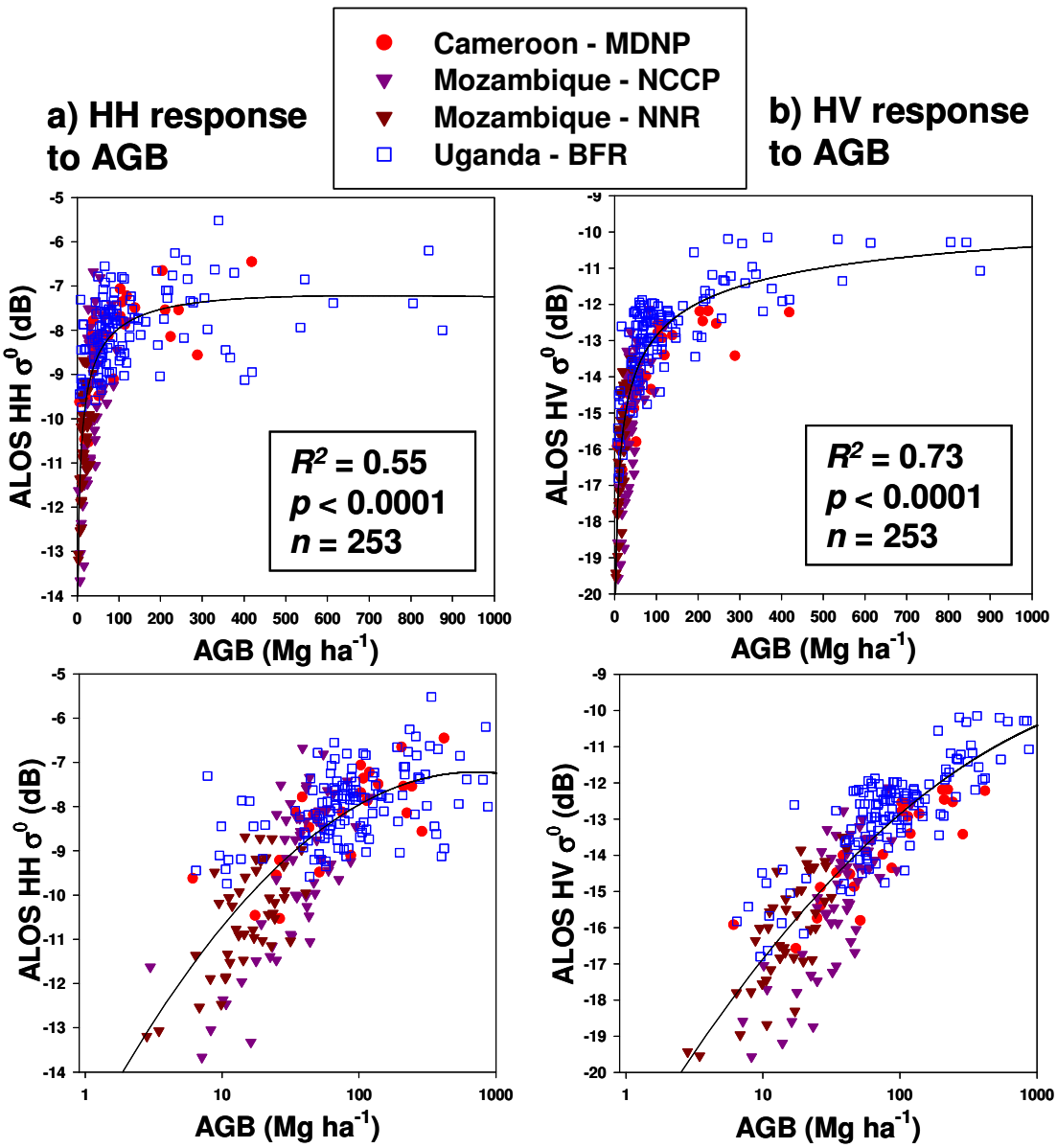

ALOS PALSAR HH and HV backscatter (σ0) are plotted against field-measured AGB (Mg ha-1) for all four sites combined, with the x-axes shown with conventional and log10 scales. Second-order log regression lines are fitted.

5.3.2 Combined AGB-backscatter relationships

Combining the HV sigma0 and AGB values of all four datasets produced a strong relationship, with an r^2 of 0.73 and $p < 0.0001$ using Equation 2, and with some sensitivity clearly still present in the data up to 150-200 Mg ha^{-1} (Figure 3b). There was also a significant relationship with HH ($r^2 = 0.56$, $p < 0.0001$), but this was less

consistent, with saturation occurring at 50-100 Mg ha^{-1} (Figure 3a). The HV relationship fitted was:

$$\sigma^0_{HV} = -22 + 2.73\ln(AGB) - 0.156(\ln(AGB))^2 \quad (3)$$

which rearranged to:

$$AGB = EXP\left[\frac{-2.73 + \sqrt{7.45 - (0.623(22 + \sigma^0_{HV}))}}{-0.311}\right] \quad (4)$$

allows the prediction of AGB from sigma0 values (Figure 4). Attempts were made to combine HH and HV data in a general linear model, but the HH terms were never significant once the HV terms had been taken into account.

Figure 4

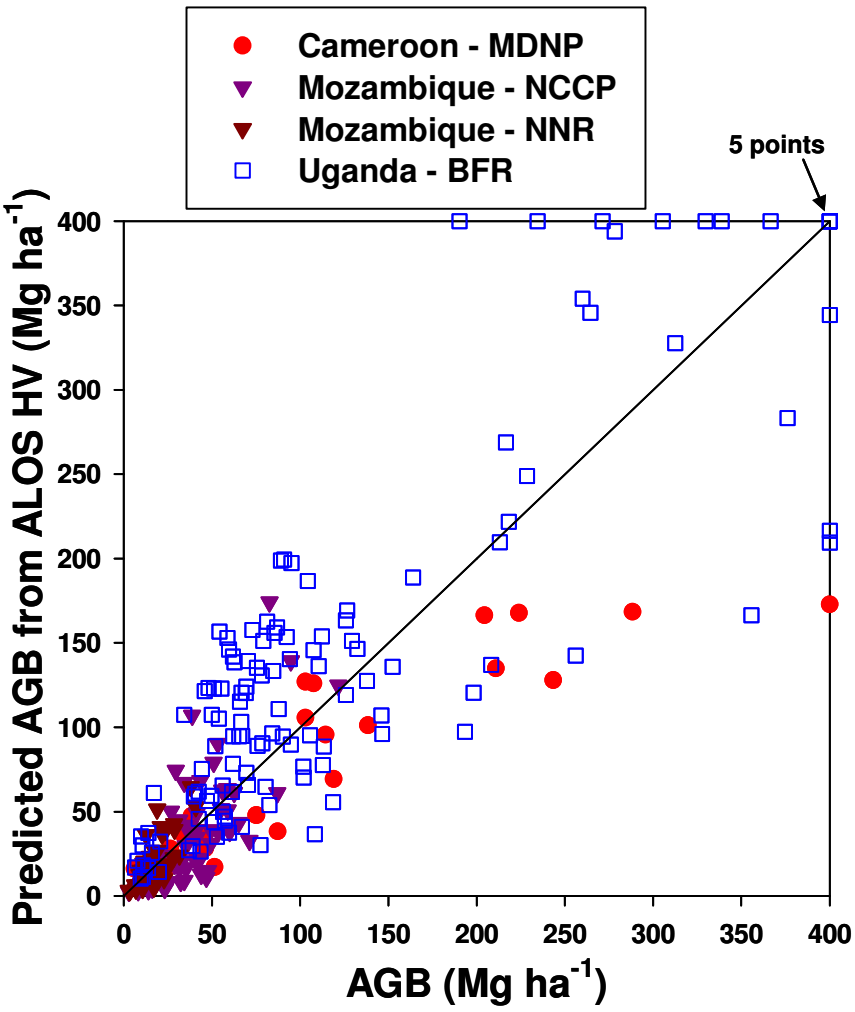

Predicted AGB (Mg ha^{-1}) derived from HV backscatter and the optimum predictive equation (Equation 4) plotted against field-measured AGB (Mg ha^{-1}). In both cases the AGB values were limited at 400 Mg ha^{-1}. A 1:1 line is shown.

5.3.3 Testing consistency

The consistency of the general relationship described above was tested using the four independent datasets. For each of the four sites, AGB predictions and resultant RMSE values were calculated using the site-specific HV equations (Figure 2, Table 2). New equations were then calculated using equations derived from the other three datasets only, and predictions made again using the HV values. Both field and predicted values were limited at 400 Mg ha^{-1}, as all possible sensitivity to AGB will be lost by this point, and thus making predictions at such high AGB values has no validity. Predictions for each site obtained by using an equation developed from the three other sites increased the RMSE by only 12-30 %, and particularly for data points with AGB <150 Mg ha^{-1} the RMSE values remained low (Table 3). The average AGB predicted using site-specific equations was within 30 % of the field-derived average AGB values, and this error increased negligibly when the equations derived from the other three sites were used (Table 3). However, as the biomass estimation error from radar depends on the errors associated with both radar and ground measurements, the true errors could be greater (Chapter 4, *Mitchard et al.*, 2011).

Table 3 –AGB and RMSE for ground plots and predicted values from radar

		Average AGB (Mg ha^{-1})			RMSE (Mg ha^{-1})		RMSE for points < 150 Mg ha^{-1}	
Site	***n***	**Ground data**	**Site-specific**	**Other-three**	**Site-specific**	**Other-three**	**Site-specific**	**Other-three**
MDNP Cameroon	24	114.7	115.5	82.1	61.5	67.5	37.4	22.3
BFR Uganda	129	137.2	176.8	174.0	67.1	74.9	48.8	69.42
NNR Mozambique	42	17.28	19.0	20.2	8.3	12.8	8.3	12.8
NCCP Mozambique	58	40.7	44.6	37.1	19.2	25.2	19.2	25.2

Average AGB and RMSE for field plots predicted from HV data and a site-specific model vs. a model derived from the three other sites (all AGB values were limited at 400 Mg ha-1).

5.4 Discussion

We have found that PALSAR HV backscatter responds strongly to AGB in a consistent manner across four African sites widely separated in space and differing greatly in their vegetation structure. The relationship derived does contain significant prediction errors (±~20 % for plots <150 Mg ha^{-1}). These are partly because L-band SAR does not respond directly to AGB, but to aspects of vegetation structure (Saatchi & Moghaddam, 2000), partially due to spatial variability in structure (Saatchi *et al.*, in press), and partially due to radar calibration and orthorectification (van Zyl, 1990) and field estimation errors propagating through the analysis (Chave *et al.*, 2004). In addition, backscatter responds differently to differing soil and vegetation moisture conditions, and the surface topography, adding to observed prediction errors. For a detailed discussion of the errors and uncertainties involved in this type of analysis see Mitchard *et al.* (2011, Chapter 4). Despite these factors, our analysis shows that AGB can be predicted using radar data for large areas dominated by differing vegetation types with useful accuracy. Notably, errors do not increase dramatically when a continental PALSAR HV-AGB equation, rather than one based on local biomass plots, is used to estimate local AGB.

The better relationship between AGB and the HV rather than HH polarization, and its higher congruence among sites, is to be expected, as this polarization is much less influenced by soil and vegetation moisture than HH (Collins *et al.*, 2009). HV is also less influenced by topography (van Zyl, 1993), though in areas of substantial topographical change significant inaccuracies in estimation and geolocation will still arise.

These results have a higher saturation point and less noise than found in previous studies using L-band HV data, *e.g.* Lucas *et al.*, (2000), Santos *et al.*, (2002), and Viergever *et al.*, (2007). This could be due to structural features of African savannas, or that the data were acquired during the dry season where errors associated with moisture are minimized. Moreover, FBD data is collected at a low incidence angle (34.3°) compared to airborne radar sensors used by the above studies, allowing the radar signal to penetrate deeper into the vegetation canopy. This, in turn, improves

the sensitivity of HV backscatter to AGB and reduces the sensitivity of HH backscatter to AGB because of impacts of soil moisture and roughness. The large number of good quality, well-geolocated field plots in relatively flat areas that were obtained for this study could also be a factor, producing more accurate results than other studies by increasing the signal-to-noise ratio.

When applying Equation 4 to any PALSAR scene over African woodlands and savannas errors of 20-30 % are to be expected (Table 3), probably increasing by another 10 % when uncertainties in allometries are included (Chave *et al.*, 2004; Williams *et al.*, 2008). Local calibration with a network of field plots will remain essential at least for validation, and for estimating a 'correction factor' for adding the AGB of grasses and stems <10 cm. However, this finding of a consistent response to AGB in these widely separated and quite different ecosystems from an operational satellite SAR sensor offers the potential of rapid, accurate, high resolution, and low cost mapping of the lower biomass woody vegetation of Africa, and potentially other regions in the world. Moreover, the 46-day repeat cycle will allow sufficient images to be captured during the year to negate any effects of seasonality and soil moisture, and allow the monitoring of landscapes for any changes in AGB. This finding suggests that utilization of PALSAR data should be essential for projects involving the mapping and monitoring of woodland and savanna biomass, thus having important implications for carbon-credit projects, such as those under proposed REDD schemes.

5.5 Acknowledgements

JAXA, ASF, and USGS provided remote sensing data. E Mitchard is funded by Gatsby Plants, and Cameroon fieldwork was also funded by TROBIT, a NERC-funded consortium, and assisted by WCS Cameroon and Bonaventure Sonké. Kirsty Laughlin assisted with data collection in BFR, where the Budongo Conservation Field Station provided local support. C Ryan was funded by NERC and data collection for NCCP was part-funded by the EU, and assisted by Envirotrade Ltd. N Ribeiro acknowledges the Eduardo Mondlane University – Department of forest engineering, IUCN-Mozambique and SGDRN (Sociedade para Gestao e

Desenvolvimento da Reserva do Niassa). S Lewis is funded by a Royal Society Research Fellowship. Jon Lloyd provided help and expertise.

5.5 References

Brown, S. (1997). *Estimating Biomass and Biomass Change of Tropical Forests*, FAO Forest Paper 134, Rome.

Chave, J., D. Coomes, S. Jansen, S.L. Lewis, N.G. Swenson, & A. E. Zanne. (2009) Towards a worldwide wood economics spectrum. *Ecology Letters,* 12, 351-366.

Chave, J., C. Andalo, S. Brown, M.A. Cairns, J.Q. Chambers, D. Eamus, H. Folster, F. Fromard, N. Higuchi, T. Kira, J. P. Lescure, B.W. Nelson, H. Ogawa, H. Puig, B. Riera, & T. Yamakura. (2005) Tree allometry and improved estimation of carbon stocks and balance in tropical forests. *Oecologia,* 145, 87-99.

Chave, J., R. Condit, S. Aguilar, A. Hernandez, S. Lao, & R. Perez. (2004). Error propagation and scaling for tropical forest biomass estimates. *Philosophical Transactions of the Royal Society of London Series B-Biological Sciences,* 359, 409-420.

Collins, J.N., L.B. Hutley, R.J. Williams, G. Boggs, D. Bell, & R. Bartolo. (2009). Estimating landscape-scale vegetation carbon stocks using airborne multi-frequency polarimetric synthetic aperture radar (SAR) in the savannahs of north Australia. *International Journal of Remote Sensing,* 30, 1141-1159.

Donnellan, A., P. Rosen, J. Graf, A. Loverro, A. Freeman, R. Treuhaft, R. Oberto, M. Simard, E. Rignot, R. Kwok, X.P. Pi, J.B. Blair, W. Abdalati, J. Ranson, H. Zebker, B. Hager, H. Shugart, M. Fahnestock, & R. Dubayah. (2008). Deformation, Ecosystem Structure, & Dynamics of Ice (DESDynI), *2008 IEEE Aerospace Conference,* 163-175.

Grassi, G., S. Monni, S. Federici, F. Achard, & D. Mollicone. (2008). Applying the conservativeness principle to REDD to deal with the uncertainties of the estimates. *Environmental Research Letters,* 3, 2008.

Le Toan, T., H. Baltzer, P. Paillou, K. Papathanassiou, S. Plummer, S. Quegan, F. Rocca, & L. Ulander. (2008). BIOMASS: Candidate Earth Explorer core mission. SP-1313/2. European Space Agency, Noordwijk, The Netherlands.

Lu, D.S. (2006). The potential and challenge of remote sensing-based biomass estimation. *International Journal of Remote Sensing,* 27, 1297-1328.

Lucas, R.M., A.K. Milne, N. Cronin, C. Witte, & R. Denham. (2000). The potential of synthetic aperture radar (SAR) for quantifying the biomass of Australia's woodlands. *Rangeland Journal,* 22, 124-140.

Mayaux, P., E. Bartholome, S. Fritz, & A. Belward. (2000). A new land-cover map of Africa for the year 2000, *Journal of Biogeography,* 31, 861-877.

Mitchard, E.T.A., S.S. Saatchi, I.H. Woodhouse, T.R. Feldpausch, S. L. Lewis, B. Sonké, C. Rowland, & P. Meir. (2011; and this thesis Chapter 4). Measuring biomass changes due to woody encroachment and deforestation/degradation in a forest-savanna boundary region of central Africa using multi-temporal L-band radar backscatter. *Remote Sensing of Environment, In Press.*

Mugasha, A.G., & S. A.O. Chamshama. (2002). Tree biomass and volume estimation for miombo woodlands at Kitulangalo, Morogoro, Tanzania. In: *Indicators and tools for restoration and sustainable management of forests in East Africa*. I-TOO Working Paper, 9.

Nangendo, G.,O. van Straaten, & A.de Gier. (2005). Biodiversity conservation through burning: a case study of woodlands in Budongo Forest Reserve, NW Uganda. In: *African forests between nature and livelihood resources: interdisciplinary studies in conservation and forest management*, edited by M. A. F. Ros-Tonen & T. Dietz. The Edin Mellen Press, New York.

Phillips, O.L., T.R. Baker, T.R. Feldpausch, & R. Brienen. (2009). Field manual for plot establishment and remeasurement, http://www.geog.leeds.ac.uk/projects/rainfor/

Podest, E., & S. Saatchi. (2002). Application of multiscale texture in classifying JERS-1 radar data over tropical vegetation. *International Journal of Remote Sensing,* 23, 1487-1506.

Ribeiro, N.S., S.S. Saatchi, H.H. Shugart, & RA. Washington-Allen. (2008). Aboveground biomass and Leaf Area Index (LAI) mapping for Niassa Reserve, northern Mozambique. *Journal of Geophysical Research-Biogeosciences*, 113, G02S02.

Ryan, C.M., (2009). Carbon cycling, fire and phenology in a tropical savanna woodland in Nhambita, Mozambique. PhD Thesis, University of Edinburgh.

Saatchi, S., M. Marlier, D. Clark, R. Chazdon, & A. Russell. (In press). Impact of Spatial Variability of forest structure on Radar Estimation of Aboveground Biomass in Tropical Forests, *Remote Sensing of Environment.*

Saatchi, S., & M. Moghaddam. (2000). Estimation of crown and stem water content and biomass of boreal forest using polarimetric SAR imagery. *IEEE Transactions on Geoscience and Remote Sensing,* 38, 697-709.

Santos, J.R., M.S.P. Lacruz, L.S. Araujo, & M. Keil. (2002). Savanna and tropical rainforest biomass estimation and spatialization using JERS-1 data. *International Journal of Remote Sensing,* 23, 1217-1229.

Shimada, M., O. Isoguchi, T. Tadono, & K. Isono. (2009). PALSAR radiometric calibration and geometric calibration. *IEEE Transactions on Geoscience and Remote Sensing*, 47, 3915-3932.

van Zyl J. (1990). Calibration of polarimetric radar images using only image parameters and trihedral corner reflector responses. *IEEE Transactions on Geoscience and Remote Sensing*, 28, 337-348.

van Zyl, J. (1993). The effect of topography on radar scattering from vegetated areas. *IEEE Transactions on Geoscience and Remote Sensing,* 31, 153-160.

Viergever, K.M., I.H. Woodhouse, & N. Stuart. (2007). Backscatter and interferometry for estimating above-ground biomass in tropical savanna woodland, *IGARSS: 2007 IEEE International Geoscience and Remote Sensing Symposium, Vols 1-12 - Sensing and Understanding Our Planet*, 2346-2349.

Williams, M., C.M. Ryan, R.M. Rees, E. Sarnbane, J. Femando, & J. Grace. (2008). Carbon sequestration and biodiversity of re-growing miombo woodlands in Mozambique. *Forest Ecology and Management,* 254, 145-155.

6. A Novel Application of Satellite Radar Data: Monitoring Carbon Sequestration and Degradation in a Community Forestry Project in Mozambique

Authors: E.T.A. Mitchard[a], P. Meir[a], C.M. Ryan[a], E.S. Woolen[a], M. Williams[a], L.E. Goodman[b], J.A. Mucavele[b], P. Watts[b], I.H. Woodhouse[a], & S.S. Saatchi[c]

a School of GeoSciences, University of Edinburgh, EH8 9XP, UK

b Envirotrade, 253 Gray's Inn Road, London, WC1X 8QT, UK

c Jet Propulsion Laboratory, California Institute of Technology, Pasadena, CA 91109, USA

This paper is currently in review with *Plant Ecology & Diversity.*

Author contributions: ETAM, PM & CMR devised the research; CMR, ESW, MW, LEG, & JAM collected the field data; ETAM conducted the analysis with assistance from PM, CMR, MW, IHW & SSS; ETAM wrote the paper with assistance and revisions from all other authors.

Abstract

Accurate, dependable and low-cost monitoring systems for Reducing Deforestation from Deforestation and Degradation (REDD+) projects are becoming ever more important, with a huge expansion of projects expected over the next few years. Monitoring systems are used not just to confirm and quantify reduced rates of deforestation in the project area, but also to determine the baseline deforestation rate in a surrounding reference area, and thus must be accurate and able to survey very large areas. Most voluntary-sector REDD+ projects currently use a combination of ground data and classification of high-resolution (10-30 m) optical satellite data. However, such systems suffer from cloud cover, can often underestimate degradation, and by artificially classifying the landscape the natural heterogeneity of biomass over forested land is absent from emission estimates.

Using extensive field data from the Gorongosa Community Carbon Project, a 56 000 ha voluntary carbon project in central Mozambique involving REDD+ and agroforestry project activities, we show that satellite radar data can quantify deforestation and carbon sequestration at a 1 ha resolution. We used cross-polarised radar mosaics from 2007 and 2009 from the ALOS PALSAR satellite sensor to create biomass maps for both time-points, using a network of 58 field plots (ranging from 0.28 – 1 ha in size). We then tracked the changes in aboveground biomass for: 500 ha of farmland where trees had been planted (agroforestry), detecting an increase of 0.4 Mg C ha^{-1} yr^{-1}; 9500 ha of REDD areas, detecting an increase of 1.1 Mg C ha^{-1} yr^{-1}; and 23 ha of known areas where degradation had taken place, detecting a decline in biomass of 3 Mg C ha^{-1} yr^{-1}. However, these averages mask considerable variation in the change detection results. Error bars are hard to assess with this dataset, as we have no ground-based data on rates of carbon accumulation/loss, so we conclude that over this time period we can only be confident in the ability of radar to detect rapid losses in AGB, with us being less confident about the true magnitude of the detected small gains. We conclude that satellite radar is a useful tool for monitoring carbon forestry projects in tropical woodlands, especially for detecting deforestation and degradation, but also, over longer time-periods reliably estimating carbon sequestration, given appropriate ground data are collected.

6.1 Introduction

Since the Reducing Emissions from Deforestation and forest Degradation (REDD+) framework was first discussed in the UN climate negotiations at Bonn in 2005 (UNFCCC, 2005), a number of projects have been set up using a similar conceptual idea, but according to various standards associated with the voluntary carbon market (FAO, 2010). This number is set to increase markedly in the coming year, and these projects will form essential case studies informing the large-scale implementation of REDD+ that will occur following an agreement to implement REDD+ globally at the UNFCCC Conference of Parties meeting in Cancun in December 2010 (UNFCCC, 2010). Although there are many potential benefits to REDD+, including reducing land use change emissions, the loss of biodiversity and ecosystem services from the world's forests, and increasing the standard of living and opportunities for the world's most vulnerable people, this potential will only be realised if it is correctly formulated. There are a number of difficult problems still to be addressed, each with the potential to greatly reduce the net benefit of the whole scheme.

One key issue is how payments will be calculated and monitoring enforced. While it is relatively easy to estimate the area of a forest (and via standard average biomass values per hectare, convert this to an approximate biomass), unlike in afforestation/reforestation/agroforestry projects it is not this quantity that is directly related to payments. Instead it is the difference between the remaining forest and some estimate of how much carbon would have been lost from the project/region/country in the absence of REDD+ activities. This 'baseline' deforestation rate is often calculated using past deforestation rates (calculated from field data, remote sensing, or published regional or national averages), combined with modelling approaches using economic and social data to predict future rates, but there is currently little knowledge of which method of monitoring or future modelling would produce the most accurate estimate (GOFC-GOLD, 2009).

Traditional remote sensing systems for monitoring deforestation are based on the classification of high resolution optical data into polygons, a system exemplified by that used by INPE to track deforestation in the Brazilian Amazon (Hansen *et al.*,

2008). However such methodologies may not be suitable for REDD+, as they do not necessarily detect small-scale deforestation and degradation. This is hard to correct using optical remote sensing, as the loss in vegetation cover caused by degradation or small-scale deforestation can be both small and short-lived (Lu *et al.*, 2005).

A plethora of different methods have been used for baseline calculations by voluntary REDD+ projects. To assess this we have reviewed different methodologies used by the seven voluntary REDD+ projects approved (at the time of writing) by the Climate Community & Biodiversity Alliance (CCBA), a leading standard for certifying the social and environmental benefits of voluntary carbon reduction projects. It can be seen that every one of these projects uses a different methodology to assess their baselines (Table 1). However, within the Project Design Documents (PDDs) for each project there is often very little (or no) justification as to why that particular method is believed appropriate for their case, and in none of the PDDs has any attempt been made to assess how the results would differ with a different method.

Table 1 – Baseline calculations among approved Climate, Community & Biodiversity Alliance (CCBA) REDD+ projects

Project Name	Location	Land use change driver	Baseline deforestation rate calculation method	Source
Kasigau Corridor, Phase 1	Rukinga Sanctuary, SE Kenya	Slash and burn by subsistence farmer population.	Landsat 5 data from 1995 and 1999, manually interpreted, no ground truth data or more recent imagery. Modelling based on fixed rate of deforestation per person per year.	http://www.climate-standards.org/projects/files/taita_taveta_kenya/Rukinga_CCB_PDD_Ver_2_0.pdf
Madre de Dios Amazon REDD Project	Acre River Basin, Madre de Dios, Peru	Illegal logging and slash and burn agriculture by local people and migrants.	Classification of Landsat 5 & 7 images from five time points from 1990 – 2008. Baseline modelled using the spatially explicit model by DINAMICA EGO.	http://www.climate-standards.org/projects/files/madre_peru/Madre_de_Dios_Amazon_REDD_Project_REVISED.pdf
Reducing carbon emissions by protecting a native forest in Tasmania	Northern Midlands Region, Tasmania, Australia	Logging concessions.	One Landsat 5 scene (2006) used to build an aboveground biomass map, using a weak relationship between a vegetation index and biomass. Baseline modelled using the spatially explicit model in the FULCAM software package.	http://www.climate-standards.org/projects/files/tasmania/REDD_Forests_CCB_PDD_FINAL_071609.pdf
Avoided Deforestation in the Coffee Forest of El Salvador	Western, Central and Eastern Regions of El Salvador	Coffee farmers cutting down trees due to falling coffee prices.	Calculated solely from probability that specific coffee farmers will go under in a specific year, with the prediction that their trees will be cut down if they cannot earn a living from coffee.	http://www.climate-standards.org/projects/files/pdd_para_sgs/ficafe_PDD_v06.pdf
The Rimba Raya Biodiversity Reserve REDD Project	Kalimantan (Borneo), Indonesia	Conversion to palm oil.	Classification of 6 Landsat scenes from 2000 – 2008 gives a baseline rate of conversion from forest to palm oil. Uses a simple, non-spatially-explicit model to extrapolate current conversion rates into the future.	http://www.climate-standards.org/projects/files/rimba_raya/CCBA_PDD_Submission_for_Public_Comments_2010_06_05.pdf
The Juma Sustainable Development Reserve Project	Amazonas State, Brazil	Agriculture and cattle grazing.	Uses a sophisticated SimAmazonia 1 spatially explicit model, incorporating INPE PRODES satellite-derived deforestation maps and an extensive set of social and GIS layers to predict future deforestation rates.	http://www.climate-standards.org/projects/files/juma/PDD_Juma_Reserve_RED_Project_v5_0.pdf
Reducing Carbon Emissions from Deforestation in the Ulu Masen Ecosystem	Aceh Province, Sumatra, Indonesia	Agriculture and logging.	Deforestation estimated at 0.86 % per year, and linearly continued into the future, based on an unpublished Conservation International report. Current carbon stocks estimated using default values for disturbed and undisturbed forest, with these two classes differentiated using SPOT satellite imagery from 2006.	http://www.climate-standards.org/projects/files/cambodia/CCB_PDD_Oddar_Meanchey_NORMAL_RES.pdf

One area of consistency within these projects is that six of the seven studies use medium/high-resolution optical imagery (predominantly 30 m resolution Landsat, but also in one case 10 m resolution SPOT) to estimate the baseline deforestation rate, with standard average biomass values for each landcover-type being used to convert this into emissions (as recommended by UNFCCC, 2005). Such data are used because they are relatively simple to interpret and widely available at a low cost. However, they are not ideal for REDD+ because their resolution is too coarse to detect degradation in most cases, and the season of the image and current water status of the vegetation can confuse the interpretation of change (Lu, 2004; Mitchard *et al.*, 2009a, Chapter 3). This latter problem is especially problematic in lower biomass regions, where the phenology of grasses, shrubs and trees can all change markedly over the season (Lu, 2006). Equally the very system of classifying the landscape into distinct classes, each given an average biomass value, can induce very large errors by over-simplification: tropical forests, woodlands and savannas are all highly heterogeneous in biomass values at the small-scale at which deforestation and degradation commonly acts (Scholes *et al.*, 1997; Chave *et al.*, 2004; Ryan *et al.*, In press-b). Therefore, in order to set up a baseline deforestation/degradation rate, and to monitor the result of the project activity, it would be much better to give every pixel a unique biomass value and update this through time.

To our knowledge, no REDD project has yet used satellite radar to monitor changes in aboveground biomass, and thus to calculate baseline deforestation rates, leakage and increases in forest biomass. This is despite the strong relationship that is known to exist between radar backscatter and biomass in tropical ecosystems (Mitchard *et al.*, 2009b), and its known ability to detect deforestation (Thiel *et al.*, 2006; Santoro *et al.*, 2010). This is in part due to the saturation of the radar response to AGB, at around 150 Mg ha^{-1} for cross-polarised L-band radar data (Mitchard *et al.*, 2009b); however this is easily high enough to cover the full range of observed biomass values in dry tropical biomes, and to detect changes in biomass in deforested areas and secondary forest in wetter systems. Satellite radar has an additional advantage over optical data: it can see through cloud, enabling the production of consistent time series over large areas, which is often not possible with optical data in the tropics.

In this paper we use a unique ground dataset including extensive forest plots and information on areas of tree planting, forest protection and degradation to examine the accuracy of a simple methodology using satellite radar backscatter scenes from two different dates. Using a relationship between the forest inventory biomass plot data and radar backscatter, we produce biomass maps from both dates and attempt to track deforestation, degradation and carbon sequestration with sufficient accuracy to enable the estimation of baseline deforestation rates, leakage and verification of reduced deforestation rates.

6.2 Study Area

The Gorongosa Community Carbon Project is located in central Mozambique in the buffer zone of the Gorongosa National Park, and has been running since 2003 as a voluntary-sector carbon forestry project involving using agroforestry and reduced deforestation (REDD) activities. It is certified by Plan Vivo, a community standard based around long-term land use change for carbon sequestration and social/environmental/biodiversity benefits (www.planvivo.org). It is currently managed by Envirotrade (Grace *et al.*, 2010). It began as a pilot scheme of 20 000 ha, but has since been expanded to include 56 000 ha.

The principle landcover type of the area is Miombo woodland, with other areas of more open savanna and shifting agriculture, as well as some gallery forest near rivers. For the years 1956-1969 and 1998-2007 good quality rainfall data is available from Chitengo meteorological station 25 km to the east of Nhambita. These data have a mean annual rainfall of 850 mm, with a standard deviation of 269 mm (Ryan, 2009). There is a strong but variable dry season from April-October, with May-September receiving on average less than 20 mm of rain per month (Ryan, 2009). The soils are highly weathered sandy loams or sandy silt loams, with most woodland burning regularly (Ryan *et al.*, In press-a).

Most farming in the area concentrates around *machambas* – clearings of 1-2 hectares in which crops such as maize, cassava and sorghum are grown for a few years

(Williams *et al.*, 2008). The project activities have concentrated on planting trees within these *machambas* ('agroforestry areas'), and also protecting large areas of Miombo woodland entirely from deforestation ('REDD areas'). The agroforestry activities has taken a variety of forms, with the nitrogen-fixing legumes *Faidherbia albida* and *Gliricidia sepium* being planted within *machambas* between crops to provide shade and improve the soil, and cashew (*Anacardium occidentale*) and mango (*Mangifera indica*) planted for their nuts/fruits, and in both cases providing revenues from voluntary-sector carbon credits to the project participants.

These agroforestry and REDD areas have been accurately mapped, as have some areas of know degradation. Additionally as part of the scientific and monitoring efforts within the area a number of field sites were set up. This makes the site ideal for testing the ability of radar data to detect the biomass changes in these different areas.

6.3 Methods

6.3.1 Field data

6.3.1.1 Biomass plots

A number of permanent and temporary vegetation plots have been set up since the project started. In order to create a ground database to calibrate the response of radar backscatter to aboveground biomass (AGB), we selected 58 plots, namely those that were measured between 2005 and 2009 and are believed to have been undisturbed since they were measured (Figure 1). These included two types of plots: firstly there were 15 x 1 ha square plots, 8 x triangular 0.28 ha plots, and 5 x circular 0.5 ha plots, measured from 2005-2007. For these plots all live stems with a diameter at breast height (1.3 m, DBH) greater than 5 cm were inventoried. Secondly, 30 plots were measured in 2009. These are 125 m x 50 m, essentially rectangular but with rounded ends, with an area of 0.57 ha. All stems with a DBH > 30 cm were measured for the whole plot, and all stems > 5 cm were additionally measured for three 20 m diameter circular subplots within the main plots (Figure 1 for detail of the shape).

Figure 1

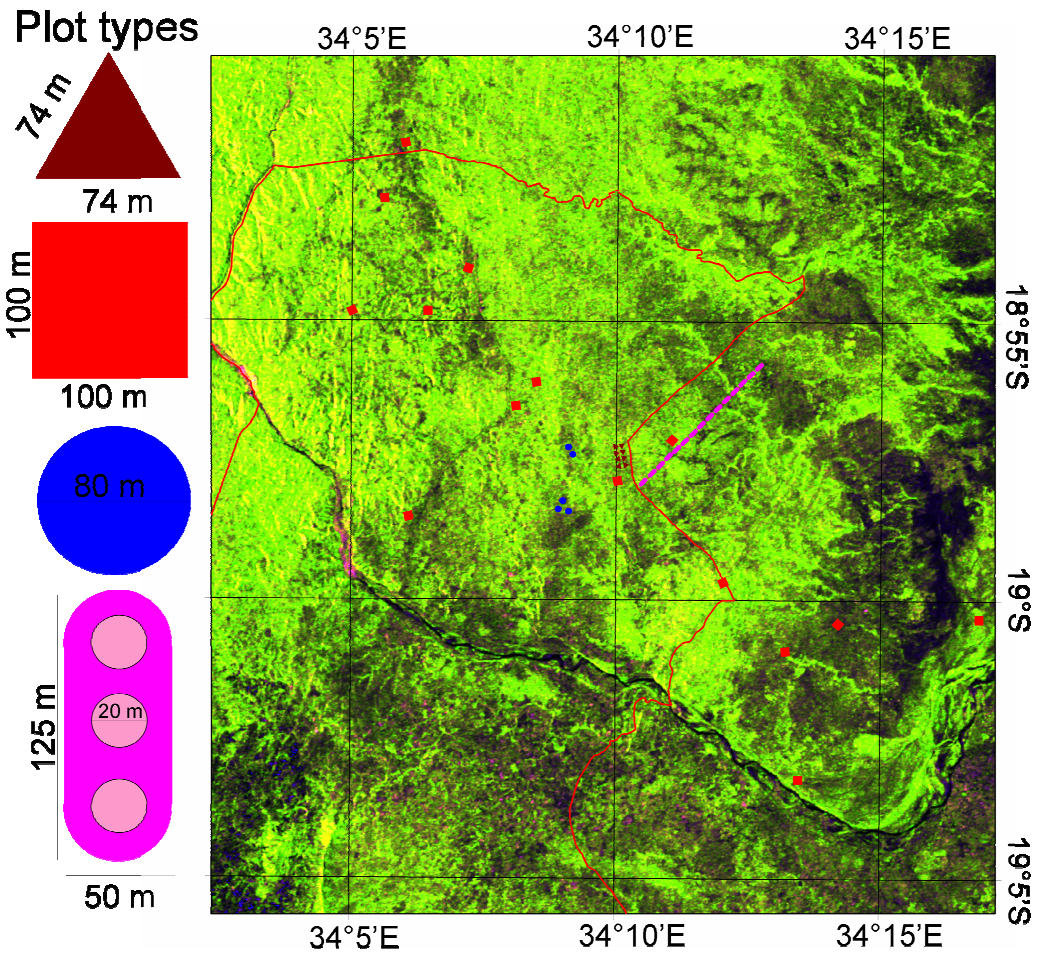

Map showing the location of the field plots used in this study. The field plots are shown with every dimension doubled (area quadrupled) compared to reality. Due to this scaling it was only possible to show 15 of the 30 ellipse-shaped plots: in reality there are two plots under every one shown. The background image is the ALOS PALSAR radar-mosaic from 2007, at 25 m resolution, with the red, green and blue bands being HH, HV, and HH/HV respectively. Bright green and yellow areas correspond to the most forested, with darker colours being low-biomass shrub and croplands. The boundary of the Gorongosa Community Carbon Project is shown in red.

AGB was calculated from DBH for all the plots using an allometric equation developed from destructive harvesting of 29 trees from the site (Ryan *et al.*, In press-a):

$$B = \mathrm{EXP}[2.601(\ln(D_{BH})) - 3.629] \quad (1)$$

Where B = Aboveground biomass (Kg C) and D_{BH} = DBH (cm). For the thirty plots where stems in the range 5 - 30 cm were only measured for subplots, correction was needed to calculate the AGB of the whole plot. To do this the total AGB for stems from 5-30 cm DBH were multiplied by 6.06, the ratio between the area of the subplots and the total plot area, and added to the AGB for stems > 30 cm.

6.3.1.2 Known afforestation and deforestation areas

Trees have been planted by farmers in the area since the carbon sequestration project started in 2003. The boundaries of every agroforestry site have been recorded by GPS, along with the type of planting that has been credited. For the purposes of this project we used all the 546 land parcels where significant tree planting had taken place, involving the planting of native trees, timber trees or fruit trees (average size 0.92 ha). Credits have also been earned by farmers in the project through "border planting", involving planting trees around the edges of their *machambas*. We chose to exclude these from the analysis as such planting would be unlikely to significantly affect the biomass of the whole parcel. We also investigated 38 REDD areas (average size 250 ha), where no new *machambas* should have been created and no significant deforestation or degradation should have occurred.

Additionally six areas where degradation is known to have occurred between 2007 and 2009 had their outlines recorded using GPS data in 2010. These were not clear-cut, but had a significant (but unquantified) portion of their aboveground biomass removed, either for agriculture or for the installation of power lines. These had an average size of 3.5 ha.

6.3.2 Remote Sensing Data

Synthetic Aperture Radar (SAR) data was collected over the field site in 2007 and 2009 from the Phased Array L-band Synthetic Aperture Radar sensor on the Advanced Land Observing Satellite (ALOS) (Table 2), with two scenes needed to cover the field site at each date. These scenes were captured in the Fine-Beam Dual-polarisation (FBD) mode, which has an incidence angle of 34.3°, a ground resolution of ~20 m, and collects in both Horizontal-send Horizontal-receive (HH) and cross-polarised, Horizontal-send Vertical-receive (HV) modes.

Table 2 - Details of ALOS PALSAR scenes

Scene ID	Date	Centre coordinate
ALPSRP075236800	10 July 2007	34.367 E, 18.899 S
ALPSRP077716800	23 June 2007	33.832 E, 18.900 S
ALPSRP196016800	28 September 2009	34.367 E, 18.899 S
ALPSRP185076800	15 July 2009	33.832 E, 18.900 S

The scenes were processed, terrain-corrected and converted to σ^0 ('sigma-nought', backscatter scaled to a log-based dB scale) using MapReady 2.3.6 (Alaska Satellite Facility), all at a 25 m resolution. The terrain-correction required the use of a Digital Elevation Model (DEM), for which we used the 90-m resolution Shuttle Radar Topography Mission (SRTM) DEM processed by the CGIAR Consortium for Spatial Information (http://srtm.csi.cgiar.org/). All subsequent remote sensing analysis was performed using ENVI 4.7 (ITT Systems). The scenes were mosaicked together, with analysis of the join showing no geolocation or brightness differences despite the difference in month of capture for the two scenes in both cases (Table 2). To ensure accurate geolocation with ground points they were warped to a 30 m resolution Landsat 7 L1T scene from the 5th May 2003 (L71167073_07320030513), using a network of 62 ground control points from permanent features such as road junctions and islands, with an RMSE of 14.2 m.

6.3.3 Data analysis

It has been shown previously that radar data relates strongly to AGB in this site (Mitchard *et al.*, 2009b). We developed relationships between the ground AGB plots and radar data separately from 2007 and 2009, and use this to produce AGB maps for both years. The σ^0 values for individual 25 m pixels covering the field sites were converted to power (m^2/m^2) before averaging, so the arithmetic rather than geometric means were used in later calculations. As errors exist on both axes we used a Reduced Major Axis (RMA) regression, as this was seen as more appropriate than ordinary least squares (OLS) regression, for which we would have to assume that the ground data has negligible error. This has not commonly been applied to remote sensing data, but we believe the extensive errors involved in ground estimation from small field plots make it a necessity (Chave *et al.*, 2004). The AGB data were log-transformed, allowing a linear relationships between log(AGB) and σ^0 to be fitted. All statistical analyses were performed using R 2.11. In order to confirm that the results were not due to artefacts inherent in the methodology, an alternative method was also used, involving the cross-calibration of the 2009 scene to 2007 using invariant targets. The methods and results of this alternative analysis are presented in Appendix 4.

As the field data inventory dates varied from 2004-2009, the same field data were used for both time points. It is not believed that the AGB of the field plots has changed much during this period (they have not been deforested, L.E. Goodman & C. Ryan *pers comm.*, and the growth rates of woodland in the area have been shown to be at most ~0.7 Mg C ha^{-1} yr^{-1} (Williams *et al.*, 2008), at the limit of what could be detected by radar). The equations were applied to the remote sensing data after it had been averaged to 100 m pixels, in order to reduce speckle noise, and reduce the impact of slight geolocation inaccuracies on the change detection. These maps were limited at 60 Mg C ha^{-1}, as this biomass value is thought to be around the highest possible in the area (the highest plot in our field dataset is 51.3 Mg C, though higher values might be possible in riverine forest areas), and is also around the limit of L-band radar's sensitivity to AGB (Mitchard *et al.*, 2009b; Mitchard *et al.*, In press).

Finally, the changes in AGB in the agroforestry, degraded and REDD parcels were compared between the two time points. From this an assessment was made as to whether radar would be a suitable forest monitoring system for this site.

6.4. Results

6.4.1 AGB to radar backscatter relationships

Significant relationships between HV radar backscatter and AGB were found for both years (Figure 2).

Figure 2

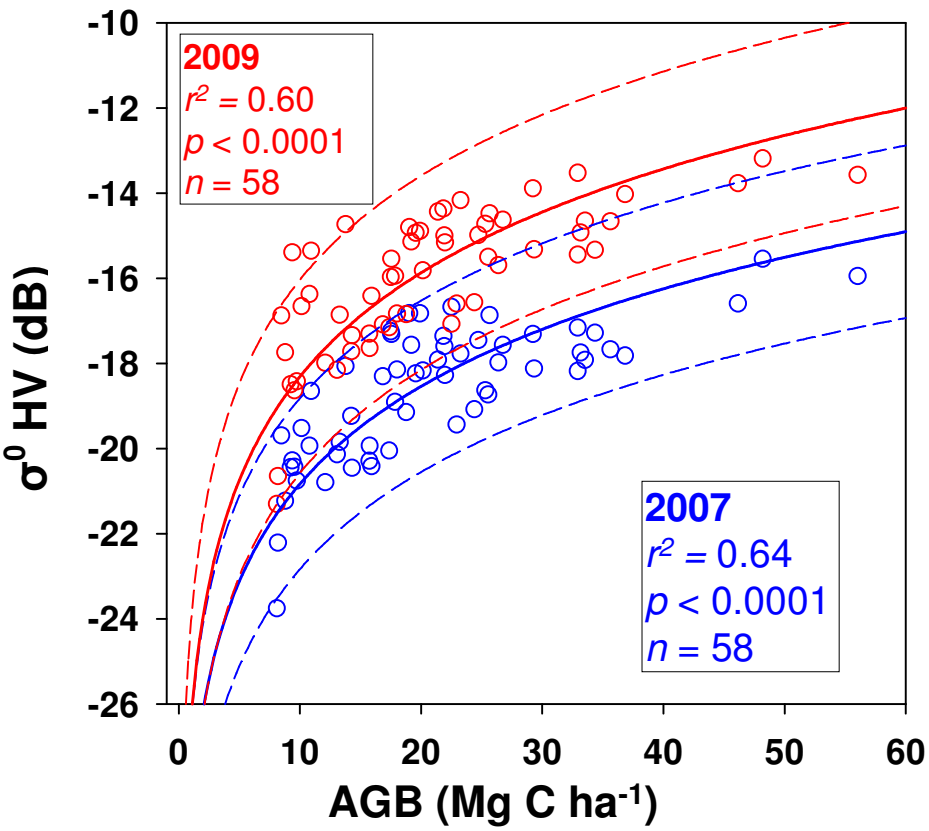

This plot shows HV radar backscatter plotted against aboveground biomass (AGB, Mg C ha^{-1}), for 2007 (blue) and 2009 (red). The field plot AGB values are assumed to be identical at both time points. The solid lines are RMA regressions of radar backscatter (sigma^0) with log AGB, the dotted lines show the prediction intervals for the regressions.

The fitted relationships (fitted using RMA regressions between log-AGB and sigma^0) were of the form:

$$\sigma^0_{HV} = a + b(\log(B)) \quad (2)$$

Which was rearranged to:

$$B = 10\text{^}\left[\frac{\sigma^0_{HV} - a}{b}\right] \quad (3)$$

With coefficients (± 95 % confidence intervals), r^2, p-value, and Root Mean Squared Error (RMSE) for the fits: 2007: a = -28.45 ± 0.96; b = 7.65 ± 0.72; r^2 = 0.64; p < 0.0001; RMSE = 6.4 Mg C ha^{-1}; 2009: a = -26.42 ± 1.12; b = 8.14 ± 0.83; r^2 = 0.60; p < 0.0001; RMSE = 6.3 Mg C ha^{-1}.

Figure 3

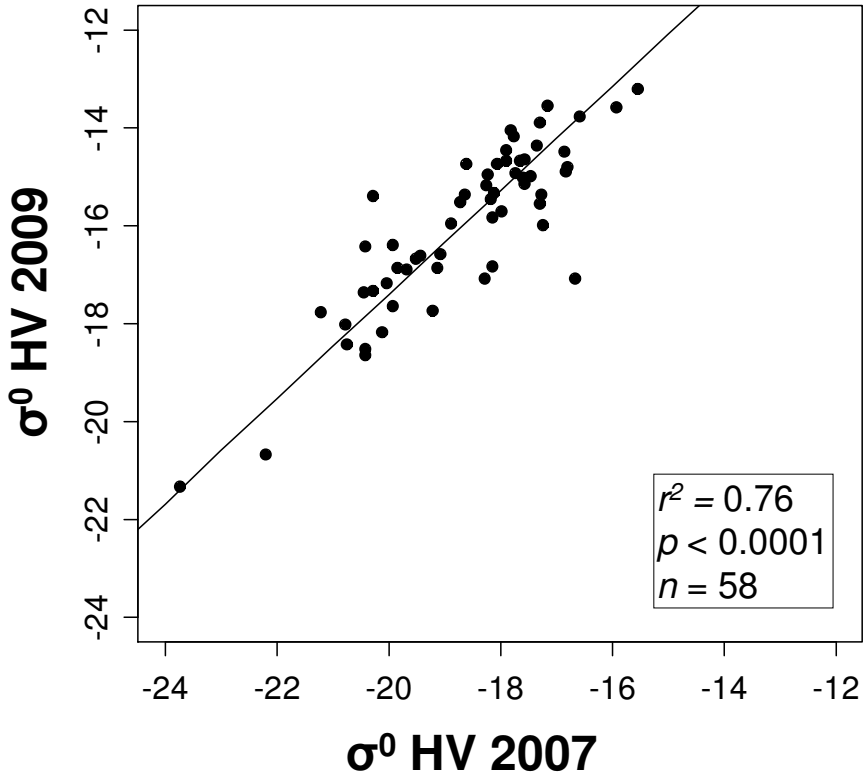

HV backscatter for the 58 plots from 2009 plotted against 2007. A linear RMA regression line is fitted.

The 95 % confidence intervals overlapped for both slope and intercept, suggesting the two relationships were not significantly different. Equally the prediction intervals for the two fits overlap (Figure 2). However, comparing the two sets of backscatter data for each plot directly suggests there are some differences in the two datasets not captured by the above analysis (Figure 3). An RMA regression performed between the backscatter values for each field plot over the two dates suggests that while there is no bias (slope is not significantly different to 1), there is some evidence of gain (the intercept is significantly different from 0 at the 95% confidence level). The fit was of the form:

$$\sigma^0_{HV\,07} = m(\sigma^0_{HV\,09}) + c \quad (4)$$

Where c = -3.63 (95% C.I.: -5.656, -1.638), m = 0.94 (95% C.I. 0.815, 1.064), r^2 = 0.76, $p < 0.0001$.

This suggests the backscatter responses over the field plots for the two years were significantly different, possibly due to calibration issues in the radar product, or possibly due to soil or vegetation moisture being different between the two dates. For the principle methodology therefore, due to the differences in radar responses, the two equations were applied individually to each year to produce biomass maps, as applying the same relationship to both could have reduced accuracy by not incorporating difference in response between backscatter and biomass in the two dates.

In order to confirm that this process was not introducing a bias, an alternative analysis is presented in Appendix 4, which uses invariant targets to cross-calibrate the radar data from 2009 to the 2007 data. This alternative methodology produces very similar change results to the results presented here.

6.4.2 AGB change

The changes within each class is summarised in Table 3 and Figure 4 (and are similar to those found with the alternative methodology, for which results see Appendix 4). AGB in the 500 ha of agroforestry parcels had a detected increase in biomass of +0.74 Mg C ha^{-1} over the two year period. There were marked differences between

the parcels, with many parcels loosing AGB, and some gaining much larger amounts (Figure 4). The increase in the REDD areas was unexpectedly higher than for the areas with active tree planting, at + 2.2 Mg C ha^{-1}, again with high variability.

For the six areas that underwent degradation between 2007 and 2009, a significant loss of biomass was observed. This loss over the two years averaged 6.1 Mg C ha^{-1}, representing approximately 20 % of the original biomass.

Table 3 – AGB change (from radar data) for each landcover history

Landcover	Mean AGB 2007 (Mg C ha^{-1})	Mean AGB 2009 (Mg C ha^{-1})	ÀGB Change (Mg C ha^{-1})	Total area (ha)	Number sites	Average size of site (ha)
Agroforestry	15.22	15.96	**+0.74**	500.45	546	0.92
Deforestation	29.35	23.26	**-6.09**	23.26	6	3.88
REDD	26.38	28.60	**+2.22**	9504.06	38	250.11

Figure 4

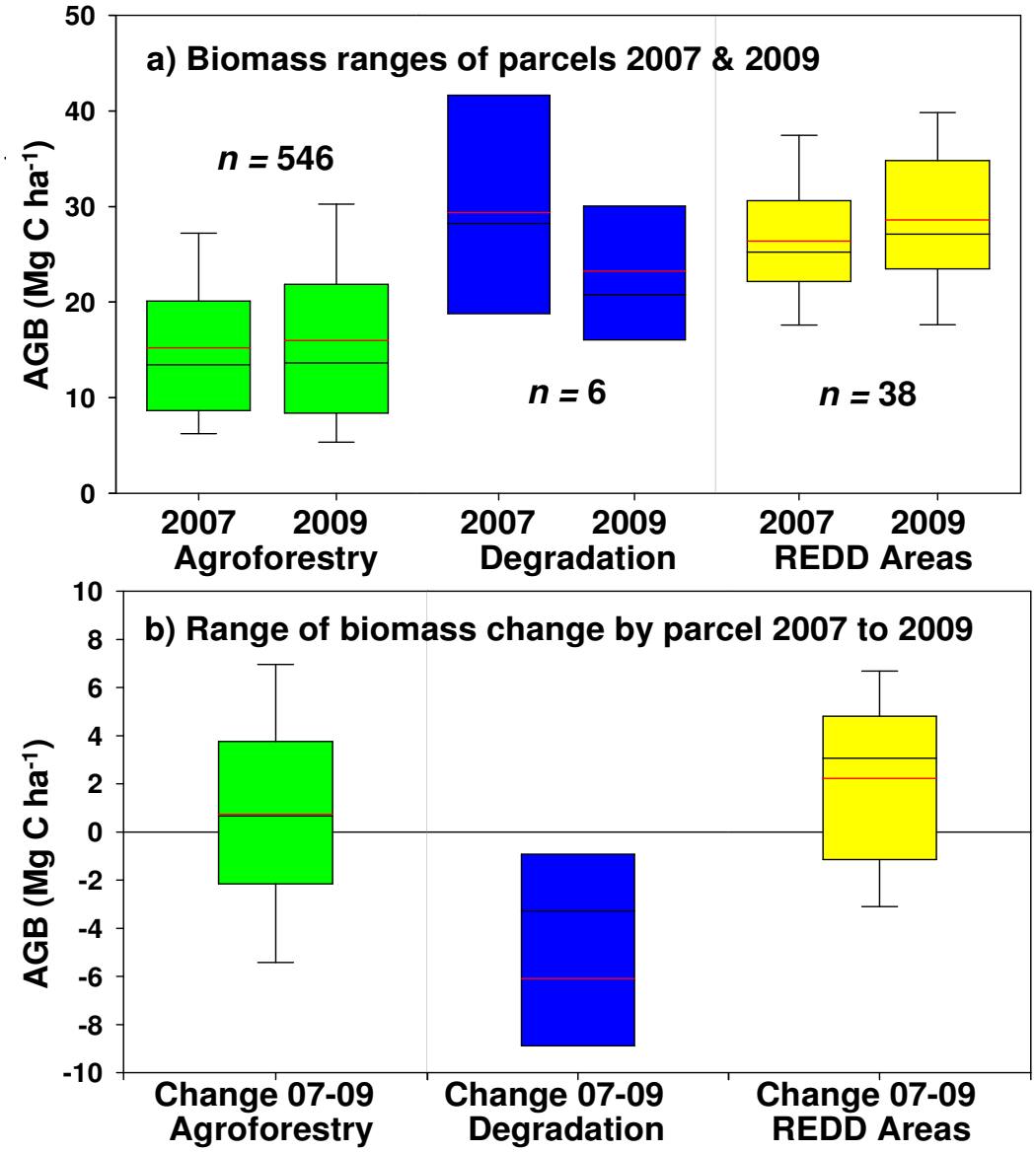

Box and whisker plots showing the a) distribution of AGB values for parcels of land in the three treatment types in 2007 and 2009, and b) the changes in AGB for each parcel from 2007 to 2009. The black line in the middle of each box gives the median value of each dataset, the red line the mean; each 'box' represents the spread of the middle 50 % of the data (between the 25th and 75th quartiles); the 'whiskers' give the 10th and 90th quartiles. For the deforested areas there are only 6 plots, so the 10th and 90th quartiles cannot be calculated.

6.5 Discussion

These results show that satellite radar data can be used to monitor projects involving forest preservation (REDD) and tree-planting. Degradation is clearly detected, and the areas known to have been protected or to have been subject to tree planting show small increases in estimated AGB. However, the high range of changes detected (Figure 4) suggests this method is not accurate enough to give exact change values, at least at a short time-period and at a high resolution (100 m). In addition to the number and size of 3-dimensional scatterers (which correlate with AGB), the radar signal is influenced by radar noise, slight geolocation errors, and moisture in vegetation and in the soil. Therefore we suspect that small changes, such as increases in AGB through the growth of trees over a two-year period, can only be confidently detected either at a coarse resolution or over a long time period. This means that radar analysis should not be used in isolation to quantify payments at a fine scale or over short time-periods, but can be used for coarse scale monitoring, in particular to detect deforestation/degradation.

6.5.1 Uncertainty and ability to detect changes

The finding of a significant difference in the AGB-backscatter relationship between the two years (Figure 2) is an important finding. This is not due to differences in the field plots as the same difference is found when using suspected invariant targets (Appendix 4), but instead must either be due to calibration differences in processing of the radar scenes, or changes in vegetation/soil moisture. The strong linear relationship found in the cross-calibration procedure with the suspected invariant targets (Appendix 4) suggests a calibration difference is the most likely cause. This finding should not affect the uncertainty associated with the results, but stresses the need for field data (ideally collected at the same time as every scene) for interpreting radar data: applying AGB-backscatter relationships without field plot data is not recommended, and thus simple change-detection algorithms relying directly on changes in dB should not be used to detect deforestation c.f. (Santoro *et al.*, 2010).

The RMSE from the original calibrations from the field plots provide some estimation of the accuracy of the methodology: this is 6.4 Mg C ha^{-1} for 2007 and 6.3

Mg C ha^{-1} for 2009. If the error of both measurements are assumed to be independent (the worst case scenario), then estimates of change, involving subtracting one estimate from the other, could be wrong by up to 12.7 Mg C ha^{-1} (though given the average plot size is 0.56 ha, this is likely to be an overestimate compared to the data parcels we are estimating). Using this assumption suggests that this method should only be able to reliably and confidently detect very large gains or losses of AGB at this resolution (in fact only losses, as over a 2-year period gains of more than 12.7 Mg C ha^{-1} are unrealistic). There is, however, some evidence from the dataset that the errors in repeat measurements are not independent, increasing the changes that can be detected. This is as we would suspect, as some of the error inherent in the RMSE is due to local vegetation and terrain conditions, which do not change as much from year to year, rather than to moisture, geolocation and radar noise (Mitchard *et al.*, In press). This evidence is that the RMSE comparing the predicted AGB from the radar data for 2007 and 2009 (which are believed to be unchanged over that 2-year period) is 3.1 Mg C ha^{-1}, which is approximately half the RMSE from the original calibrations. This suggests that estimates of changes over the same area are about 50 % more accurate than either original estimate, and extrapolating this reasoning suggests that changes of ±6 Mg C ha^{-1} between two images should be reliably detectable at a 1-ha resolution.

It has been suspected that errors in change detection are random rather than biased (Mitchard *et al.* in press). This applies only to change estimates, as opposed to estimates of absolute carbon stocks: this is because errors that can introduce biases, for example errors in allometric equations, should affect both AGB estimates approximately equally, cancelling out when one is subtracted from the other (Mitchard *et al.* in press). This would allow the stock and change data derived from radar to be considered more accurate when many pixels are summed together than for individual pixels or land parcels treated alone. Thus, even though the analysis above suggests changes at an individual pixel-level should not necessarily be trusted unless their magnitude is relatively large, when averaging all parcels we should expect the mean value of change to be relatively accurate.

It is possible that the direct relationship between backscatter and AGB results in an underestimate of AGB loss from degradation/deforestation in this environment. This is because after trees have been cut significant resprouting and coppicing occurs (Ryan, 2009), and it is possible that this change in structure will result in higher radar backscatter than its biomass would suggest. Our data do not allow us to quantify this effect, but it warrants further investigation.

6.5.2 Accuracy of detected increases in AGB

This leaves the question as to why the REDD areas appear to have increased considerably faster than the agroforestry areas (2.2 Mg C ha^{-1} vs. 0.74 Mg C ha^{-1} over the two year period). It is possible that this is genuinely occurring on the ground: it is not out of the realms of possibility that the REDD areas could have increased this fast, and for the agroforestry areas new young trees do not necessarily grow that quickly. Regrowing miombo woodland in this area has been observed to increase by 0.5-1.0 Mg C ha^{-1} yr^{-1} (Williams *et al.*, 2008), so an increase of 1.11 Mg C ha^{-1} yr^{-1} observed in the REDD areas is comparable to field data (it should be noted that under the alternative methodology this increase is +0.9 Mg C ha^{-1} yr^{-1}, within this observed range (Appendix 4)). However, this rate is definitely higher than would be expected for relatively mature miombo woodland. As regards the relatively low value for the agroforestry plots, it is possible that changes in the structure of the agroforestry areas (for example, clearing shrubs) could be reducing the perceived increase in backscatter, resulting in an underestimate of biomass increase in these areas. Once again, this can only be assessed by further investigation, involving biomass assessments on plots in these different areas. However, both these changes have a small magnitude and high range (Figure 4), and given the short detection period and errors and uncertainties inherent in this methodology perhaps the only conclusion that can be made is that both agroforestry and REDD areas are on average maintaining or slightly increasing their biomass.

6.5.3 Comparisons and combinations

The radar data we present here has been much more useful to the project management team than attempts to monitor the site using optical data (L. Goodman,

pers. comm.). The detection of degradation (in addition to true deforestation) is very useful, as will be the assessments as to which areas are gaining AGB fastest. Ignoring the issue of cloud cover, optical data cannot detect changes in biomass directly in these ecosystems, instead only being able to detect step changes in the vegetation type. Even then differences in the time of year of the imagery can confound the analyses, as the tree and grass layers gain and loose their vegetation at different times. However, by giving information on landcover, optical data can contribute to the interpretation of the radar data.

Ultimately airborne LiDAR is the most accurate remote-sensing tool for tracking changes in biomass. By giving a three-dimensional picture of a forest at a very high resolution, even small changes can be detected, with no saturation point (Clark *et al.*, 2004). However, though large-scale LiDAR analyses are becoming more feasible (Asner *et al.*, 2010), it still remains very expensive, beyond the budget of the vast majority of carbon forestry projects, and also very time-consuming over large areas. Radar satellite data represents a good alternative, especially for implementing REDD+ monitoring at a national scale.

At a far lower cost to the user than airborne LiDAR is spaceborne LiDAR data. However, there are currently no spaceborne LiDAR systems in operation, and the launch dates for new satellites will not be before 2016. Even then such satellites will not replace radar data, as unlike aircraft-borne LiDAR they will only sample the landsurface, using footprints on the order of 20 m in diameter, rather than centimetres as in aircraft-borne LiDAR. Instead satellite LiDAR will be an excellent tool for calibrating and extrapolating the other remote sensing methodologies.

6.6 Conclusions

We have shown that satellite radar data can be used to monitor changes in AGB in a Miombo woodland agroforestry and avoided deforestation project. Degraded areas showed a marked decrease in estimated carbon stocks, whereas agroforestry and REDD areas showed a small increase. Our field data did not include estimates from the ground as to the magnitude of changes within these areas, so further work is

needed to estimate accuracies of the change detection results. However, these results suggest that a series of annual radar mosaics has the potential to be a very useful monitoring tool for carbon forestry projects.

Acknowledgements

The European Space Agency provided the ALOS PALSAR scenes for this study through a Category 1 application to Edward Mitchard. Landsat data were provided free of charge by the USGS and NASA. The radar data were originally collected and processed by JAXA. SRTM data was collected by NASA, and processed by the CGIAR Consortium for Spatial Information (http://srtm.csi.cgiar.org/). Mapready software, used for processing the radar data, was provided free of charge by the Alaska Satellite Facility. The European Development Fund, NERC and Envirotrade funded the field data collection; Envirotrade also provided logistical support. We acknowledge the following Envirotrade employees who assisted in collecting the field data: Joao 'Dois' Eduardo, Manuel Francisco, Gary Goss, Alfonso Jornal, Zito Lindo, Neto Moulinho, Salomaõ 'Baba' Nhangue, Ramaio Saimone with the supervision of Alastair MacCrimmon, Antonio Serra, and Philip Powell. Meg Coates-Palgrave carried out the tree identification on the Permanent Sample Plots.

Financial Declaration

Envirotrade has a financial interest in the success of the Gorongosa Community Carbon Project, and LG, JM & PW are employees of Envirotrade. This has not influenced the analysis nor the findings presented. EM, PM, CR, EW, MW, IW & SS have no financial interests in the project, and are independently funded as research scientists by their respective institutions.

6.7 References

Asner, G.P., Powell, G.V.N., Mascaro, J., Knapp, D.E., Clark, J.K., Jacobson, J., Kennedy-Bowdoin, T., Balaji, A., Paez-Acosta, G., Victoria, E., Secada, L., Valqui, M., Hughes, R.F., (2010). High-resolution forest carbon stocks and emissions in the Amazon. *Proceedings of the National Academy of Sciences of the United States of America* 107, 16738-16742.

Chave, J., Condit, R., Aguilar, S., Hernandez, A., Lao, S., Perez, R., (2004). Error propagation and scaling for tropical forest biomass estimates. *Philosophical Transactions of the Royal Society of London Series B-Biological Sciences* 359, 409-420.

Clark, M.L., Clark, D.B., Roberts, D.A., (2004). Small-footprint lidar estimation of sub-canopy elevation and tree height in a tropical rain forest landscape. *Remote Sensing of Environment* 91, 68-89.

FAO, (2010). *Global Forests Resources Assessment 2010*. FAO Forestry Paper 163, Rome.

GOFC-GOLD, (2009). *A sourcebook of methods and procedures for monitoring and reporting anthropogenic greenhouse has emissions and removals caused by deforestation, gains and losses of carbon stocks in forests, remaining forests, and forestation.* GOFC-GOLD, Alberta, Canada.

Grace, J., Ryan, C.M., Williams, M., Powell, P., Goodman, L., Tipper, R., (2010). A pilot project to store carbon as biomass in African woodlands. *Carbon Management* 1, 227-235.

Hansen, M.C., Shimabukuro, Y.E., Potapov, P., Pittman, K., (2008). Comparing annual MODIS and PRODES forest cover change data for advancing monitoring of Brazilian forest cover. *Remote Sensing of Environment* 112, 3784-3793.

Lu, D., Mausel, P., Batistella, M., Moran, E., (2005). Land-cover binary change detection methods for use in the moist tropical region of the Amazon: a comparative study. *International Journal of Remote Sensing* 26, 101-114.

Lu, D.S., (2004). Change detection techniques. *International Journal of Remote Sensing* 25, 2365-2401.

Lu, D.S., (2006). The potential and challenge of remote sensing-based biomass estimation. *International Journal of Remote Sensing* 27, 1297-1328.

Mitchard, E.T.A., Saatchi, S.S., Gerard, F.F., Lewis, S.L., Meir, P. (2009a, and this thesis Chapter 3). Measuring Woody Encroachment along a Forest-Savanna Boundary in Central Africa. *Earth Interactions* 13, 1-29.

Mitchard, E.T.A., Saatchi, S., Woodhouse, I., Feldpausch, T., Lewis, S., Sonké, B., Rowland, C., Meir, P. (2011, and this thesis Chapter 4). Measuring biomass changes due to woody encroachment and deforestation/degradation in a forest-savanna boundary region of central Africa using multi-temporal L-band radar backscatter. *Remote Sensing of Environment, In Press*.

Mitchard, E.T.A., Saatchi, S.S., Woodhouse, I.H., Nangendo, G., Ribeiro, N.S., Williams, M., Ryan, C.M., Lewis, S.L., Feldpausch, T.R., Meir, P., (2009b, and this thesis Chapter 5). Using satellite radar backscatter to predict above-ground woody biomass: A consistent relationship across four different African landscapes. *Geophysical Research Letters* 36, L23401.

Ryan, C., (2009). *Carbon cycling, fire and phenology in a tropical savanna woodland in Nhambita, Mozambique*. PhD Thesis, University of Edinburgh, Edinburgh.

Ryan, C., Williams, M., (In press-a). How does fire intensity and frequency affect miombo woodland tree populations and biomass? *Ecological Applications*.

Ryan, C.M., Williams, M., Grace, J., (In press-b). Above- and Belowground Carbon Stocks in a Miombo Woodland Landscape of Mozambique. *Biotropica*.

Santoro, M., Fransson, J.E.S., Eriksson, L.E.B., Ulander, L.M.H., (2010). Clear-Cut Detection in Swedish Boreal Forest Using Multi-Temporal ALOS PALSAR Backscatter Data. *IEEE J. Sel. Top. Appl. Earth Observ. Remote Sens*. 3, 618-631.

Ribeiro, N.S., S.S. Saatchi, H.H. Shugart, & RA. Washington-Allen. (2008). Aboveground biomass and Leaf Area Index (LAI) mapping for Niassa Reserve, northern Mozambique. *Journal of Geophysical Research-Biogeosciences*, 113, G02S02.

Scholes, R.J., Archer, S.R., (1997). Tree-grass interactions in savannas. *Annual Review of Ecology and Systematics* 28, 517-544.

Thiel, C., Drezet, P., Weise, C., Quegan, S., Schmullius, C., (2006). Radar remote sensing for the delineation of forest cover maps and the detection of deforestation. *Forestry* 79, 589-597.

UNFCCC, (2005). Reducing emissions from deforestation in developing countries: approaches to stimulate action – draft conclusions proposed by the president. UNFCCC Secretariat, Bonn, Germany. Available at http://unfccc.int/resource/docs/2005/cop11/eng/l02.pdf.

UNFCCC, (2010). Decision CP16 Section III C, http://unfccc.int/files/meetings/cop_16/application /pdf/cop16_lca.pdf.

Williams, M., Ryan, C.M., Rees, R.M., Sarnbane, E., Femando, J., Grace, J., (2008). Carbon sequestration and biodiversity of re-growing miombo woodlands in Mozambique. *Forest Ecology and Management* 254, 145-155.

7. Mapping tropical forest biomass with radar & spaceborne LiDAR in Lopé National Park, Gabon: overcoming problems of high biomass and persistent cloud

Authors: E.T.A. Mitchard[a], S.S. Saatchi[b], L.J.T. White[c,d,e], K.A. Abernethy[d,e], K.J. Jeffery[c,d,e], S.L. Lewis[f], M. Collins[g], M.A. Lefsky[h], M.E. Leal[i], I.H. Woodhouse[a], & P. Meir[a]

a *School of GeoSciences, The University of Edinburgh, EH8 9XP, UK*

b *Jet Propulsion Laboratory, California Institute of Technology, Pasadena, CA 91109, USA*

c *Agence Nationale des Parcs Nationaux, Batterie IV, B.P. 20379, Libreville, Gabon*

d *School of Natural Sciences, University of Stirling, Stirling, FK9 4LA, UK*

e *Institut de Recherche en Ecologie Tropicale, CENAREST, BP 13354, Libreville*

f *Earth and Biosphere Institute, School of Geography, University of Leeds, LS2 9JT , UK*

g *Grantham Research Institute on Climate Change and the Environment, London School of Economics, London, WC2A 2AZ, UK*

h *Natural Resource Ecology Laboratory, Colorado State University, Fort Collins, Colorado, USA*

i *Missouri Botanical Garden, P.O. Box 299, St. Louis, MO 63166, USA*

As published in *Biogeosicences,* 2011[1].

Author contributions: ETAM, PM, SSS & LJTW devised the research; MC, LJTW, KAA, KJJ, & SLL collected the field data; MAL processed and provided the ICESat GLAS data; ETAM processed the remote sensing data and conducted the analysis with SLL, with input from all other authors; ETAM wrote the paper with assistance and revisions from all other authors.

[1] *In press, Biogeosciences.* Previously published as an interactive discussion paper in *Biogeosicences Discussions, doi:10.5194/bgd-8-8781-2011*, see Appendix 5.

Abstract

Spatially-explicit maps of aboveground biomass are essential for calculating the losses and gains in forest carbon at a regional to national level. The production of such maps across wide areas will become increasingly necessary as international efforts to protect primary forests, such as the REDD+ (Reducing Emissions from Deforestation and forest Degradation) mechanism, come into effect, alongside their use for management and research more generally. However, mapping biomass over high-biomass tropical forest is challenging as (1) direct regressions with optical and radar data saturate, (2) much of the tropics is persistently cloud-covered, reducing the availability of optical data, (3) many regions include steep topography, making the use of radar data complex, (4) while LiDAR data does not suffer from saturation, expensive aircraft-derived data are necessary for complete coverage.

We present a solution to the problems, using a combination of terrain-corrected L-band radar data (ALOS PALSAR), spaceborne LiDAR data (ICESat GLAS) and ground-based data. We map Gabon's Lopé National Park (5000 km^2) because it includes a range of vegetation types from savanna to closed-canopy tropical forest, is topographically complex, has no recent cloud-free high-resolution optical data, and the dense forest is above the saturation point for radar. Our 100 m resolution biomass map is derived from fusing spaceborne LiDAR (7142 ICESat GLAS footprints), 96 ground-based plots (average size 0.8 ha) and an unsupervised classification of terrain-corrected ALOS PALSAR radar data, from which we derive the aboveground biomass stocks of the park to be 78 Tg C (173 Mg C ha^{-1}). This value is consistent with our field data average of 181 Mg C ha^{-1}, from the field plots measured in 2009 covering a total of 78 ha, and which are independent as they were not used for the GLAS-biomass estimation. We estimate an uncertainty of ±25 % on our carbon stock value for the park. This error term includes uncertainties resulting from the use of a generic tropical allometric equation, the use of GLAS data to estimate Lorey's height, and the necessity of separating the landscape into distinct classes.

As there is currently no spaceborne LiDAR satellite in operation (GLAS data is available for 2003-2007 only), this methodology is not suitable for change-detection.

This research underlines the need for new satellite LiDAR data to provide the potential for biomass-change estimates, although this need will not be met before 2015.

7.1 Introduction

Tropical forest ecosystems have a variety of values, monetary and otherwise, that vary markedly with the scale considered. However, many of these, especially the more general benefits at a larger scale, are often not included in decisions relating to whether a forest area remains forest or is converted to another land-use (Engel *et al.* 2008; Stern 2008). At a local scale the individual plants and animals have value, providing non-timber forest products, bushmeat, fuel, and timber (Ahrends *et al.* 2010); at a regional scale they can provide protection from extreme weather events and preserve water supplies (Kaiser & Roumasset 2002; Swetnam *et al.* 2011); and at a global scale they influence global energy budgets through regulation of evapotranspiration, rainfall, and other climatic variables (Meir *et al.* 2006), also acting as a large store of carbon, and as a carbon sink (Phillips *et al.* 2008; Lewis *et al.* 2009a, 2009b). The fate of an area of forest has tended to be controlled by the opportunity to liquidate its considerable timber value (Geist & Lambin 2002) by destructively harvesting its trees, or clearing the land to convert it to a more productive land-use, e.g. agriculture (though in many cases local people derive no benefit from conversion (Rodrigues *et al.* 2009)). Further difficulties arise in the optimum allocation of land to differing uses due to ownership, sovereignty, governance, and the ability and will to monitor forests, particularly at larger scales (Chhatre & Agrawal 2008, 2009).

One approach to preventing this loss of forests has been attempts to place a price on forests, based on the carbon stored, with the avoided emissions from deforestation producing carbon credits tradable on carbon markets. Carbon is only one element of the benefits provided by living forests, but it is one that is relatively tangible and easy to quantify. Past international structures largely excluded pricing existing forest carbon, for example under the United Nations Clean Development Mechanism (CDM), which formed part of the Kyoto Treaty, carbon credits for forestry were

given only for planting new forests or for reforestation, rather than for protecting threatened forests. However, the 2010 Cancun Agreement, agreed at the UNFCCC COP-16 Conference, has created an international framework for valuing forest carbon within the Reducing Emissions from Deforestation and forest Degradation (REDD+) scheme. The aim is to rapidly and radically reduce the rate of deforestation across the tropics, via performance-related payments to countries who reduce deforestation and degradation related carbon emissions (Clements 2010). Though the details of REDD+ are yet to be finalised, its adoption was agreed at COP16 at Cancun, and considerable funds have already been committed (USD 28.3 billion have been committed by the developed world to developing world as fast-start finance for climate mitigation programs, including REDD+ (WRI 2010)). Additionally, REDD+ transfers through government-government agreements and through the voluntary sector have already started, and are accelerating (Clements *et al.* 2010).

Whilst recognising the numerous limitations and problems associated with valuing forests for their carbon alone, a carbon price may establish a minimum value for forests, which may alter the decisions of land-owners in the future. Yet such a price associated with an area of forest can only be assessed if the carbon stocks of an area of forest can be accurately determined, with known uncertainties giving a minimum carbon stock at each time point, and then such a carbon map updated regularly in order to calculate deforestation rates, and therefore payments.

Scientific forest inventory plots are thought to provide the most accurate data on the aboveground biomass (AGB) of an area: these usually involve measuring the diameter at breast height (DBH), and ideally the height and species too, of every tree with a DBH > 10 cm (Brown 1997; Phillips *et al.* 2009). AGB is then estimated from these measurements using either locally-derived or standard allometric equations; there are thought to be significant errors associated with these equations, as destructive harvesting data is not available for specific species and areas. Often for tropical forests a pantropical equation is used, derived from 2410 destructively harvested trees from 27 sites (Chave *et al.* 2005). It includes equations stratified by

forest type, with DBH, height and wood density as parameters. The approach not only reduces the model error compared with using DBH alone, but also increases applicability to tree-types not used to define the original equations.

However, for reasons of resources, time and access, it is not possible to place a sufficient number of plots across a forested area, let alone a country, in order to be able to use such plots to estimate AGB for the whole area directly. Instead remote sensing data is used to extrapolate the plot data across the landscape, with the methods used split into two major categories:

1) Direct statistical relationship between AGB and a remote sensing variable (or variables, possibly including modelled variables and environmental data layers), allowing the production of a continuous AGB map for the area. With the notable exception of LiDAR (see below), such relationships are strong for lower AGB levels but tend to decrease in accuracy and eventually saturate as AGB increases, making higher biomass areas hard to map. This saturation point varies greatly depending both on the source data and vegetation type – ranging from 15 – 70 Mg ha^{-1} for visible/near-infrared vegetation indices (Lu 2006), or from 40 to 150 Mg ha^{-1} for L-band radar data (Lu 2006; Mitchard *et al.* 2009).
2) Classification into landcover type, usually using optical remote sensing data, with each forest type then given an AGB value and these classes then summed to estimate AGB over the whole site. Ideally the average AGB of each class is derived from field data, but often national or continental average values are used (GOFC-GOLD 2009).

An exception to the above is LiDAR data, which by sending a short pulse of laser light either from an aircraft or from space can be used to elucidate the height and even vertical structure of a forest. Tree height, and other LiDAR-derived metrics, have been shown to relate strongly to forest biomass, with no saturation at higher biomass values (Lefsky *et al.* 2005). Unfortunately aircraft LiDAR data acquisition is costly, and the capacity to collect annual data over whole countries does not exist currently. However, space-borne LiDAR data was collected by the ICESat sensor

from 2003 to 2007 (Lefsky 2010), and more such data will be collected firstly by ICESat-2 (Abdalati *et al.* 2010), due for launch in 2015. Aircraft LiDAR tends to be imaging LiDAR, with small footprints collected at a very high density, leading to a detailed 3-dimensional image of the area of interest; however current spaceborne systems are profiling LiDARs, collecting isolated, widely separated footprints, thus sampling the landscape. As a result in order to create full-coverage spatial layers from spaceborne LiDAR the data must be fused with other datasets. It has been shown previously that satellite LiDAR data has great potential for estimating biomass over large areas when fused with radar data (Shugart et al., 2010).

Methods for estimating AGB using the methods above are relatively well established, and have been employed as part of the monitoring schemes for many pilot REDD+ projects (CCBA, 2011), principally involving the classification approach given as 2) above. However, much of the tropics is suboptimal for the above methods in three respects. Firstly, many areas exhibit frequent cloud-cover, making classification using optical data next to impossible. Secondly, many areas include high biomass forest, at which most direct AGB-estimation methods saturate. Third, many forest overlay areas of steep topography, making radar data less useful. Thus methods to overcome these obstacles are needed: this paper aims to demonstrate a new methodology for overcoming these problems.

Here we use the mountainous and persistently cloud-covered Lopé National Park in Gabon to show how a novel AGB estimation method, involving terrain-corrected L-band radar data, field data and GLAS LiDAR data, can accurately determine AGB over a densely forested landscape with specified and relatively high accuracy. The use of high resolution optical data was not possible over this site, as there are no cloud-free SPOT, ASTER or Landsat scenes covering over 50 % of the study site from 2000 to the present day.

7.2 Study Site

The study area is the Lopé National Park (LNP), which is situated in central Gabon (Figure 1), and covers an area of 4948 km^2; it has been a wildlife reserve since 1946,

and a National Park since 2002 (Figure 1). Though surrounded by closed-canopy tropical rainforest typical of the Congo basin, the north of the park is characterised by savanna and a mosaic of low-biomass forest types (principally monodominant Okoumé (*Aucoumea klaineana*) forest, and distinctive open-canopy Marantaceae forest, so-called because the understory is dominated by a thick layer of herbaceous plants of the Marantaceae and Zingiberaceae families). The forest-savanna mosaic is a remnant of the landscape that dominated much of the Congo basin during the Last Glacial Maximum (LGM) (White, 2001). At the LGM savanna covered the majority of LNP, but the increase in precipitation has since caused an expansion of forest to cover nearly the whole area, with forest continuing to expand into the savannas today (White, 2001). Certain forests in the south of the study area may represent Pleistocene refuges that survived through successive glacial maxima that resulted in savanna expansion (Leal 2001), but much of the northern half of LNP was dominated by savanna until an apparent large reduction in the human population c. 1400 BP (Oslisly & White 1995). In about 1920 the colonial administration moved all villages from the interior of the LNP, initiating large-scale forest regeneration in previously cultivated zones (Pourtier 1989). The savanna that remains is maintained by a combination of now limited human burning and the rain-shadow of the Massif du Chaillu, which reduces rainfall to 1500 mm yr^{-1} in the north of the park (White & Abernethy 1997); whereas rainfall in the south of the park is ~2500 mm yr^{-1} (Tropical Rainfall Measuring Mission (TRMM) 3B43 V6 data January 1998 to January 2010). The site features significant topographic variation and dissection: the altitude ranges from 72 to 980 m above sea level, and 23.7 % of the study area has a slope great than 20 % (11.3°).

Figure 1

a) Landcover map

b) PALSAR radar (2009) with GLAS footprints

c) Lopé National Park only, showing field plots

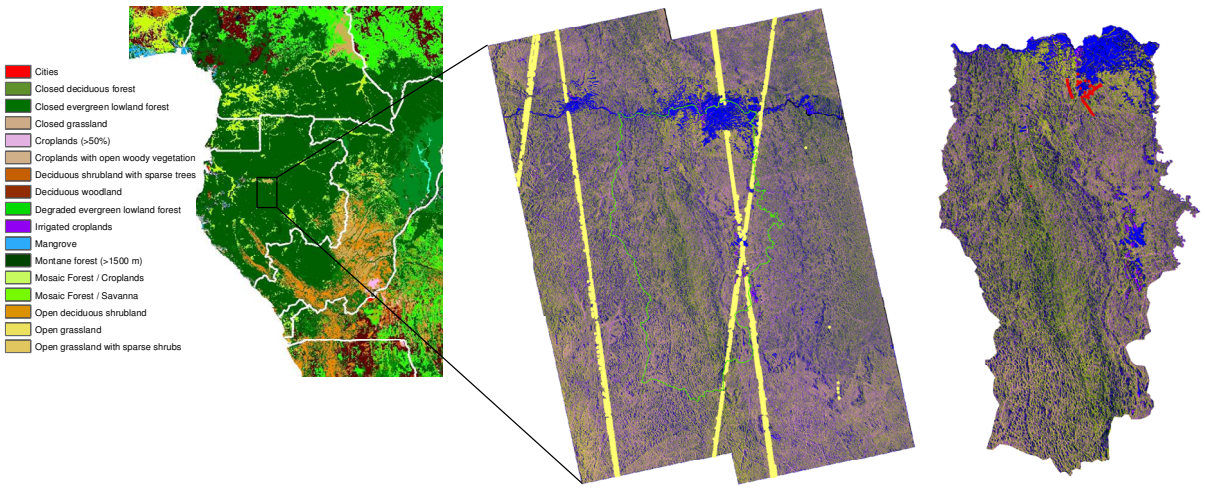

a) Map showing the location of the field site within a landcover map for the year 2000 (Mayaux et al., 2004), b) the ALOS PALSAR radar mosaic (HH in red, HV in green, and HH/HV in blue) shown with the location of the GLAS lidar footprints post-filtering, c) the same radar image, but cut out around Lopé National Park, showing the location of the field plots.

7.3 Methods

The processing chain is displayed in Figure 2, and described in the 7.3.1-7.3.5 below.

7.3.1 Field Data

A wealth of forestry data has been collected in the LNP since 1983. However, in order to investigate the relationship between radar data and AGB we only used the plots that were re-measured in 2009, which include 3 transects of length 5 km, 20 plots of 20m x 40 m, and one plot of 100 m x 100 m.

Figure 2 – Processing Chain

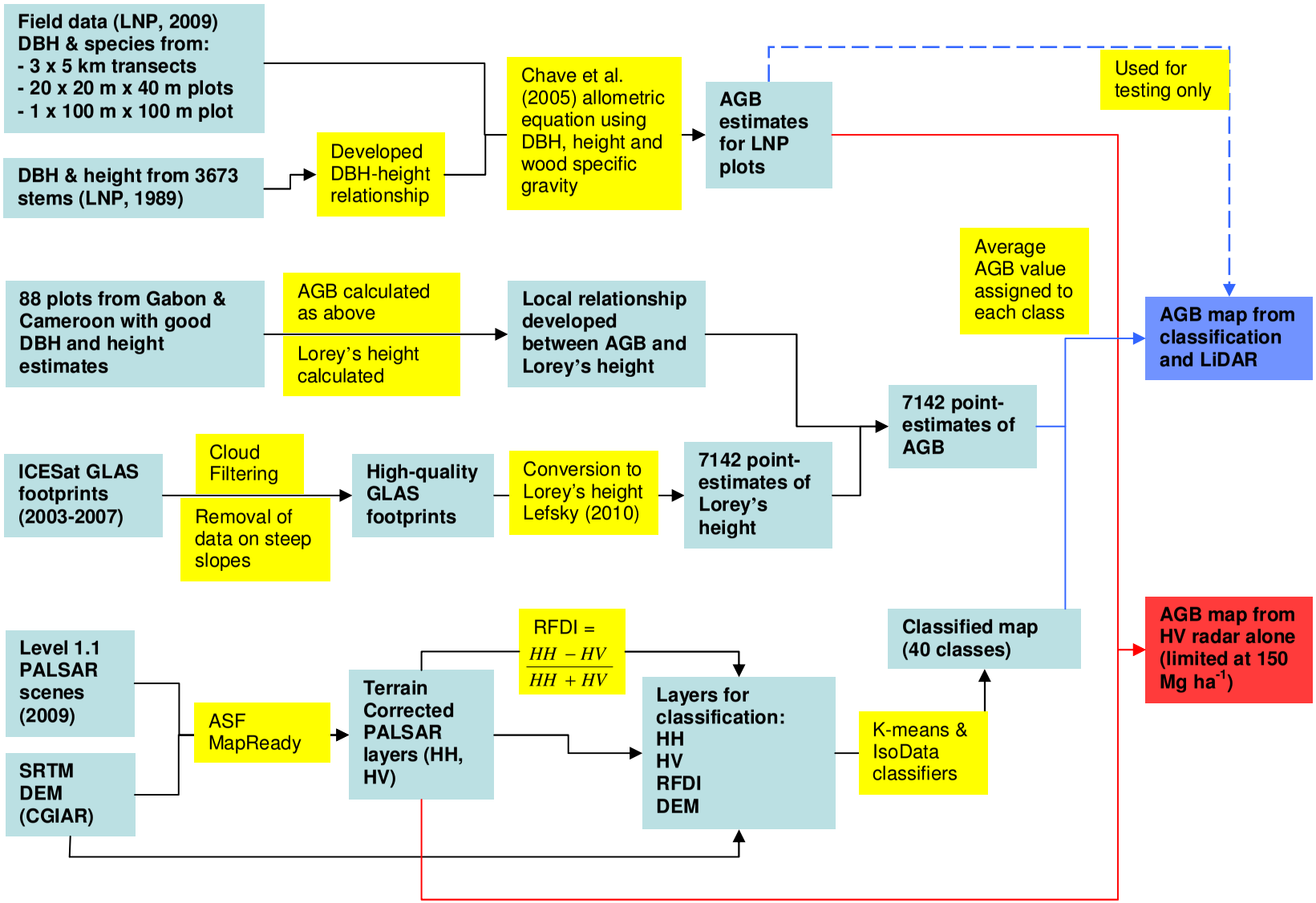

For the 20 x 40 m plots and the 100 m x 100 m plot all stems with a diameter at breast height (DBH) ≥10 cm had their DBH measured and were identified to the species level (or genus if species identification was not possible). The locations of all four corners of each plot were determined using a Garmin 60 CSx GPS. For the 5 km transects all stems > 10 cm DBH were only measured for a 5 m wide band, with stems > 70 cm DBH being measured for a 50 m band. We therefore split each transect into 25 sections of 200 m x 50 m, giving 25 plots of 1 ha size per transect. To calculate AGB values for each 1 ha section of the 50 m wide band, the AGB of the stems between 10 and 70 cm DBH (in the 5 m band) were multiplied by ten and added to the AGB for the >70 cm stems.

Tree heights were measured in addition to DBH for 3673 stems along the 5 m band of the five transects in 1989. The tree heights were estimated to the nearest meter using a clinometer. These data were used to build a site-specific relationship between tree height and DBH.

AGB was estimated using the moist tropical forest equation from (Chave et al., 2005), involving DBH (*D*), height (*H*) and wood specific gravity (ρ):

$$AGB = 0.0509\left[\rho D^2 H\right] \quad (1)$$

This equation gives AGB in kg dry biomass; throughout this study AGB has been reported in Mg ha^{-1} dry biomass, but where appropriate this has been converted to carbon (Mg C) using the standard conversion factor of 0.5 (IPCC 2003). Wood specific gravity data were derived from the Global Wood Density database (Chave *et al.* 2009a; Chave *et al.* 2009b): species-specific data were available for 64 % of stems, for the rest the average density for members of the genus from tropical Africa were used.

7.3.2 Lorey's height to AGB relationships

The method used to process the LiDAR data gave an estimate of Lorey's height, a basal-area weighted measure of height (Section 3.4). In order to develop a relationship between Lorey's height and AGB, Lorey's height (*L*) was calculated for

each plot using height in metres (H) and basal area in m^2 (A_B, calculated as $\pi(DBH/2)^2$) for each stem using the following equation:

$$L = \frac{\sum(H.A_B)}{\sum A_B} \quad (2)$$

For calculating Lorey's height from the ground plots we preferred plots for which we had height measurements for every stem – using DBH-height relationships reduces the accuracy of height measurements, and also introduces a spurious correlation as both axes will scale directly with basal area, with only wood density providing the scatter. We therefore used the 5 m band data of the five LNP transects from 1989 (split into 0.25 ha sections, a similar size to the LiDAR footprints, giving 50 plots in total), but this did not give a sufficient number of plots, especially for lower AGB values, to enable us to build up a suitable relationship. To resolve this issue we added the 20 plots of 20 m x 40 m plots from LNP; though we had to use the DBH-height relationship for these, every stem that was broken off, damaged or deformed was noted in the field notes, reducing errors. We also added plots from nearby areas where DBH and height had been measured for every stem, adding four more 1 ha plots from Gabon (Lewis *et al.* 2009b), and 14 plots from Mbam Djerem National Park, on the forest-savanna transition zone in Cameroon, which has a similar vegetation type and rainfall to LNP (Mitchard *et al.* In press). In total this gave 88 plots where field-measured Lorey's height and AGB could be compared.

7.3.3 Radar data

Six ALOS PALSAR (Advanced Land Observing Satellite Phased Array L-band SAR) scenes captured on the 25th June 2009 (3 scenes) and 24th July 2009 (3 scenes) were acquired through an ESA (European Space Agency) Category-1 Proposal. These were FBD (Fine-Beam Dual-polarization) scenes, provided at the 1.1 processing level. We projected the scenes using the Alaska Satellite Facility's software package MapReady 2.3. Terrain slope has a significant impact on radar scenes, impacting both the projection of the slant-range image, and the backscatter values, which due to changes in the radar incidence angle are increased on slopes facing the sensor, and reduced on slopes facing away. To perform the terrain

correction we needed a Digital Elevation Model (DEM): we used the 90 m resolution Shuttle Radar Topography Mission (SRTM) dataset, using the void-filled Version 4 product produced by CGIAR-CSI (http://srtm.csi.cgiar.org). We used MapReady to correct geolocation and radiometric problems due to terrain (including adjusting pixel areas due to incidence angle, adjusting backscatter values to account for radar incidence angle, and interpolating layover/shadow regions). The terrain correction was successful, with the topography not visible in the corrected HH and HV images, and there being no residual correlation between the corrected backscatter values and the radar incidence angle.

All processing, including the extraction of radar data values for the field plots, was performed at a 100 m (1 ha) spatial resolution: the same scale as the majority of the field plots (76 out of 96), and a scale at which the heterogeneity of forest structure is normally distributed (Chave *et al.* 2004), and at which we are confident in our geolocation.

7.3.4 LiDAR data

Space-borne LiDAR data were collected from 2003-2007 over LNP by the Geoscience Laser Altimeter System (GLAS) on the Ice Cloud and Land Elevation Satellite (ICESat). These data are in the form of circular footprints, with each footprint ranging from 0.2 – 0.25 ha in size, depending on the terrain slope. In total data for 37 021 individual footprints overlapping with the PALSAR scenes were recorded. However, the majority of these were removed through cloud filtering, with a further 3000 points removed as they fell on steep slopes (> 20 %), where accuracy decreases markedly (Lefsky *et al.* 2005). This left 7140 GLAS footprints coincident with the six radar scenes (Figure 1b). Features of the waveforms were correlated with measured Lorey's height from 95 plots in three forest sites in the Amazon, with field plots coincident with GLAS data (r^2 = 0.83, RMSE = 3.3 m, n=95), see (Lefsky 2010) for details.

7.3.5 Unsupervised classification

Due to saturation, direct regression between the field plots data and radar backscatter, as performed for example in (Mitchard *et al.* 2009), was thought to be poorly suited to estimating AGB for LNP, apart from in the small area of savanna in the north. Though we performed the analysis for comparison, it is the LiDAR data that has the potential to estimate the AGB of LNP above the saturation limit of the radar. Rather than simply averaging the heights of the LiDAR footprints to get an average value for the park, we pursued a solution that would include the spatial information on vegetation structure contained in the radar data.

The Radar Forest Degradation Index (RFDI) (Saatchi *et al.*, in press) is a ratio between the power of the HH and HV polarizations, designed to assess the strength of the double-bounce term. It is defined as:

$$RFDI = \frac{HH - HV}{HH + HV} \quad (3)$$

and picks out this term because HH is sensitive to both volume scattering and double bounce, whereas HV is mostly sensitive to volume scattering. We therefore found it to be a useful layer in helping to differentiate different vegetation types, pulling out more information from the dual-polarisation radar data.

We therefore used the radar backscatter (in HH and HV polarisations), RFDI, and elevation (from the DEM) to develop an unsupervised classification of the park (Figure 3). We aimed to use as many classes as possible, to enable us to fully characterise the different vegetation structures, and after experimentation we chose 40 classes as this left each class with at least 100 LiDAR observations.

Figure 3

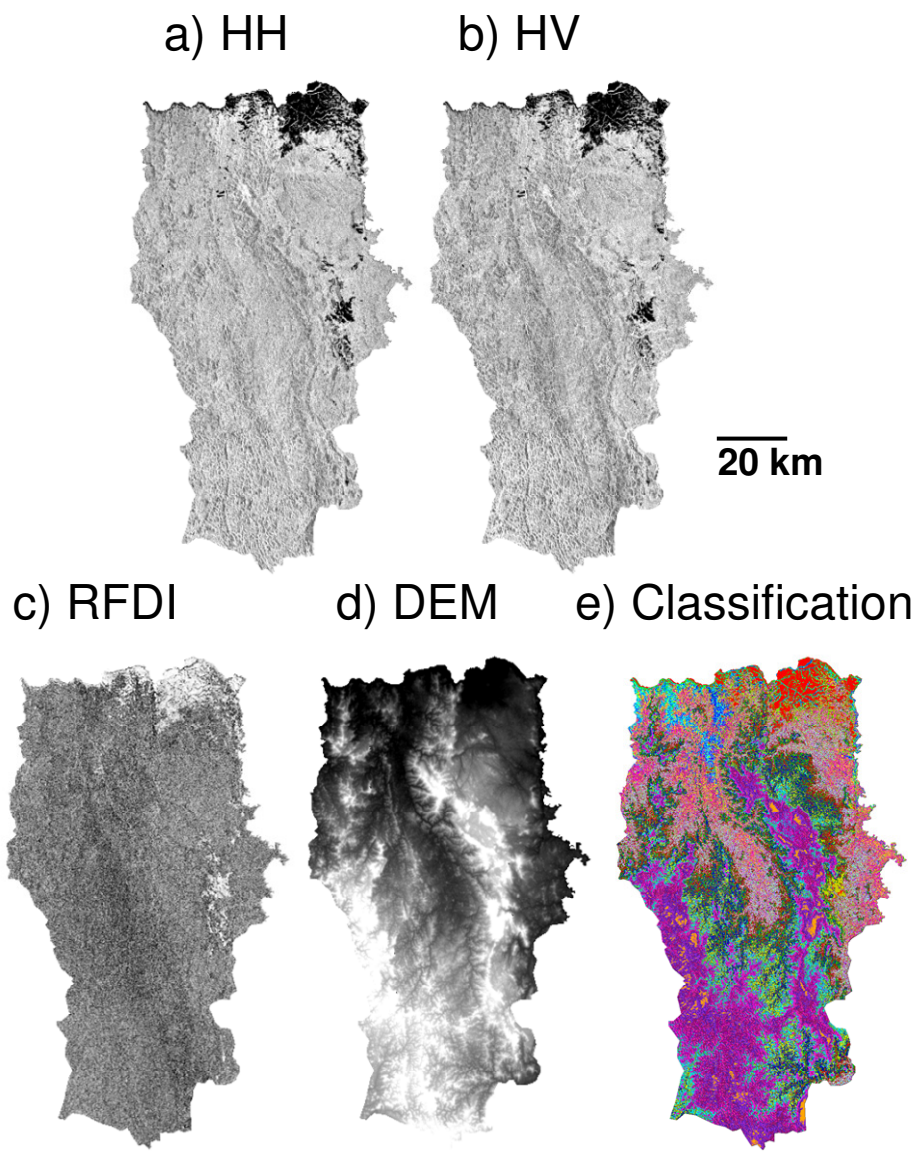

Images of Lopé National Park using a) PALSAR HH, b) PALSAR HV, c) Radar Forest Degradation Index (RFDI), d) Digital Elevation Model (DEM), e) Classified map, showing 40 classes with arbitrary colours.

The classification was performed using ENVI 4.7 (ITT Systems), using both the K-means and IsoData unsupervised classification methods, with 40 classes and 100 iterations. All four bands (HH, HV, RFDI & DEM height) were scaled to have an identical mean and standard deviation. At this number of iterations both methodologies produced an identical classified map. We then extracted the derived AGB value from each GLAS footprint within each class, averaged these AGB

values, and assigned these mean AGB values to each class in order to produce an AGB map.

7.4 Results

7.4.1 Stem heights to DBH

We required AGB estimates for the field plots, but though we had DBH and species data for every stem, no stem height data was collected in 2009. Therefore we wished to develop a site-specific relationship between DBH and stem height, based on 3673 stem DBH and heights measured over four transects in 1989. The stem heights (H) were strongly correlated with DBH (D) (r^2= 0.62, p < 0.0001, standard error of estimate = 4.97 m, Figure 4).

Figure 4

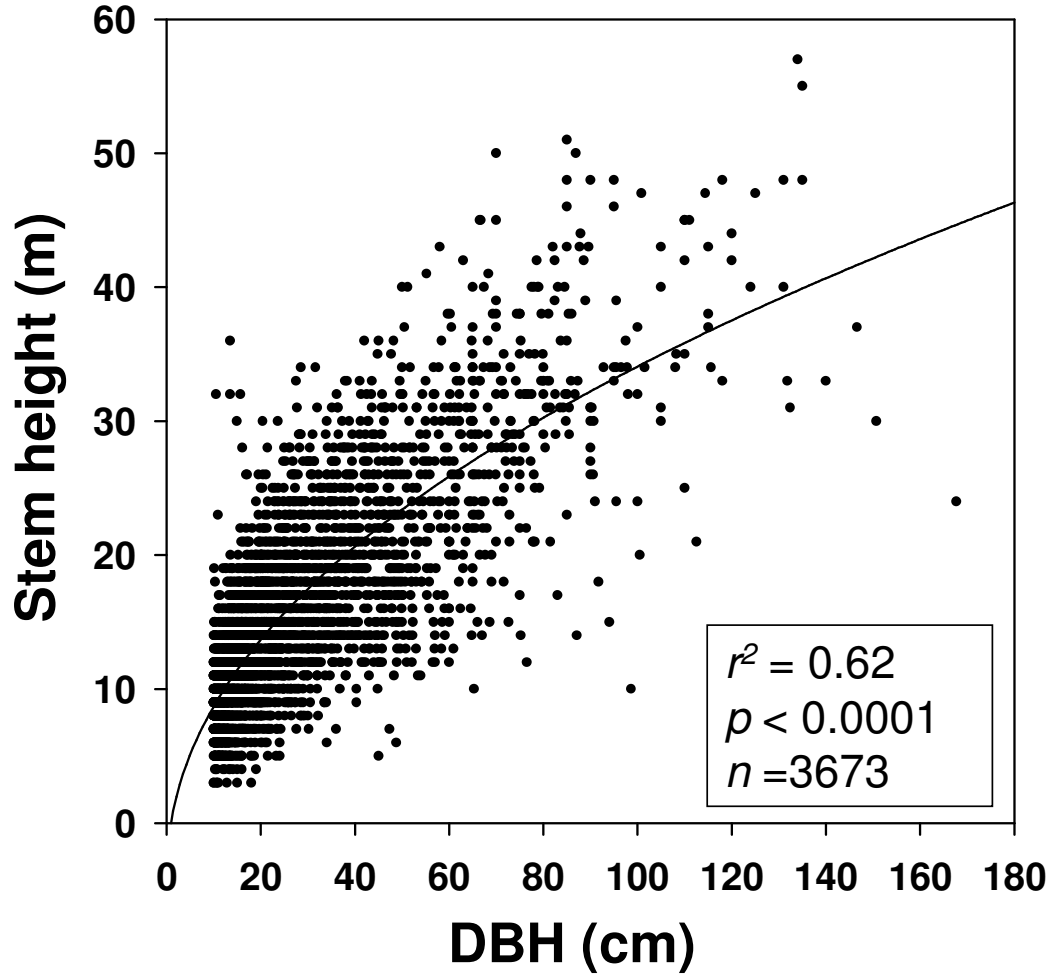

The relationship between diameter (DBH, cm) and height (m) for 3673 trees measured in Lopé National Park in 1989.

The fitted equation was:

$$H = a + b\left[D^{c} \right] \quad (3)$$

with coefficients (± standard errors): a = -4.25 ±1.20, b = 4.37 ±0.90, c = 0.472 ± 0.037. This relationship was applied to the stems measured in 2009, allowing AGB to be calculated from the Chave *et al.* (2005) equation involving DBH, wood density and height.

Figure 5

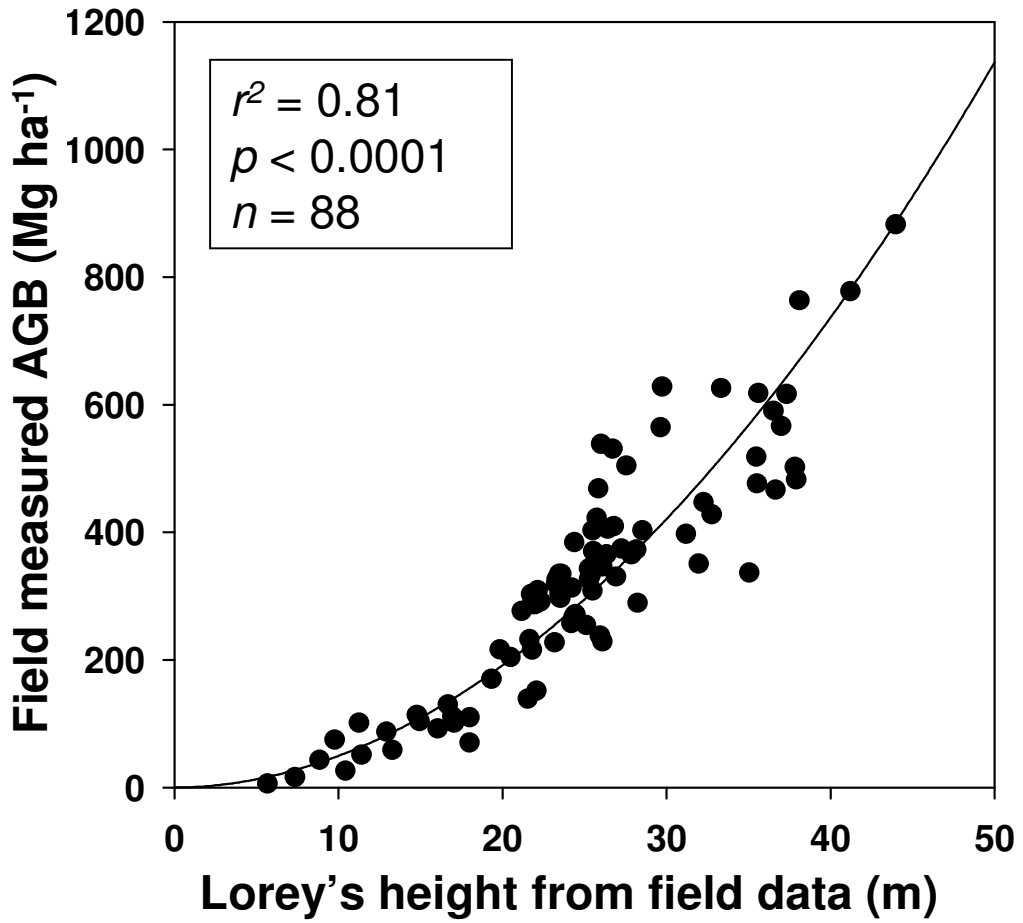

Field measured AGB for 88 field plots from Lopé in Gabon, nearby plots in Gabon, and Mbam Djerem National Park in Cameroon, plotted against field-measured Lorey's height for these plots. This plot dataset is different to that used for the radar-biomass relationship, as the emphasis here was for plots from the same vegetation-type where every stem was measured, to produce an accurate regression relationship between Lorey's height and AGB.

7.4.2 Lorey's height to field biomass

We had estimates of Lorey's height from the LiDAR data, but needed to use field plot data to convert these Lorey's height estimates into AGB. To do this we used Lorey's heights (H_L) from the 88 field sites (both from within and near Lopé, and from the Mbam Djerem National Park in Cameroon) where height had been measured for every stem (see Methods). We found that Lorey's height was strongly related to AGB of these plots (r^2= 0.81, p < 0.0001, Figure 5); we treated AGB as the dependent variable here, as it was this that we wished to predict from Lorey's height. The fitted equation was:

$$AGB = a\left[\left(H_L\right)^b\right] \quad (4)$$

with coefficients (± standard errors): a = 0.564 ±0.013, b = 1.945 ±0.096.

7.4.3 Direct biomass estimation with radar

We then correlated the terrain-corrected radar data (in both the HH and HV polarisations) with the field data. We found a strong relationship with both polarisations, with a saturation point around 100 Mg ha^{-1} for HH, and around 150 Mg ha^{-1} for HV (Figure 6). The best fit model was the same as that used in Mitchard *et al.* (*in press*, Chapter 4), also identical in form to the Water Cloud Model (Attema & Ulaby 1978) (for coefficients see Table 1):

$$\sigma^0_{dB} = a + b\left[1 - EXP\left(c.AGB\right)\right] \quad (5)$$

Table 1 – Coefficients in radar-biomass regressions (± standard errors)

Polaraisation	*a*	*b*	*c*	r^2	*p*	*n*
HH	-15.01 ±1.82	6.85 ±1.77	-0.012 ±0.003	0.4	< 0.0001	96
HV	-23.40 ±2.79	10.00 ±1.76	-0.017 ±0.003	0.76	< 0.0001	96

Equation 5 was rearranged as follows to allow the production of an AGB map over the study area using the HV PALSAR data:

$$AGB = \frac{1}{c}.\ln\left[1 - \frac{\sigma^0_{dB} - a}{b}\right] \quad (6)$$

Figure 6

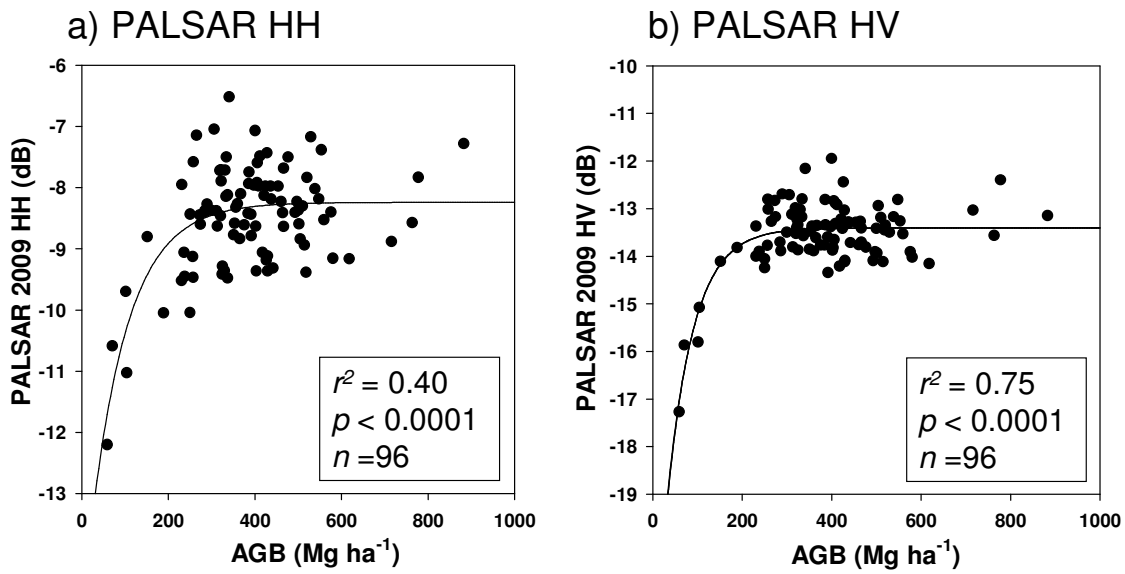

ALOS PALSAR backscatter in a) HH and b) HV polarisations is plotted against AGB for 96 field plots (including 75 x 1 ha sections of long transects).

The relationship between PALSAR HV and AGB saturates at ~150 Mg ha^{-1} (Figure 6b, Mitchard et al. 2011, Chapter 4), and thus the map produced was limited at this value (Figure 6a). Using this upper limit means that using radar data in this way to estimate the AGB of LNP will results in a large underestimation; however for comparison, and as an absolute lower limit, this methodology estimates the aboveground biomass of LNP to be 67.5 Tg, equivalent to 33.7 Tg C (Figure 7a).

Figure 7

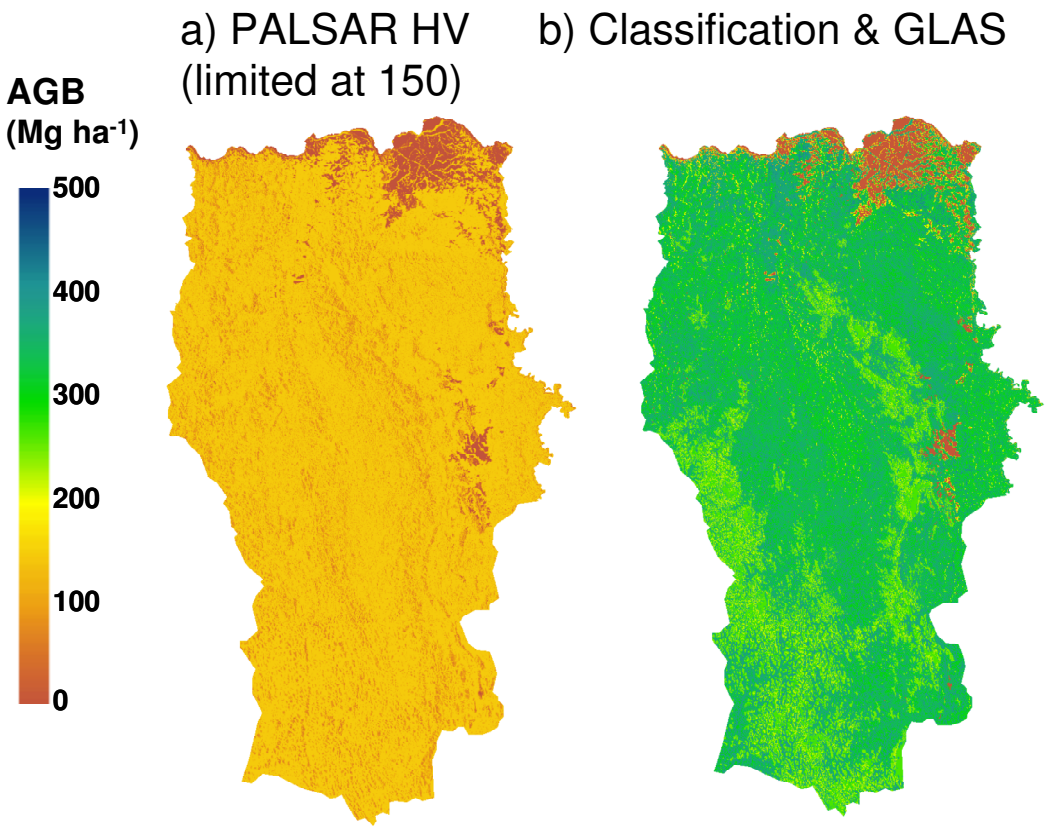

Two different AGB maps for Lopé national park are displayed. a) is for the regression with PALSAR HV, which is limited at 150 Mg ha^{-1} due to the saturation of these data; b) is for the map produced by classifying PALSAR data and giving the 40 classes AGB values derived from GLAS footprints.

7.4.4 Classification and mapping by GLAS

A K-means and IsoData classification with 40 classes and 100 iterations were found to give identical results, and a classification that, based on our field knowledge, classified separately and accurately all the major vegetation types. No more than 40 classes, were used as experimentation showed that more would have resulted in fewer than 100 GLAS footprints falling within each class.

Each class was given an average AGB value by converting each GLAS footprint into an AGB estimate (Equation 4), then averaging these AGB estimates within each class. This gives a carbon stock estimate for LNP of 156 Tg biomass, 78 Tg C

(Figure 7b). It gives the average AGB as 315 Mg ha^{-1}, which compares much better to the field plots and LiDAR data-derived averages (390 and 251 Mg ha^{-1} respectively) than the 136 Mg ha^{-1} from the (limited at 150 Mg ha^{-1}) PALSAR HV-derived map.

7.4.5 Comparisons with independent data

The LiDAR data were not used in the creation of the radar-based AGB map, and similarly the field data were not used to create the classification-based map. This allows a test of the accuracy of both approaches using independent data.

Comparison of radar-derived AGB map to LiDAR data

Due to geolocation errors and differences in scale a direct comparison between the 100 m AGB pixels and the 0.2-0.25 ha GLAS footprints would not give an appropriate estimation of error; even with a perfect AGB map there would be a lot of scatter in the result. Instead the HV-derived AGB map was divided into 6 classes (0-25, 25-50, 50-75, 75-100, 100-150, & >150 Mg ha^{-1}), and the mean and standard deviation of the LiDAR-derived AGB values in each class compared (Table 2). The mean of the LiDAR-derived AGB values for each class fall within that class, suggesting the PALSAR HV-derived map is producing consistent, unbiased results throughout its sensitivity range.

Table 2 – Mean LiDAR-derived AGB in radar-derived biomass classes

AGB class from PALSAR HV (Mg ha^{-1})	Mean AGB from LiDAR footprints within this class (Mg ha^{-1})	Standard Deviation LiDAR-AGB (Mg ha^{-1})	Number of LiDAR footprints
0-25	14.1	13.1	148
25-50	43.1	25.1	131
50-75	68.7	33.8	158
75-100	89.9	35.1	236
100-150	134.4	45.5	1847
>150	297.2	102.9	4522

Comparison of LiDAR and classification-derived AGB map to field data

We do not have access to a sufficient number of field plots to enable the use of these to confirm the accuracy of all 40 classes. However, ten of the classes, covering 34.7 % of LNP in total, had four or more field plots located within them. The mean of these field plots were an average of 9.5 % (range: 1% - 16%) different from the mean AGB derived from the field data plots (Table 3). These data provide evidence of a small bias, with the average AGB values for the field data being on average 4.5 % higher than the mean value for the class derived from LiDAR data.

Table 3 – Comparison of mean AGB for classes from LiDAR with mean AGB from field plots found within these classes

Class number	Class mean AGB (from GLAS) (Mg ha^{-1})	Mean AGB field plots (Mg ha^{-1})	Standard Deviation of field plots AGB (Mg ha^{-1})	Number field plots in class
14	296.1	305.2	44.6	5
5	313.0	310.0	82.1	5
9	314.5	271.6	109.0	13
15	325.6	359.9	74.5	8
12	337.3	370.0	163.8	16
23	338.5	405.3	52.4	6
28	347.7	363.9	111.2	11
18	366.1	320.7	90.7	5
11	393.0	453.6	152.7	8
20	421.1	458.9	95.0	4
Mean	***345.3***	***361.9***	***97.6***	***8.1***

Accuracy assessment for ten of the 40 classes in the AGB map, where sufficient field plots were found in the radar-derived class to test the accuracy of the GLAS mean AGB for that class.

7.5 Error estimation

When providing estimates of carbon stocks for REDD+ and other carbon forestry projects, an estimate is useless without an associated estimate of accuracy. Normally the number of carbon credits awarded is based on the most conservative estimate (*i.e.* the largest carbon stock estimate about which the estimate is relatively) (Grassi *et al.* 2008; GOFC-GOLD 2009). The results in Section 4.5 provide some confidence in

our methodologies, but due to the limited number and spatial distribution of the field plots, and the inaccuracies inherent in LiDAR-AGB estimation, these do not provide an estimate of the true error of the analysis.

There are two major types of estimation error we should be concerned with, which we shall call random errors and uncertainties. Random errors are caused by spatial and structural heterogeneity, geolocation errors, changes in vegetation between observations, and measurement error, and are responsible for much of the random noise observable in Figures 4-6, and the differences between field plot averages and the GLAS-averages of their classes reported in Section 4.5.2 and Table 3. These random errors are thought to be approximately normally distributed about the mean, and, while they can markedly reduce the accuracy when estimating AGB at a pixel level, should cancel out when estimating carbon stocks of a large area. This does not mean they should be ignored: for any methodology that wishes to assess change they are very important (see Mitchard *et al.*, 2011, Chapter 4), but we shall discuss them no further in this section, as they do not affect the uncertainty of the AGB estimate for the whole park. Uncertainties, however, can be biased, and therefore do not necessarily reduce when averaging across a large area. Thus uncertainties should be estimated and reported when trying to estimate carbon stocks over a large area.

7.5.1 Uncertainties in the LiDAR-classification map

a) Allometric equations: the AGB values derived from both the field and LiDAR data are ultimately derived from measurements of the diameter, height and species of trees. These are converted to AGB for this study using the Chave *et al.* (2005) equations, which while believed to be the best available, have significant, but hard to estimate, uncertainties. They are not derived from African trees, which may be a problem as there are known to be differences in height-DBH relationships between the continents (Feldpausch *et al.* 2010); however our use of a locally-derived DBH-height relationship should correct for this, and Lewis et al. (2009) showed that locally-derived relationships did not dramatically alter their biomass estimates from African forests (Lewis *et al.* 2009b). We therefore estimate the potential bias due to the allometric equation at ±10 %, which though twice the figure published in the

original paper with this equation (Chave *et al.* 2005), is similar to that discovered by Lewis *et al* (2009), who propagated estimated height and diameter errors in their biomass estimates, and by Djomo *et al.* (2010), who used destructive sampling of trees in Africa to estimate the accuracy of various pantropical equations.

b) LiDAR waveform to Lorey's height: the relationship used to derive Lorey's height from the LiDAR waveforms is based on field plots coincident with LiDAR footprints from three sites in the Brazilian Amazon (Lefsky 2010). Unfortunately no LiDAR footprints intersected with our field plots from LNP, so we cannot discern the extent to which this could cause inaccuracies, though the results in Section 4.5 provide some confidence. There are structural differences between the two continents' forests (Djomo *et al.* 2010), so we add an uncertainty of ±5 % , similar in magnitude to the detected potential bias in Section 4.5.2, to account for this.

c) Classification: classifying the image into forty different clusters, based on similar radar returns and altitude, is bound to introduce errors by both over-simplification (the resulting vegetation types will not necessarily have identical average AGB values in different spatial locations) and mis-classification. As the clusters are only covered by LiDAR data from a spatially-limited portion of the image (Figure 1b), this is likely to introduce biases. To test this we ran four additional models, excluding LiDAR data from one quarter of the park each time, and comparing the biomass results produced from that quarter with the original biomass estimates. This resulted in changes in the biomass estimate for each quarter of 4.8 % (range 4 – 7 %). This procedure only estimates part of the potential error due to this source, so to be conservative we add an error of ±10 %.

7.5.2 Summing uncertainties

As these errors are all independent, and in order to use the most conservative method, these errors should be summed to give an estimate of the most extreme error: this is ±25 %. This gives the total AGB stocks of LNP, using the LiDAR data and unsupervised classification methodology, to be between 58.5 and 97.5 Tg C, with the lower number being that recommended for carbon payment purposes.

7.6 Discussion

Despite the high biomass and persistent cloud-cover, we have produced a high resolution (100 m) map of AGB over Lopé National Park in Gabon. This estimate was made possible through a novel fusion of radar and spaceborne LiDAR data. Also, using a conservative error-estimation method optimised for carbon payments for REDD+, we have shown that these estimates at a park level have a ±25 % uncertainty, due to potential biased errors in our input data and estimations. We have shown from our field data that there is a strong relationship between Lorey's height and field-derived AGB, and then used this to give us an additional 7042 point-based AGB estimates from spaceborne LiDAR waveforms, which can estimate Lorey's height with high confidence (Lefsky, 2010). Finally we used the information in our dual-polarisation radar data, along with a DEM, to classify the vegetation into units with distinct biophysical parameters, enabling the spatial extrapolation of the radar data. While none of these steps are novel or controversial, we believe this new combination of methodologies provides an excellent pathway for combining the strengths of GLAS and radar data to produce AGB maps of high biomass forest.

This methodology enables the production of carbon maps for a tropical region or country, a requirement, for example, in advance of a deforestation-reduction program such as REDD+. However, the high resolution and spatially-explicit nature of these maps goes beyond the requirements of the lower two assessment standards given by the International Panel on Climate Change (IPCC), which rely on maps giving changes in landcover type and not on spatially-explicit AGB maps. Therefore using such a methodology could give data required for the highest tier, Tier 3 (GOFC-GOLD, 2009). Running Tier 3 assessments may be advantageous, as the increased certainty may lead to a larger number of certified emissions reductions for a landscape. Additionally, Tier 3 monitoring may increase investor confidence leading to increased investments in REDD. Furthermore, such monitoring may lead to this carbon being trade at a price premium if the REDD scheme moves to become a market-based scheme. The method developed here shows that a large investment in a high density of field plots or airborne LiDAR data may not be necessary to reach the

accuracy required by this tier: a high density of GLAS plots, combined with optical or radar data for vegetation classification, may suffice, as long as there are sufficient field plots for validation.

Our approach to the uncertainty analysis, using conservative estimates of potential biases from a wide variety of sources, and then summing them, is conservative, but appropriate to the problem in hand. For such a large area it will produce much wider confidence intervals than commonly used estimates based on standard errors of means, but this is appropriate as for the purposes of conserving carbon stocks we must find the minimum likely carbon stocks of the park, not a mean estimate. We believe such an approach is essential for the monitoring of deforestation, where the conservativeness principle outlined by Grassi et al. (2008), that for the purposes of forest conservation the most conservative estimate of any parameter must always be used, must apply. This conservative approach is essential for two reasons. Firstly, if avoided deforestation credits are to be used to offset actual fossil fuel carbon emissions, then any overestimate of carbon savings realised would result in REDD+ have a net negative impact on net CO_2 emissions, exactly the opposite of its original intentions. Secondly, the majority of the errors included in our analysis are very hard to quantify, that is these uncertainties are themselves very uncertain. Therefore our conservative approach assists in ensuring that the confidence bands presented span the full range of possible values.

GLAS-LiDAR is clearly not the ideal tool for mapping biomass: its footprints cover only a tiny percentage of the total land-area of the planet, and the footprints, at 0.2 - 0.25 ha, are too large for detailed mapping. It would always be preferable to use airborne LiDAR, as for example Asner et al. (2010) have done in the Peruvian Amazon, using a similar approach as described here but with airborne-LiDAR, extrapolated to other areas using the classification of high-resolution optical rather than radar data. However, airborne LiDAR data is expensive to collect, thus whole country censuses, let alone with annual repeat, are unlikely in the near future. GLAS represents a spatially distributed set of footprints, with hundreds of thousands to millions of footprints freely available across every country (Lefsky, 2010), and as

such is a useful resource to assist mapping forest biomass carbon stocks. The patchy coverage necessitates using another dataset to classify the landscape: here we use radar data and a DEM due to data availability, but if cloud-free optical data (or other high quality spatially-explicit datasets) were available they should be added into the classification procedure.

A limitation with the approach we set out here is that IceSAT GLAS is no longer operational: suitable data were only produced from 2003 until 2009. A new satellite carrying a spaceborne LiDAR system, ICESat-2, is planned for launch in late 2015 (http://icesat.gsfc.nasa.gov/icesat2/). Unlike ICESat, ICESat-2 will use a micropulse multi-beam approach, which will produce a greater number of smaller footprints, with great potential for biomass retrieval; however, this new approach will necessitate new algorithm development and testing. The lack of data from 2009-2015 will mean that though this method may be used to produce carbon maps for the mid- to late- 2000s, it will not be possible to use this for change detection or deforestation monitoring in the near future. However this is still a useful development: both optical and radar systems can easily be used to detect changes in forest *area*, and so having an accurate carbon map at one time-point will allow the emissions caused by deforestation to be better estimated from landcover-change results.

7.7 Acknowledgements

This paper is dedicated to the memory of Fabiane Lima de Oliveira, who passed away in Gabon in 2009 after falling ill whilst on fieldwork for this project. Her deep knowledge and love of the forest was highly respected by all who she met. She is greatly missed by family, and friends and the scientific community.

ESA provided the ALOS PALSAR radar data at cost price through a Category 1 Application. These data were ultimately collected and processed by JAXA. ICESat GLAS data were provided by NASA. SRTM data were provided by NASA and processed by CGIAR-CSI (http://srtm.csi.cgiar.org). Funding for this work was provided by a PhD Studentship to Edward Mitchard, with the fieldwork being funded by a grant from the Gordon and Betty Moore Foundation and the Packard

Foundation. Simon Lewis is supported by a Royal Society University Research Fellowship. The Gabonese Agence Nationale des Parcs Nationaux, the Station d'Etudes des Gorilles et Chimpanzés, and Etienne Massard provided essential logistical support to the fieldwork effort.

7.8 References

Abdalati W., Zwally H.J., Bindschadler R., Csatho B., Farrell S.L., Fricker H.A., Harding D., Kwok R., Lefsky M., Markus T., Marshak A., Neumann T., Palm S., Schutz B., Smith B., Spinhirne J. & Webb C. (2010) The ICESat-2 Laser Altimetry Mission. *Proceedings of the IEEE*, 98, 735-751

Ahrends A., Burgess N.D., Milledge S.A.H., Bulling M.T., Fisher B., Smart J.C.R., Clarke G.P., Mhoro B.E. & Lewis S.L. (2010) Predictable waves of sequential forest degradation and biodiversity loss spreading from an African city. *Proceedings of the National Academy of Sciences of the United States of America*, 107, 14556-14561

Asner G.P., Powell G.V.N., Mascaro J., Knapp D.E., Clark J.K., Jacobson J., Kennedy-Bowdoin T., Balaji A., Paez-Acosta G., Victoria E., Secada L., Valqui M. & Hughes R.F. (2010) High-resolution forest carbon stocks and emissions in the Amazon. *Proceedings of the National Academy of Sciences of the United States of America*, 107, 16738-16742

Attema E.P.W. & Ulaby F.T. (1978) Vegetation Modeled as a Water Cloud. *Radio Science*, 13, 357-364

Brown S. (1997) *Estimating Biomass and Biomass Change of Tropical Forests*. FAO Forest Paper 134, Rome.

CCBA (2011) List of accepted CCBA projects. *http://www.climate-standards.org/projects/index.html*

Chave J., Andalo C., Brown S., Cairns M.A., Chambers J.Q., Eamus D., Folster H., Fromard F., Higuchi N., Kira T., Lescure J.P., Nelson B.W., Ogawa H., Puig H., Riera B. & Yamakura T. (2005) Tree allometry and improved estimation of carbon stocks and balance in tropical forests. *Oecologia*, 145, 87-99

Chave J., Condit R., Aguilar S., Hernandez A., Lao S. & Perez R. (2004) Error propagation and scaling for tropical forest biomass estimates. *Philosophical Transactions of the Royal Society of London Series B-Biological Sciences*, 359, 409-420

Chave J., Coomes D., Jansen S., Lewis S., Swenson N. & Zanne A. (2009a) Data from: Towards a worldwide wood economics spectrum. In. Dryad Data Repository

Chave J., Coomes D., Jansen S., Lewis S.L., Swenson N.G. & Zanne A.E. (2009b) Towards a worldwide wood economics spectrum. *Ecology Letters*, 12, 351-366

Chhatre A. & Agrawal A. (2008) Forest commons and local enforcement. *Proceedings of the National Academy of Sciences of the United States of America*, 105, 13286-13291

Chhatre A. & Agrawal A. (2009) Trade-offs and synergies between carbon storage and livelihood benefits from forest commons. *Proceedings of the National Academy of Sciences of the United States of America*, 106, 17667-17670

Clements G.R., Sayer J., Boedhihartono A.K., Venter O., Lovejoy T., Koh L.P. & Laurance W.F. (2010) Cautious Optimism over Norway-Indonesia REDD Pact. *Conservation Biology*, 24, 1437-1438

Clements T. (2010) Reduced Expectations: the political and institutional challenges of REDD. *Oryx*, 44, 309-310

Djomo A.N., Ibrahima A., Saborowski J. & Gravenhorst G. (2010) Allometric equations for biomass estimations in Cameroon and pan moist tropical equations including biomass data from Africa. *Forest Ecology and Management*, 260, 1873-1885

Donnellan A., Rosen P., Graf J., Loverro A., Freeman A., Treuhaft R., Oberto R., Simard M., Rignot E., Kwok R., Pi X.P., Blair J.B., Abdalati W., Ranson J., Zebker H., Hager B., Shugart H., Fahnestock M. & Dubayah R. (2008) Deformation, Ecosystem Structure, and Dynamics of Ice (DESDynI). *2008 IEEE Aerospace Conference*, 163-175

Engel S., Pagiola S. & Wunder S. (2008) Designing payments for environmental services in theory and practice: An overview of the issues. *Payments for Environmental Services in Developing and Developed Countries*, 65, 663-674

Feldpausch T.R., Banin L., Phillips O.L., Baker T.R., Lewis S.L., Quesada C.A., Affum-Baffoe K., Arets E.J.M.M., Berry N.J., Bird M., Brondizio E.S., de Camargo P., Chave J., Djagbletey G., Domingues T.F., Drescher M., Fearnside P.M., Fransa M.B., Fyllas N.M., Lopez-Gonzalez G., Hladik A., Higuchi N., Hunter M.O., Iida Y., Abu Silam K., Kassim A.R., Keller M., Kemp J., King D.A., Lovett J.C., Marimon B.S., Marimon-Junior B.H., Lenza E., Marshall A.R., Metcalfe D.J., Mitchard E.T.A., Moran E.F., Nelson B.W., Nilus R., Nogueira E.M., Palace M., Patia S., Peh K.S.H., Raventos M.T., Reitsma J.M., Saiz G., Schrodt F., Sonké B., Taedoumg H.E., Tan S., White L., Wa H. & Lloyd J. (2010) Height-diameter allometry of tropical forest trees. *Biogeosciences Discuss.*, 7, 7727-7793

Geist H.J. & Lambin E.F. (2002) Proximate causes and underlying driving forces of tropical deforestation. *Bioscience*, 52, 143-150

GOFC-GOLD (2009) A sourcebook of methods and procedures for monitoring and reporting anthropogenic greenhouse has emissions and removals caused by deforestation, gains and losses of carbon stocks in forests, remaining forests, and forestation. In, Alberta, Canada

Grassi G., Monni S., Federici S., Achard F. & Mollicone D. (2008) Applying the conservativeness principle to REDD to deal with the uncertainties of the estimates. *Environmental Research Letters*, 3, 035005

IPCC (2003) Good practice guidance for land use, land-use change and forestry. In, IPCC

Kaiser B. & Roumasset J. (2002) Valuing indirect ecosystem services: the case of tropical watersheds. *Environment and Development Economics*, 7, 701-714

Leal M.E. (2001) Microrefugia, Small Scale Ice Age Forest Remnants. *Systematics and Geography of Plants*, 71, 1073-1077

Lefsky M. (2010) A global forest canopy height map from the Moderate Resolution Imaging Spectroradiometer and the Geoscience Laser Altimeter System. *Geophysical Research Letters*, 37, L15401

Lefsky M.A., Harding D.J., Keller M., Cohen W.B., Carabajal C.C., Espirito-Santo F.D., Hunter M.O. & de Oliveira R. (2005) Estimates of forest canopy height and aboveground biomass using ICESat. *Geophysical Research Letters*, 32

Lewis S.L., Lloyd J., Sitch S., Mitchard E.T.A. & Laurance W.F. (2009a) Changing Ecology of Tropical Forests: Evidence and Drivers. *Annual Review of Ecology, Evolution, and Systematics*, 40, 529-549.

Lewis S.L., Lopez-Gonzalez G., Sonke B., Affum-Baffoe K., Baker T.R., Ojo L.O., Phillips O.L., Reitsma J.M., White L., Comiskey J.A., Djuikouo M.N., Ewango C.E.N., Feldpausch T.R., Hamilton A.C., Gloor M., Hart T., Hladik A., Lloyd J., Lovett J.C., Makana J.R., Malhi Y., Mbago F.M., Ndangalasi H.J., Peacock J., Peh K.S.H., Sheil D., Sunderland T., Swaine M.D., Taplin J., Taylor D., Thomas S.C., Votere R. & Woll H. (2009b) Increasing carbon storage in intact African tropical forests. *Nature*, 457, 1003-1006

Lu D.S. (2006) The potential and challenge of remote sensing-based biomass estimation. *International Journal of Remote Sensing*, 27, 1297-1328

Meir P., Cox P. & Grace J. (2006) The influence of terrestrial ecosystems on climate. *Trends in Ecology & Evolution*, 21, 254-260

Mitchard E.T.A., Saatchi S., Woodhouse I., Feldpausch T., Lewis S., Sonké B., Rowland C. & Meir P. (2011, and this thesis Chapter 4) Measuring biomass changes due to woody encroachment and

deforestation/degradation in a forest-savanna boundary region of central Africa using multi-temporal L-band radar backscatter. *Remote Sensing of Environment, in press*

Mitchard E.T.A., Saatchi S.S., Woodhouse I.H., Nangendo G., Ribeiro N.S., Williams M., Ryan C.M., Lewis S.L., Feldpausch T.R. & Meir P. (2009, and this thesis Chapter 5) Using satellite radar backscatter to predict above-ground woody biomass: A consistent relationship across four different African landscapes. *Geophysical Research Letters*, 36*, L23401*

Oslisly R. & White L.J.T. (1995) La relation homme-milieu dans la reserve de la Lopé (Gabon) au cours de l'Holocène; les implications sur l'environnement. In: *Dynamique à long terme des Ecosystèmes Forestiers Intertropicaux* (eds. Servant M & Servant-Vildary S), pp. 241-250. ORSTOM

Phillips O.L., Baker T.R., Feldpausch T.R. & Brienen R. (2009) Field manual for plot establishment and remeasurement, http://www.geog.leeds.ac.uk/projects/rainfor/. URL http://www.geog.leeds.ac.uk/projects/rainfor/

Phillips O.L., Lewis S.L., Baker T.R., Chao K.J. & Higuchi N. (2008) The changing Amazon forest. *Philosophical Transactions of the Royal Society B-Biological Sciences*, 363, 1819-1827

Pourtier R. (1989) *Le Gabon. Tome 2: Etat et Développement.* Editions L'Harmattan, Paris.

Rodrigues A.S.L., Ewers R.M., Parry L., Souza C., Verissimo A. & Balmford A. (2009) Boom-and-Bust Development Patterns Across the Amazon Deforestation Frontier. *Science*, 324, 1435-1437

Saatchi S.S., Harris N.L., Brown S., Lefsky M., Mitchard E.T.A., Salas W., Zutta B., Buermann W., Lewis S., Hagen S., Petrova S., White L., Silman M., Morel A. (In press) Benchmark map of forest carbon stocks in tropical regions across three continents. *Proceedings of the National Academy of Sciences of the United States of America.*

Shugart H.H., Saatchi S.S. & Hall F.G. (2010) Importance of structure and its measurement in quantifying function of forest ecosystems. *J. Geophys. Res.*, 115, G00E13

Stern N.H. (2008) *The economics of climate change : the Stern review*. Cambridge University Press, Cambridge.

Swetnam T., Falk D.A., Hessl A.E. & Farris C. (2011) Reconstructing landscape patter of historical fires and fire regimes. In: *The lanscape ecology of fire* (eds. McKenzie D, Miller C & Falk DA), pp. 165-192. Springer. Ecological Studies, vol. 213.White L.J.T. (2001) Forest-savanna dynamics and the origins of 'Marantaceae Forest' in the Lopé Reserve, Gabon. In: *African Rain Forest Ecology and Conservation* (eds. Weber B, White LJT & Vedder A), pp. 165-192. Yale University Press

White L.J.T. & Abernethy K. (1997) *A guide to the vegetation of the Lopé Reserve*. Wildlife Conservation Society, New York.

WRI (2010) Summary of Developed Country "Fast-Start" Climate Finance Pledges. World Resources Institute, http://www.wri.org/.

Interpreting and improving first generation biomass maps: Comment on Baccini *et al.* (2008) 'A first map of tropical Africa's above-ground biomass derived from satellite imagery'

Authors: E.T.A. Mitchard[a], S.S. Saatchi[b], S.L. Lewis[c], T.R. Feldpausch[c], F.F. Gerard[d], I.H. Woodhouse[a], and P. Meir[a]

a School of GeoSciences, University of Edinburgh, EH8 9XP, UK

b Jet Propulsion Laboratory, California Institute of Technology, Pasadena, CA 91109, USA

c Earth and Biosphere Institute, School of Geography, University of Leeds, LS2 9JT, UK

d Centre for Ecology and Hydrology, Maclean Building, Benson Lane, Crowmarsh Gifford, Wallingford, Oxfordshire, OX10 8BB, UK

As published in Environmental Research Letters[1]*, November 2011*

Author contributions: ETAM, SSS, & PM designed the research; some field data was collected by ETAM, SLL & TRF, the rest was collated by ETAM from various sources, detailed in the acknowledgements; ETAM conducted the analysis with assistance from all other authors; ETAM wrote the paper with assistance and revisions from all other authors.

[1]*Environmental Research Letters,* 6, 049001. doi:10.1088/1748-9326/6/4/049001. See Appendix 6.

Abstract

We present a critical evaluation of the aboveground biomass (AGB) map of Africa published in this journal by Baccini *et al.* (2008). We first test their map against an independent dataset of 1154 scientific inventory plots from 16 African countries, and find only weak correspondence between our field plots and the AGB value given for the surrounding 1 km pixel by Baccini *et al*. Separating our field data using a continental landcover classification suggests the Baccini *et al.* map underestimates the AGB of forests and woodlands, while overestimating the AGB of savannas and grasslands. Secondly, we compare their map to 216,000 x 0.25 ha spaceborne LiDAR footprints. A comparison between Lorey's height (basal-area weighted average height) derived from the LiDAR data for 1-km pixels containing at least 5 LiDAR footprints again does not support the hypothesis that the Baccini *et al.* map is accurate, and suggests it significantly underestimates the AGB of higher-AGB areas. We conclude that this is due to the unsuitability of some of the field data used by Baccini *et al.* to create their map, and overfitting in their model, resulting in low accuracies outside the small areas from which their field data is drawn.

8.1. Introduction

The ERL paper by Baccini *et al.* (2008), 'A first map of tropical Africa's above-ground biomass derived from satellite imagery', was a timely attempt to combine available field and remotely sensed data to produce the first aboveground biomass (AGB) map of a significant portion of sub-Saharan Africa. The authors used passive optical remote sensing data, which generally has not been found to be very sensitive to AGB at higher biomass values (Zheng *et al.*, 2004; Lu, 2006; GOFC-GOLD, 2009; Mitchard *et al.* 2009). Still, Baccini *et al.* report a high accuracy, with the map explaining 82 % of the variance in AGB for 10 % of field plots held back for validation, with a Root Mean Squared Error (RMSE) of 50.5 Mg ha^{-1}. They then perform a test against spaceborne LiDAR height metrics from across the whole spatial extent of the map, and report an r^2 of 0.90 in a regression between mean LiDAR derived height and AGB (averaged over 10 Mg ha^{-1} AGB classes). We tested the Bacinni *et al.* results against independent and spatially extensive field data, and newly-calculated spaceborne LiDAR results, and found little support for the accuracy of the map (Figure 1, Figure 2, Table 1). Our conclusion is that this is due to the low accuracy and limited spatial extent of the field data used to train and validate the RandomForest model used to produce the AGB map.

8.2. Test against field data

We first test the accuracy of the Baccini *et al.* map directly using AGB derived from 1154 scientific inventory plots from 16 African countries, ranging in size from 0.1 – 10 ha (mean plot size 0.32 ha, mean 1.5 ha inventoried per 1 km pixel, Figure 1, Table 2 for plot details). In order to ensure sufficient sampling within each 1 km pixel, small plots (< 0.5 ha) are included in this analysis only if the 1 km pixel in which they are located contains at least 0.5 ha of inventory plots. If multiple field plots occurred within one pixel, we calculated a mean AGB value, weighted by the square root of plot size. There are on average 4.8 field plots per 1 km pixel, so we compared field plots and the AGB map in a total of 239 pixels. The plots were collected from 1995 to 2010, with a mean julian date corresponding to July 2005

(compared to the remote sensing data in the Baccini *et al.* map from 2000 to end 2003).

We find a significant, but very weak correlation, between our field plot AGB values and those in the Baccini *et al.* map: a linear regression gave $r^2 = 0.28$, $p < 0.001$ (F-test), slope of 0.37, and RMSE of 145 Mg ha^{-1} (Figure 1b). In this the best fit line had an intercept and slope significantly different from 0 and 1 respectively ($p < 0.01$). Errors range from an overestimate of 295 Mg ha^{-1} to an underestimate of -734 Mg ha^{-1}; the Baccini *et al.* map has a much smaller range of AGB values than our field plots, with all higher AGB plots underestimated.

When the plots are grouped by landcover type, using the Global Land Cover 2000 (GLC 2000) dataset (Mayaux *et al.* 2004), the AGB of forest and woodland classes are underestimated by the Baccini *et al.* map by ~50 %, while shrubland/grassland classes are mostly overestimated (Table 1, only landcover classes where we had at least 10 ha of field plots covering at least ten 1 km pixels were considered).

Figure 1

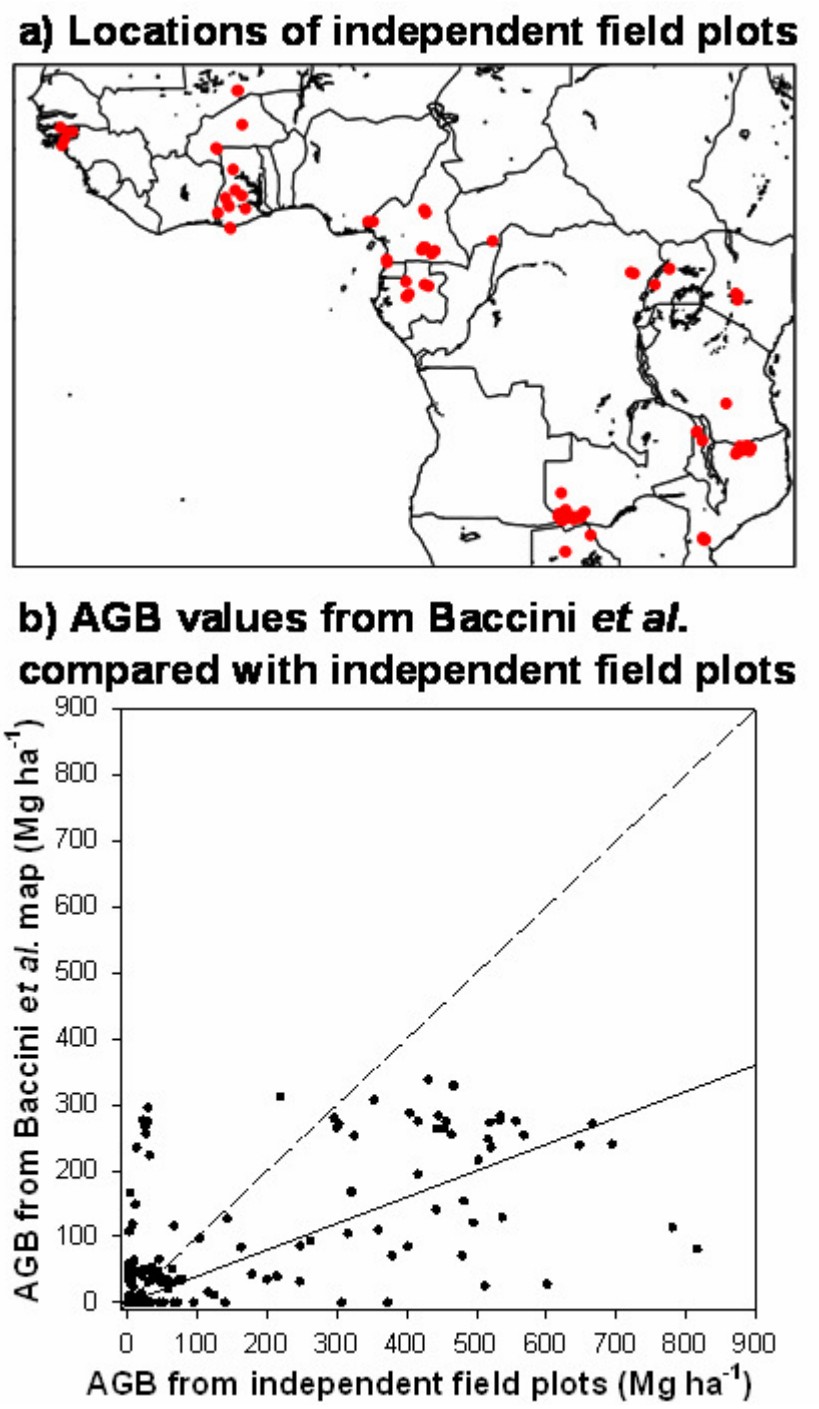

a) location of the 1154 scientific inventory plots used to compare to the Baccini *et al.* AGB map; **b)** AGB values from pixels of the Baccini *et al.* map containing inventory plots plotted against the weighted average AGB of independent inventory plots; also shown is the best fit line (solid line), and the 1:1 line (dotted).

Table 1. Difference between Baccini *et al.* map and field plots by GLC2000 landcover class.

GLC2000 land cover class	Number of pixels sampled	Total number of field plots within sampled pixels	Total area of field plots within sampled pixels (ha)	Mean AGB from Baccini *et al.* (Mg ha^{-1})	Mean AGB from independent field plots (Mg ha^{-1})	Difference (Mg ha^{-1})
Closed evergreen lowland forest	29	38	75.1	202.5	445.1	-242.6
Submontane forest (900 -1500 m)	11	16	20.2	210.0	438.1	-228.1
Deciduous woodland	66	308	76.7	20.2	36.5	-16.3
Deciduous shrubland with sparse trees	44	196	42.1	14.8	4.3	10.4
Open deciduous shrubland	28	371	46.0	0.2	4.1	-3.9
Closed grassland	16	99	32.5	27.0	3.9	23.0

Table 2: Field data sources

Who collected?	Country(s)	Dates collected	Number of plots used	Min plot size (ha)	Max plot size (ha)	Min AGB (Mg ha-1)	Max AGB (Mg ha-1)	Reference (if published) or source of further information
AFRITRON Consortium	Liberia, Ghana, Nigeria, Cameroon, Gabon, Democratic Republic of Congo, Uganda, Central African Republic, Cote D'Ivoire	1995 - 2007	44	0.25	10	142.9	780.7	Simon L. Lewis, Gabriela Lopez-Gonzalez, Bonaventure Sonke, Kofi Affum-Baffoe, Timothy R. Baker, Lucas O. Ojo, Oliver L. Phillips, Jan M. Reitsma, Lee White, James A. Comiskey, Marie-Nool Djuikouo K, Corneille E. N. Ewango, Ted R. Feldpausch, Alan C. Hamilton, Manuel Gloor, Terese Hart, Annette Hladik, Jon Lloyd, Jon C. Lovett, Jean-Remy Makana, Yadvinder Malhi, Frank M. Mbago, Henry J. Ndangalasi, Julie Peacock, Kelvin S.-H. Peh, Douglas Sheil, Terry Sunderland, Michael D. Swaine, James Taplin, David Taylor, Sean C. Thomas, Raymond Votere & Hannsjorg Woll. 2009. Increasing carbon storage in intact African tropical forests, Nature, 457, 1003-7. http://www.geog.leeds.ac.uk/projects/afritron/
CARBOVEG Consortium	Gunea-Bisau	2007-2009	10	0.13	0.13	20.6	478.7	http://carboveg-gb.dpp.pt
Casey Ryan & Mat Williams, University of Edinburgh	Mozambique	2006-2009	27	0.3	1	16.2	73.7	Ryan, C.M. , M. Williams & J Grace (in press) Above and Below Ground Carbon Stocks in a Miombo Woodland Landscape of Mozambique. Biotropica. Williams M, CM Ryan, RM Rees, E Sambane, J Fernando and J Grace. (2008) Carbon sequestration and biodiversity of re-growing miombo woodlands in Mozambique. Forest Ecology and Management, 254: 145-155.
Edward Mitchard, University of Edinburgh	Cameroon & Uganda	2007-2008	14	0.25	1.86	199.7	815.9	Mitchard, E.T.A., S.S. Saatchi, I.H. Woodhouse, G. Nangendo, N.S. Ribeiro, M. Williams, C.M. Ryan, S.L. Lewis, T.R. Feldpausch, & P. Meir. 2009. Using satellite radar backscatter to predict above-ground woody biomass: A consistent relationship across four different African landscapes. Geophysical Research Letters, 36, L23401
TROBIT Consortium	Burkina Faso, Cameroon, Ghana, Mali	2006-2007	25	0.4	1	0.0	372.4	http://www.geog.leeds.ac.uk/groups/trobit Mitchard, E.T.A., S.S. Saatchi, I.H. Woodhouse, G. Nangendo, N.S. Ribeiro, M. Williams, C.M. Ryan, S.L. Lewis, T.R. Feldpausch, & P. Meir. 2009. Using satellite radar backscatter to predict above-ground woody biomass: A consistent relationship across four different African landscapes. Geophysical Research Letters, 36, L23401
Emily Woollen, University of Edinburgh	Mozambique	2009	31	0.57	0.57	22.5	78.1	http://www.geos.ed.ac.uk/homes/s0452637/
Gemma Casells, University of Edinburgh	Malawi	2009	5	0.5	1.25	20.8	63.6	http://web.me.com/gemmacassells/
Leon Theron, Peace Parks Foundation	Zambia	2009	905	0.1	0.1	0.0	13.2	http://ppf.org.za/Home.htm
Lyndon Estes, University of Virginia	Kenya	2006	36	0.1	0.1	1.5	29.3	Estesm LD, Okin, GS, Mwangi, AG, Shugard, HH. 2008. Habitat selection by a rare forest antelope: a multi-scale approach combining field data and imagery from three sensors. Remote Sensing of Enivronment 112, 2033-2050
Natasha Ribeiro	Mozambique	2005	50	0.7	0.7	0.8	9.4	Ribeiro, N. S., S. S. Saatchi, H. H. Shugart, and R. A. Washington-Allen (2008), Aboveground biomass and leaf area index (LAI) mapping for Niassa Reserve, northern Mozambique, J. Geophys. Res., 113, G02S02
Southern African Regional Science Initiative (SAFARI 2000)	Zambia, Botswana	2000	4	9	9	1.8	51.9	Privette JI, and roy DP. 2005. Southern Africa as a remote sensing test bed: the SAFARI 2000 Special Issue overview. International Journal of Remote Sensing, 26, 4141-4158

There are five possible explanations for this discrepancy if the Baccini *et al.* map is accurate; however regressions with subsets of our field data do not support any of these hypotheses. In all the following regressions the best fit lines are significant ($p < 0.01$), and intercepts and slopes are significantly different from 0 and 1 respectively ($p < 0.05$). First, this could be caused by our field plots having a larger AGB range than the AGB map. This is not the case, as excluding pixels with an average AGB >338 Mg ha^{-1} (the maximum in the Baccini *et al.* dataset) gives an r^2 of 0.12, slope of 0.36, and an RMSE of 79.6 Mg ha^{-1} (n = 204 pixels): as would be expected the RMSE is reduced by removing the high AGB plots, but the overall accuracy (based on the r^2 and slope) actually decreases. Second, the non-normal distribution of biomass for very small plots (Chave *et al.* 2003) may drive the poor fit. This is not the case, as if we limit our field data to pixels that have a total plot area ≥1 ha (1% coverage of the 1 km^2 pixel), although the r^2 increases to 0.32, the slope does not change at 0.38 (n = 128), and the RMSE of 169.5 Mg ha^{-1} is higher than for the whole dataset; additionally we have four plots of 10 ha in size from eastern Democratic Republic of Congo – these have an average AGB value of 463 Mg ha^{-1}, but the two Baccini *et al.* pixels in which they fall (of which these plots sample 15 %), are given AGB values of 273 and 283 Mg ha^{-1}. Third, our independent validation compares field-measured values from small plots to 1 km pixels (mean plot size = 0.3 ha, mean 4.8 plots per 1 km pixel); such plots may not sample the whole pixel sufficiently to accurately estimate its AGB. However, we do not think this third hypothesis can explain the extent of the poor correlation, as the error increases when we only consider the 70 pixels that have more than five field plots located within them (mean 13 plots per 1 km pixel for this reduced dataset): r^2 = 0.14, slope = 0.42, RMSE = 170.2 Mg ha^{-1}. Fourth, there is a potential for changes in the landcover of our field plots (which range from 1995 to 2010, compared to 2000 to 2003 for the remote sensing data of Baccini *et al.*); however considering only field plots from 2000-2003 the results do not improve, with r^2 = 0.36, slope = 0.39, and RMSE = 291 Mg ha^{-1} (n = 38). Finally, our fifth hypothesis relates to differences in the choice of the allometric equations relating measured tree parameters to AGB. The allometrics chosen differ between our datasets and those of Baccini *et al.*: Baccini *et al.* use the

Brown *et al.* (2005) equation involving diameter alone for the majority of their field plots, whereas we use a combination of the Chave *et al.* (2005) 'moist forest' equation involving diameter, height and wood density for our forest plots, and for savanna/woodland vegetation we used either the Chave *et al.* (2005) dry forest equation or locally-derived area-specific equations (Table2). We tested the impact of equation choice for 87 of our field plots where we have access to the raw stem data (from savannas and tall forests in Cameroon, Gabon and Uganda, with similar characteristics to the field data used by Baccini *et al.*): the plots had a mean AGB of 363 Mg ha^{-1} using a combination of the Chave *et al.* (2005) dry and moist equations, and 376 Mg ha^{-1} using the Brown *et al.* 2005 equation involving diameter alone. A direct comparison of individual plot values using both allometric equations provides little support for bias at low or high biomass values: linear RMA regression gave intercept = 3.2, slope = 0.98, $r^2 = 0.97$, $p < 0.0001$.

8.3. Test against LiDAR data

In our second test, we examine the spaceborne LiDAR verification as performed by Baccini *et al.* To do this we used a dataset of ICESat Geoscience Laser Altimeter System (GLAS) footprints collected between 2003 and 2007, which were processed to provide estimates of Lorey's height, a basal-area weighted average height that can be estimated accurately from GLAS waveforms (Lefsky *et al.* 2005, Lefsky, 2010). We use Lorey's height, as opposed to maximum height and HOME as used by Baccini *et al.*, because the evidence suggests it can more accurately be determined from GLAS data, and because it has a stronger relationship with AGB (Lefsky *et al.* 2005, Lefsky, 2010). After cloud- and terrain- filtering (Saatchi *et al*. in press), we selected pixels that contained ≥5 GLAS footprints (Baccini *et al.*'s used three; each footprint covers 0.20-0.25 ha), giving a total of 35,034 test pixels, using 215,733 GLAS footprints. We find only a very weak relationship between Lorey's height and Baccini *et al.*'s AGB values when considering individual pixel values (Figure 2a, linear regression: slope = 0.02, r^2 = 0.045). We also averaged the Lorey's height values in 10 Mg ha^{-1} bins, replicating the display method used in Figure 7 of the Baccini *et al.* study, and reproduced here as Figure 2b. We could not replicate their strong relationship between mean height and AGB, instead finding just a weak trend towards increasing height with increasing AGB up to ~80 Mg ha^{-1}, and no relationship thereafter. We extend this analysis further by using a Lorey's height (H_L)-AGB relationship derived from plot data in Africa (AGB=0.3542($H_L^{2.0528}$), n = 75, r^2 = 0.85, p < 0.001, Saatchi *et al.*, in press); again this suggests the Baccini *et al.* map underestimates AGB in higher AGB areas, and has a low accuracy throughout the range of AGB values (Figure 2c, linear regression: slope = 0.05, r^2 = 0.01, RMSE = 173 Mg ha^{-1}).

Figure 2

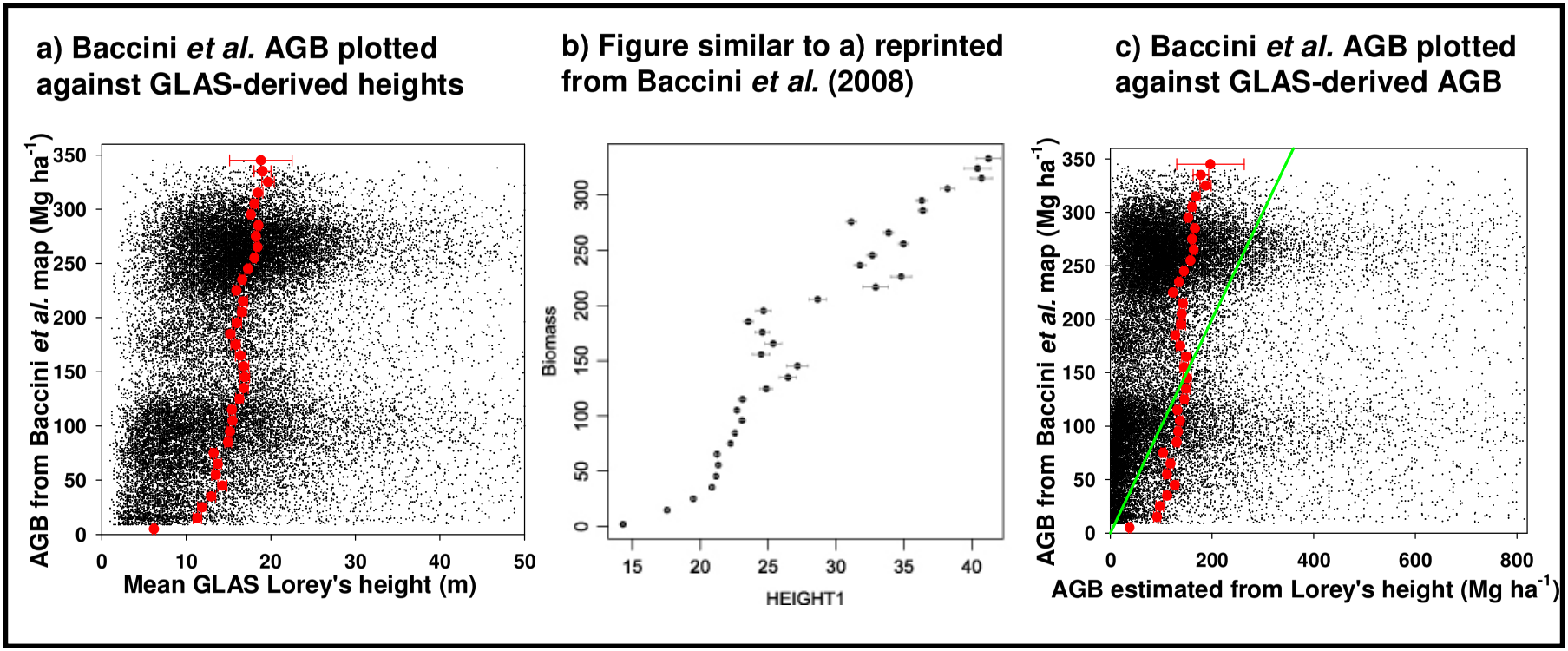

a) AGB from 35,034 pixels from the Baccini *et al.* map plotted against the mean Lorey's height from that pixel, each estimated from ≥5 ICESat GLAS footprints; also shown in red is the mean height estimated for each 10 Mg ha^{-1}, with error bars showing standard errors; **b)** reprint of Figure 7a from Baccini *et al.*, showing the mean maximum height for each pixel averaged into 10 Mg ha^{-1} biomass classes, with errors bars showing standard errors; **c)** as for a), but with the Lorey's height values transformed into estimates of AGB (using an equation derived from African plot data), and with a 1:1 line shown in green.

We are unable to explain this discrepancy between our GLAS analysis and that of Baccini *et al.*, though one factor could be that the metric derived from the raw GLAS waveform that we used (Lorey's height) is different from the metric they used (an estimate of canopy height, and the ratio of HOME to height). As Lorey's height is an average height weighted by basal area, its value will always be lower than maximum height for the same forest. However, it should be more sensitive to AGB than any estimate of height alone, and yet it does not appear to increase with AGB here. The result we report here does appear to concur with the results of the field data comparison, that is, that the Baccini *et al.* map appears to have a low accuracy, in contrast to those reported within the paper. The possible causes of this low accuracy are fourfold: (i) the quality of the field data, which were mostly not scientific plots; (ii) The field data were not collected at a similar time to the remote sensing data; (iii) Some of the 'field data' points used by Baccini *et al.* are derived from a landcover map, itself derived from remote sensing; (iv) The field data were from a very limited spatial distribution, and not from across the continent. These issues are discussed below.

8.4. Discussion of Baccini *et al.*'s field data

We fully sympathise with the difficulties faced by Baccini *et al.* in obtaining sufficient numbers of high quality field plots across a continent, as this is extremely challenging. However, the field data used by Baccini *et al.* are unlikely to be suitable for developing an accurate AGB map, as in addition to likely high randomly-distributed inaccuracies, they are also likely to have consistent biases. We shall specifically examine the three datasets Baccini *et al.* used in detail in order to highlight the potential problems with these types of data:

1. The commercial forest inventory plots in the Republic of Congo (collected 2001-2003) relied on measuring the diameters of just 1 % of stems >40 cm diameter, 0.5 % of stems 20-40 cm, and 0.2 % of 'commercial species only' 2-20 cm. This very low proportion of diameters measured is likely to lead to inaccurate AGB estimates and, unless the small proportion chosen for measurement is strictly random (with regards to both species and diameters), will lead to biased estimates. Additionally, logging companies, until very recently, have not collected data to estimate biomass

stocks, but to assess the approximate density and size-class distribution of timber trees. Therefore: (i) the plot sizes and tree diameters may be inaccurate (indeed it is not specified whether or not the trees were measured here, often in such commercial inventories trees are placed in broad DBH classes rather than measured to the nearest mm); and (ii) the trees to be measured were unlikely to be a strict random subset of all the trees present. Though Réjou-Méchain *et al.* (2011) did not find that commercial forestry inventories have a strong bias towards commercial species, as is often assumed, the above problems are still sufficient to result in large errors in AGB estimates. Baccini *et al.* only used these data when at least three biomass plots were located within the same 1 km pixel. However, this averaging step will only reduce noise in the dataset; it will not correct for any systematic biases introduced by the methodology. This dataset makes up 65 % of the pixels used by Baccini *et al.* for training and validation.

2. The dataset used by Baccini *et al.* from Cameroon involved measuring the diameters of all stems greater than 10 cm DBH for 3 x 1 ha plots within each of 61 pixels. Unfortunately the diameters were only recorded as being within 10 cm bands rather than measured to the nearest millimetre, as is normal for scientific inventory plots: this will reduce accuracy. The biomass results for these plots appear very low for "dense humid forest" from South-Central Cameroon (mean c. 100 Mg ha^{-1}, maximum 220 Mg ha^{-1}, based on Baccini *et al.*'s Fig 3). Other field plots published from within this area all have AGB values >400 Mg ha^{-1} (Djuikouo *et al.* 2010; Lewis *et al.* 2009). Furthermore the plots were measured in 1994, while the remote sensing dataset is from 2000-2003: Baccini *et al.* use Landsat TM scenes from 1990 and 2000 to exclude plots that have undergone "forest cover change" over this period, but quite significant changes will not necessarily be visible in TM data (GOFC-GOLD, 2009). The accuracy of this dataset is therefore hard to assess, but it makes up only 4 % of the pixels used in the Baccini *et al.* study.

3. Baccini *et al.*'s dataset from Uganda is possibly the least accurate. Again, very little description of these plots is given in the paper, however the referenced Drichi (2003) 'National biomass study' from the Uganda Forest Department presents a landcover map of Uganda, with the country divided into vegetation classes using SPOT remote sensing data from 1990-1994, with data from a field campaign

involving 4000 small forest inventory plots being used to give each vegetation class an average AGB value. However, the actual field plots were not used for this study, but instead Baccini *et al.* interpolated AGB values for their pixels from this "high resolution land cover type map", i.e. the proportion of each landcover class within each 1 km MODIS pixel was multiplied by its AGB value in order to give a weighted mean AGB value for that pixel. Landsat TM data was then used to select <0.2 % of the ~236 000 pixel dataset (442 pixels are used, selected using undefined criteria). The use of optical remote sensing data to define the original landcover classes could explain the high accuracies reported by Baccini *et al.*, as similar spectral information is used both to define and later separate biomass values; this will inevitably lead to higher accuracies than when truly independent field data is used. Equally, the use of a single average AGB value for each landcover class introduces pseudoreplication, as multiple pixels containing the same landcover class will be given identical AGB values (derived from the same plot data), but are treated as independent data points by the analysis. This dataset provides almost all the savanna and woodland training points used in the Baccini *et al.* map, which is the landcover of 91 % of the total area predicted (Mayaux *et al* 2004).

8.5. Discussion

Given the likely quality of the field data, it is surprising that the model Baccini *et al.* develop appears to be so accurate against their test data. For example, it performs well against 10 % of data held back for testing (training: 96 % variance explained and RMSE 23.5 Mg ha^{-1} vs testing: 82 % and 50.5 Mg ha^{-1}). This apparent contradiction, with the model performing well against the three datasets included in Baccini *et al.*, but not in the field data we compiled, may be because of the circularity of using a landcover map partially derived from remote sensing data to derive the Uganda dataset, the pseudoreplication inherent in the Uganda dataset, and the small biomass range in the Baccini *et al.* dataset compared to our dataset. However, an alternative explanation may be that the complex RandomForest model developed using a suite of MODIS variables to relate to AGB is not invariant across the continent. This is a significant danger: the Baccini field plots are located in three relatively small areas from approximately 1 to 4 degrees N, and most vegetation types, or ecoregions, were not sampled. In general using RandomForest (or other non-parametric models) with

limited and uneven spatial sampling of variables, results in over-fitting the training data and produces large predictive errors outside the training regions (Genuer et al., 2008). We suggest that their model may work relatively well for these three regions containing training data, while being poor in other regions, if, as is conceptually likely, the complex interactions of reflectance data that correspond to different AGB values within their model are not invariant across the full extent of the predicted AGB map.

8.6. Conclusion

In conclusion, we present evidence that the Baccini *et al.* biomass map of Africa has large errors, with discrepancies between their map and independent scientific inventory plots resulting in an RMSE of 145 Mg ha^{-1}, and field data averaged by vegetation class suggesting that the AGB values for forest areas are underestimated, and for savanna areas mostly overestimated. Three major lessons should be taken from this analysis, to avoid these types of errors in the future: these apply equally to all studies that attempt to use point-data to extrapolate an ecological variable across a landscape. The first lesson is that care must be taken to use good quality, unbiased field data: if there are sufficient plots then it is not necessary for the individual field data points to have a high accuracy, but if they have inherent biases then the resulting map will not be valid. The second lesson is that field data must be drawn from across the spatial extent and ecological variability of the prediction area; due to logistical constraints an even spatial distribution of plots is rarely possible. However, if plots are unevenly distributed then this must be considered in the analysis, and ideally a map showing an estimated distribution of accuracy should be included. Finally, accuracy assessments should be done against truly independent datasets, not a small random subset of the input data, which may suffer from the same biases or be related in other ways than just the parameter of interest.

8.7 Acknowledgements

We thank Alessandro Baccini and his coauthors for providing their AGB map for us to compare to our data. Michael Lefsky provided processed ICESat GLAS Lorey's height data. We thank the following people and institutions for providing help in collecting field data, or for permission to use their field data for this study: Tropical Biomes in Transition (TROBIT, NERC Consortium project, NE/D005590/1): Jon Lloyd, University of Queensland, Bonaventure Sonké, Université de Yaoundé I, Cameroon; CARBOVEG Guinea-Bissau (funded by the Ministry of Environment, Portugal (PA), the Ministry of Science and Technology, Portugal (FCT) & The Gulbenkian Foundation): João Carreiras, Tropical Research Institute (IICT), Lisbon, Portugal, Maria José Vasconcelos, IICT, Lisbon, Portugal; Nhambita Carbon & Communities Project (funded by the EU, NERC): Casey Ryan, University of Edinburgh, UK, Emily Woollen, University of Edinburgh, UK, Mathew Williams, University of Edinburgh, UK; Malawi data (funded by NERC, Moss Centenary Scholarship, Natural Resources International Foundation Travel Award): Gemma Cassells, University of Edinburgh, in-country support provided by the Department of Forestry and Department of Land Management at Mzuzu University, Bennet Mataya and Jarret Mhango; Zambia data: Ministry of Forestry, Zambia, Leon-Jaques Theron & Dr Solomon Tesfamichael, Peace Parks Foundation, Stellenbosch, South Africa; Lyndon Estes, University of Virginia, USA; Natascha Ribiero, Universidade Eduardo Mondlane, Mozambique; the Southern African Regional Science Initiative 2000 (SAFARI 2000) project; Biomass collection work in Lopé national park was funded by the Gordon and Betty Moore Foundation and the Packard Foundation, and supported by the Gabonese Agence Nationale des Parcs Nationaux, the Station d'Etudes des Gorilles et Chimpanzés, Murray Collins, Lee White, Kate Abernethy, Kath Jeffery, & Etienne Massard; Uganda data: Doug Sheil (ITFC), Kirsty Laughlin, and the Budongo Conservation Field Station (funded by the Royal Zoological Society of Scotland). Simon Lewis is supported by a Royal Society University Research Fellowship. Edward Mitchard is funded by Gatsby Plants.

8.7. References

Baccini A, Laporte N, Goetz SJ, Sun M and Dong H (2008) A first map of tropical Africa's above-ground biomass derived from satellite imagery *Environmental Research Letters,* 3, 045011

Brown S, Pearson T, Moore N, Parveen A, Ambagis S and Shoch D (2005) Impact of selective logging on the carbon stock of tropical forests: Republic of Congo as a case study Technical Report 6 Winrock International http://www.winrock.org

Chave J, Condit R, Lao S, Caspersen JP, Foster RB and Hubbell, SP (2003) Spatial and temporal variation of biomass in a tropical forest: results from a large census plot in Panama. *Journal of Ecology*, 91, 240-252.

Chave J., Andalo C., Brown S., Cairns M., Chambers J., Eamus D., Fölster H., Fromard F. et al. (2005) Tree allometry and improved estimation of carbon stocks and balance in tropical forests. *Oecologia* 145, 87-99

Drichi P (2003) National biomass study Technical Report Forest Department, PO Box 1613, Kampala, Uganda

Djuikouo MNK, Doucet J-L, Nguembou CK, Lewis SL and Sonké B (2010) Diversity and aboveground biomass in three tropical forest types in the Dja Biosphere Reserve, Cameroon. *African Journal of Ecology.* 48 1053–1063

Genuer R, Poggi J-M, Tuleau C (2008) Random Forests: some methodological insights. Research report INRIA Saclay, RR-6729. http://hal.inria.fr/inria-00340725/fr/

GOFC-GOLD (2009) Reducing greenhouse gas emissions from deforestation and degradation in developing countries: a sourcebook of methods and procedures for monitoring, measuring and reporting GOFC-GOLD Report, Version COP14-2, Alberta, Canada

Lefsky MA, Harding DJ, Keller M, Cohen WB, Carabajal CC, Espirito-Santo FDB, Hunter MO, and de Oliveira R (2005) Estimates of forest canopy height and aboveground biomass using ICESat *Geophysical Research Letters,* 32 L22S02

Lefsky MA (2010) A global forest canopy height map from the Moderate Resolution Imaging Spectroradiometer and the Geoscience Laser Altimeter System *Geophysical Research Letters,* 37 043622.

Lewis SL, Lopez-Gonzalez G, Sonké B, Affum-Baffoe K, Baker TR, Ojo LO, Phillips OL, Reitsma J, White L, Comiskey J, Ewango C, Feldpausch TR, Hamilton AC, Gloor M, Hart T, Hladik A, Djuikouo MNK, Lloyd J, Lovett J, Makana J-R, Malhi Y, Mbago FM, Ndangalasi HJ, Peacock J, Peh KS-H, Sheil D, Sunderland T, Swaine, MD, Taplin J, Taylor D, Sean CT, Votere R and Hannsjo W. (2009) Increasing carbon storage in intact African tropical forests *Nature,* 457, 1003–1006

Lu D (2006) The potential and challenge of remote sensing-based biomass estimation *Intenational Journal of Remote Sensing,* 27 1297–32

Mayaux P, Bartholome E, Fritz S and Belward A (2004) A new land-cover map of Africa for the year 2000J. *Biogeography*, 31, 1–17

Mitchard ETA, Saatchi SS, Gerard FF, Lewis SL, and Meir P (2009, and Chapter 3) Measuring woody encroachment from 1982-2006 along a forest-savanna boundary in central Africa. *Earth Interactions.* 18, 8

Réjou-Méchaina M, Fayolle A, Nasi R, Gourlet-Fleury S, Doucet J-L, Gally M, Hubert D, Pasquier A, and Billand A (2011) Detecting large-scale diversity patterns in tropical trees: Can we trust commercial forest inventories? *Forest Ecology and Management* 261, 187–194

Saatchi S.S., Harris N.L., Brown S., Lefsky M., Mitchard E.T.A., Salas W., Zutta B.R., Buermann W., Lewis S.L., Hagen S., Petrova S., White L., Silman M. & Morel A. (2011) Benchmark map of forest carbon stocks in tropical regions across three continents. *Proceedings of the National Academy of Sciences*, in press.

Zheng D, Rademacherb J, Chena J, Crowc T, Bresee M, Moined J L and Ryu S 2004 Estimating aboveground biomass using Landsat 7 ETM+ data across a managed landscape in northern Wisconsin, USA *Remote Sensing of Environment,* 93, 402–11

9. Conclusions

9.1 Summary

In this thesis, field data and satellite remote sensing have been used to demonstrate the following, fulfilling the six aims stated in Section 1.3:

- Chapter 3 (Mitchard *et al.* 2009a, *Earth Interactions*): Dry-season NDVI is tightly correlated to canopy cover in a forest-savanna transition area of Cameroon (r^2 = 0.87, n = 32). This relationship was used with a novel change metric, after cross-calibration of the images, to show that extensive woody encroachment has occurred in the forest-savanna transition area of the Mbam Djerem National Park, Cameroon, from 1986 - 2006.

- Chapter 4 (Mitchard *et al.* 2011a, *Remote Sensing of Environment*): Cross-polarised (HV) L-band Synthetic Aperture Radar (hereafter referred to as 'radar') data from the ALOS PALSAR satellite is strongly correlated with aboveground biomass (AGB) up to a saturation point of around 150 Mg ha^{-1} (r^2 = 0.86, n = 25), using data from the Mbam Djerem National Park of Cameroon in 2007. As in Chapter 3, cross-calibration was used to allow the use of remote sensing data from the past, when field data had not been collected: in this case JERS-1 radar data from 1996. The change analysis concurred with Chapter 3 in finding significant areas of woody encroachment in and around the national park, but over the wider 15 000 km^2 area analysed deforestation dominated.

- Chapter 5 (Mitchard et al., 2009b, *Geophysical Research Letters*): The relationship developed between HV radar and AGB is similar across four widely-separated sites, in Cameroon, Uganda, northern Mozambique and central Mozambique. A combined HV-AGB equation was developed (r^2 = 0.86, n = 253), which allowed the prediction of AGB with an accuracy of ±20 % (limited at 150 Mg ha^{-1}). An important conclusion of this study for using such radar data in areas without field data was that prediction errors (RMSE

values) increased by only 12-30 % when an AGB-HV equation developed from the other three sites was used, compared to an equation developed using the field data from that one site alone.

- Chapter 6 (in review: *Plant Ecology & Diversity*): L-band HV radar can be used to monitor forest degradation in a Miombo woodland REDD+ and reforestation project, identifying degradation with confidence (known areas of degradation were observed using radar to have decreased in AGB by 3 Mg ha^{-1}). However, this method struggled to detect small increases in AGB accurately over the two year period investigated. This study shows that radar has the capability to monitor avoided deforestation and reforestation projects.

- Chapter 7 (Mitchard *et al.*, 2011b, *Biogeosciences*): Using ground plot data from the high-biomass Lopé National Park in Gabon, AGB can be mapped using L-band radar, despite the majority of the area being above the saturation point shown elsewhere to be ~150 Mg ha^{-1}. This study used the L-band SAR to segment the image into vegetation types, and ICESat GLAS spaceborne LiDAR data to obtain biomass estimates for the segments; the total AGB of the park was estimated to be 78 Tg C (173 Mg C ha^{-1}), with ±25 % uncertainty. This novel methodology showed that L-band radar can still be useful in mapping AGB beyond its saturation point, as the backscatter values and ratio between the polarisations still contains information about vegetation structure.

- Chapter 8 (Mitchard *et al.*, 2011c, *Environmental Research Letters*): an extensive field dataset of 1154 plots from 16 African countries, and the complete dataset of ICESat GLAS data over the region, were used to test the accuracy of an AGB map of tropical Africa produced by Baccini *et al.* (2007). Only a weak correspondence was found between the field plots or LiDAR data and the Baccini *et al.* AGB map. Analyses of subsets of the data suggested this was not due to artefacts of the data comparison, but instead

due to inaccuracies and biases inherent in the field data and methodology used by Baccini *et al.*

9.2 Implications

These results have important implications for three major areas: a) for use in estimating and monitoring woody cover and biomass in conservation, avoided deforestation (REDD+) and reforestation projects, across Africa and globally; b) for policy makers involved in mitigating climate change, forest conservation, and research and satellite funding; and c) for the wider research community, both in the fields of forest ecology and remote sensing.

9.2.1 Implications for forest monitoring for conservation, REDD+, and LULUCF projects

The managers of national parks and conservation projects, LULUCF projects (Land Use, Land Use Change, and Forestry, which include afforestation and reforestation projects), and REDD+ projects (Reducing Emissions from Deforestation and Degradation), all need to be able to robustly map woody cover and woody biomass stocks, and changes in these stocks. For the purposes of conservation, this process of mapping and monitoring can inform management decisions, enabling such decisions to be made to maximise the species diversity and ecological value of an area. Equally, effective satellite monitoring allows for rapid responses to recent degradation or deforestation. For LULUCF and REDD+ projects, having an effective system for monitoring woody biomass is an essential part of the project management, as the carbon credits earned are directly related to changes in biomass stocks.

This thesis presents analysis methods for three different types of remote sensing data that can be used to assess and monitor woody cover and/or biomass. A major finding from this thesis is that radar and LiDAR datasets offer many advantages over optical datasets in terms of their ability to map AGB and AGB change. This had already been appreciated (e.g. GOFC-GOLD 2009), but it is hoped that the data from this thesis will help encourage project management plans to move beyond simple classifications of optical imagery into more sophisticated optical, radar and LiDAR

analyses, which can give quantitative values of canopy cover and/or AGB for each pixel, with known uncertainties.

The specific implications of the results of this thesis for each type of remote sensing data are presented below in the same order as in Chapter 2.

Optical data: Chapter 3 showed that optical remote sensing can be used to map woody cover and changes in woody cover, using cross-calibrated vegetation index (NDVI). This was not unexpected, but the relationship between NDVI and canopy cover was perhaps stronger than has often been found elsewhere. This is likely to be because in this area of Cameroon the majority of the woodland trees retain their leaves during the dry season, whereas the grass layer is dead for the majority of this season, meaning that in a dry-season NDVI image the vast majority of the NDVI signal is coming from leaves on trees. This does not occur in every tree-grass system, but in most cases trees do have a different phenlogical cycle to grasses that can be exploited (Ryan, 2009 Chapter 4; Archibald & Scholes, 2007). This result will be very useful for many projects that contain mixed tree-grass systems, allowing a first-stage assessment of how canopy cover has changed as far back as the early 1970s, when the first Landsat data were collected, and also an early-warning system for deforestation. However, once canopy cover reaches 100 % the signal saturates, making this method less useful for determining absolute biomass stocks or detecting the degradation of forests. There are some situations where optical data can differentiate biomass beyond canopy closure (Saatchi *et al.* 2007), but this will not normally be through a direct and simple relationship with a vegetation index, making the monitoring of changes more difficult.

In summary, optical data can be useful for assessing changes in woody cover up to full canopy closure provided the influence of non-woody vegetation can be negated, but is less useful at determining AGB or changes where the canopy cover stays intact.

Radar data: Chapters 4, 5, 6 & 7 all found a strong relationship between L-band cross-polarised radar backscatter and AGB. Such relationships between L-band radar and AGB have been found before. However, the relatively high saturation point consistently found here (~150 Mg ha^{-1}, Chapters 4, 5 & 7), and the consistency between widely separated and different sites (Chapter 5), will assist in changing satellite radar from an experimental technique with potential for the future, to a tool that can be used by land managers now to assess biomass stocks and changes in these stocks. A voluntary-sector REDD+ and afforestation/reforestation project (Envirotrade's Sofala Carbon and Communities Project) was used as a study site in Chapter 6; Envirotrade have found the biomass maps produced from radar in 2007 and 2009 useful for their project implementation, monitoring and verification (Chapter 6). Equally the biomass maps produced for the Mbam Djerem National Park (Chapter 4) and for Lopé National Park (Chapter 7) have been used by the park authorities, the Wildlife Conservation Society, and the Cameroonian and Gabonese governments respectively, to help create forest-loss baselines and plan a management regime for their REDD+ development.

New radar satellites are planned (L-band: ALOS-2, P-band: BIOMASS), and much of the data from such satellites (and the current JAXA L-band satellite ALOS) will be given out free for use in monitoring forest carbon stocks (GOFC-GOLD 2009; Khalasa *et al.* 2009). It is not likely that the relationship between AGB and backscatter will be the same everywhere, so calibration with local field plots remains important. However, the methods and results presented here should allow project managers to justify including such data in their monitoring plans, and increase accuracy in the monitoring of forest carbon stock changes. Equally, by finding strong relationships between AGB and HV backscatter, more complex decompositions of the radar signal are not seen as necessary, reducing the complexity involved in using radar data. However, the use of more complex metrics, especially from full-polarisation data, has the potential to increase accuracies but extracting more information from the radar signal, and should remain an area of active research.

LiDAR: This thesis has not concentrated on LiDAR data, only touching it in passing except in Chapter 8 (and an introduction to the principles in Chapter 2). Despite LiDAR's unique potential for very high accuracy characterisation of the structure of woody vegetation, it is currently not possible to easily apply such data at a project scale. Firstly this is because of the paucity of such data collected systematically from satellites: there is currently no suitable satellite collecting data, with ICESat GLAS having collected data only from 2003-2009. ICESat-2 is not scheduled for launch until 2016. Secondly, satellite LiDAR is still not ideal for mapping and monitoring AGB, as it only samples a small proportion on the surface in widely separated circular footprints, and thus must be combined with other data sources to create maps (Chapter 7). This lack of available data, and the necessity of combining it with other data sources, makes optical and radar data more applicable for monitoring vegetation changes for REDD+/LULUCF and other conservation projects.

Both these problems (incomplete coverage and lack of a satellite data) can be solved by using LiDAR data from aircraft: there have never been more active airborne LiDARs, and the density of laser footprints from such systems (with many footprints per square meter) means that full coverage of an area can be collected at a very high resolution (10's of footprints per m^2). LiDAR from aircraft has the ability to map the canopy height, and to a certain extent the three-dimensional structure, of forests, allowing accurate estimates of biomass to be produced (Asner *et al.* 2010). However, such data are expensive and time-consuming to collect and process, and thus are not easily applicable to most REDD+, LULUCF and conservation projects; though these costs may decrease in the future. Aircraft-derived LiDAR data can also be used to help calibrate and validate carbon-stock and change estimates derived from radar and optical data (Weishampal *et al.* 2000; Clark *et al.* 2004; Asner *et al.* 2010), for example using data from a small part of a study area, or to test the general applicability and reliability of methodologies to be applied more widely. However, for the majority of REDD+ and conservation projects, aircraft-derived LiDAR data will not be available.

9.2.2 Implications for policy makers

Non-optical data: The first (of three) major implications of this research for policy-makers is the importance of non-optical data in obtaining accurate estimates of canopy cover and AGB mapping and changes. Optical data are highly useful, because of the large number of satellites currently collecting data, the long historical record (from 1972, and earlier using comparable aircraft data), and ease of interpretation. However, these data do not contain information about the three-dimensional structure of vegetation, and thus are a poor tool for mapping changes in the AGB of woodlands or forests. Active sensors, (*i.e.* LiDAR or radar) can penetrate the forest canopy and collect such data. Therefore, providing funding for new satellites collecting active remote sensing data, for research into methodologies for using such data, and building capacity in-country to analyse such data, should remain an essential component of government policies for conservation and forest protection.

Continuous-fields: Secondly, policy makers should encourage a move from classification-based analysis towards continuous-fields. That is to say, rather than giving every pixel in an analysis a land-cover class such as 'forest' or 'savanna', pixels should be given absolute values of AGB or canopy cover (ideally with an associated estimate of uncertainty and precision). Data and methodologies now exist to perform these more sophisticated analyses, and movement towards using them should be encouraged: by its very nature cutting up a landscape into artificial classifications will always reduce accuracy. This is especially vital for REDD+ projects, which are a global policy priority, as small negative and positive changes in carbon stocks within the same vegetation class are of vital importance. Similarly such data are essential for answering large-scale scientific questions about the carbon balance of these ecosystems. For example, assessing forest degradation, or assessing the size of the terrestrial CO_2 sink (which may be being caused by CO_2 fertilisation), can only be quantified by using a continuous-field methodology.

Uncertainty: Thirdly, throughout this thesis the importance of uncertainty estimation has been stressed. Too many remote sensing studies and forest management plans have in the past provided estimates without associated uncertainty values, which can make them of little value for many purposes. Policy makers, including governments and organisations such as UNREDD, the FAO, and GOFC-GOLD can influence this by demanding that studies include measurements of both accuracy and precision for each stage of their analysis, and propagate these through to their final results. Accuracy and precision are both measures of uncertainty and so are often confused, but they are very different:

> **Accuracy:** accuracy is a measure of the difference between the averages of many measurements and the true value. In a typical remote sensing for AGB estimation example, this includes biases within allometric equations and field methods, and biases in the regression between field data and remote sensing data when applied to the pixel of interest.
>
> **Precision:** precision is a measure of the repeatability of a measurement – if the same measurement was taken many times independently, with the same methodology, how much would they differ? Again, using the example of the remote sensing of AGB, this is affected by noise in the remote sensing signal, and how different atmospheric and vegetation conditions (not accounted for in the methodology) could affect the estimate.

Another way to consider these when examining a time series of AGB estimates for a particular pixel: accuracy is the mean error of the absolute AGB value, whereas precision is an estimate of the accuracy of the AGB change between each timepoint. In many circumstances there are good reasons to suggest that the precision of a monitoring system could be quite high, allowing fairly accurate change estimates, even if the absolute accuracy is comparatively low (Chapter 6). Both of these components of uncertainty are difficult to quantify (*i.e.* estimates of uncertainty themselves are often very uncertain) However, even rough estimates are very useful. Policy makers should aim to create a landscape where these estimates become a routine part of every stage in quantifying forest cover and AGB.

9.2.3 Implications for researchers

This PhD has left numerous scientific questions unanswered, and many lines of research remain to be completed. Many are discussed in the Discussion sections of Chapters 3-8, and will not be repeated here. However, there are four key issues that are returned to throughout the thesis, which should be considered and addressed urgently by the research community:

Uncertainty: The importance of quantifying uncertainty (see Section 9.2.2 above) also applies strongly to researchers: as a community we must collectively think carefully about the best methods of estimating uncertainty, and include these estimates in all studies. New primary research is called for, among forest ecologists, remote sensing scientists, and statisticians. The increase in field data (especially in regularly remeasured field plots) that will be collected due to the rapid expansion of REDD+ and AFOLU projects will provide the ideal opportunity.

Resolution & Scale: so many processes in ecology are scale-dependent, and the distribution of biomass and canopy cover in forests is no exception. The range and normality of AGB values derived from plot data is highly dependent on their plot size (Chave *et al.* 2004); canopy cover shows similar trends (Chapter 3). Within remote sensing studies, there is often a mismatch between field data and pixel size; this is hard to account for statistically, but must be included as a source of error. Further investigation of this issue must be continued, especially in terms of what size of degradation or deforestation event can be detected by sensors acting at different resolutions.

The findings in this thesis have shown that radar satellite data can be used to quantify AGB. However we do not as yet truly understand the radar response to vegetation. This constrains analysis, especially with respect to predicting how radar will respond to different vegetation structures and moisture conditions, and how uncertainty can be reduced. While empirical relationships between field-derived AGB and backscatter can be used, ultimately a more fundamental understanding of the physics involved in the radar response to woody vegetation is essential. Currently there is a

disagreement as to which scatter types dominate, and why saturation occurs (Imhoff 1995; Lin & Sarabandi 1999, Woodhouse 2006): research must focus on resolving these issues.

Spaceborne LiDAR: The use of airborne LiDAR is well understood, and offers the potential to enable researchers to use it to both map and quantify changes in AGB with a high accuracy. However, airborne LiDAR is expensive and the capacity does not currently exist to cover more than a very small percentage of the forested area of the tropics. Spaceborne LiDAR instruments have the potential to improve and verify estimates of AGB and AGB change, as the estimates of canopy height and vegetation density they provide correlate very strongly to AGB. The scientific question here is how such data, which typically consists of widely-separated, non-randomly distributed footprints, can be used to assist other remote sensing and ground data layers in producing accurate maps of AGB and AGB change. Also, the current lack of spaceborne LiDAR system creates an opportunity to design new systems optimal for this purpose, for example with smaller footprints, or potentially novel methodologies such as photon-counting (Mitev, 2011) or multi-spectral capabilities (Morsdorf *et al.* 2009).

9.3 References

Archbald, S., & Scholes, R.J. (2007). Leaf green-up in a semi-arid African savanna – separating tree and grass responses to environmental cues. *Journal of Vegetation Science,* 18, 583-594.

Chave J., Condit R., Aguilar S., Hernandez A., Lao S. & Perez R. (2004) Error propagation and scaling for tropical forest biomass estimates. *Philosophical Transactions of the Royal Society of London Series B-Biological Sciences*, 359, 409-420

Clark M.L., Clark D.B. & Roberts D.A. (2004) Small-footprint lidar estimation of sub-canopy elevation and tree height in a tropical rain forest landscape. *Remote Sensing of Environment*, 91, 68-89

Asner G.P., Powell G.V.N., Mascaro J., Knapp D.E., Clark J.K., Jacobson J., Kennedy-Bowdoin T., Balaji A., Paez-Acosta G., Victoria E., Secada L., Valqui M. & Hughes R.F. (2010) High-resolution forest carbon stocks and emissions in the Amazon. *Proceedings of the National Academy of Sciences of the United States of America*, 107, 16738-16742

GOFC-GOLD (2009) *A sourcebook of methods and procedures for monitoring and reporting anthropogenic greenhouse has emissions and removals caused by deforestation, gains and losses of carbon stocks in forests, remaining forests, and forestation*. GOFC-GOLD, Alberta, Canada

Imhoff M.L. (1995) A Theoretical-Analysis of the Effect of Forest Structure on Synthetic-Aperture Radar Backscatter and the Remote-Sensing of Biomass. *IEEE Transactions on Geoscience and Remote Sensing*, 33, 341-352

Y.-C. Lin, Y.-C. & Sarabandi, K. (1999). A Monte Carlo coherent scattering modelfor forest canopies using fractal-generated trees. *Transactions on Geoscience and Remote Sensing,* 37, 440–451.

Khalsa S.J.S., Nativi S. & Geller G.N. (2009) The GEOSS Interoperability Process Pilot Project (IP3). *IEEE Transactions on Geoscience and Remote Sensing*, 47, 80-91

Mitchard, E.T.A., Saatchi, S.S., Gerard, F.F., Lewis, S.L., & Meir, P. (2009a; and this thesis Chapter 3). Measuring woody encroachment along a forest-savanna boundary in central Africa. *Earth Interactions,* 13, 8.

Mitchard, E.T.A., Saatchi, S.S., Woodhouse, I.H., Nangendo, G., Ribeiro, N.S., Williams, M., Ryan, C.M., Lewis, S.L., Feldpausch, T.R. & Meir, P. (2009b ; and this thesis Chapter 5) Using satellite radar backscatter to predict above-ground woody biomass: A consistent relationship across four different African landscapes. *Geophysical Research Letters, 36*, L23401.

Mitchard, E.T.A., S.S. Saatchi, I.H. Woodhouse, T.R. Feldpausch, S. L. Lewis, B. Sonké, C. Rowland, & P. Meir. (2011; and this thesis Chapter 4). Measuring biomass changes due to woody encroachment and deforestation/degradation in a forest-savanna boundary region of central Africa using multi-temporal L-band radar backscatter. *Remote Sensing of Environment, In Press*.

Mitev V. (2011) Compact micropulse backscatter lidar: airborne and ground-based applications. *Environmental Engineering and Management Journal*, 10, 161-168

Morsdorf F., Nichol C., Malthus T. & Woodhouse I.H. (2009) Assessing forest structural and physiological information content of multi-spectral LiDAR waveforms by radiative transfer modelling. *Remote Sensing of Environment*, 113, 2152-2163

Ryan, C.M. (2009). Chapter 4: Tree green-up precedes rainfall across Southern African woodlands. In: *Carbon cycling, fire and phenology in a tropical savanna woodland in Nhambita, Mozambique*. PhD Thesis, University of Edinburgh.

Saatchi S.S., Houghton R.A., Alvala R., Soares J.V. & Yu Y. (2007) Distribution of aboveground live biomass in the Amazon basin. *Global Change Biology*, 13, 816-837

Weishampel J.F., Blair J.B., Knox R.G., Dubayah R. & Clark D.B. (2000) Volumetric lidar return patterns from an old-growth tropical rainforest canopy. *International Journal of Remote Sensing*, 21, 409-415

Woodhouse I.H. (2006) Predicting backscatter-biomass and height-biomass trends using a macroecology model. *IEEE Transactions on Geoscience and Remote Sensing*, 44, 871-877

Appendix 1

Published version of Chapter 3, plus its supplementary information

Earth Interactions • Volume 13 (2009) • Paper No. 8 • Page 1

Measuring Woody Encroachment along a Forest–Savanna Boundary in Central Africa

E. T. A. Mitchard*

School of Geosciences, University of Edinburgh, Edinburgh, United Kingdom

S. S. Saatchi

Jet Propulsion Laboratory, California Institute of Technology, Pasadena, California

F. F. Gerard

Centre for Ecology and Hydrology, Wallingford, United Kingdom

S. L. Lewis

Earth and Biosphere Institute, School of Geography, University of Leeds, Leeds, United Kingdom

P. Meir

School of Geosciences, University of Edinburgh, Edinburgh, United Kingdom

Received 14 August 2008; accepted 20 May 2009

ABSTRACT: Changes in net area of tropical forest are the sum of several processes: deforestation, regeneration of previously deforested areas, and the changing spatial location of the forest–savanna boundary. The authors conducted a long-term (1986–2006) quantification of vegetation change in a 5400 km^2

* Corresponding author address: E. T. A. Mitchard, Institute of Geography, School of Geosciences, University of Edinburgh, Drummond St, Edinburgh, EH8 9XP, UK.
E-mail address: edward.mitchard@ed.ac.uk

DOI: 10.1175/2009EI278.1

forest–savanna boundary area in central Cameroon. A cross-calibrated normalized difference vegetation index (NDVI) change detection method was used to compare three high-resolution images from 1986, 2000, and 2006. The canopy dimensions and locations of over 1000 trees in the study area were measured, and a very strong relationship between canopy area index (CAI) and NDVI was found. Across 5400 km^2 12.6% of the area showed significant positive change in canopy cover from 1986 to 2000 (0.9% yr^{-1}) and 7.8% from 2000 to 2006 (1.29% yr^{-1}), whereas <0.4% of the image showed a significant decrease in either period. The largest changes were in the lower canopy cover classes: the area with <0.2 m^2 m^{-2} CAI decreased by 43% in 20 years. One cause may be a recent reduction in fire frequency, as documented by Along Track Scanning Radiometer-2/Advanced ATSR (ATSR-2/AATSR) data on fire frequency over the study area from 1996 to 2006. The authors suggest this is due to a reduction in human pressure caused by urbanization, as rainfall did not alter significantly over the study period. An alternative hypothesis is that increasing atmospheric CO_2 concentrations are altering the competitive balance between grasses and trees. These data add to a growing weight of evidence that forest encroachment into savanna is an important process, occurring in forest–savanna boundary regions across tropical Africa.

KEYWORDS: Woody encroachment; Ecotone; Change detection

1. Introduction

It has long been appreciated that the woody cover of large areas of tropical Africa has undergone rapid changes in the recent past, with forest having retreated to a small fraction of its present area because of an arid period from circa 4000 to 1300 years before present, and having expanded to its present extent by around 900 years before present despite increasing human pressure (Maley 1996; Salzmann and Hoelzmann 2005). Many factors interact to control the woody cover of an area, including rainfall, soil characteristics, seasonality, temperature, and the level and history of disturbance (Sankaran et al. 2005; Bucini and Hanan 2007). The majority of the woody savannas of Africa would, in the absence of disturbance, become forest: Sankaran et al. (Sankaran et al. 2005) show that if mean annual precipitation (MAP) is greater than 650 mm, then only disturbance (fire, herbivory, timber extraction) prevents canopy closure. This has been confirmed by the observation of rapid woody encroachment in long-term fire exclusion experiments in Ghana (Swaine et al. 1992), Burkina Faso (Menaut 1977), and Ivory Coast (Vauttoux 1976).

Assessing the dynamics of the tropical forest–savanna boundary is important, as change will have large influences on people, ecosystems, and human populations. Changes in tree cover in the wide ecotone between rain forest and dry savannas in Africa depend on the relative strengths of many processes, the most important of which are forest clearance for agriculture and pasture, forest degradation for timber and fuel, changes in fire frequency, and climate change (which includes increasing atmospheric CO_2 concentrations, increasing air temperature, and changes in precipitation; Malhi and Wright 2004). Climate change excepted, increased human presence increases the first three of these, reducing the tree cover of an area, whereas reduced human impact will result in a reduction in these factors, and both an expansion of forest into savannas and a general increase in the woody cover of

those savannas (Bucini and Hanan 2007). The importance of fire frequency cannot be overstated here: almost all fires in African savannas are anthropogenic in origin, and given the ability of fires to spread widely from where they are set they have the potential to influence the vegetation across large areas, even far from human settlements (Favier et al. 2004). The impact of anthropogenic climate change on these ecosystems is still uncertain: although increasing temperatures are likely to reduce the competitiveness of trees over C4 grasses, increasing CO_2 concentrations do the reverse, reducing the advantage C4 grasses have over C3 trees (Lloyd and Farquhar 2008). Increased atmospheric CO_2 concentrations have also been hypothesized to lead to increased success of trees in savannas because of a reduced transpiration rate leading to increased water percolation and reduced seedling mortality (Polley et al. 1997), and by increasing the ability of saplings to resprout successfully following fire damage, thus making it more likely that they will escape the flame zone (Bond and Midgley 2000). While it is appreciated that increased rainfall would over the long term increase tree cover, provided the effect is not negated by increasing temperature (Hély et al. 2006), significant uncertainties exist as to the long-term precipitation trends in the region (Bernstein et al. 2007). These uncertainties are exacerbated by the fact that changes in vegetation in this sensitive region will result in strong feedbacks with climate (Zeng and Neelin 2000).

There is a large body of evidence that woody encroachment (involving both trees and shrubs) into semiarid savannas and grasslands is occurring (Archer et al. 2001; Eamus and Palmer 2007); Archer et al. (Archer et al. 2001) found 28 studies showing increases in woody vegetation in Africa and 202 studies finding such changes worldwide. There are fewer studies finding such an increase in tropical savannas, but some do exist: for example in northern Australia (Hopkins et al. 1996; Bowman et al. 2001; Russell-Smith et al. 2004; Brook and Bowman 2006), the Western Ghats of India (Puyravaud et al. 2003), and South America (Duarte et al. 2006; Durigan and Ratter 2006; Marimon et al. 2006; Roitman et al. 2008). In Africa just four studies showing increasing tree cover in tropical rain forest–savanna boundary regions have been reported. Boulvert (Boulvert 1990) drew on anecdotal evidence to suggest that woody expansion was occurring in the forest–savanna ecotones of central Africa because of the urbanization of the population but provided little concrete evidence. Happi (Happi 1998) compared a high-resolution aerial photograph from 1950 with Landsat thematic mapper (TM) data from 1990 to find gallery forest encroachment into surrounding savannas at a rate of 0.6–2 m yr^{-1} in central Cameroon. Guillet et al. (Guillet et al. 2001) used field studies and soil carbon isotopes ($^{13}C/^{12}C$, ^{14}C) along two transects in eastern Cameroon to show both significant expansion of the forest and that increased woody cover of the savanna has occurred over the past century. Nangendo et al. (Nangendo et al. 2005) used a combination of field studies and vegetation index–based satellite change detection to find a 14% increase in woody vegetation over a 14-yr period in the woodlands of the Budongo Forest Reserve, Uganda. However, all the African studies are small in scale and reliant on detailed local field data for success, and as such their methods are not easily applicable to a larger spatial scale, which is necessary to assess whether this forest encroachment is indeed widespread. No studies showing the opposite process, woody regression, were found for Africa apart from in areas where there has been an increase in anthropogenic activity, for example, around cities and in areas of agricultural encroachment.

Mapping woody cover from remote sensing data can follow a wide range of different methods. Manual interpretation is best suited to hyperspatial satellite data and aerial photographs (Couteron et al. 2001; Xiao and Moody 2005). Classification-based methodologies can be effective (Sedano et al. 2005; Su et al. 2007), but the imposition of artificial classes can result in a tendency toward subjectivity and lead to an overestimation of dominant classes and underestimation of rare classes (e.g., Couteron et al. 2001) and was thought especially unsuitable for this study as finding changes in woody cover within a class (e.g., woody savanna) is not possible. Empirical regressions between vegetation indices or red reflectance can be successful, often finding very strong relationships (Leprieur et al. 2000; Lu et al. 2003; Ferreira et al. 2004; Ferreira and Huete 2004), though problems of soil reflectance (Chen et al. 1998; Leprieur et al. 2000) and the influence of the herbaceous vegetation (Fuller et al. 1997; Qin and Gerstl 2000) must be considered. More sophisticated techniques that can consider more bands—for example, spectral mixture analysis or neural networks, or metrics that include image texture in addition to spectral information—are becoming increasingly accepted; they are, however, very sensitive to differing environmental conditions, sensor type and calibration, solar-target geometry, and atmospheric conditions, and as such are not appropriate for change detection unless there are good ground data for all dates (Coppin et al. 2004; Lu et al. 2004; Lu 2006).

Numerous techniques have been developed for bitemporal change detection, but they can be broadly classed into three categories: postclassification comparisons, image differencing/ratioing, and more sophisticated multiband algorithms (such as change vector analysis or cross-calibration analysis) (Coppin et al. 2004; Lu et al. 2004). Which methodology is chosen depends on the environment being analyzed and the types of data being used: remotely sensed or ground data. In general, when changes in clear categories of land cover are being assessed, classification-based methodologies are appropriate; where the variable being assessed is relatively simple and different sensors or exact atmospheric correction is not possible, image differencing is preferred; and where identical sensors are used and good atmospheric and field data are available, more sophisticated change algorithms may be appropriate, though in most cases they do not give superior results to image differencing–based methodologies (Coppin et al. 2004).

In this paper we examine changes in woody cover in a large study area in central Cameroon. The normalized difference vegetation index (NDVI) derived from Landsat and Advanced Spaceborne Thermal Emission and Reflection Radiometer (ASTER) remote sensing platforms is used in combination with field studies, coarse spatial resolution data [Advanced Very High Resolution Radiometer (AVHRR)], and very high spatial resolution satellite imagery (Quickbird) to identify and characterize with great confidence the changes in woody cover from 1986 to 2006. The methods presented here, because of their relative simplicity and the ready availability of historical NDVI data, allow the possibility of scaling up to a regional level using coarser-resolution data.

2. Study area

The study area is a 5400 km^2 region in central Cameroon, centered on 6°1′22″N, 12°48′40″E, and encompasses the northern two-thirds of the Mbam Djerem

National Park and the area to the north of the park, including the town of Tibati and Lake Mbakauo. This region was chosen as it includes a complete range of regional vegetation types, from forest in the south contiguous with the Congo basin rain forest belt, through a forest–savanna matrix in the north of the park, to savanna with narrow gallery forests in the north of the study area (see Figure 1). It experiences an annual rainfall of 1650 mm, with a pronounced dry season (average 4 mm month^{-1}) from December to March [Climatic Research Unit (CRU) TS 2.1 dataset (Mitchell and Jones 2005) and Tropical Rainfall Measuring Mission (TRMM) 3B43 V6 satellite data (Kummerow et al. 2001)]. The human population of the southern part of the study area is very small and has decreased over the study period because of the formation first of the Reserve de Faune de Pangar et Djerem in 1982, which encompasses 2400 km^2, and then the Mbam Djerem National Park in 2000, which expanded this to 4165 km^2. The population density in the northern half of the study area is higher but still low, with the only major population center being the town of Tibati, which has increased in population by almost 90% over the study period, from 15 522 in the 1987 census to an estimated 28 981 by 2007 (CIESIN 2004). Small-scale agriculture occurs around settlements, and there is a limited amount of nomadic cattle herding passing through the area; local people believe this has decreased significantly over the past 20–30 years. Significant levels of fishing occur within the park, though there are attempts to reduce this (Ministère des Forêts et de la Faune 2007), and also occur in all the rivers and lakes in the study area.

3. Methods

3.1. Field data

The study area was visited October–December 2007 as part of the Tropical Biomes in Transition field campaign (TROBIT; www.geog.leeds.ac.uk/groups/trobit/). Eight transects 20 m wide and 100–200 m long were set up and positioned in three different areas near the Djerem River in the north to middle of the Mbam Djerem National Park (see Figure 1). Seven of these transects ran from forest to savanna, with one entirely in forest. All trees with a diameter at 1.3 m [diameter at breast height (DBH)] greater than 5 cm had their diameter, height, canopy dimensions (distance from trunk to outermost leaf measured for all four compass points), and species identity recorded. A total of 1009 trees, representing 79 species from 33 families, were measured (see appendix A for species list). Each tree was located using a handheld differential GPS (Trimble GeoHX, Trimble, United States); these positions were later corrected using data from the Scripps Orbit and Permanent Array Center (SOPAC) N'Koltang ground station in Libreville, Gabon, using the H-Star differential correction facility in the software GPS Pathfinder Office 3.10 (Trimble, United States), resulting in accuracies of $<$0.5 m in the horizontal direction and $<$1 m in the vertical dimension. The transects were divided into 30-m sections, and the canopy dimensions used to calculate the vertically projected canopy area for each region of the transects (an elliptic canopy shape was assumed), which we named the canopy area index (CAI). The changes in species composition in the different portions of the eight transects are detailed in appendix A.

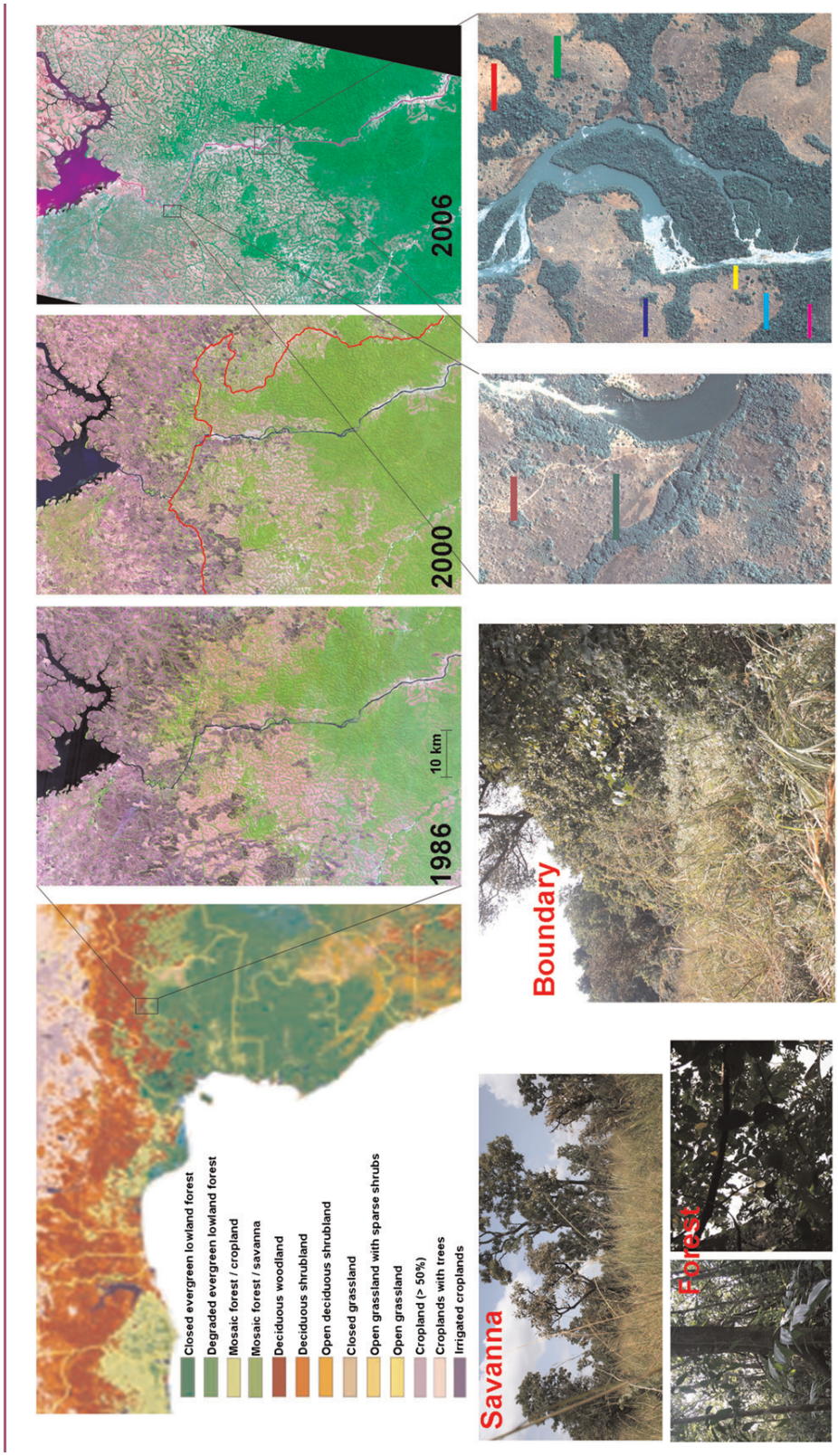
2006
2000
1986
10 km
Closed evergreen lowland forest
Degraded evergreen lowland forest
Mosaic forest / cropland
Mosaic forest / savanna
Deciduous woodland
Deciduous shrubland
Open deciduous shrubland
Closed grassland
Open grassland with sparse shrubs
Open grassland
Cropland (> 50%)
Croplands with trees
Irrigated croplands
Boundary
Savanna
Forest

3.2. Remote sensing data

A Landsat TM image captured on 30 December 1986 and a Landsat Enhanced TM Plus (ETM+) image captured on 12 December 2000, both for path 156 row 56, were downloaded from the Global Land Cover Facility. Both were provided at a pixel size of 28.5 m. Two ASTER scenes, between them covering almost the whole study area, captured 4 December 2006, were acquired from the National Aeronautics and Space Administration (NASA) Land Processes Distributed Active Archive Center. Of the ASTER scene only the visible and near-infrared bands were used in further analysis, which were provided at a 15-m pixel size. Two 0.6-m-resolution Quickbird images were acquired from Eurimage covering all the field sites, by a combination of a 12 × 8 km archive image from 19 February 2004 covering the northern field sites, and a 10 × 10 km new acquisition, captured 23 January 2008, covering the southern field sites.

To remove atmospheric effects from the TM, ETM+, and ASTER data, atmospheric correction was performed using atmospheric/topographic correction software package (ATCOR)-2 (ReSe, Switzerland). This model used the post-launch offsets and gains and a tropical atmospheric model to produce reflectance images. The software package ENVI (ITT, United States) was used for all subsequent remote sensing analysis. The two ASTER scenes were mosaicked together, and visual analysis of the join showed it to be seamless. No sharp changes in the reflectance values of any bands were apparent in 20 transects placed across the join of the two images, so no further correction of the individual scenes was considered necessary. This outcome was expected given that the scenes were captured with the same sensor within 10 s of each other.

The 60 × 90 km study area was subsetted from the 2000 ETM+ image, and the 1986 TM image was georeferenced to this using a network of 40 visually selected ground control points taken from features such as road junctions, islands, small clumps of trees, and branching points of gallery forests, with a resulting root-mean-square error (RMSE) of 0.37 pixels (10.5 m). Similarly the 2006 ASTER mosaic was georeferenced to the 2000 ETM+ image, with a network of 38 ground control points resulting in an RMSE of 0.35 pixels (10 m). The ASTER image was subsequently resampled to 28.5-m pixels using the pixel aggregate method.

Given the difficulties of calibrating images captured by different sensors under different unknown atmospheric conditions, we decided to analyze the changes using normalized univariate image differencing, implemented on cross-calibrated

←

Figure 1. (top row) Vegetation map taken from Mayaux et al. (Mayaux et al. 2004) showing the location of the study area within Cameroon, with the three satellite images compared in this study: Landsat TM from 1986, Landsat ETM+ from 2000, and ASTER mosaic from 2006. The north and east borders of the Mbam Djerem National Park are shown in red on the 2000 image. (bottom row) Pictures taken from the study area in 2007, showing typical forest and savanna biomes, as well as the sharp transition between the two; portions of Quickbird images showing the location of the eight transects where canopy cover was measured.

vegetation indices. Univariate image differencing essentially subtracts one date of imagery from another date and is often chosen as the preferred change detection approach for tropical environments (Coppin et al. 2004; Lu et al. 2004), with Coppin et al. (Coppin et al. 2004) stating in their conclusions summary that "image differencing and linear transformations appear to perform generally better than other bitemporal change detection methods." More sophisticated change detection techniques were thought to be unsuitable for this analysis, as the sensor used at each time point is different, and absolute atmospheric correction of the earlier scenes is not possible.

Using vegetation indices, which are in effect a ratio between two spectral bands, reduces the errors inherent in univariate change detection analyses because ratios between bands are affected to a smaller degree by different atmospheric conditions and different sensor characteristics than raw reflectance values (Coppin et al. 2004; Pettorelli et al. 2005). These indices are developed from the red and near-infrared bands, and their response to vegetation cover is widely acknowledged (e.g., Huete et al. 2002). The visible red wavelengths are absorbed by chlorophyll in vegetation, and near-infrared wavelengths are strongly reflected by the plant cuticle and cell wall, giving higher values for vegetation than for nonvegetated surfaces. As all three images were captured in the early dry season, when the grass layer is dead and dry, containing no chlorophyll, but leaves are still present on most trees, it is to be expected that the value of a vegetation index in a pixel will correspond directly to the CAI of that pixel (Fuller et al. 1997; Qin and Gerstl 2000; Archibald and Scholes 2007). Vegetation indices have been shown to be strongly related to woody cover in savanna environments on a number of occasions (e.g., Lu et al. 2003; Ferreira et al. 2004; Ferreira and Huete 2004). Typical problems with using these indices, such as topography and soil reflectance, were minimized in this study as the study area has little relief and is not large enough to have much heterogeneity in the CAI to vegetation index relationship.

We investigated the use of three vegetation indices: the NDVI, the modified soil adjusted vegetation index (MSAVI) (Qi et al. 1994), and the enhanced vegetation index (EVI) (Huete et al. 1994). The EVI, though it appeared to be very sensitive to vegetation and as such was good for comparing the two Landsat scenes, was abandoned because of the necessity of a blue band (450–515 nm), which is not present in ASTER data. MSAVI, designed to minimize the influence of soil reflectance, produced a small dynamic range for this ecosystem, and though it did differentiate forest from savanna well, it was less successful than NDVI. NDVI was therefore the vegetation index chosen for all subsequent analysis. Its formula is

$$\mathrm{NDVI} = \frac{b_n - b_r}{b_n + b_r}, \tag{1}$$

where b_n is the near-infrared band (750–900 nm) and b_r is the red band (630–690 nm).

The NDVIs from the 1986 TM and 2006 ASTER images were then calibrated to the 2000 ETM+ image using linear regression models derived from 25 known invariant targets (i.e., their land-cover type and appearance did not change in any of the three images). These targets were drawn from water bodies, grasslands, and dense tropical forest [1986–2000, $\mathrm{NDVI}_{\mathrm{adj}} = -0.1804 + 0.9009(\mathrm{NDVI}_{86})$,

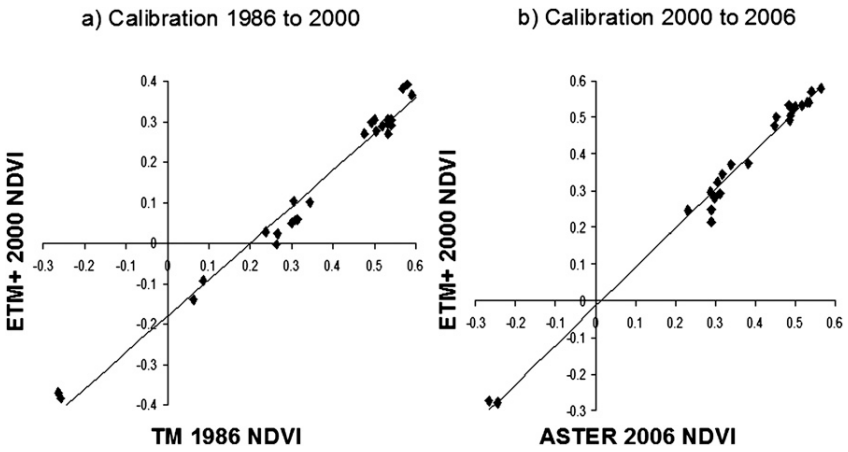

Figure 2. NDVI cross-calibration points, drawn from suspected unchanged areas such as water bodies, grasslands, and dense tropical forest, plotted for (a) ETM+ 2000 against TM 1986 and (b) ETM+ 2000 against ASTER 2006.

$r^2 = 0.98$; 2006–00, $\text{NDVI}_{\text{adj}} = -0.0226 + 1.069(\text{NDVI}_{06})$, $r^2 = 0.98$, see Figure 2]. This process should have removed most remaining calibration problems between the different sensors and atmospheres, and it is as successful as absolute radiative correction (Songh et al. 2001; Coppin et al. 2004), which is not possible here because of the lack of accurate atmospheric data for the 1986 image.

To test that NDVI is correlated with woody cover, the NDVI values extracted from the ASTER 2006 pixels covering each 30-m section of the eight transects were regressed against the CAI measured in situ (defined as m^2 canopy divided by m^2 ground area). A different georeferencing was used here, involving two 10×10 km sections taken from the 15-m adjusted-NDVI ASTER image and performing a very detailed tie-point matching process with the ground control point-corrected Quickbird data (which is estimated to be geocorrected to <2 m). RMSE values were always less than 0.3 ASTER pixels (<4.5 m), based on at least 50 tie points, so it is possible to be very confident that the NDVI values extracted correspond to the portions of the transects measured on the ground.

To examine whether precipitation was similar during November–December 1986, 2000, and 2006, a combination of the weather station and modeling-derived CRU TS 2.1 dataset (1901–2002; Mitchell and Jones 2005) and the TRMM Microwave Imager (TMI) 3B43 V6 satellite data (1998–2007; Kummerow et al. 2001) were used to estimate the rainfall in these months. The monthly precipitation data at a 0.5° resolution were used in both cases, making these two data sources readily comparable. These datasets were also analyzed for long-term rainfall and temperature trends over the study area (1901–2007).

To confirm that trends observed at individual time slices are representative of a genuine trend and not merely caused by problems with calibration or different environmental conditions, NDVI values from the Global Inventory Modeling and Mapping Studies (GIMMS) AVHRR 8-km dataset (Pinzon et al. 2005; Tucker et al. 2005) were extracted over the study area. These data were examined for trends in

the annual average NDVI as well as the annual average NDVIs for the dry and wet seasons.

As fire frequency is considered an important factor in controlling woody cover, an estimate of the changes in fire frequency over the study area was also desirable. No data of sufficient sensitivity exist for the whole study period (AVHRR fire data detected just six hot spots in the study area from 1986 to 2006), so data were acquired from the Along Track Scanning Radiometer-2 and Advanced ATSR (ATSR-2/AATSR) World Fire Atlas from 1996 to 2006. Fires detected from within the study area were extracted and the number of fires counted for each year. This thermal anomaly dataset is known to be accurate, having very good geolocation and low commission errors (Arino et al. 2005; George et al. 2006), but it is also acknowledged that it underestimates the total fire number because of both a lack of sensitivity to low-intensity fires and the nighttime detection missing daytime fires. However, this is not of concern here, as we are interested in the trend in fire frequency, not the absolute rate of fire occurrence.

3.3. Change detection

Image comparisons were performed between 1986 and 2000 and 2000 and 2006. However, before any comparisons, water bodies and urban areas were masked from all images by excluding any pixels with a negative NDVI. A proportion of savanna areas were clearly burn scars and found to have an NDVI between 0.05 and 0.16. Leaving these areas in the analysis with their raw NDVI values would bias the analysis, as the same area changing from burnt grassland to unburnt grassland would appear to have increased in woody cover, whereas in fact no change would have occurred. Rather than exclude these areas from the analysis, which would reduce the area available to detect changes, the value of all unmasked pixels with an NDVI < 0.2 was adjusted to 0.2. This in effect converted all the burnt areas in the images to areas with the same NDVI as savanna with a CAI of 0–0.2 $m^2\ m^{-2}$, as it is assumed that areas that burn in this way, early in the dry season, will have a low CAI (Lambin et al. 2003; Felderhof and Gillieson 2006). The validity of this procedure was confirmed by the observation that the majority of burnt patches in the 1986 image have similar NDVI values to their surrounding, unburnt, areas after this procedure is applied. To confirm that this procedure is not driving the observed results, an identical analysis was performed without this process, instead using a supervised classification to remove all the burnt areas (see appendix B).

Rather than comparing the simple differences in NDVI between the various time points [as recommended by Singh (Singh 1989) and used by, e.g., Nangendo et al. (Nangendo et al. 2005)], we decided to normalize the changes by comparing the difference ratioed by the sum of the pixels, as this further increases confidence in the results of vegetation index differencing change detection (Coppin et al. 2004). This is because difference values of the same absolute magnitude vary in significance depending on the size of the original NDVI values: an increase from 0.25 to 0.35 is much more significant than an increase from 0.45 to 0.55 (see Figure 3), but a simple differencing method will predict the same magnitude of change for both. The formula used for the change detection was, therefore,

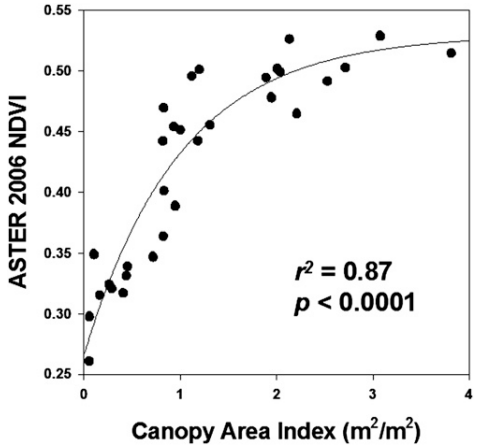

Figure 3. Adjusted ASTER 2006 NDVI regressed against field-measured CAI (m^2 canopy per m^2 area) for 30-m sections of field transects.

$$\text{Change} = \frac{\text{NDVI}_{\text{new}} - \text{NDVI}_{\text{old}}}{\text{NDVI}_{\text{new}} + \text{NDVI}_{\text{old}}}. \tag{2}$$

This produces change images, with every pixel having a value from -1 to $+1$, where zero indicates no change, positive values positive change (i.e., an increase in woody cover), and negative values negative change (i.e., a decrease in woody cover). The resulting distribution of points was tested for normality using a Shapiro–Wilk normality test, and then the standard deviation of the distribution was calculated, allowing an assessment of how much of a deviation from zero indicates a significant change in woody cover. The pixels were therefore grouped into classes according to the number of standard deviations each pixel deviated from zero, with $<\pm$ one standard deviation considered no change, $>\pm$ one standard deviation considered marginally significant change, and $>\pm$ two standard deviations considered significant change at approximately the 95% confidence level.

The tight relationship between the in situ measured CAI and ASTER NDVI makes it possible to look at absolute changes in the extent of woody cover over the study area. To do this the relationship between NDVI and projected CAI was applied to the NDVI image in each of the three time points, and the ground area in five cover classes quantified (water bodies, urban areas, and areas not present in the 2006 mosaic were not included).

4. Results

4.1. Sensitivity of NDVI to CAI

NDVI is shown to be strongly correlated with field-measured CAI ($m^2\ m^{-2}$) in this environment ($r^2 = 0.87$, $p < 0.0001$, $n = 32$; see Figure 3). CAI is directly

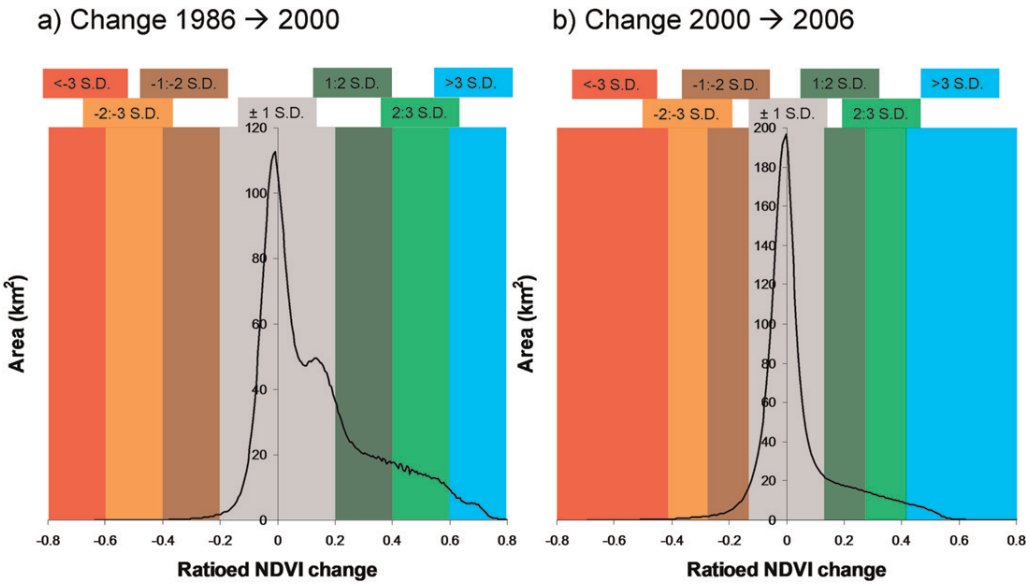

Figure 4. Histograms showing the area covered by pixels in each 0.05 range of ratioed NDVI change, for the 1986–2000 and 2000–06 analyses. Standard deviations of the distribution are overlaid, with colors corresponding to those used in Figure 5.

proportional to the density and size of trees per unit area and believed therefore to be a good measure of woody cover. The fitted line is

$$\mathrm{NDVI} = 0.27 + 0.26(1 - e^{-\mathrm{CAI}}), \tag{3}$$

which can be rearranged to

$$\mathrm{CAI} = -\ln\left(\frac{0.53 - \mathrm{NDVI}}{0.26}\right). \tag{4}$$

Sensitivity decreases rapidly above a CAI of 2 $\mathrm{m}^2\ \mathrm{m}^{-2}$, but NDVI is undoubtedly a very good metric for detecting changes in the woodiness of savannas and the position of the forest–savanna boundary, giving confidence that the change detection shown below relates to genuine changes in woody vegetation.

4.2. Change detection

Both normalized image differencing analyses produced normal distributions centered on 0, with a positive skew, suggesting, respectively, that the cross-calibration process was effective and that increases in NDVI were observed

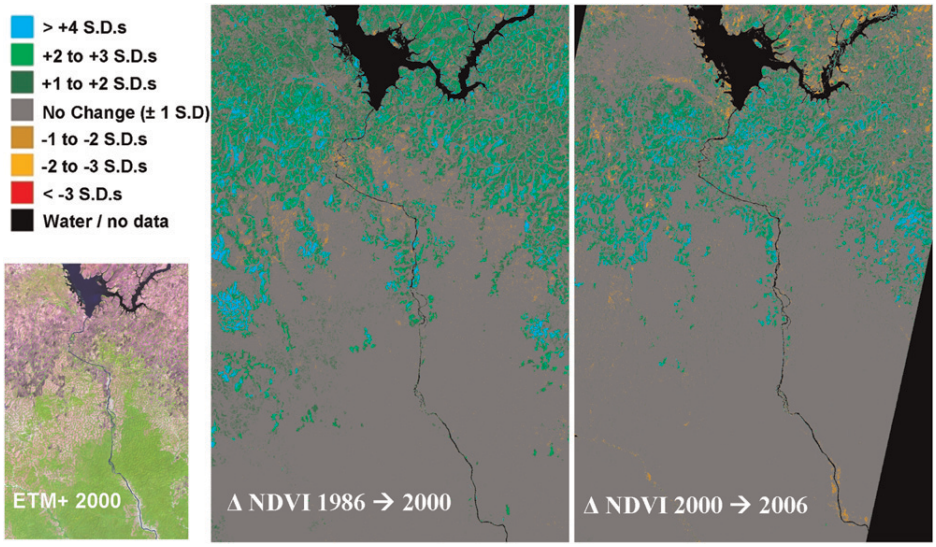

Figure 5. Two images showing the change in NDVI between 1986 and 2000 and 2000 and 2006, in standard deviations (see text). Changes >± two standard deviations should be considered significant at the 95% level. The 5–4–3 composite image from 2000 is also included to show that the increases in NDVI occurred in the savannas, consistent with an increase in woody vegetation.

(Figure 4). When thresholded according to standard deviations, very significant increases in NDVI over savanna regions are found both between 1986 and 2000 and 2000 and 2006, as displayed in Figure 5 and Table 1. A significant positive increase in NDVI (> two standard deviations, approximately equivalent to a 95% confidence level) can be seen in 12.57% of the study area from 1986 to 2000 and 7.76% from 2000 to 2006. There is evidence from this that the rate of woody encroachment has risen over the 20-yr period, as the percentage increase divided by the number of years of comparison is 0.9% yr^{-1} from 1986 to 2000 but 1.29% yr^{-1} from 2000 to 2006. In contrast, the number of pixels showing significant negative trends is negligible in both comparisons.

Applying Equation (4) to the NDVI images allowed an assessment of how the area covered by each vegetation type has changed over the study period. The results of this are displayed in Figure 6. While less sensitive than the change detection analysis, because of inaccuracies in the CAI–NDVI relationship and the necessity to categorize the vegetation into distinct classes, this analysis is useful in that it can quantify which cover classes experienced the most rapid change. This showed that the largest changes are occurring in the low CAI classes, with the area of grassland (less than 0.2 m^2 CAI per m^2 ground) decreasing by 43% over the 20 years, from 2132 km^2 in 1986 to 1214 km^2 in 2006. All the other classes increase over the study period, with the largest increase in the 0.2–0.4 m^2 m^{-2} CAI class and the smallest in the >1 m^2 m^{-2} CAI class.

Table 1. Percentage and area of change images falling into each change class in the two comparisons, TM 1986 with ETM+ 2000 and ETM+ 2000 with ASTER 2006. The percentage significant positive change divided by the number of years of comparison is also included.

Class	1986–2000		2000–06	
	Percent	Area (km^2)	Percent	Area (km^2)
Significant positive change (>+2 std dev)	12.57	679.2	7.76	419.1
Marginally significant positive change (>+1 std dev)	12.46	673	8.02	433
No change (−1 to +1 std dev)	70.28	3795.1	73.35	3960.7
Marginally significant negative change (<−1 std dev)	1.32	71.2	1.68	90.7
Significant negative change (<−2 std dev)	0.08	4.3	0.38	20.4
Masked (water/urban areas/areas not present in 2006 mosaic)	3.28	177.1	8.82	476.0
Significant positive change per year (%)	0.9% yr^{-1}		1.29% yr^{-1}	

Similar trends were found in the analysis where burnt areas where removed prior to the change analysis (see appendix B). The trends found were approximately half the magnitude of the changes above, as would be expected given the large areas of savanna that were removed; however, this provides evidence that the above results are not an artifact of the thresholding methodology used to enable to inclusion of burnt areas.

4.3. High temporal resolution NDVI record

The AVHRR GIMMS NDVI record shows no significant trend in the annual average or the wet-season average from 1982 to 2006. However, there is a very clear increasing trend in the dry-season NDVI (see Figure 7), showing that the trends found in the high spatial but low temporal resolution dry-season analysis are part of a larger trend.

4.4. Rainfall, temperature, and fire frequency

No significant long-term trends were found in the rainfall or temperature data for the study site. Average annual temperature fluctuated from just 22.5° to 23.6°C, with no obvious trends and, while annual rainfall was more variable, most of the variation was due to fluctuations in the wettest months, and still no trends were apparent (see Figure 8). For the above remote sensing–based change detection to be valid it is essential that precipitation in the months preceding the image capture are identical, otherwise the results could be due to changes in the greenness of the vegetation (especially grasses) not to changes in CAI. A comparison was made of precipitation in the month of image capture, 3 months before image capture, and 6 months before image capture; no differences are apparent between years in the month of image capture or the average of the previous 3 months (see Figure 9). However, there does appear to have been greater average rainfall in 2006 than in the other 2 years when the 6-month average is compared. This should not interfere with the results as the grass layer should still have been dead in 2006; however, it

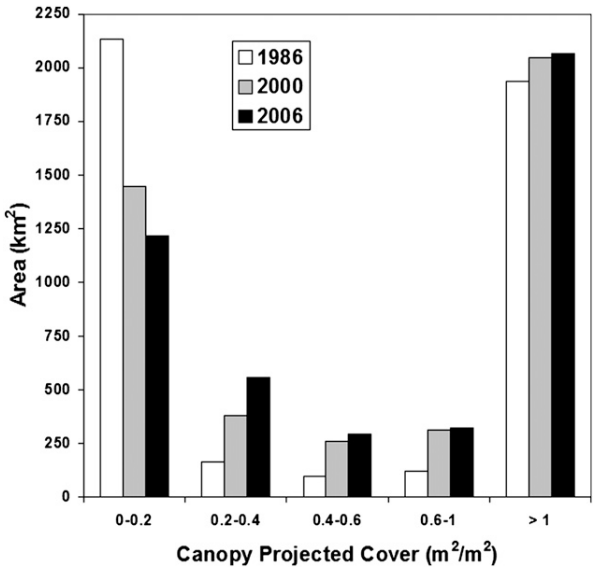

Figure 6. Changes in the total area of vegetation found in different CAI classes in 1986, 2000, and 2006.

should be considered when interpreting the results of the second period of change detection.

Analysis of the ATSR-2/AATSR data provides some evidence that fire occurrence in the study area decreased over the second half of the study period (from 1996 to the present); unfortunately, there are no suitable data for the first half, as AVHRR data have too coarse a resolution and are not sufficiently sensitive to detect these small-scale fires. Figure 10 displays the result, with linear regression finding a significant negative trend in fire frequency against time (gradient $= -1.08$ fires per year, $r^2 = 0.57$, $p < 0.01$, $n = 11$).

5. Discussion

5.1. Woody encroachment

Woody encroachment is occurring rapidly in the Mbam Djerem National Park, corroborating smaller-scale (40–600 km^2) studies showing woody expansion in the forest–savanna ecotones of Africa. This also confirms observations within the study area in November 2007, where forest edges were dominated by young pioneer trees, with dead and dying savanna trees prevalent, which is strong evidence that this constituted young encroaching forests (E. T. A. Mitchard and S. L. Lewis 2007, personal observation; and also the presence of savanna trees in the forest sections of all transects; see appendix A). When looking at the change maps, it is possible to see changes along some gallery forests, suggesting they have increased in width. However, the resolution of the comparisons, 28.5 m, means that even

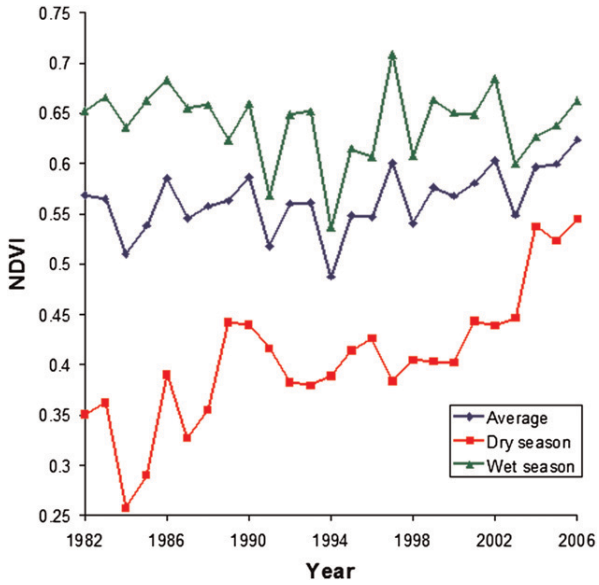

Figure 7. Trends in AVHRR average NDVI for the study area derived from GIMMS data (Pinzon et al. 2005; Tucker et al. 2005). Red points show the average dry-season NDVI (December–March), green points the average wet-season NDVI (April–November), and blue the annual average NDVI.

relatively rapid increases in the size of forests are unlikely to be detected by this method: the forest advance rate of 2 m yr^{-1} found in a nearby region by Happi (Happi 1998) would equate to a movement of 28 m (one pixel) in the 1986–2000 comparison, and 12 m (under half a pixel) in the 2000–06 comparison, both of which could be missed because of slight inaccuracies in the georeferencing. The majority of the increases detected are thus an increase in the woodiness of the savannas, rather than an increase in forest area, as can be seen in Figure 6. We note that, though we are confident the changes we observe genuinely represent an increase in woody cover, the lack of historical field data and local rainfall data prevents us from rejecting the possibility that some or all of these changes are artifacts caused by increases in dry-season rainfall causing greener grasses. We believe the data presented in Figures 7–9 show that this is unlikely to be the case, but without historical field data we cannot be entirely certain, especially for the second period of change detection (2000–06), where, though the rainfall for the preceding 3 months is similar to that in the other 2 years, the preceding wet season had higher rainfall (though it is possible this could be an artifact of using TRMM data, which appears to produce much more variable results in the wet season than the CRU 2.1 dataset; see Figure 8).

While the legal formation of the Mbam Djerem National Park is responsible for some of this gain, slightly over half of the significant positive change in both comparisons occurred outside the park. The likely cause of these changes is hard to determine with confidence, but local people considered the changes due to reductions in human population density, caused by urbanization, resulting in

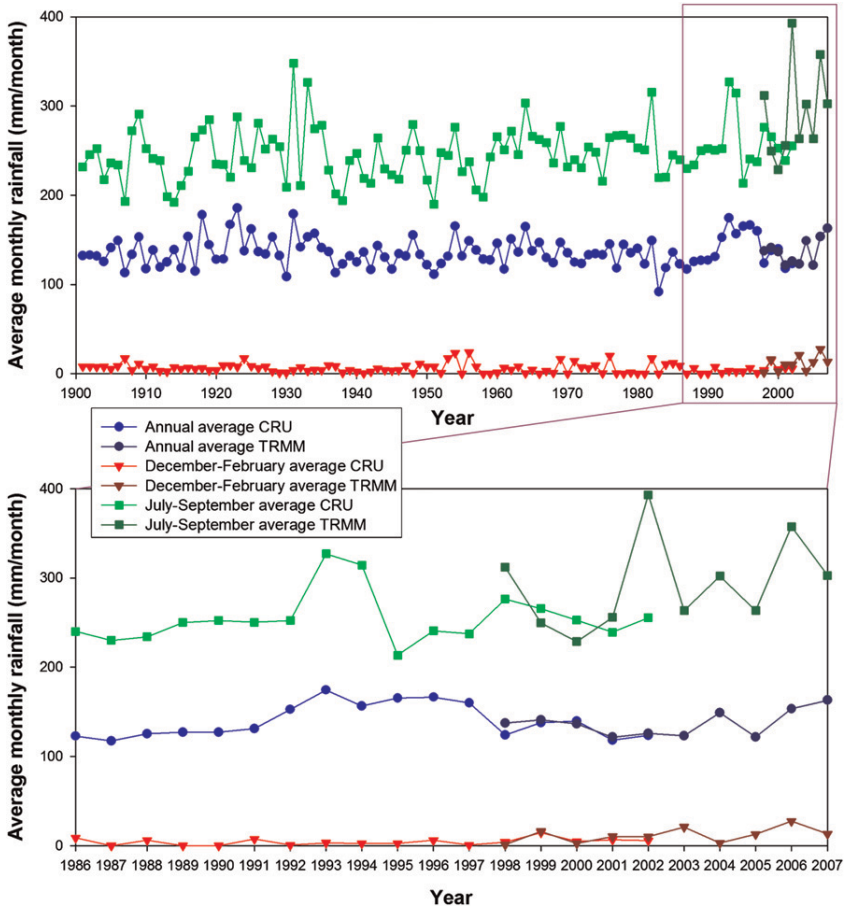

Figure 8. Rainfall data for the study area from 1901 to 2007, showing the average annual rainfall (mm month^{-1}), average rainfall in the driest 3 months (December–February, with December taken from the previous year), and average rainfall in the wettest 3 months (July–September). The data shown are CRU 2.1 modeled/measured data (1901–2002) and TRMM 3B43 V6 satellite data (1998–2007). The study period is also shown in more detail.

decreased burning of the savannas and thus an increase in the number and size of trees (E. T. A. Mitchard and S. L. Lewis 2007, personal communication). They also observe that nomadic cattle herding has moved to other more profitable areas, so burning to produce a flush of grass for cattle is also less widespread. The establishment of the Chad–Cameroon Petroleum Development and Pipeline Project by the World Bank in 2000 may also be an important factor. This project brought the prospect of jobs and consequently caused a shift in the labor force from the mid-1990s (Guyer 2002). The Mbam Djerem National Park also owes its creation in 2000 to this project, which was initially funded by the World Bank with the aim of offsetting some of the environmental damage caused by the project. There is a low-frequency trend distinguishable in the increase in

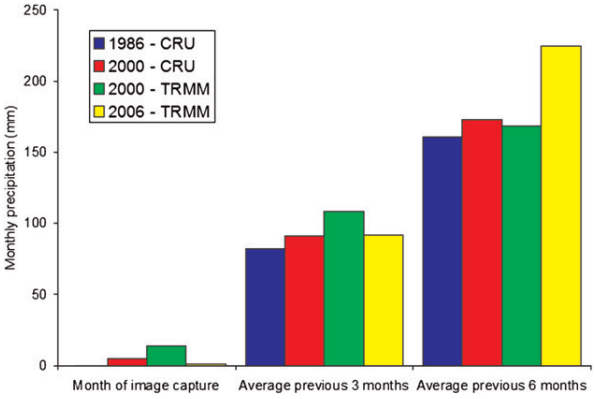

Figure 9. Monthly rainfall over the study site for the month of image capture—average of 3 previous months and average of previous 6 months—for 1986, 2000, and 2006. For 1986 the data are derived from the CRU 2.1 dataset, for 2000 from both the CRU 2.1 and TRMM 3B43 V6 data, and for 2006 only TRMM data.

dry-season GIMMS NDVI data (Figure 7), with rapid increases in the 1980s and 2000s, but a stagnation in the 1990s. The increase from 2000 is easy to explain as it coincides both with the creation of the Mbam Djerem National Park and the Chad–Cameroon Pipeline, as discussed above. The change in the 1980s may be concurrent with urbanization and a reduction in cattle herding, though it is harder to explain why this increase disappears in the 1990s without better local demographic data.

Our analysis of the ATSR-2/AATSR World Fire Map data for the study area from 1996 to 2006 goes some way toward confirming the reduction in fire activity in the area, putatively caused by a reduction in human impact. Although this satellite sensor is not able to detect low-intensity fires, which represent the majority of fires in the study area, the data are unbiased and as such general trends are thought likely to correspond to genuine changes in fire frequency in an area (Arino et al. 2005). The approximate halving in fire frequency over a 10-yr period we see here therefore provides some evidence that a reduction in fire frequency has occurred. Unfortunately, it is impossible to know what the fire frequency was in the mid-1980s over this area as the only satellite data available are not sensitive enough to detect the small-scale fires typical of this ecosystem, but we hypothesize that it was considerably higher than present.

There are no reliable population data available at a sufficient resolution to ascertain whether population levels have genuinely fallen in the study area over the time period considered here. Data for the whole of Cameroon show that, while the urban population has risen at an average 4.44% yr^{-1} from 1986 to 2006, rural population has only increased by only 0.69% yr^{-1} over the same period (World Bank 2007). It is therefore possible that the rural population could have fallen in this small area, as local people suggest, especially given that the population density is already very low (excluding the towns of Tibati and Yoko, the Global

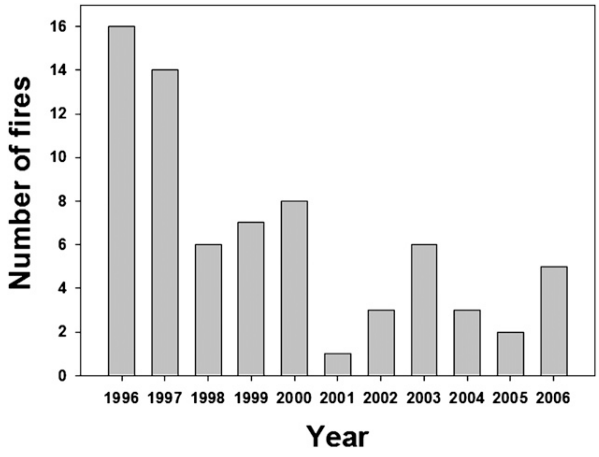

Figure 10. Annual fire count for the study area from 1996 to 2006 derived from ATSR-2 and AATSR World Fire Atlas, using the more sensitive algorithm 2.

Rural–Urban Mapping Project estimates the population density of the area to be just two people per square kilometer; CIESIN 2004).

Analysis of the rainfall and temperature data suggests that this woody encroachment is not environmentally driven. However, it is possible that part of the increase could be due to slight increases in average rainfall. In particular the years 1992–97 stand out as 6 consecutive years where the average annual rainfall is consistently above the long-term average (Figure 8). There is no increase in the average dry-season rainfall during this period, however, where an increase in rainfall would be most likely to influence the survival of woody vegetation both through reduced water stress and a reduction in fire intensity and area (Hély et al. 2006), and equally this increase in precipitation occurs in a period where no increase in dry-season NDVI is detected in the coarse-resolution GIMMS dataset (Figure 7). It has also been suggested that, while rainfall may not have increased, there is evidence of a global reduction in pan evaporation, putatively caused by decreased wind speed and decreased receipt of solar radiation due to increased cloud cover and atmospheric aerosol content (Eamus and Palmer 2007). Such a reduction would have the same effect as an increase in rainfall, increasing soil moisture, which in combination with the potential reduction in stomatal conductance caused by an increase in the CO_2 concentration (Lloyd and Farquhar 2008) could explain woody encroachment. Though Eamus and Palmer's (Eamus and Palmer 2007) model is more suited to arid and semiarid systems than the more mesic environment studied here, the intense dry season makes this a possible causal factor.

5.2. Potential of methodology

The finding that NDVI is very well correlated with CAI in forest–savanna ecotones opens a realm of possibilities for change detection and monitoring of

tropical woody vegetation. NDVI can be calculated from numerous sensors at a full range of resolutions and is easily available in products such as the GIMMS AVHRR data, which has global coverage at an 8-km resolution from 1982 to the present. In this study the trend of increasing CAI detected at a high resolution is clearly matched by an increase in NDVI in the dry-season GIMMS dataset. This provides potential for using dry-season coarse-resolution NDVI data to examine changes both at a continental scale [e.g., using AVHRR or Moderate Resolution Imaging Spectroradiometer (MODIS)] to assess large-scale changes in woody vegetation, and at a more localized scale (e.g., using Landsat and ASTER), for example, to monitor the success of avoided deforestation or carbon sequestration forestry projects. However, heterogeneity of climate and soil may introduce difficulties when using this methodology at a larger scale, though these could potentially be overcome with good ground truthing and potentially further reduced by analysis of the annual NDVI cycle made possible by the daily revisits of coarser-resolution satellite sensors. It is clear that such data must always be analyzed with reference to a precipitation dataset.

Acknowledgments. The authors wish to thank two anonymous reviewers for their detailed comments on an earlier draft of the manuscript. Gatsby Plants for provided ETAM's Ph.D. studentship, and TROBIT, a NERC-funded consortium, Grant NE/D005590/1, funded the rest of the fieldwork. SLL is funded by a Royal Society Research Fellowship; PM is funded by a Royal Society of Edinburgh Research Fellowship. Jon Lloyd, TROBIT P.I., provided useful advice and expertise. Jeanette Sonké, Wildlife Conservation Society-Cameroon (WCS-Cameroon), the University of Yaounde I, and 14 canoeists from Mbakaou provided invaluable support in Cameroon. Adam Freedman provided useful advice on the sources of accurate population data, and Thijs vanden Bergh helped collate the fire data. Remote sensing data were provided by the USGS Global Landcover Facility (Landsat and ASTER), Eurimage (Quickbird), ESA ATSR World Fire Atlas (ATSR-2/AATSR hot spot data), and the NASA Giovanni Rainfall Archive (TRMM rainfall data). The CRU TS 2.1 dataset was downloaded from the University of East Anglia's Climate Research Unit at www.cru.uea.ac.uk/~timm/grid/CRU_TS_2_1.html.

Appendix A

The Locations of Tree Species Found

This is a complete list of tree species found in the eight transects. The species are divided into forest and savanna species, based on knowledge of the ecology of the species in question. Each of the eight transects are divided into three sections according to their average CAI: savanna (CAI < 0.5), transitional forest (CAI 0.5–1), and forest (CAI > 1). Transect 4 did not contain a savanna portion. Note the presence of 24 individuals of savanna species in the forest sections of the transects (all old trees, all but one of which had a DBH > 20 cm), compared with just three individuals of forest species found in the savanna (all of which were young trees with a DBH < 10 cm). These data support the hypothesis that forest is expanding into savanna.

Appendix A.

			Savanna							Transition								Forest							
		Transect number	1	2	3	5	6	7	8	1	2	3	4	5	6	7	8	1	2	3	4	5	6	7	8
Species type	Family	Species																							
Savanna tree	Annonaceae	*Annona senegalensis*	6	4		19											3								
	Araliaceae	*Cussonia arborea*				1			2																
	Arecaceae	*Borassus aethiopum*			4			2								1									2
	Bombacaceae	*Ceiba pentandra*														1									
	Celastraceae	*Maytenus senegalensis*	7					2	3																
	Combretaceae	*Combretum molle*	2	3	5	1						1					2								
		Terminalia albida		1	7	16	23								2					1			1		
		Terminalia avicennioides			4																				
		Terminalia indet					9								4										
		Terminalia macroptera	11	4		1				4	4			1				1							
		Terminalia schimperiana						1																	
	Euphorbiaceae	*Bridelia ferruginea*	7		2						1							1	1						
		Bridelia speciosa		1							1														
		Hymenocardia acida	9	6	23	47	15	13	2	1	2	2	2	8	10	1					2	2	1		
		Maprounea africana							2																
		Maprounea membranacea	4			2								1											
		Phyllanthus muellerianus							1																
	Fabaceae	*Entada africana*		2		2		12								1									
		Piliostigma indet					10								3								3		
		Piliostigma reticulatum			7							1													
		Piliostigma thonningii	12	10				1	3	1							5	1	1						
	Hypericaceae	*Psorospermum febrifugum*				2																			
	Meliaceae	*Trichilia emetica*	1	2		8			1	1	1										1	1			
	Moraceae	*Ficus abutilifolia*				1																			
		Ficus exasperata	2														1								
		Ficus mucuso																			1				
		Ficus sycomorus			2											2								1	
	Myrtaceae	*Syzygium guineense*	12		2												3								

APPENDIX A. (*Continued*)

			Savanna							Transition								Forest							
		Transect number	1	2	3	5	6	7	8	1	2	3	4	5	6	7	8	1	2	3	4	5	6	7	8
	Ochnaceae	*Lophira lanceolata*	7			5			1					1			1									
		Ochna schweinfurthiana				2																				
	Proteaceae	*Protea madiensis*	2																							
	Rubiaceae	*Crossopteryx febrifuga*	9	1		23		5	10					4			2					1				
		Nauclea indet			1																					
		Sarcocephalus latifolia	3	2					2				1			1						1				1
	Simaroubaceae	*Quassia undulata*							1																	
Forest tree	Anacardiaceae	*Sorindeia indet*																1			16					
		Spondias indet																		1	8					
		Spondias mombin											2								3		10			
	Annonaceae	*Xylopia aethiopica*									1		2	4					4		6	8	1			2
	Apocynaceae	*Funtumia africana*																					1			
		Funtumia elastica											2	1							10	5				
	Bignoniaceae	*Markhamia tomentosa*																2	1							
	Boraginaceae	*Cordia africana*																							1	
	Chrysobalanaceae	*Parinari indet*																			1					
	Clusiaceae	*Garcinia indet*																								4
	Ebenaceae	*Diospyros zenkeri*																			2					
	Euphorbiaceae	*Bridelia indet*																	2							
		Margaritaria discoidea														1				1					1	1
		Uapaca guineense									2	1		1					18	10	2	2		19	6
	Fabaceae	*Afzelia africana*															1									
		Albizia zygia				1				2				1		2		1	1							
		Aphanocalyx djumaensis																			1					
		Berlinia grandiflora																			2				9	
		Daniellia oliveri															6									2
		Detarium macrocarpum																				4				3
		Erythrophleum ivorense												1								4	1			
		Parkia biglobosa																			1				4	

Flacourtiaceae	*Oncoba dentata*					1								12			
	Oncoba indet											1		1			1
	Oncoba spinosa																2
Hypericaceae	*Harungana madagascariensis*										1			4			
Irvingiaceae	*Klainedoxa gabonensis*													1			
Lauraceae	*Beilschmiedia indet*													2			
Meliaceae	*Khaya ivorensis*													1			
	Khaya senagalensis																1
Moraceae	*Ficus indet*										2						
Myristicaceae	*Pycnanthus angolensis*														4	1	
Ochnaceae	*Ochna afzelii*			1	2	1	3	2				2		11	21	3	
Olacaceae	*Olax subscorpioidea*								3							1	
Phyllanthaceae	*Antidesma laciniatum*						4							4		8	1
	Antidesma membranaceum					5								11			
	Antidesma venosum	1															1
Sapindaceae	*Allophylus africanus*			4	1		1		1		3	2	1			9	5
Sterculiaceae	*Cola lateritia*															1	
	Cola laurifolia													3			
	Sterculia tragacantha									1	1						
Ulmaceae	*Celtis zenkeri*											1					
Verbenaceae	*Vitex doniana*		1		1				1		1	1		6	2	1	1
	Vitex grandifolia													2	4		

Earth Interactions • Volume 13 (2009) • Paper No. 8 • Page 24

Table B1. Percentage and area of change images falling into each change class in the two comparisons, TM 1986 with ETM+ 2000 and ETM+ 2000 with ASTER 2006, with pixels that were burnt in either or both images masked out. The percentage significant positive change divided by the number of years of comparison is also included.

	1986–2000		2000–06	
Class	Percent	Area (km^2)	Percent	Area (km^2)
Significant positive change (>+2 std dev)	6.78	366.3	2.85	153.9
Marginally significant positive change (>+1 std dev)	8.08	436.4	4.05	218.5
No change (−1 to +1 std dev)	51.01	2754.6	65.24	3522.9
Marginally significant negative change (<−1 std dev)	3.7	200.2	0.69	37.7
Significant negative change (<−2 std dev)	0.22	12.3	0.41	22.3
Masked (burnt in at least one time point)	25.8	1393.4	16.98	917.1
Masked (water bodies and urban areas)	4.4	236.6	4.23	228.4
Masked (areas not present in 2006 mosaic)	N/A	N/A	5.54	299.2
Significant positive change per year (%)	0.48% yr^{-1}		0.47% yr^{-1}	

Appendix B

Additional Analysis with Fire Scars Removed

B.1. Methodology

A supervised spectral angle mapper classification was applied at each time point, using all available bands, and a training dataset of 25 areas chosen based on local field knowledge. It is impossible to assess the accuracy of these classifications, but they appeared consistent with our field knowledge, with the purple areas known to correspond to burn scars in 5–4–3 composites clearly picked out. The normalized image differencing technique was then applied as before, but with burnt areas as well as water bodies removed, and no thresholding of low NDVI values.

B.2. Results

The results are summarized Table B1 and Figure B1.

B.3. Discussion

While the areas and percentages increasing in both time points have been reduced by around half by this methodology, that is to be expected, as a large area of savanna has been removed from both comparisons. However, the areas of increase are still very significant (366 km^2 showing a significant increase from 1986 to 2000, 154 km^2 from 2000 to 2006), showing that the increases observed are not merely an artifact caused by the thresholding of low NDVI values as in the original analysis.

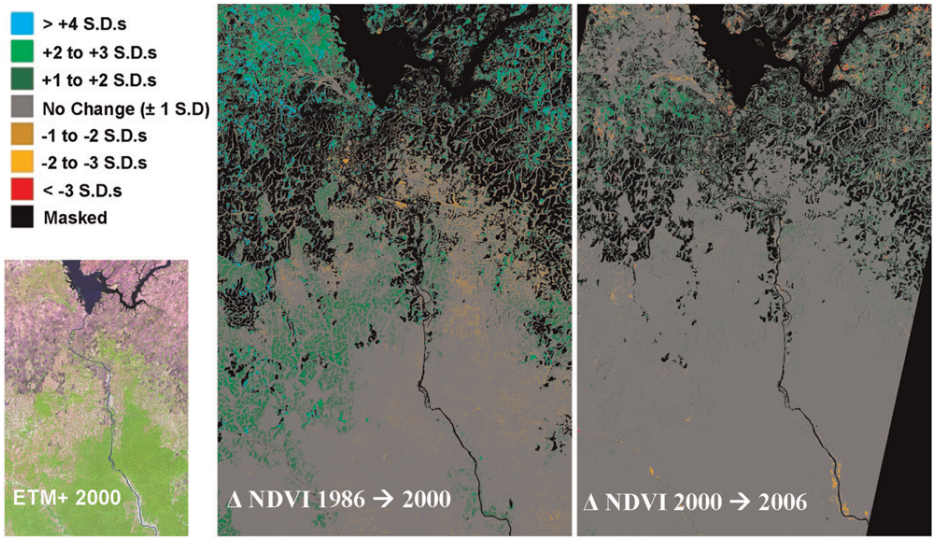

Figure B1. Two images showing the change in NDVI between 1986 and 2000 and 2000 and 2006, in standard deviations, with fire scars present at either time point in each comparison masked. Changes >±2 standard deviations should be considered significant at the 95% level. The 5–4–3 composite image from 2000 is also included.

The increase in percentage significant change per year observed using the original analysis has disappeared here, suggesting that this observed increase may not be significant. However, this is caused by a decrease in burnt area found in the 2006 images as compared to the 2000 image, which results in this technique removing a significant quantity of the positive change that occurred over this time period.

The analysis as presented in the paper is appropriate and robust; however, this analysis is considerably more conservative as it removes all burnt areas, following the methodology of, for example, Nangendo et al. (Nangendo et al. 2005). It should be viewed as supplementary verification that the observed results are not an artifact of the methodology.

References

Archer, S., T. W. Boutton, and K. A. Hibbard, 2001: Trees in grasslands: Biogeochemical consequences of woody plant expansion. *Global Biogeochemical Cycles in the Climate System,* E.-D. Schulze et al., Eds., Academic Press, 115–133.

Archibald, S., and R. J. Scholes, 2007: Leaf green-up in a semi-arid African savanna—Separating tree and grass responses to environmental cues. *J. Veg. Sci.,* **18,** 583–594.

Arino, O., S. Plummer, and D. Defrenne, 2005: Fire disturbance: The ten years time series of the ATSR world fire atlas. *Proc. MERIS (A)ATSR Workshop 2005,* Frascati, Italy, ESRIN, 30.1.

Bernstein, L., and Coauthors, 2007: *Climate Change 2007: Synthesis Report*. IPCC, Geneva, Switzerland, 104 pp.

Bond, W. J., and G. F. Midgley, 2000: A proposed CO_2-controlled mechanism of woody plant invasion in grasslands and savannas. *Global Change Biol.,* **6,** 865–869.

Boulvert, Y., 1990: Avancée ou recul de la forêt centroafricaine. Changements climatiques, influence de l'homme et notamment de feux. *Paysages Quaternaries de l'Afrique Central Atlantique,* R. Lanfranchi and D. Schwartz, Eds., Initiations et Didactiques, Orstrom, 353–366.

Bowman, D. M. J. S., A. Walsh, and D. J. Milne, 2001: Forest expansion and grassland contraction within a Eucalyptus savanna matrix between 1941 and 1994 at Litchfield National Park in the Australian monsoon tropics. *Global Ecol. Biogeogr.,* **10,** 535–548.

Brook, B. W., and D. Bowman, 2006: Postcards from the past: Charting the landscape-scale conversion of tropical Australian savanna to closed forest during the 20th century. *Landscape Ecol.,* **21,** 1253–1266.

Bucini, G., and N. P. Hanan, 2007: A continental-scale analysis of tree cover in African savannas. *Global Ecol. Biogeogr.,* **16,** 593–605.

Center for International Earth Science Information Network (CIESIN), cited 2004: Global Rural-Urban Mapping Project. (GRUMP): Urban/rural population grids. [Available online at http://sedac.ciesin.columbia.edu/gpw/.]

Chen, Z., C. D. Elvidge, and D. P. Groeneveld, 1998: Monitoring seasonal dynamics of arid land vegetation using AVIRIS data. *Remote Sens. Environ.,* **65,** 255–266.

Coppin, P., I. Jonckheere, K. Nackaerts, B. Mys, and E. Lambin, 2004: Digital change detection methods in ecosystem monitoring: A review. *Int. J. Remote Sens.,* **25,** 1565–1569.

Couteron, P., M. Deshayes, and C. Roches, 2001: A flexible approach for woody cover assessment from SPOT HRV XS data in semi-arid West Africa. Application in northern Burkina Faso. *Int. J. Remote Sens.,* **22,** 1029–1051.

Duarte, L. D. S., R. E. Machado, S. M. Hartz, and V. D. Pillar, 2006: What saplings can tell us about forest expansion over natural grasslands. *J. Veg. Sci.,* **17,** 799–808.

Durigan, G., and J. A. Ratter, 2006: Successional changes in cerrado and cerrado/forest ecotonal vegetation in western Sao Paulo State, Brazil, 1962–2000. *Edinburgh J. Bot.,* **63,** 119–130.

Eamus, D., and A. R. Palmer, 2007: Is climate change a possible explanation for woody thickening in arid and semi-arid regions? *Res. Lett. Ecol.,* **2007,** 37364, doi:10.1155/2007/37364.

Favier, C., J. Chave, A. Fabing, D. Schwartz, and M. A. Dubois, 2004: Modelling forest-savanna mosaic dynamics in man-influenced environments: Effects of fire, climate and soil heterogeneity. *Ecol. Modell.,* **171,** 85–102.

Felderhof, L., and D. Gillieson, 2006: Comparison of fire patterns and fire frequency in two tropical savanna bioregions. *Austral Ecol.,* **31,** 736–746.

Ferreira, L. G., and A. R. Huete, 2004: Assessing the seasonal dynamics of the Brazilian Cerrado vegetation through the use of spectral vegetation indices. *Int. J. Remote Sens.,* **25,** 1837–1860.

——, H. Yoshioka, A. Huete, and E. E. Sano, 2004: Optical characterization of the Brazilian savanna phyiognomies for improved land cover monitoring of the cerrado biome: Preliminary assessments from an airborne campaign over an LBA core site. *J. Arid Environ.,* **56,** 425–447.

Fuller, D. O., S. D. Prince, and W. L. Astle, 1997: The influence of canopy strata on remotely sensed observations of savanna-woodlands. *Int. J. Remote Sens.,* **18,** 2985–3009.

George, C., C. Rowland, F. Gerard, and H. Balzter, 2006: Retrospective mapping of burnt areas in Central Siberia using a modification of the normalised difference water index. *Remote Sens. Environ.,* **104,** 346–359.

Guillet, B., G. Achoundong, J. Y. Happi, V. K. K. Beyala, J. Bonvallot, B. Riera, A. Mariotti, and D. Schwartz, 2001: Agreement between floristic and soil organic carbon isotope ($^{13}C/^{12}C$, ^{14}C) indicators of forest invasion of savannas during the last century in Cameroon. *J. Trop. Ecol.,* **17,** 809–832.

Guyer, J. I., 2002: Briefing: The Chad-Cameroon petroleum and pipeline development project. *Afr. Aff.,* **101,** 109–115.

Happi, J. Y., 1998: *Arbres contre graminees: La lenta invasion de la savane par la foret au center-Cameroun*. Doctoral thesis, Université de Paris Sorbonne, 237 pp.

Hély, C., L. Bremond, S. Alleaume, B. Smith, M. T. Sykes, and J. Guiot, 2006: Sensitivity of African biomes to changes in precipitation regime. *Global Ecol. Biogeogr.,* **15,** 258–270.

Hopkins, M. S., J. Head, J. E. Ash, R. K. Hewett, and A. W. Graham, 1996: Evidence of a Holocene and continuing recent expansion of lowland rain forest in humid, tropical north Queensland. *J. Biogeogr.,* **6,** 737–745.

Huete, A., C. Justice, and H. Liu, 1994: Development of vegetation and soil indices for MODIS EOS. *Remote Sens. Environ.,* **49,** 224–234.

——, K. Didan, T. Miura, E. P. Rodriguez, X. Gao, and L. G. Ferreira, 2002: Overview of the radiometric and biophysical performance of the MODIS vegetation indices. *Remote Sens. Environ.,* **83,** 195–213.

Kummerow, C., and Coauthors, 2001: The evolution of the Goddard Profiling Algorithm (GPROF) for rainfall estimation from passive microwave sensors. *J. Appl. Meteor.,* **40,** 1801–1820.

Lambin, E. F., K. Goyvaerts, and C. Petit, 2003: Remotely-sensed indicators of burning efficiency of savannah and forest fires. *Int. J. Remote Sens.,* **24,** 3105–3118.

Leprieur, C., Y. H. Kerr, S. Mastorchio, and J. C. Meunier, 2000: Monitoring vegetation cover across semi-arid regions: Comparison of remote observations from various scales. *Int. J. Remote Sens.,* **21,** 281–300.

Lloyd, J., and G. D. Farquhar, 2008: Effects of rising temperatures and [CO_2] on the physiology of tropical forest trees. *Philos. Trans. Roy. Soc. London,* **B363,** 1811–1817.

Lu, D., 2006: The potential and challenge of remote sensing-based biomass estimation. *Int. J. Remote Sens.,* **27,** 1297–1328.

——, P. Mausel, E. Brondizio, and E. Moran, 2004: Change detection techniques. *Int. J. Remote Sens.,* **25,** 2365–2401.

Lu, H., M. R. Raupach, T. R. McVicar, and D. J. Barrett, 2003: Decomposition of vegetation cover into woody and herbaceous components using AVHRR NDVI time series. *Remote Sens. Environ.,* **86,** 1–18.

Maley, J., 1996: The African rain-forest—Main characteristics of changes in vegetation and climate from the Upper Cretaceous to the Quaternary. *Proc. Roy. Soc. Edinburgh,* **104,** 31–73.

Malhi, Y., and J. Wright, 2004: Spatial patterns and recent trends in the climate of tropical rainforest regions. *Philos. Trans. Roy. Soc. London,* **B359,** 311–329.

Marimon, B. S., E. S. Lima, T. G. Duarte, L. C. Chieregatto, and J. A. Ratter, 2006: Observations on the vegetation of northeastern Mato Grosso, Brazil. IV. An analysis of the cerrado-Amazonian forest ecotone. *Edinburgh J. Bot.,* **63,** 323–341.

Mayaux, P., E. Batholomé, S. Fritz, and A. Belward, 2004: A new land-cover map of Africa for the year 2000. *J. Biogeogr.,* **31,** 861–877.

Menaut, J. C., 1977: Evolution of plots protected from fire since 13 years in a Guinea savanna of Ivory Coast. *Actas IV Simposium Internacional Ecología Tropical,* Impresora Nación, LNAC, Panama, 541–481.

Ministère des Forêts et de la Faune, 2007: Parc National du Mbam et Djerem, Plan d'Aménagement 2007-2011. Republique du Cameroun, 137 pp. [Available online at http://archive.wcs.org/media/file/MbamDjeremMangementPlanDraft.pdf.]

Mitchell, T. D., and P. D. Jones, 2005: An improved method of constructing a database of monthly climate observations and associated high-resolution grids. *Int. J. Climatol.,* **25,** 693–712.

Nangendo, G., O. van Straaten, and A. de Gier, 2005: Biodiversity conservation through burning: A case study of woodlands in Budongo Forest Reserve, NW Uganda. *African Forests between Nature and Livelihood Resources: Interdisciplinary Studies in Conservation and Forest Management,* M. A. F. Ros-Tonen and T. Dietz, Eds., Edwin Mellen, 113–128.

Pettorelli, N., J. O. Vik, A. Mysterud, J. M. Gaillard, C. J. Tucker, and N. C. Stenseth, 2005: Using the satellite-derived NDVI to assess ecological responses to environmental change. *Trends Ecol. Evol.,* **20,** 503–510.

Pinzon, J., M. E. Brown, and C. J. Tucker, 2005: Satellite time series correction of orbital drift artifacts using empirical mode decomposition. *Hilbert-Huang Transform: Introduction and Applications,* N. Huang, Ed., World Scientific, 167–186.

Polley, H. W., H. S. Mayeux, H. B. Johnson, and C. R. Tischler, 1997: Viewpoint: Atmospheric CO_2, soil water and shrub/grass ratios on rangelands. *J. Range Manage.,* **50,** 278–284.

Puyravaud, J. P., C. Dufour, and S. Aravajy, 2003: Rain forest expansion mediated by successional processes in vegetation thickets in the Western Ghats of India. *J. Biogeogr.,* **30,** 1067–1080.

Qi, J., A. Chehbouni, A. R. Huete, and Y. H. Kerr, 1994: A modified soil adjusted vegetation index. *Remote Sens. Environ.,* **48,** 119–126.

Qin, W., and S. A. W. Gerstl, 2000: 3-D Scene modeling of semidesert vegetation cover and its radiation regime. *Remote Sens. Environ.,* **74,** 145–162.

Roitman, I., J. M. Felfili, and A. V. Rezende, 2008: Tree dynamics of a fire-protected *cerrado sensu stricto* surrounded by forest plantation, over a 13-year period (1991-2004) in Bahia, Brazil. *Plant Ecol.,* **197,** 255–267.

Russell-Smith, J., P. J. Stanton, A. C. Edwards, and P. J. Whitehead, 2004: Rain forest invasion of eucalypt-dominated woodland savanna, Iron Range, north-eastern Australia: II. Rates of landscape change. *J. Biogeogr.,* **31,** 1305–1316.

Salzmann, U., and P. Hoelzmann, 2005: The Dahomey Gap: An abrupt climatically induced rain forest fragmentation in West Africa during the late Holocene. *Holocene,* **15,** 190–199.

Sankaran, M., and Coauthors, 2005: Determinants of woody cover in African savannas. *Nature,* **438,** 846–849.

Sedano, F., P. Gong, and M. Ferrao, 2005: Land cover assessment with MODIS imagery in southern African Miombo ecosystems. *Remote Sens. Environ.,* **98,** 429–441.

Singh, A., 1989: Review article: Digital change detection techniques using remotely-sensed data. *Int. J. Remote Sens.,* **10,** 989–1003.

Songh, C., C. E. Woodcock, K. C. Seto, M. P. Lenney, and S. A. Macomber, 2001: Classification and change detection using Landsat TM data: When and how to correct atmospheric effects? *Remote Sens. Environ.,* **75,** 230–244.

Su, L., M. J. Chopping, A. Rango, J. V. Martonchik, and D. P. C. Peters, 2007: Support vector machines for recognition of semi-arid vegetation types using MISR multi-angle imagery. *Remote Sens. Environ.,* **107,** 299–311.

Swaine, M. D., W. D. Hawthorne, and T. K. Orgle, 1992: The effects of fire exclusion on savanna vegetation at Kpong, Ghana. *Biotropica,* **24,** 166–172.

Tucker, C. J., J. E. Pinzon, M. E. Brown, D. Slayback, E. W. Pak, R. Mahoney, E. Vermote, and N. El Saleous, 2005: An extended AVHRR 8-km NDVI data set compatible with MODIS and SPOT vegetation NDVI data. *Int. J. Remote Sens.,* **26,** 4485–4498.

Vauttoux, R., 1976: Contribution a l'etude de l'evolution des strates arboree et arbustive dans la savane de Lamto (Cote-d'Ivore). *Ann. Univ. Abidjan,* **13,** 35–63.

World Bank, cited 2007: World Bank Development Indicators Database. World Bank, Washington DC. [Available online at http://www.worldbank.org/data/onlinedatabases/wdi.]

Xiao, J., and A. Moody, 2005: A comparison of methods for estimating fractional green vegetation cover within a desert-to-upland transition zone in central New Mexico, USA. *Remote Sens. Environ.,* **98,** 237–250.

Zeng, N., and D. Neelin, 2000: The role of vegetation–climate interaction and interannual variability in shaping the African savanna. *J. Climate,* **13,** 2665–2670.

Appendix 1A: table showing the locations of tree species found

			Savanna							Transition								Forest							
		Transect Number	1	2	3	5	6	7	8	1	2	3	4	5	6	7	8	1	2	3	4	5	6	7	8
Species Type	Family	Species																							
Savanna tree	Annonaceae	*Annona senegalensis*	6	4		19																			
	Araliaceae	*Cussonia arborea*				1			2								3								
	Arecaceae	*Borassus aethiopum*			4			2								1									2
	Bombacaceae	*Ceiba pentandra*														1									
	Celastraceae	*Maytenus senegalensis*	7					2	3																
	Combretaceae	*Combretum molle*	2	3	5	1						1					2								
		Terminalia albida		1	7	16	23								2					1			1		
		Terminalia avicennioides			4																				
		Terminalia indet					9								4										
		Terminalia macroptera	11	4		1				4	4			1				1							
		Terminalia schimperiana						1																	
	Euphorbiaceae	*Bridelia ferruginea*	7		2						1							1	1						
		Bridelia speciosa		1							1														
		Hymenocardia acida	9	6	23	47	15	13	2	1	2	2	2	8	10	1					2	2	1		
		Maprounea africana							2																
		Maprounea membranacea	4			2								1											
		Phyllanthus muellerianus							1																
	Fabaceae	*Entada africana*		2		2		12								1									
		Piliostigma indet					10								3								3		
		Piliostigma reticulatum			7							1													
		Piliostigma thonningii	12	10				1	3	1							5	1	1						
	Hypericaceae	*Psorospermum febrifugum*				2																			
	Meliaceae	*Trichilia emetica*	1	2		8			1	1	1										1	1			
	Moraceae	*Ficus abutilifolia*				1																			
		Ficus exasperata	2														1								
		Ficus mucuso																			1				
		Ficus sycomorus			2											2								1	
	Myrtaceae	*Syzygium guineense*	12		2												3								
	Ochnaceae	*Lophira lanceolata*	7			5			1					1			1								
		Ochna schweinfurthiana				2																			
	Proteaceae	*Protea madiensis*	2																						
	Rubiaceae	*Crossopteryx febrifuga*	9	1		23		5	10					4			2					1			
		Nauclea indet			1																				
		Sarcocephalus latifolia	3	2					2				1			1						1			1
	Simaroubaceae	*Quassia undulata*							1																
Forest tree	Anacardiaceae	*Sorindeia indet*																1			16				
		Spondias indet																		1	8				
		Spondias mombin											2								3		10		
	Annonaceae	*Xylopia aethiopica*									1		2	4					4		6	8	1		2
	Apocynaceae	*Funtumia africana*																					1		
		Funtumia elastica											2	1							10	5			
	Bignoniaceae	*Markhamia tomentosa*																2	1						
	Boraginaceae	*Cordia africana*																						1	
	Chrysobalanaceae	*Parinari indet*																			1				
	Clusiaceae	*Garcinia indet*																							4
	Ebenaceae	*Diospyros zenkeri*																			2				
	Euphorbiaceae	*Bridelia indet*																	2						
		Margaritaria discoidea														1				1				1	1
		Uapaca guineense									2	1		1					18	10	2	2		19	6
	Fabaceae	*Afzelia africana*															1								
		Albizia zygia				1				2				1		2		1	1						
		Aphanocalyx djumaensis																			1				
		Berlinia grandiflora																			2			9	
		Daniellia oliveri															6								2
		Detarium macrocarpum																				4			3
		Erythrophleum ivorense												1								4	1		
		Parkia biglobosa																			1			4	
	Flacourtiaceae	*Oncoba dentata*											1								12				
		Oncoba indet																	1		1				1
		Oncoba spinosa																							2
	Hypericaceae	*Harungana madagascariensis*																1			4				
	Irvingiaceae	*Klainedoxa gabonensis*																			1				
	Lauraceae	*Beilschmiedia indet*																			2				
	Meliaceae	*Khaya ivorensis*																			1				
		Khaya senagalensis																							1
	Moraceae	*Ficus indet*																2							
	Myristicaceae	*Pycnanthus angolensis*																				4	1		
	Ochnaceae	*Ochna afzelii*								1	2		1	3	2				2		11	21	3		
	Olacaceae	*Olax subscorpioidea*														3							1		
	Phyllanthaceae	*Antidesma laciniatum*												4							4		8		1
		Antidesma membranaceum											5								11				
		Antidesma venosum				1																			1
	Sapindaceae	*Allophylus africanus*								4	1			1		1		3	2	1			9		5
	Sterculiaceae	*Cola lateritia*																					1		
		Cola laurifolia																			3				
		Sterculia tragacantha															1	1							
	Ulmaceae	*Celtis zenkeri*																	1						
	Verbenaceae	*Vitex doniana*					1				1					1		1	1		6	2	1		1
		Vitex grandifolia																			2	4			

Legend to Appendix A: This is a complete list of tree species found in the eight transects. The species are divided into forest and savanna species, based on knowledge of the ecology of the species in question. Each of the eight transects are

divided into three sections according to their average CAI: savanna (CAI < 0.5), transitional forest (CAI 0.5 – 1), and forest (CAI > 1). Transect 4 did not contain a savanna portion. Note the presence of twenty-four individuals of savanna species in the forest sections of the transects (all old trees, all but one of which had a DBH > 20 cm), compared with just three individuals of forest species found in the savanna (all of which were young trees with a DBH < 10 cm). These data support the hypothesis that forest is expanding into savanna.

Appendix 1B: additional analysis with fire scars removed

Methodology

A supervised spectral angle mapper classification was applied at each time point, using all available bands and a training dataset of 25 areas chosen based on local field knowledge. It is impossible to assess the accuracy of these classifications, but they appeared consistent with our field knowledge, with the purple areas known to correspond to burn scars in 5-4-3 composites clearly picked out. The normalised image differencing technique was then applied as before, but with burnt areas as well as water bodies removed, and no thresholding of low NDVI values.

Results

The results are summarised Table B1 and Figure B1.

Table B1

Percentage and area of change images falling into each change class in the two comparisons, TM 1986 with ETM+ 2000, and ETM+ 2000 with ASTER 2006, with pixels that were burnt in either or both images masked out. The percentage significant positive change divided by the number of years of comparison is also included.

Class	1986-2000		2000-2006	
	%	Area (km^2)	%	Area (km^2)
Significant positive change (> +2 S.D.s)	**6.78**	**366.3**	**2.85**	**153.9**
Marginally significant positive change (> +1 S.D.s)	8.08	436.4	4.05	218.5
No Change (-1 to +1 S.D.s)	51.01	2754.6	65.24	3522.9
Marginally significant negative change (< -1 S.D.s)	3.7	200.2	0.69	37.7
Significant negative change (< -2 S.D.s)	**0.22**	**12.3**	**0.41**	**22.3**
Masked (burnt in at least one time-point)	25.8	1393.4	16.98	917.1
Masked (water bodies & urban areas)	4.4	236.6	4.23	228.4
Masked (areas not present in 2006 mosaic)	n/a	n/a	5.54	299.2
% Significant positive change per year	***0.48 % yr^{-1}***		***0.47 % yr^{-1}***	

Figure B1

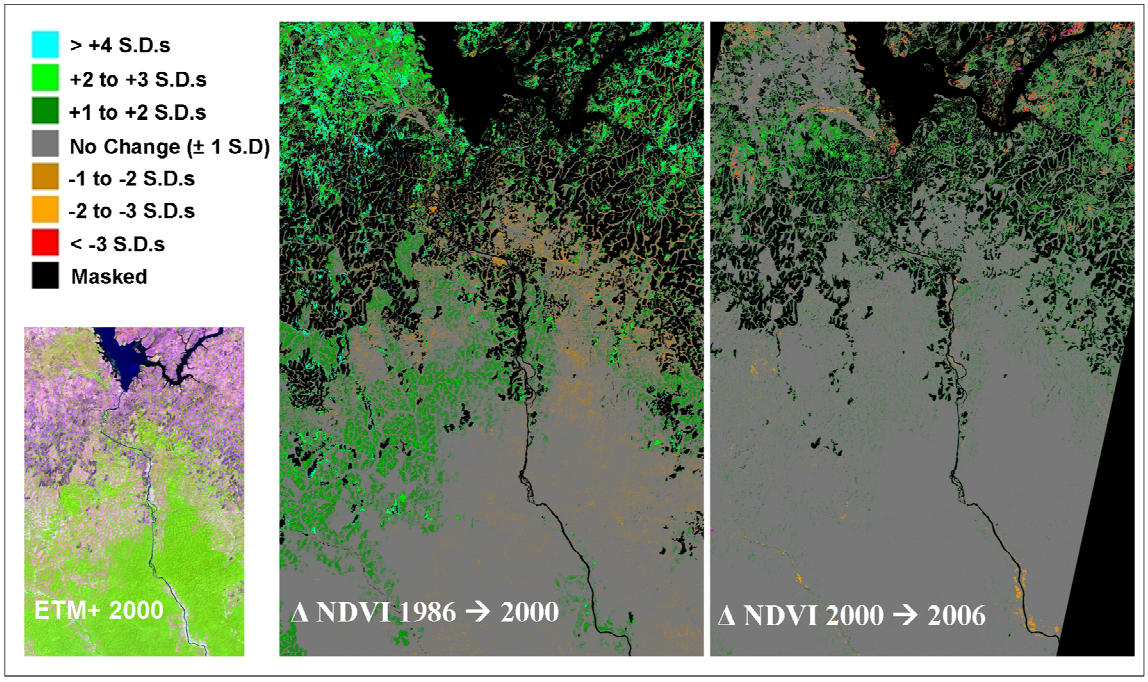

Two images showing the change in NDVI between 1986 and 2000, and 2000 to 2006, in standard deviations, with fire scars present at either time point in each comparison masked. Changes > ±2 standard deviations should be considered significant at the 95 % level. The 5-4-3 composite image from 2000 is also included.

Discussion

While the areas and percentages increasing in both time points have been reduced by around half by this methodology, that is to be expected, as a large area of savanna has been removed from both comparisons. However, the areas of increase are still very significant (366 km^2 showing a significant increase from 1986 to 2000, 154 km^2 from 2000 to 2006), showing that the increases observed are not merely an artefact caused by the thresholding of low NDVI values as in the original analysis.

The increase in percentage significant change per year observed using the original analysis has disappeared here, suggesting that this observed increase may not be significant. However this is caused by a decrease in burnt area found in the 2006 images as compared to the 2000 image, which results in this technique removing a significant quantity of the positive change that occurred over this time period.

The analysis as presented in the paper is appropriate and robust, however this analysis is considerably more conservative as it removes all burnt areas, following the methodology of for example Nangendo *et al.* (2005). It should be viewed as supplementary verification that the observed results are not an artefact of the methodology.

Appendix 2

Published version of Chapter 4

Contents lists available at ScienceDirect

Remote Sensing of Environment

journal homepage: www.elsevier.com/locate/rse

Measuring biomass changes due to woody encroachment and deforestation/degradation in a forest–savanna boundary region of central Africa using multi-temporal L-band radar backscatter

E.T.A. Mitchard [a,*], S.S. Saatchi [b], S.L. Lewis [c], T.R. Feldpausch [c], I.H. Woodhouse [a], B. Sonké [d], C. Rowland [e], P. Meir [a]

[a] School of GeoSciences, University of Edinburgh, EH8 9XP, UK
[b] Jet Propulsion Laboratory, California Institute of Technology, Pasadena, CA 91109, USA
[c] Earth and Biosphere Institute, School of Geography, University of Leeds, LS2 9JT, UK
[d] Department of Biology, University of Yaoundé 1, P.O. Box 047, Yaoundé, Cameroon
[e] CEH Lancaster, Lancaster Environment Centre, Lancaster, LA1 4AP, UK

ARTICLE INFO

Article history:
Received 9 April 2009
Received in revised form 12 October 2009
Accepted 7 February 2010
Available online 6 May 2011

Keywords:
ALOS PALSAR
Aboveground biomass
Cameroon
Change detection
Deforestation
Degradation
Ecotone
Forest–savanna boundary
JERS-1
SAR
Radar
REDD
Woody encroachment

ABSTRACT

Satellite L-band synthetic aperture radar backscatter data from 1996 and 2007 (from JERS-1 and ALOS PALSAR respectively), were used with field data collected in 2007 and a back-calibration method to produce biomass maps of a 15 000 km^2 forest–savanna ecotone region of central Cameroon. The relationship between the radar backscatter and aboveground biomass (AGB) was strong ($r^2 = 0.86$ for ALOS HV to biomass plots, $r^2 = 0.95$ relating ALOS-derived biomass for 40 suspected unchanged regions to JERS-1 HH). The root mean square error (RMSE) associated with AGB estimation varied from ~25% for AGB < 100 Mg ha^{-1} to ~40% for AGB > 100 Mg ha^{-1} for the ALOS HV data. Change detection showed a significant loss of AGB over high biomass forests, due to suspected deforestation and degradation, and significant biomass gains along the forest–savanna boundary, particularly in areas of low population density. Analysis of the errors involved showed that radar data can detect changes in broad AGB class in forest–savanna transition areas with an accuracy >95%. However, quantitative assessment of changes in AGB in Mg ha^{-1} at a pixel level will require radar images from sensors with similar characteristics collecting data from the same season over multiple years.

1. Introduction

The interface between tropical forest and savanna in west and central Africa is a wide, structurally and floristically diverse mosaic of vegetation types, with forest penetrating deeply into the savanna biome as gallery forests along river banks, and also as forest patches on plateaus and in between rivers (Dai et al., 2004; Hely et al., 2006; Menaut, 1983). The savannas in this region are not maintained by precipitation, there being enough rainfall to support full canopy closure except in the poorest or inundated soils. Instead they are maintained largely by anthropogenic disturbance such as fire and clearance for grazing, agriculture and timber (Bucini & Hanan, 2007; Sankaran et al., 2005). Changes in these disturbance regimes can therefore result in rapid changes in the woody cover of this region. Due to the large extent of the tropical forest–savanna ecotone in Africa (1.28 million km^2 is forest–savanna mosaic, compared with 2.36 million km^2 forest and 4.12 million km^2 woodland; Mayaux et al., 2004), any changes in the woody vegetation cover and the resulting feedbacks could have significant implications for biodiversity and the carbon cycle (Lewis, 2006). Such ecotones are also important as they are transitional habitats that appear to be areas of evolutionary dynamism, storing genetic diversity and acting as an important locus for the generation of new species (Smith et al., 1997, 2001).

Dynamics of woody vegetation in this ecotone are the result of the integration of a variety of different competing processes, each of largely unknown magnitude and spatial distribution. Forest is being cleared for agriculture, and woody savannas are often burnt to assist agriculture and cattle grazing (FAO, 2007; Zhang et al., 2006). Forest and woody savannas are also undergoing degradation, especially around settlements, for timber (legal logging concessions and illegal

* Corresponding author.
E-mail address: edward.mitchard@ed.ac.uk (E.T.A. Mitchard).

0034-4257/$ – see front matter © 2011 Elsevier Inc. All rights reserved.
doi:10.1016/j.rse.2010.02.022

extraction), wood fuel and charcoal (Goetze et al., 2006; Mertens & Lambin, 2000). Changes in climate also have the potential to alter the area of forest and savanna, for example increases in dry season length will favor savanna, as would rising temperatures (Dai et al., 2004; Hely et al., 2006; Zeng & Neelin, 2000). In contrast, there are also processes that could cause forest to expand into savanna and savannas to increase in woodiness: reduced anthropogenic fire, caused by reduced human activity in an area; increased CO_2 concentration, which has the potential to increase tree growth in forests and therefore biomass (Lewis et al., 2004, 2009) by favoring the growth of trees with a C3 photosynthetic pathway, over grasses that have a C4 pathway[1] (Lloyd & Farquhar, 1996, 2008); and if rainfall increased, which would again favor trees over grasses (Hely et al., 2006).

It has been suggested that forest is expanding into savannas in central Africa because of urban-migration and a consequent reduction in fire frequency (Boulvert, 1990). Indeed, this forest encroachment has been found to be occurring in other tropical forest–savanna ecotones, including northern Australia (Bowman et al., 2001; Brook & Bowman, 2006; Hopkins et al., 1996), the Western Ghats of India (Puyravaud et al., 2003), and South America (Duarte et al., 2006; Durigan & Ratter, 2006; Marimon et al., 2006). However, little quantitative analysis followed Boulvert's initial observations in Africa: a literature search found only three studies reporting woody expansion in African tropical forest–savanna transitions, though there is much evidence of woody encroachment in semi-arid environments in Africa (Archer et al., 2001; Eamus & Palmer, 2007). In an ecotonal region of central Cameroon, optical remote sensing data and field measurements were used to show that over a period of 40 years (1950–1990), gallery forests encroached into the savanna landscape at a rate of 0.6 to 2 m a year (Happi, 1998). In eastern Cameroon, analysis of soil carbon isotopes ($^{13}C/^{12}C$, ^{14}C) along two transects showed both significant expansion of the forest, and that increased woody cover of the savanna has occurred over the past century (Guillet et al., 2001). In Budongo Forest Reserve, Uganda, a combination of field studies and vegetation index-based satellite change detection were used to demonstrate a 14% increase in woody vegetation (Nangendo, 2005). In combination, these studies provide some evidence that forest expansion is occurring, but none used a method that can be extrapolated to larger areas without a huge investment of resources: all involved extensive field studies or the manual interpretation of high-resolution remotely sensed images.

The use of space-borne radar backscatter data is becoming increasingly accepted as a useful method for measuring woody biomass over much larger areas in the tropics because of the capability of radar to penetrate through the forest canopy, and its capacity for all-weather acquisition (Lu, 2006; Ribeiro et al., 2008; Sano et al., 2005; Santos et al., 2002). Radar data are likely to be particularly applicable to forest–savanna boundary regions, as theory suggests there will be a substantial increase in backscatter as both the density and size of trees increase (Podest & Saatchi, 2002; Woodhouse, 2006), and biomass changes from savanna to forest are in the lower biomass ranges, where radar is most sensitive. As radar backscatter responds to the density, size, orientation, and water content of scattering elements on the surface (Rosenqvist et al., 2007), rather than just the color and density of leaves, it has the potential to be more sensitive to changes in the woodiness of savanna than spectral data. This is especially true because the radar signal will be much less sensitive to grasses than spectral data, especially when longer radar wavelengths are used. The spectral vegetation signal from trees can be very hard to distinguish from that of grasses unless hyperspatial data, capable of resolving individual trees (Lu, 2006), or multi-temporal data which enables the phenology of different landcover types to be separated (Loveland et al., 2000), are used.

The successful launch of the Advanced Land Observing Sattelite's Phased Array-type L-band Synthetic Aperture Radar (ALOS PALSAR) in 2006 has increased the potential to use radar to measure biomass, as this is the first long-wavelength (L-band, 23-cm wavelength) synthetic aperture radar (SAR) satellite sensor to have the capability of collecting cross-polarized (HV, horizontal-send, vertical receive) data in addition to horizontal-send, horizontal-receive (HH) data. This is an advantage for detecting biomass because for HV only scattering elements that change the polarization of the incoming electromagnetic radiation will be detected, so complex three-dimensional structures such as trees will produce a strong response, but soil moisture, which does not change the polarization of the incoming radiation, will not be detected.

Radar has been used only rarely to quantify biomass in forest–savanna transition regions, though when used it has been with considerable success (Lucas et al., 2000; Ribeiro et al., 2008; Sano et al., 2005; Santos et al., 2002). It has to our knowledge never previously been used for long-term biomass change detection in forest–savanna transition regions, despite the availability and potential of the data. Here, we compare satellite L-band radar data from 1996 and 2007 over a large ecotonal region of central Cameroon, both to assess changes in aboveground woody biomass in this region, and as a proof of concept for its application for large scale monitoring of changes in biomass from space.

2. Study area

The study area covers a 15 000 km^2 region in central Cameroon, centered around 6°4′18″ N, 12°53′18″ E, encompassing the Mbam Djerem National Park and the surrounding area to the north and east (Fig. 1). This region was chosen as it extends across a range of tropical vegetation types, from humid forests contiguous with the Congo Basin tropical forest belt in the south to savanna with narrow gallery forests in the north. It experiences an annual rainfall of 1720 mm, with a standard deviation of 213 mm (derived from Tropical Rainfall Measuring Mission (TRMM) 3B43 V6 data from January 1998 to December 2008). There is a pronounced dry season from December to March, with an average rainfall of 20 mm per month. The Mbam Djerem National park was established in the year 2000 as an expanded version of the longer-standing Pangare Djerem reserve with funds from Chad-Cameroon Pipeline Project, and is currently maintained by the Wildlife Conservation Society. It has a high species diversity, containing over 360 bird and 50 mammal species (Anonymous, 2007), and is regarded as having critical importance for the preservation of Central African biodiversity (Doumenge et al., 2003). The park itself has a very low human population density, with almost no permanent residents. Major anthropogenic disturbances in the park are fishing, bushmeat hunting in the southern forests, and grazing accompanied by burning in areas along the northern forest–savanna boundary. The regions surrounding the park are more populated, especially on the eastern side, with the two major towns being Tibati on the western side of Lake Mbakaou, and Ngaoundal in the northeast of the study area. The population of both towns has increased by approximately 85% in the past twenty years, from 15 522 and 11 382 respectively in 1987 to 28 981 and 21 239 in 2006 (CIESIN, 2004; PNUD, 1999).

[1] C3 photosynthesis is the photosynthetic pathway that occurs in most plants including all trees. C4 photosynthesis is an alternative used by some grasses, including the majority found in this area, that gives increased efficiency of photosynthesis with respect to water 'use' (i.e. water loss through transpiration), and is therefore beneficial in drier and hotter environments (Taiz & Zeiger, 2006). However, the advantage which C4 plants have over C3 plants is reduced as the concentration of CO_2 in the atmosphere increases (energetically costly adaptations that increase the concentration of CO_2 in leaf cells becomes less advantageous; Lloyd & Farquhar, 2008). Thus increasing CO_2 concentrations could be responsible for woody encroachment by reducing the competitiveness of C4 grasses compared with C3 plants. However, increasing temperatures or a reduction in rainfall, that may occur concurrently with an increase in CO_2 concentration, could negate this effect by increasing the competitive advantage of C4 grasses over C3 trees.

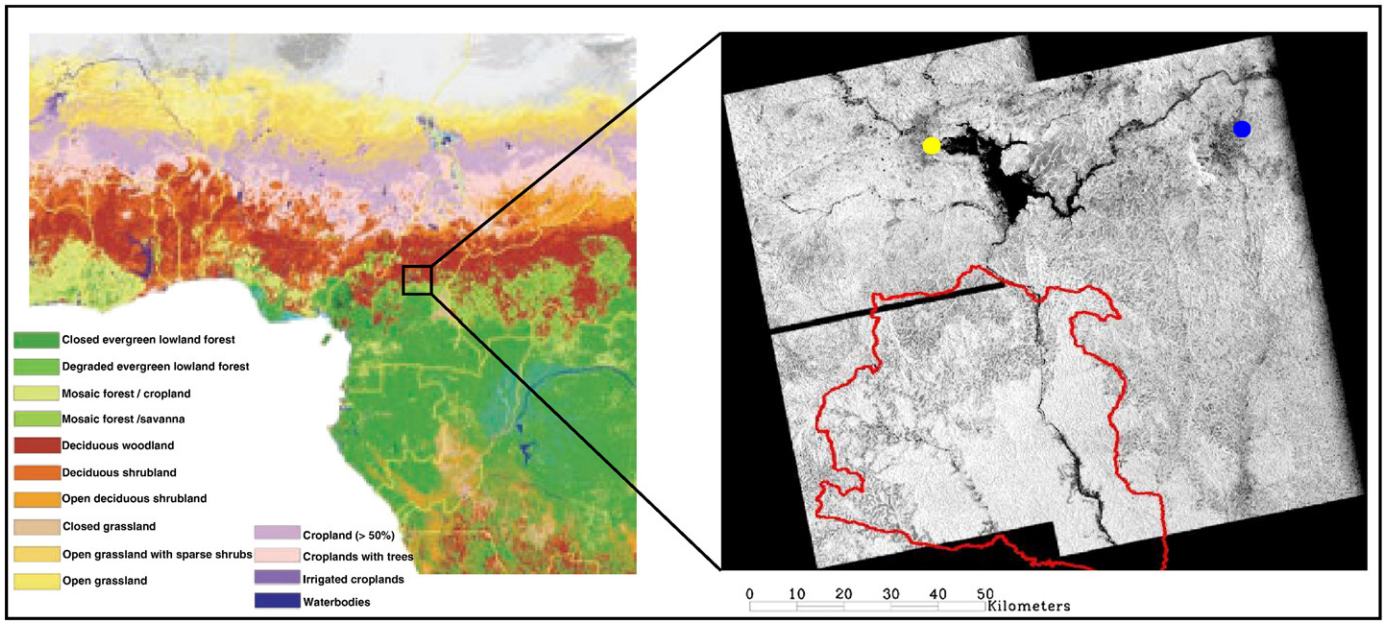

Fig. 1. A section of a vegetation map of Africa taken from Mayaux et al. (2004), showing the location of the study area within Cameroon, with the ALOS HV 2007 mosaic showing the Mbam Djerem National Park outlined in red, Tibati in yellow and Ngaoundal in blue.

3. Methods

3.1. Field data

The study area was visited in October–December 2007 as part of the Tropical Biomes in Transition project (TROBIT, www.geog.leeds.ac.uk/research/trobit). Vegetation was sampled in four regions from the top to the middle of the Mbam Djerem National Park. In all, data were collected from four one-hectare savanna plots, four one-hectare forest plots, a pair of 0.4 ha plots (one in transitional forest, one savanna), and eight 20×200 m transects (8×100 m×100 m; 2×40 m×100 m; 8×20 m×200 m). Seven transects ran from forest into savanna, and as the transition from forest to savanna was very sharp (typically occurring in under five meters), they were each split into a forest and a savanna portion, hence each giving two data points. We did not sub-divide these transects further (nor divide the ten larger plots), in order to remove any problems of autocorrelation: all data-points are sufficiently separated in space or vegetation type to be considered independent. One transect was solely located in forest, and for this AGB was averaged across its whole length. So, in total, 25 biomass plots were used in this study, 13 from forest and transitional forest, and 12 from savanna.

Within these 18 sampling locations data were collected for every tree with a diameter ≥10 cm at 1.3 m along the stem, or above buttresses or stem deformities, a forestry convention called 'diameter at breast height' (DBH). The variables used in this study were the species, DBH, and height (the latter measured for only a subset of trees). Height was estimated using vertex hypsometers (Laser Vertex Hypsometer/Vertex Hypsometer III, Haglöf, Sweden). The height of every tree was measured for the 8 transects and for the remaining 10 plots height was collected for only a random subsample of trees, and site-specific power-law regression equations used to estimate height from diameter for the remaining trees (average $n=56$ trees for each plot, average RMSE<1.6 m, $p<0.001$ in all cases). The field sites were located using a handheld differential GPS (Trimble GeoHX, Trimble, USA). The GPS positions were later corrected using data from the SOPAC N'Koltang ground station in Libreville, Gabon, using the H-STAR differential correction facility in the software GPS Pathfinder Office 3.10 (Trimble, USA), resulting in accuracies of <0.5 m in the horizontal direction and <1 m in the vertical.

The aboveground biomass (AGB) in kilograms of each tree was estimated using the optimal pan-tropical allometric equations as derived by Chave et al. (2005). For the savanna species the dry forest equation (Eq. 1) was used, for forest species the moist forest equation (Eq. 2) was used:

$$\mathrm{AGB} = exp\left[-2.187 + 0.916\, ln\left(\rho D^2 H\right)\right] \quad (1)$$

$$\mathrm{AGB} = exp\left[-2.977 + ln\left(\rho D^2 H\right)\right] \quad (2)$$

where ρ is the wood mass density (oven-dry wood mass divided by green volume, g/cm^3), D is the DBH in cm at 1.3 m, and H is the tree height in meters. Species were differentiated into forest and savanna species based on knowledge of the ecology of the species from BS & SLL, and in which environment they were predominantly found. Wood mass density (also known as wood specific gravity) data were collated from the Global Wood Density Database (Chave et al., 2009; Zanne et al., 2009), in which wood density values measured at 12% or 18% moisture were converted to wood mass density. We also calculated biomass for the forest species using the dry forest allometric equation (Eq. 1). Though this reduced the biomass of the forest plots by 5–10%, this did not change any of the conclusions reported in the paper so the results are not shown.

The biomass values produced using the allometric equations and all three tree-specific variables were then summed and normalized by the area of the plots to produce estimates of woody AGB in Mg ha^{-1}. Stems with a DBH<10 cm were not measured for all plots, so the term AGB for the remainder of this paper refers to the dry biomass of stems with a DBH≥10 cm, which are likely to comprise >95% of the woody biomass in these ecosystems (based on the 8 transects which were measured to a 5 cm minimum diameter, and pan-African estimates from Lewis et al., 2009). These larger trees will be the component to which L-band radar responds most strongly.

3.2. Remote sensing data

JERS-1 HH L-band SAR data were collated from the Global Rainforest Mapping Project (GRMP) (De Grandi et al., 2000), for the study area from the beginning and end of the dry season (November and March) of 1996. The scenes had been geometrically corrected, radiometrically calibrated, mosaicked into one image, and resampled from the original 12.5 m pixel spacing to 100 m pixels using wavelet decomposition, maintaining as much of the true signal as possible while greatly reducing speckle and noise (De Grandi et al., 2000). These data were converted from digital number (DN) to sigma^0 values using the equation and calibration coefficients provided by the GRMP (see http://southport.jpl.nasa.gov/GRFM/), using ENVI 4.4 (ITT, USA):

$$\text{sigma}^0[\text{dB}] = 20 \cdot \log_{10}(6 \cdot \text{DN} + 250) - 68.2. \quad (3)$$

The 2007 data comprised four ALOS PALSAR scenes collected in the FBD (Fine Beam Double-polarization) mode that were acquired from the Alaska Satellite Facility, having been provided to them by JAXA. Two were captured on the 26th July 2007, and the other two on the 12th of August 2007. These are, like the JERS data, L-band, but are polarimetric, including HH and HV polarizations, and were provided at the original 12.5 m pixel spacing.

Quickbird data (60 cm panchromatic resolution and 2.4 m multispectral resolution) were acquired from Eurimage for all the sites by purchasing an archive image from 19th February 2004 for the southern sites and requesting a new acquisition, captured on 30th January 2008, for the northern sites. These ground-point corrected Quickbird data are estimated to be geo-correct to <2 m. In order to reduce speckle noise, the ALOS image was resampled by averaging blocks of 2×2 pixels to produce an image at 25 m resolution. Areas of the ALOS scenes covering the field data plots were georeferenced by eye to the Quickbird data, by using 30 ground control points taken from features such as islands, small clumps of trees and branching points of gallery forests, with resulting RMSE<0.4 ALOS pixels (10 m).

The ALOS scenes were converted to sigma^0 values using the following equation and data-specific calibration factors, identical for all scenes:

$$\text{sigma}^0[\text{dB}] = 10\left(\log_{10}\text{DN}^2\right) + CF \quad (4)$$

where *CF* is the calibration factor, set at −80.2 for the HV polarization and −83.2 for the HH polarization for scenes generated before 1st January 2009 (Shimada et al., 2009).

3.3. Radar sensitivity to structure and biomass

The sigma^0 values for pixels covering the plots were converted to the power domain before averaging, to ensure the use of the arithmetic, not geometric, means. Eighteen of the twenty-five biomass plots fell on the overlap between the two scenes captured seventeen days apart. A regression analysis between the two sets of backscatter values found that they were very well correlated ($dB_{SE} = 1.0074(dB_{SW})$, $r^2 = 0.88$, $p < 0.00001$, where dB_{SE} and dB_{SW} are the sigma^0 HV backscatter values for the 18 sites found in both the south-east and south-west images respectively), and were not significantly different from each other (paired *t*-test of difference not equal to zero, $p = 0.384$), therefore the mean of the two raw power averages for each site was used in all presented analyses. The sigma^0 values for both polarizations were then regressed against structural features of the plots (basal area, average height, stem density and average DBH), and then against the AGB values for each site. Best fit empirical relationships were then calculated comparing backscatter with these variables, as no consensus has yet been reached as to what functional form *a priori* best describes these relationships. These comparisons with structural features are important as the majority of previous studies relating such data to backscatter are from temperate plantation forests (Lu, 2006; Woodhouse, 2005), and as such there is little data from natural heterogeneous tropical savanna–forest mosaics. All regression analyses were performed with the software SigmaPlot 10.0 (Systat Software, USA).

3.4. Biomass change detection

To allow comparison with the JERS data, the ALOS data were mosaicked and subsequently resampled to 100 m pixels. The JERS data were then georeferenced to the ALOS data using a network of 40 ground control points, selected by eye, which resulted in an RMSE of 0.48 pixels (48 m); areas in the JERS image not present in the ALOS mosaic were then masked.

As there were no field data available for this area from 1996, and the field data collected in 2007 is from areas near the forest edges that are suspected to have increased in biomass over the preceding eleven years (Mitchard et al., 2009), it was necessary to back-calibrate the JERS HH data to the ALOS-derived AGB values from areas that were unlikely to have changed over the time period. This methodology relies on the fact that there are identifiable areas where AGB is relatively stable in forest–savanna transition regions and the impacts of environmental variables on the radar backscatter such as soil and canopy moisture are relatively small (Hovestadt et al., 1999; Jeltsch et al., 1999; Ratter, 1992; Santos et al., 2002). Pixels were randomly selected from the image, and when they were judged to have fallen in an area that was unlikely to have changed (e.g. dense forest, or known grassland, confirmed by visual analysis of a Landsat ETM+ scene from 2000 compared with ASTER images from 2006/7), pixel values were extracted and averaged for a homogeneous area of 5×5 pixels around this pixel from both images (25 ha). These larger areas were used in order to limit errors caused by speckle and geolocation problems, with this averaging across homogeneous areas greatly increasing the confidence in the relationship produced. A regression between the ALOS-derived AGB values and the sigma^0 values from the JERS image was then performed, using the same relationship as with ALOS HH to ensure that the biomass of young and regenerating forests was calibrated correctly, and the derived relationship used to create a biomass map for the JERS image. Although there is evidence for a general increase in AGB across higher biomass tropical African forests (Lewis et al., 2009), at most this increase would be a small fraction of the total biomass of these sites (<4%), too small to be detectable by the radar backscatter data at these high biomass values. Hence we assumed that no detectable change had occurred in the AGB of the selected high biomass sites.

The accuracy of the derived relationship between JERS HH and AGB was evaluated by examining the relationship between ALOS HH and AGB, as both sensors have similar characteristics and incidence angles. We did not use the HH channel from both sensors to perform the change detection directly (using differences in dB value after a cross-calibration procedure) because the ALOS HH data were acquired in the wet season and as such were not comparable, as the HH channel responds strongly to soil moisture as well as to AGB.

The biomass class widths were chosen to be approximately equal to the RMSE of the biomass estimation at that level, and thus the classes increase in width as biomass increases, with the highest class taking as its lowest value the point where there is no evidence of a significant positive relationship between biomass and backscatter above that point. The area covered by the different classes at the two time points was compared, and a change map was produced showing the changes in average biomass at a 500 m (25 ha) resolution. Subsequently, an assessment of the sources and likely magnitude of uncertainties was performed.

4. Results

4.1. Field data

In total 4368 trees were measured, representing 205 species from 142 genera and 58 families. AGB measurements for the 25 data points ranged from 6 to 424 Mg ha^{-1}. Table 1 gives the full plot data combined with the ALOS HH and HV backscatter data. As expected biomass values were strongly related to basal area, with a fitted linear relationship giving an r^2 of 0.92 (Fig. 2). However the influence of height and wood density values on the biomass estimates using these equations can be seen here, as if an allometric equation that used only DBH values had been used this relationship would have an r^2 of 1. Biomass was also significantly related to average height ($r^2 = 0.70$) and to stem density ($r^2 = 0.45$), though in both cases the quadratic terms were significant in the regression, suggesting a reduction in the strength of the relationship at higher biomass values. There was a weaker but still significant correlation between biomass and the average DBH for each plot when a quadratic relationship was fitted ($r^2 = 0.30$, $p < 0.01$).

4.2. ALOS backscatter sensitivity to vegetation structure

Significant log relationships were found between ALOS HV and HH sigma^0 backscatter and basal area, average height, and stem density (Fig. 3). No significant relationship was found between average DBH for the plot and either polarization. As expected, both polarizations responded most strongly to basal area (HV: $r^2 = 0.76$, HH: $r^2 = 0.55$), with HV having the smaller residuals. HV backscatter responded almost as strongly to average height ($r^2 = 0.73$), though HH responded less strongly to this variable ($r^2 = 0.48$). A loss of sensitivity appeared to occur quite early in both cases, with a strong relationship with height up to about 9 m and little evidence of a predictive relationship above this point. There was a significant response to stem density in both polarizations (HV $r^2 = 0.47$, $p < 0.0005$, HH $r^2 = 0.48$, $p < 0.0001$); interestingly in this case, HH is more strongly correlated than HV, even if only marginally and insignificantly so. This is possibly due to the influence of ground-trunk scattering, which should increase with stem density, and is a more influential component of the HH than HV backscatter (Woodhouse, 2005).

4.3. ALOS to biomass regression

One biomass plot was on a significant slope (*c.* 25°), in radar shadow, and consequently had an anomalously low radar return (Woodhouse, 2005). It was therefore thought most appropriate to remove this point from subsequent analyses, as all other plots were located on comparatively flat ground (0°–7° slope), and therefore were unsuitable for developing and testing a slope-correction procedure to apply to the anomalous plot. Attempts were made to fit a relationship between AGB and a combination of HH and HV polarizations, however the strongest relationship was found between ALOS HV sigma^0 alone and AGB, using an exponential rise-to-maximum model, as this best fitted the backscatter data, with the loss of sensitivity at approximately 150–200 Mg ha^{-1} well modeled (see Fig. 4a). This fitted model happens to be equivalent to the simple Water Cloud Model (Attema & Ulaby, 1978), but the equation was chosen because it had a higher r^2 than any other relationship that was tested, rather than for theoretical reasons. For this analysis, data points were weighted according to the square root of their area (Zar, 2007), to correct for the differences between the sizes of the sample plots. The fitted relationship was:

$$ALOS\ HV_{sigma^0} = a + b\left[1 - e^{-c.AGB}\right] \quad (5)$$

where $a = -16.59 \pm 0.46$, $b = 4.63 \pm 0.44$, and $c = 0.014 \pm 0.004$ (uncertainties in parameter estimation are standard errors). The r^2 for the fitted regression was 0.86, an F-test for the regression found it to be highly significant ($F_{2,22} = 63.23$, $p < 0.0001$), and the data passed a Shapiro–Wilk normality test ($p = 0.47$).

Table 1
Biomass (Mg ha^{-1}), stem density (stems ha^{-1}), average height (m), basal area (m^2 ha^{-1}) and ALOS 2007 HH and HV sigma^0 (dB) are given for all the field plots. The plot in italics was not used in the biomass regression analysis because it was on a steep slope facing away from the sensor, and thus in radar shadow, whereas the other plots were all from relatively flat ground.

Biomass Mg ha^{-1}	Stem density stems ha^{-1}	Average height m	Average DBH cm	Basal area m^2 ha^{-1}	ALOS HH sigma^0 dB	ALOS HV sigma^0 dB
6.1	42	6.6	11.7	1.4	−9.42	−15.72
17.4	136	6.5	17.7	4.3	−10.26	−16.37
24.9	213	6.2	16.4	5.9	−9.35	−15.54
26.3	108	8.1	20.3	4.5	−9.01	−14.69
26.4	201	5.7	12.3	6.7	−10.33	−15.19
34.5	241	8.0	18.5	8.1	−7.93	−14.28
38.4	315	6.9	18.1	14.0	−7.58	−13.8
43.2	278	6.2	11.6	10.7	−8.27	−14.22
46.3	455	5.3	11.4	11.1	−7.98	−14.77
51.4	249	6.3	15.2	9.3	−9.28	−15.6
75.1	390	6.7	15.5	15.4	−7.92	−13.78
87.2	281	7.3	17.7	17.3	−7.1	−14.15
102.9	575	12.8	11.9	13.9	−7.48	−12.59
103.1	277	8.9	14.5	15.1	−6.86	−12.34
107.8	460	15.4	19.1	16.2	−7.16	−12.35
114.7	797	9.1	11.9	24.1	−7.67	−12.73
119.7	510	11.8	14.7	18.7	−7.02	−13.2
141.2	473	12.0	12.4	22.6	−7.29	−12.65
204.4	642	13.6	13.9	27.7	−6.45	−11.99
212.3	465	13.6	20.3	25.6	−7.34	−12.26
240.5	467	16.8	20.8	25.6	−7.94	−11.98
247.1	641	12.5	13.4	29.7	−7.34	−12.33
306.97	*611*	*17.4*	*23.1*	*35.6*	*−8.36*	*−13.22*
456.13	516	14.6	24.6	50.5	−6.25	−12.02

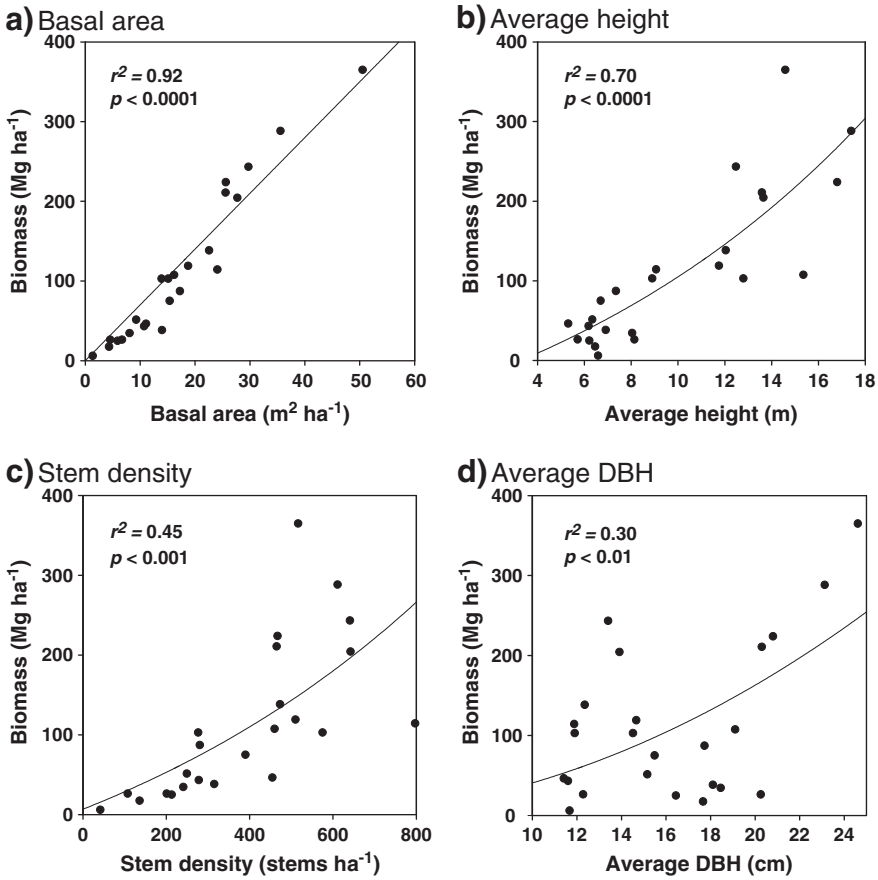

Fig. 2. Biomass values for the field plots against a) basal area, b), average height, c) stem density, and d) average DBH. The fit for a is linear, for b, c and d quadratic.

To create a biomass map from the ALOS HV backscatter data Eq. (5) was rearranged to:

$$AGB = \frac{1}{c} \times - \ln\left[1 - \frac{ALOSHV_{sigma^0} - a}{b}\right]. \quad (6)$$

There was also a good, but weaker, relationship with the ALOS HH polarization alone, which gives an estimate of the accuracy of the relationship between JERS HH data from 1996 and AGB ($r^2 = 0.64$, $F_{2,22} = 17.96$, $p < 0.0001$, Fig. 4b).

4.4. Accuracy of ALOS-biomass regression

The accuracy of the ALOS HV AGB predictions decrease as biomass increases (Fig. 5). The overall root mean square error (RMSE) for these data is 49 Mg ha^{-1}; however this decreases to 29 Mg ha^{-1} if only values below 150 Mg ha^{-1} are considered, and to 24 Mg ha^{-1} using only data points <100 Mg ha^{-1}. These results led us to map AGB in classes chosen to be similar in size to the RMSE at each level: 0–25, 25–50, 50–75, 75–100, 100–150, 150–200, and >200 Mg ha^{-1}. The large degree of scatter and possible bias observable in Fig. 5 for values >200 Mg ha^{-1} suggests that no subdivision of biomass classes above this point is appropriate.

The relationship between ALOS HH and biomass is clearly noisier, with a loss of sensitivity occurring earlier than for the HV data, at around 100–150 Mg ha^{-1} (Fig. 4b). The RMSE values are consequently higher: 65 Mg ha^{-1} for the whole dataset, 52 Mg ha^{-1} for points <150 Mg ha^{-1}, and 39 Mg ha^{-1} for values <100 Mg ha^{-1}. Note that the acquisition of these ALOS data was in the wet season, where the HH polarization would be expected to be responding to soil moisture as well as to biomass, and this perhaps explains the poorer than expected performance at lower biomass values. The JERS HH data were captured in the dry season and would therefore be expected to considerably outperform the ALOS HH backscatter. However, to be conservative, it was assumed that the dry season JERS HH is only as accurate as the wet season ALOS HH. Thus much broader biomass classes were used for the JERS data (and thus also the change detection): 0–50, 50–100, 100–150, and >150.

4.5. JERS to ALOS-derived biomass regression

A strong relationship was found between the 40 suspected unchanged areas in the JERS HH sigma^0 data from March 1996 (dry season) with the ALOS HV biomass data ($r^2 = 0.95$, $F_{2,48} = 341.1$, $p < 0.0001$; Fig. 6). The equation used was identical to Eq. (5), but with coefficients: a = −10.98 ± *0.12*, b = 4.03 ± *0.16*, and c = 0.014 ± *0.002*. The relationship with the JERS HH sigma^0 data from November 1996 (wet season) was less strong ($r^2 = 0.72$, data not shown), confirming that radar data are more sensitive to biomass in the dry season. The reason the r^2 is higher here than with the ALOS HV data is because of the large areas used to calibrate the relationship (25 ha each), greatly reducing the geolocation errors and noise apparent when a relationship is derived from comparatively small field plots, as in the ALOS to biomass regression. This higher r^2 value should not be taken to show that JERS HH is more sensitive to biomass than ALOS HV, as in general its accuracy is likely to be similar to that for ALOS HH (though in all likelihood better as the drier conditions should result in less soil moisture influence). The relationship was used to estimate AGB from JERS HH imagery and a map was produced by classifying AGB into 4 classes with 50 Mg ha^{-1} intervals, chosen to capture the estimation uncertainties predicted using the ALOS HH data (Fig. 7a), the training data is put in the correct class with a 94% accuracy using these classes.

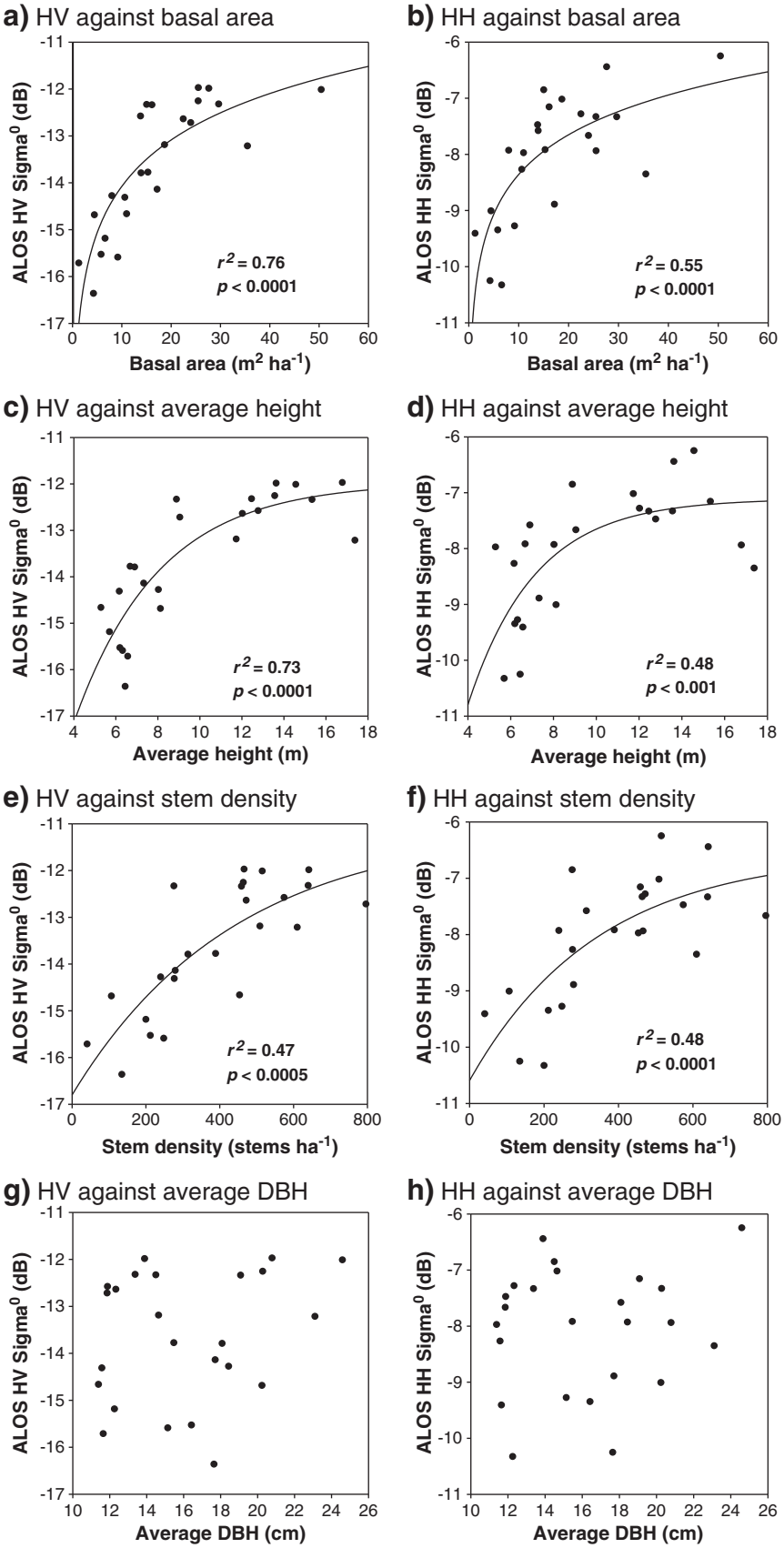

Fig. 3. ALOS 2007 HV and HH sigma^0 plotted against basal area, average height, stem density and average DBH (stem diameter at 1.3 m). Best fit log relationships were fitted for a–f; no significant relationships were found for g and h.

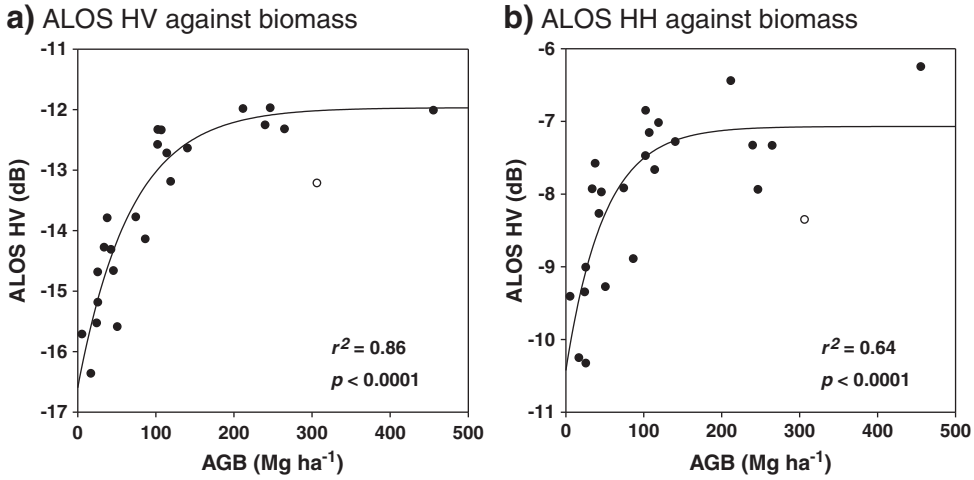

Fig. 4. a) ALOS HV sigma^0 (dB) and b) ALOS HH sigma^0 (dB) plotted against field-measured AGB (Mg ha^{-1}), with area-weighted negative exponential relationships fitted. The point in white is from a steep slope and for this reason was excluded from the regression calculations.

For comparison the ALOS HV map with its seven classes is included as Fig. 7b.

4.6. Change detection

The biomass change map was produced by tracing the number of biomass classes each 500 m pixel changed between the two periods (Fig. 7c). Although the ALOS biomass map has smaller intervals and a larger biomass range, we produced the change map by using 50 Mg ha^{-1} as the class interval and 150 Mg ha^{-1} as the upper limit, as these are the best that can be confidently predicted using the JERS data. The resulting map shows biomass losses and gains dominating in different parts of the study area, with losses of higher biomass classes in the eastern side, and gains on the western side. Changes in the absolute area covered by each biomass class are also shown in Fig. 8, both for the whole study area, and for the eastern and western sides individually. A loss of the high biomass classes dominates the east of the study area, which appears to be concentrated around the major population centers and along the railway line (Fig. 9). Here the area covered by forest >150 Mg ha^{-1} has declined almost by half, from 2700 km^2 in 1996 to 1400 km^2 in 2007. However, there are also areas of positive change (i.e. biomass gain), concentrated in the western side of the study area, particularly in the savanna areas of the Mbam Djerem National Park and the area north of it. Increases in biomass appear to occur in all the woodland–savanna areas without a high human population density. These increases are shown by a reduction in the area of biomass classes <100 Mg ha^{-1}, and an increase in area for both cover classes >100 Mg ha^{-1}.

4.7. Uncertainty analysis

There are two major sources of uncertainty in this analysis: uncertainties in calculating biomass values from field data using allometric equations, and uncertainties in using radar remote sensing data to estimate biomass. Uncertainties in the first case seem unlikely to affect the results of the change detection, so increases and decreases should be correctly located, but the magnitude of the biomass classes could be incorrect. Uncertainties inherent in using radar remote sensing data to estimate biomass across an area may, however, affect the results of the change detection, and these errors are particularly uncertain for the JERS data from 1996 as there are no field data, making an assessment of the accuracy of that classification

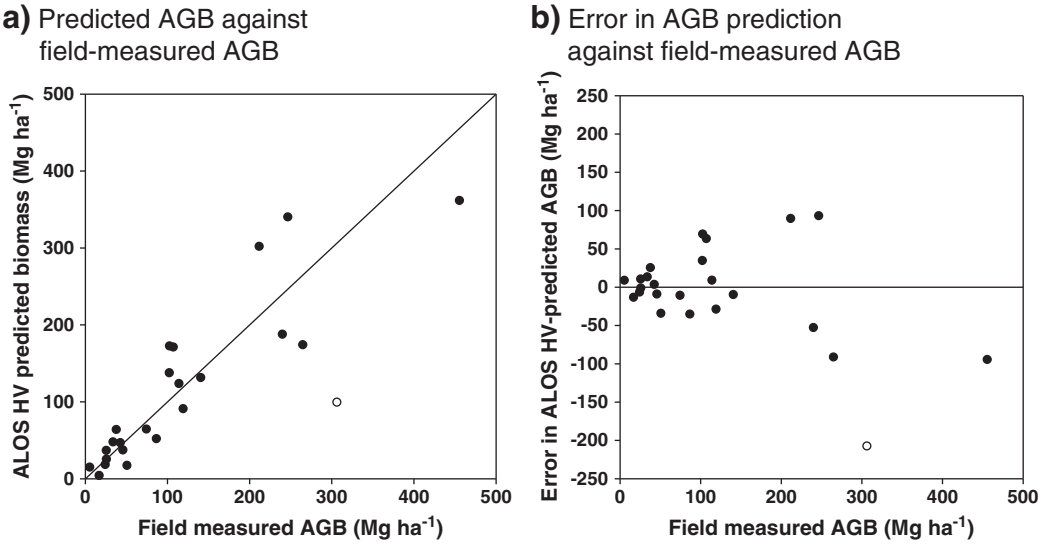

Fig. 5. Errors in predicting biomass from the ALOS HV relationship are shown by a) ALOS HV-predicted AGB plotted against field-measured AGB (Mg ha^{-1}), with an x = y line shown, and b) the error in ALOS HV biomass prediction plotted against field-measured biomass.

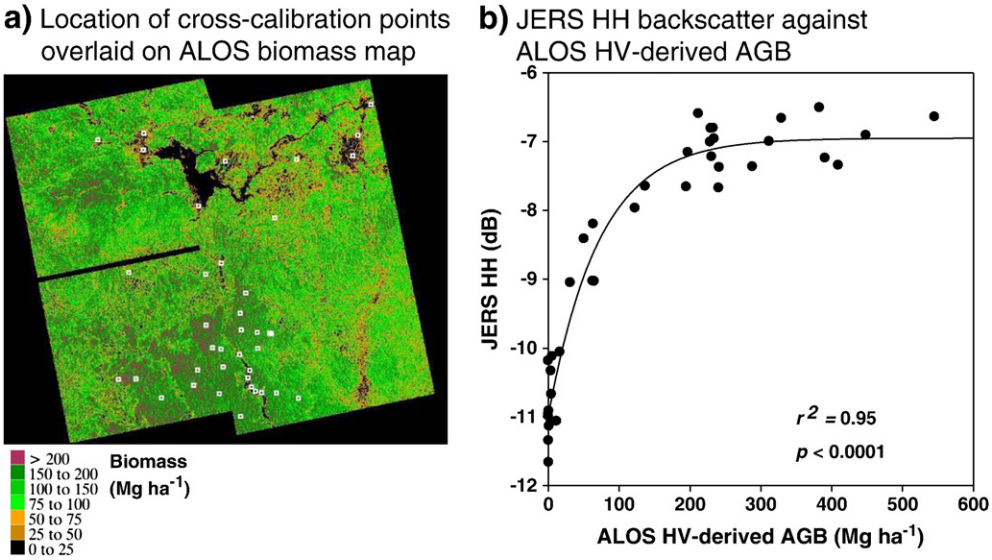

Fig. 6. a) Location of 40 × 500 m × 500 m suspected unchanged areas used to back-calibrate JERS HH data to ALOS HV-derived AGB, and b) JERS HH sigma^0 from 1996 (dB) plotted against ALOS HV-derived AGB (Mg ha^{-1}) from 2007 for these 40 suspected unchanged 25 ha areas.

difficult. Here we will subdivide these uncertainties into their major sources, and estimate the likely contribution from each.

4.7.1. Errors in field data to AGB estimation

4.7.1.1. Uncertainties in diameter, height and species measurements. Diameter measurements are considered very accurate (Alder & Synnott, 1992), and though height measurements are less precise, an in-field assessment, involving re-measuring 10 trees across the full height range at least 8 times from different angles and on different days, suggested that our methods were accurate to greater than ±10%. All species were identified in the field by expert local botanists, and as such mis-identifications are likely to be relatively few, and given the similarities of wood density within a genus, unlikely to have a major effect on the biomass estimation (Chave et al., 2006, 2009).

4.7.1.2. Uncertainties in the allometric equation. It is not possible to use species-specific, or even region-specific, allometric equations for most tropical ecosystems, as the species diversity is too large and the relevant data have not been collected. However using a pan-tropical equation including height, diameter and species-specific wood density minimizes overall uncertainty in biomass estimates to an estimated ±10% (though Chave et al. (2005) optimistically estimate ±5% for the equation we used). This error could be considerably higher for larger trees, where accurate biomass data are very scarce.

We therefore estimate that the biomass classes used could be inaccurate by at worst ±20%, assuming a consistent 10% error in height estimation combined with the allometric equation used that poorly predicts tree biomass and consistently over- or under-estimating by a further 10%. The consequence of this is that, for example, the 100–150 Mg ha^{-1} biomass class could in fact at worst be 80–120 Mg ha^{-1} or 120–180 Mg ha^{-1}.

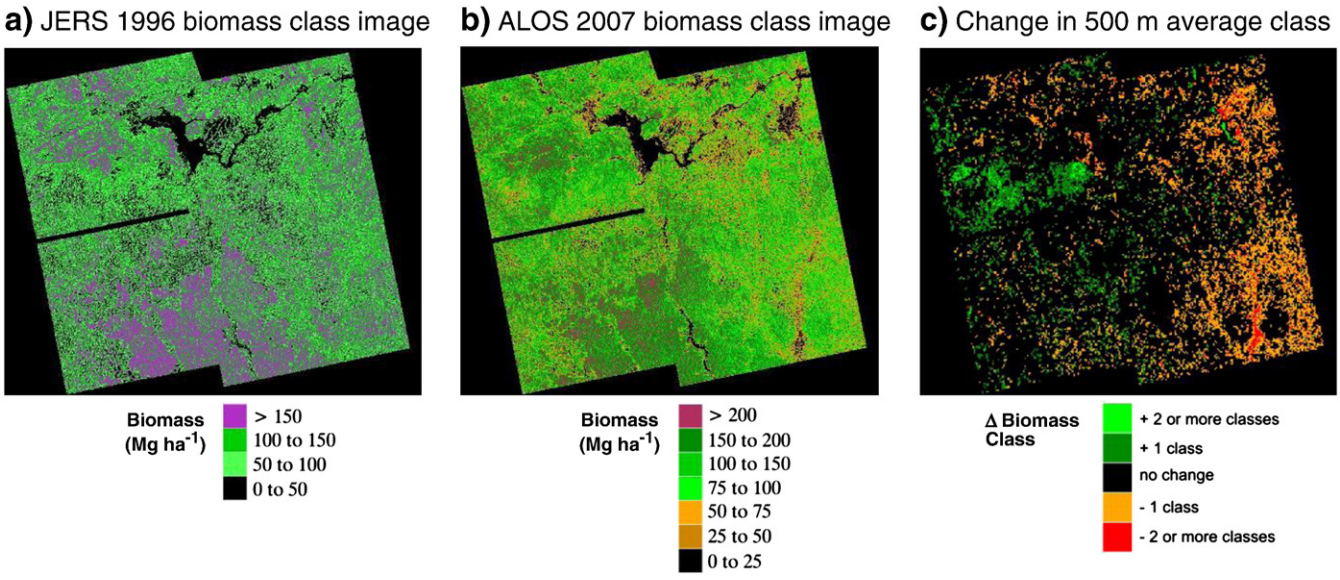

Fig. 7. Biomass class images produced using a) JERS HH 1996 data and b) ALOS HV 2007 data, using scales with the size of biomass classes based on RMSE error values, with broader classes for the JERS HH 1996 data than the ALOS HV 2007 data; and c) change in 500 m average class (JERS class image subtracted from ALOS class image) for the two images (using the broader JERS classes).

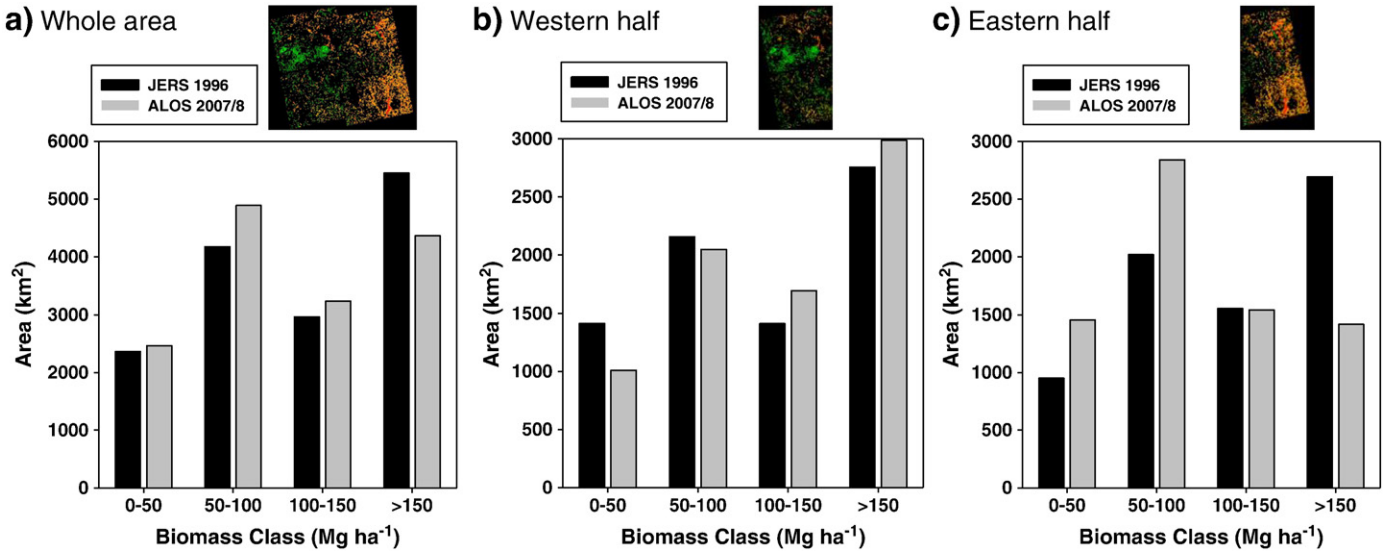

Fig. 8. The total area in km^2 against biomass class (Mg ha^{-1}) for the two biomass maps from 1996 and 2007 for: a) the whole data set; b) the less-populated western half of the study region; and c) the more-populated right hand half.

4.7.2. Uncertainties in radar to biomass estimation

We now consider the errors involved in putting a pixel into the correct biomass class. This was estimated using the RMSE values from the original biomass estimation, as discussed in Section 4.5, though these RMSE values are likely to overestimate the true error value because of their small plot size. The biomass class sizes were chosen to be approximately equal to the RMSE values at the respective biomass level. Assuming errors are normally distributed, this should result in approximately 68% of data points being placed in the correct class, and approximately 95% in the correct class or a neighboring class (Zar, 2007). These are indeed approximated in the field data, with 65% of the data points being correctly classified for the ALOS HV data, and 96% being placed in the correct or neighboring class; for ALOS HH (with the wider biomass classes) these values are 57% and 96% respectively.

These errors in classifying pixels should, unlike those for the biomass estimation, be randomly distributed, with no bias (i.e. there is assumed to be an equal chance of over- and under-estimation for every point). Thus while the chances of a randomly chosen pixel being correctly classified is just 66%, the large number of pixels considered in all the classes suggests the overall accuracy in estimating the total area of this class is much higher. This assumption would not be valid if the number of pixels varied

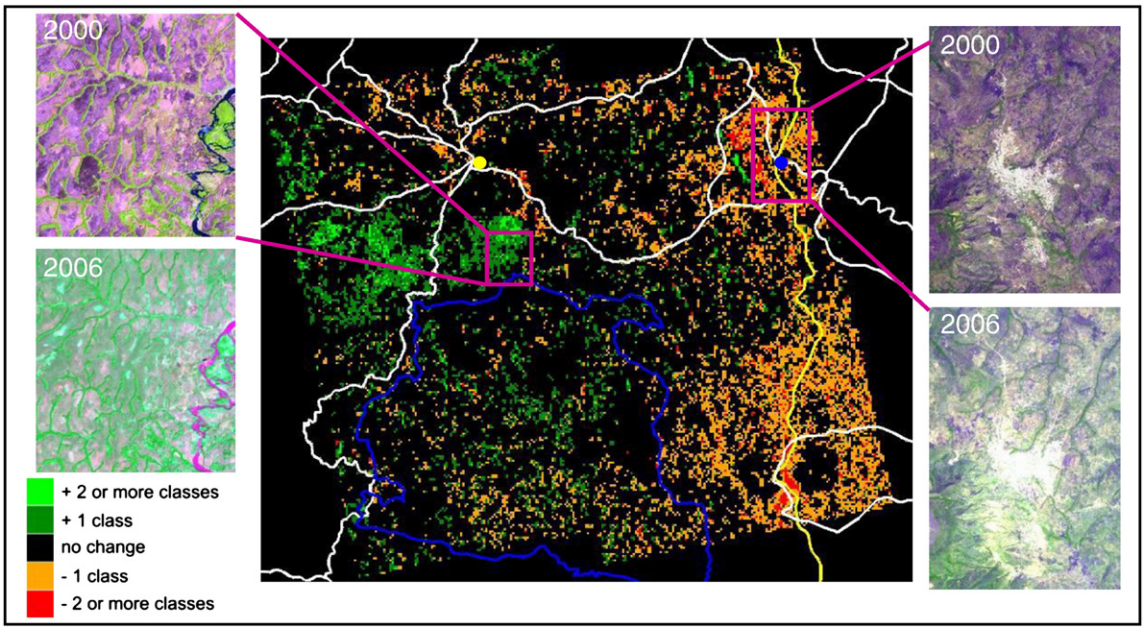

Fig. 9. Change in class image using the same method as for Fig. 6c. The major towns of Tibati and Ngaundal are shown as yellow and blue circles respectively, Mbam Djerem National Park is outlined in blue, roads are shown in white, and the railway line in yellow. Optical close-up images are Landsat ETM+ from 2000 (bands 5–4–3) and ASTER from 2006 (bands 3n–2–1), showing the widening of gallery forests and increased woody vegetation on the left-hand pair, and the rapid clearing of woody vegetation around the town of Ngaundal on the right-hand pair. Note that the differences in color are caused by the different bands available from two sensors, however in both the green channel is an infra-red band that responds strongly to vegetation cover, which will mostly be woody in these dry season images.

considerably between classes, as rare classes would be overestimated due to mis-estimation from neighboring classes; however as all the classes are of a similar magnitude this is unlikely to be a serious problem. Equally, 25 pixels are averaged to produce each average class at a 500 m resolution before the change detection routine is performed. Therefore the total area covered by each class in Fig. 8, and the changes in average biomass class at a 500 m resolution in Fig. 7, are thought accurate to at least a 95% (based on a simple statistical simulation model), and possibly higher, suggesting that the changes observed are robust. However, using this methodology to track changes in individual 100 m pixels is likely to give poor estimates, so we produced a biomass change map at a 500 m resolution, as the averaging of the class of 25 pixels gives a level of confidence in the results (>95%) which could not be achieved with a higher resolution (Fig. 7c).

5. Discussion

5.1. Using radar data to detect changes in forest–savanna ecotones

We detected forest expansion over a large, less-populated western part of our study area, and rapid forest loss in the eastern side. This strongly suggests that satellite L-band SAR data can be used to detect biomass changes in forest–savanna transition regions. While a reduction in signal sensitivity at higher biomasses makes the accurate estimation of forest biomass difficult, detecting changes in the woodiness of savannas, and detecting deforestation and degradation, is possible using a combination of JERS and ALOS PALSAR, and in future with two PALSAR images. The errors in the analysis have been assessed, and shown to be small compared to the signal in the data, increasing our confidence in results derived from L-band SAR data combined with on-the-ground field measurements.

The lack of field data corresponding to the 1996 satellite data increases the error in the results, but apparently not dramatically so; although this error is impossible to quantify precisely, we can be confident in the results given the conservative methodology and broad biomass classes used. These broad classes mean that only pixels that have undergone rapid biomass change will be detected, thus providing confidence that any observed changes are genuine and not caused by noise or mis-calibration of the datasets.

The ALOS data were captured in the wet season, and the HH signal is therefore likely to be less sensitive to differences in biomass than if the imagery had been obtained during the dry season with lower soil moisture influences. Consequently, the HH data from JERS captured in the dry season is likely to have considerably smaller errors than suggested by the ALOS HH data. The benefits of using HV over HH can be seen clearly, with a relationship found with $r^2 = 0.86$ for the ALOS HV data, despite the wet season image capture. This is due to the minimal impact of soil moisture on L-band HV, which has been shown elsewhere (Dubois et al., 1995; Oh et al., 1992).

5.2. Forest expansion

The smaller-scale (40–300 km^2) reports of Boulvert (1990), Happi (1998) and Guillet et al. (2001) showing woody expansion in Cameroon are consistent with our larger scale (15 000 km^2) study: woody expansion is indeed occurring in some forest–savanna transition regions, and it is occurring rapidly, with many pixels increasing by two biomass classes over the eleven year study period, equivalent to at least a doubling in biomass. While this increase is rapid, it is not necessarily unrealistic: increases of 1.4–2.0 Mg $ha^{-1} yr^{-1}$ have been observed in the drier Miombo woodlands (Chidumayo, 1997; Williams et al., 2008), and increases >10 Mg $ha^{-1} yr^{-1}$ have been found for secondary forest growth in Amazonia (Feldpausch et al., 2004; Gehring et al., 2005; Houghton et al., 2000), in wetter, less seasonal conditions. We therefore estimate that increases in the order of 5 Mg $ha^{-1} yr^{-1}$ would be possible in this area, which is sufficient to produce the observed increases over the eleven years.

This also corroborates a recent study using high resolution spectral vegetation index data over a 5000 km^2 region equivalent to the central-west section of this study area from 1986 to 2006, which found significant increases in the woody cover of the savanna regions (Mitchard et al., 2009). Equally, this finding agrees with informal independent field observations in the Mbam Djerem National Park: the first 30 m or so of most gallery forests were dominated by young pioneer trees, with a scattering of older dead and dying savanna trees being shaded by the arrival of faster growing and ultimately taller forest biome species (Mitchard et al., 2009 & personal observation by ETAM, TRF, SLL & BS).

It is likely that the expansion of forest is caused by a reduction in human disturbance, especially fire, which may have resulted from a combination of urban migration, changes in lifestyle away from cattle herding, and the formation of the Mbam Djerem National Park. These factors have previously been shown to be the cause of woody encroachment in a number of semi-arid environments in Africa (Dalle et al., 2006; Ward, 2005). Although it is difficult to quantify the total positive effect of the designation of the area as a National Park on biomass gain, the study does show the potential for national parks in forest–savanna ecotone regions to be managed to sequester carbon. It is possible that adopting a policy of limiting savanna burning and exploitation might enable such parks to earn valuable funds, either in the voluntary carbon market or the proposed Reduced Emissions from Deforestation and Degradation (REDD) scheme. By contrast, it demonstrates that a policy of savanna burning may need to be implemented in Mbam Djerem National Park in order to maintain the unique diversity of ecosystem types present.

This study also demonstrates that a combination of satellite radar data with field studies can provide sufficiently robust evidence to claim and validate carbon stocks (though robust baseline data will also be needed to enable calculations of carbon credits). Ideally however a still-more robust analysis would be performed, using L- or P-band data from the same sensor in the same season under similar ground moisture conditions, in combination with field data collected in the same year as each radar scene. This would increase the accuracy and confidence in the results, removing any need for back calibration, and allowing direct estimation of biomass changes per pixel, without the need for broad biomass classes. It would also reduce the influence of soil moisture. The impact of soil moisture in this study cannot be ruled out entirely, although we believe it could not explain the biomass increases observed in this study, because (a) forest–savanna boundaries and gallery forests in the ALOS HV image are clearly visible, (b) these boundaries correspond well with the Quickbird data, and (c) we used a large number of biomass plots and calibration points around the area which showed the biggest biomass increase.

5.3. Forest loss

Despite the significant gains shown in the west, the overall biomass trend for the study area is negative, with a net loss of 20% (1090 km^2) of high biomass forest (>150 Mg ha^{-1}) over the 11 year study period. The losses along the railway line and paved road on the eastern side of the study area are very obvious, and similarly around the town of Ngaoundal in the north-east (Fig. 9). We suspect strongly that this change is due to human-driven deforestation and degradation (SLL personal observation), but cannot rule out the possibility that it is due to forest die-back following a localized drought (Dai et al., 2004). The population density there is higher, and as well as farming and timber extraction for fuel (both woodfuel for local use and charcoal for transport to towns and cities), there are logging operations in the forest areas outside the park. Clearly, the fate of woody vegetation in this region is currently largely in the hands of humans, and without intervention it seems likely that rapid net forest biomass losses will

continue; biomass gains in protected areas are very unlikely to be large enough to offset losses of forest and biomass elsewhere. However, recent population trends leave some room for cautious optimism regarding biomass stocks: although the urban population of Cameroon grew by 3.61% per year from 2002 till 2006, the rural population actually fell slightly, at an average rate of −0.023% per year (World Bank, 2007). Yet, the growing urban population will, of course, have larger demands for fuel, food and timber, so while remote or protected areas may have the potential for an increase in biomass, areas of forest and woody savanna near settlements and access routes are likely to continue to decrease in biomass unless affordable alternatives are available to local biomass-based products. The Mbam Djerem National Park is relatively well protected and the savannas are not currently systematically burned, and as such the land in the park may continue sequestering carbon into the future. Given the rate of loss outside the park, perhaps community projects in this area attempting to reduce deforestation and promote the planting of trees may be more successful at carbon sequestration than relying on natural regeneration within undisturbed savannas (Williams et al., 2008). However, as Geist and Lambin (2002) showed in a meta-analysis of 152 sub-regional deforestation studies, the principal cause of deforestation is demand from remote foreign markets, so local intervention may not alone provide a solution. In addition to local action large-scale, concerted international solutions such as REDD, involving making performance-based payments to reduce deforestation and degradation rates alongside demand management for wood products, may be necessary.

5.4. Implications for future radar satellites

While the methods used in this study are sufficient to accurately find areas of large-magnitude biomass change, using these data we cannot be very exact in assessing the precise magnitude of such changes, nor of absolute carbon stocks. However, in the future it is likely to be possible to produce quantitative estimates of biomass change using radar backscatter images captured during the same season over different years from identical or similar L- or P-band polarimetric sensors. The similar geometric configuration and radiometric accuracy of the sensors will allow the use of established radar change detection algorithms which directly compare backscatter values (Carincotte et al., 2006; Rignot & Vanzyl, 1993; Touzi et al., 1999). This will be possible using ALOS PALSAR data (which will be continued by ALOS-2), but also with more informative data including information about tree heights from new satellites such as NASA's interferometric L-band SAR and lidar DESDynI, and ESA's planned interferometric P-band BIOMASS. Such data should allow for accurate large-scale, high resolution and long-term monitoring of forest degradation and regeneration.

It is also possible that the accuracy of the biomass maps produced at each time point could be improved by the addition of optical data and digital elevation models (DEMs) to the radar data, using multivariate analysis techniques. Optical data, such as vegetation indices, provide a different suite of information about forest structure in these ecosystems (for example canopy cover; Mitchard et al., 2009) that might be beneficial in producing more robust biomass maps, and DEMs could be used to correct for the influence of slope on radar backscatter. This technique of incorporating many different layers to produce biomass maps has been conducted at a coarse resolution in Amazonia (e.g. Saatchi et al., 2007), but would suffer from the difficulties of acquiring comparable, high resolution and cloud-free images captured at a similar time to the radar images for each year for this kind of high resolution change detection. In general, however, more information should provide greater constraints on potential errors and improve accuracy, so this type of combined-data approach should be investigated.

Acknowledgments

The authors would like to acknowledge Gatsby Plants for providing ETAM's PhD studentship, and TROBIT, a NERC-funded consortium, grant ref: NE/D005590/1, for funding the rest of the work. SLL was funded by a Royal Society University Research Fellowship. Jon Lloyd, TROBIT P.I., provided useful advice and expertise. Three anonymous referees provided helpful suggestions and comments on an earlier version of the manuscript that were instrumental in improving the study. Adam Freedman provided advice on the sources of accurate population data. Jeanette Sonké, Wildlife Conservation Society-Cameroon (WCS-Cameroon), The University of Yaounde I, and 14 canoeists from Mbakaou provided invaluable support in Cameroon. Remote sensing data were provided by the Alaska Satellite Facility, the Global Rainforest Mapping Project, NASA and Eurimage; Landsat and ASTER images were provided free of charge by Terralook, courtesy of USGS EROS and NASA's Jet Propulsion Laboratory; TRMM 3B43 data was downloaded from the Giovanni online data system, developed and maintained by the NASA Goddard Earth Sciences (GES) Data and Information Services Center (DISC).

References

Alder, D., & Synnott, T. J. (1992). Permanent sample plot techniques for mixed tropical forest. *Oxford Forestry Institute Tropical Forestry Papers*, *25*.

Anonymous (2007). *Park National du Mbam et Djerem, Plan d'Aménagement 2007–2011*. Cameroun: Le Ministère des Forêts et de la Faune.

Archer, S., Boutton, T. W., & Hibbard, K. A. (2001). Trees in grasslands: Biogeochemical consequences of woody plant expansion. In E. -D. Schulze, S. Harrison, M. Heimann, E. Holland, J. Lloyd, I. Prentice, & D. Schimel (Eds.), *Global biogeochemical cycles in the climate system* (pp. 115–133). San Diego: Academic Press.

Attema, E. P. W., & Ulaby, F. T. (1978). Vegetation modeled as a water cloud. *Radio Science*, *13*, 357–364.

Boulvert, Y. (1990). Avancée ou recul de la forêt centroafricaine. Changements climatiques, influence de l'homme et notamment de feux. In R. Lanfranchi, & D. Schwartz (Eds.), *Paysages Quaternaries de l'Afrique Central Atlantique* (pp. 353–366). Paris: Initiations et Didactiques ORSTROM.

Bowman, D., Walsh, A., & Milne, D. J. (2001). Forest expansion and grassland contraction within a Eucalyptus savanna matrix between 1941 and 1994 at Litchfield National Park in the Australian monsoon tropics. *Global Ecology and Biogeography*, *10*, 535–548.

Brook, B. W., & Bowman, D. (2006). Postcards from the past: Charting the landscape-scale conversion of tropical Australian savanna to closed forest during the 20th century. *Landscape Ecology*, *21*, 1253–1266.

Bucini, G., & Hanan, N. P. (2007). A continental-scale analysis of tree cover in African savannas. *Global Ecology and Biogeography*, *16*, 593–605.

Carincotte, C., Derrode, S., & Bourennane, S. (2006). Unsupervised change detection on SAR images using fuzzy hidden Markov chains. *IEEE Transactions on Geoscience and Remote Sensing*, *44*, 432–441.

Center for International Earth Science Information Network (CIESIN) Columbia University, International Food Policy Research Institute (IPFRI), World Bank, & Centro Internacional de Agricultura Tropical (CIAT) (2004). *Global Rural–Urban Mapping Project (GRUMP): Urban/Rural Population grids*. Palisades, NY: CIESIN, Columbia University Downloaded from http://sedac.ciesin.columbia.edu/gpw/.

Chave, J., Andalo, C., Brown, S., Cairns, M. A., Chambers, J. Q., Eamus, D., et al. (2005). Tree allometry and improved estimation of carbon stocks and balance in tropical forests. *Oecologia*, *145*, 87–99.

Chave, J., Coomes, D., Jansen, S., Lewis, S. L., Gwenson, N. G., & Zanne, A. E. (2009). Towards a worldwide wood economics spectrum. *Ecology Letters*, *12*, 351–366.

Chave, J., Muller-Landau, H. C., Baker, T. R., Easdale, T. A., Ter Steege, H., & Webb, C. O. (2006). Regional and phylogenetic variation of wood density across 2456 neotropical tree species. *Ecological Applications*, *16*, 2356–2367.

Chidumayo, E. N. (1997). *Miombo ecology and management: An introduction*. London: IT Publications in association with the Stockholm Environment Institute.

Dai, A. G., Trenberth, K. E., & Qian, T. T. (2004). A global dataset of Palmer Drought Severity Index for 1870–2002: Relationship with soil moisture and effects of surface warming. *Journal of Hydrometeorology*, *5*, 1117–1130.

Dalle, G., Maass, B. L., & Isselstein, J. (2006). Encroachment of woody plants and its impact on pastoral livestock production in the Borana lowlands, southern Oromia, Ethiopia. *African Journal of Ecology*, *44*, 237–246.

De Grandi, G., Mayaux, P., Rauste, Y., Rosenqvist, A., Simard, M., & Saatchi, S. S. (2000). The Global Rain Forest Mapping Project JERS-1 radar mosaic of tropical Africa: Development and product characterization aspects. *IEEE Transactions on Geoscience and Remote Sensing*, *38*, 2218–2233.

Doumenge, C., Ndinga, A., Nembot, T. F., Tchanou, Z., Ondo, V. M., Nze, N. O., et al. (2003). Forest biodiversity conservation in Atlantic regions of central Africa: II. Identifying a network of critical sites. *Bois et Forest des Tropiques*, *296*, 43–58.

Duarte, L. D. S., Machado, R. E., Hartz, S. M., & Pillar, V. D. (2006). What saplings can tell us about forest expansion over natural grasslands. *Journal of Vegetation Science*, *17*, 799–808.

Dubois, P. C., Vanzyl, J., & Engman, T. (1995). Measuring soil-moisture with imaging radars. *IEEE Transactions on Geoscience and Remote Sensing*, *33*, 915–926.

Durigan, G., & Ratter, J. A. (2006). Successional changes in cerrado and cerrado/forest ecotonal vegetation in western Sao Paulo State, Brazil, 1962–2000. *Edinburgh Journal of Botany*, *63*, 119–130.

Eamus, D., & Palmer, A. (2007). Is climate change a possible explanation for woody thickening in arid and semi-arid regions? *Research Letters in Ecology*.

FAO (2007). *State of the world's forests 2007*. Rome: Food and Agriculture Organization of the United Nations.

Feldpausch, T. R., Rondon, M. A., Fernandes, E. C. M., Riha, S. J., & Wandelli, E. (2004). Carbon and nutrient accumulation in secondary forests regenerating on pastures in central Amazonia. *Ecological Applications*, *14S*, S164–S176.

Gehring, C., Denich, M., & Vlek, P. L. G. (2005). Resilience of secondary forest regrowth after slash-and-burn agriculture in central Amazonia. *Journal of Tropical Ecology*, *21*, 519–527.

Geist, H. J., & Lambin, E. F. (2002). Proximate causes and underlying driving forces of tropical deforestation. *Bioscience*, *52*, 143–150.

Goetze, D., Horsch, B., & Porembski, S. (2006). Dynamics of forest–savanna mosaics in north-eastern Ivory Coast from 1954 to 2002. *Journal of Biogeography*, *33*, 653–664.

Guillet, B., Achoundong, G., Happi, J. Y., Beyala, V. K. K., Bonvallot, J., Riera, B., et al. (2001). Agreement between floristic and soil organic carbon isotope (C-13/C-12, C-14) indicators of forest invasion of savannas during the last century in Cameroon. *Journal of Tropical Ecology*, *17*, 809–832.

Happi, J. Y. (1998). *Arbres contre graminees: la lenta invasion de la savane par la foret au center-Cameroun.* Paris: Université de Paris Sorbonne.

Hely, C., Bremond, L., Alleaume, S., Smith, B., Sykes, M. T., & Guiot, J. (2006). Sensitivity of African biomes to changes in the precipitation regime. *Global Ecology and Biogeography*, *15*, 258–270.

Hopkins, M. S., Head, J., Ash, J. E., Hewett, R. K., & Graham, A. W. (1996). Evidence of a Holocene and continuing recent expansion of lowland rain forest in humid, tropical North Queensland. *Journal of Biogeography*, *23*, 737–745.

Houghton, R. A., Skole, D. L., Nobre, C. A., Hackler, J. L., Lawrence, K. T., & Chomentowski, W. H. (2000). Annual fluxes of carbon from deforestation and regrowth in the Brazilian Amazon. *Nature*, *403*, 301–304.

Hovestadt, T., Yao, P., & Linsenmair, K. E. (1999). Seed dispersal mechanisms and the vegetation of forest islands in a West African forest–savanna mosaic (Comoe National Park, Ivory Coast). *Plant Ecology*, *144*, 1–25.

Jeltsch, F., Moloney, K., & Milton, S. J. (1999). Detecting process from snapshot pattern: Lessons from tree spacing in the southern Kalahari. *Oikos*, *85*, 451–466.

Lewis, S. L. (2006). Tropical forests and the changing Earth system. *Philosophical Transactions of the Royal Society of London Series B-Biological Sciences*, *361*, 195–210.

Lewis, S. L., Lopez-Gonzalez, G., Sonke, B., Affum-Baffoe, K., Baker, T. R., Ojo, L. O., et al. (2009). Increasing carbon storage in intact African tropical forests. *Nature*, *457*, 1003-U1003.

Lewis, S. L., Malhi, Y., & Phillips, O. L. (2004). Fingerprinting the impacts of global change on tropical forests. *Philosophical Transactions of the Royal Society of London Series B-Biological Sciences*, *359*, 437–462.

Lloyd, J., & Farquhar, G. D. (1996). The CO_2 dependence of photosynthesis, plant growth responses to elevated atmospheric CO_2 concentrations and their interaction with soil nutrient status. 1. General principles and forest ecosystems. *Functional Ecology*, *10*, 4–32.

Lloyd, J., & Farquhar, G. D. (2008). Effects of rising temperatures and [CO_2] on the physiology of tropical forest trees. *Philosophical Transactions of the Royal Society B-Biological Sciences*, *363*, 1811–1817.

Loveland, T. R., Reed, B. C., Brown, J. F., Ohlen, D. O., Zhu, Z., Yang, L., et al. (2000). Development of a global land cover characteristics database and IGBP DISCover from 1 km AVHRR data. *International Journal of Remote Sensing*, *21*, 1303–1330.

Lu, D. S. (2006). The potential and challenge of remote sensing-based biomass estimation. *International Journal of Remote Sensing*, *27*, 1297–1328.

Lucas, R. M., Milne, A. K., Cronin, N., Witte, C., & Denham, R. (2000). The potential of synthetic aperture radar (SAR) for quantifying the biomass of Australia's woodlands. *Rangeland Journal*, *22*, 124–140.

Marimon, B. S., Lima, E. S., Duarte, T. G., Chieregatto, L. C., & Ratter, J. A. (2006). Observations on the vegetation of northeastern Mato Grosso, Brazil. IV. An analysis of the cerrado-Amazonian forest ecotone. *Edinburgh Journal of Botany*, *63*, 323–341.

Mayaux, P., Bartholome, E., Fritz, S., & Belward, A. (2004). A new land-cover map of Africa for the year 2000. *Journal of Biogeography*, *31*, 861–877.

Menaut, J. C. (1983). The vegetation of African savanna. In F. Bourliere (Ed.), *Ecosystems of the world: Tropical savannas*. Amsterdam: Elsevier.

Mertens, B., & Lambin, E. F. (2000). Land-cover-change trajectories in southern Cameroon. *Annals of the Association of American Geographers*, *90*, 467–494.

Mitchard, E. T. A., Saatchi, S. S., Gerard, F. F., Lewis, S. L., & Meir, P. (2009). Measuring woody encroachment along a forest–savanna boundary in central Africa. *Earth Interactions*, *13*, 8.

Nangendo, G. v. S. O. d. G. A. (2005). Biodiversity conservation through burning: a case study of woodlands in Budongo Forest Reserve, NW Uganda. In M. A. F. D. T. Ros-Tonen (Ed.), *African forests between nature and livelihood resources: interdisciplinary studies in conservation and forest management* (pp. 113–128). New York: The Edin Mellen Press.

Oh, Y., Sarabandi, K., & Ulaby, F. T. (1992). An empirical-model and an inversion technique for radar scattering from bare soil surfaces. *IEEE Transactions on Geoscience and Remote Sensing*, *30*, 370–381.

PNUD (UNDP, United Nations Development Program). (1999). *Rapport sur le pauvreté rurale au Cameroun.* Yaoundé: PNUD.

Podest, E., & Saatchi, S. (2002). Application of multiscale texture in classifying JERS-1 radar data over tropical vegetation. *International Journal of Remote Sensing*, *23*, 1487–1506.

Puyravaud, J. P., Dufour, C., & Aravajy, S. (2003). Rain forest expansion mediated by successional processes in vegetation thickets in the Western Ghats of India. *Journal of Biogeography*, *30*, 1067–1080.

Ratter, J. A. (1992). Transitions between cerrado and forest vegetation in Brazil. In P. A. Furley, J. Proctor, & J. A. Ratter (Eds.), *Nature and dynamics of forest–savanna boundaries*. London: Chapman and Hall.

Ribeiro, N. S., Saatchi, S. S., Shugart, H. H., & Washington-Allen, R. A. (2008). Aboveground biomass and Leaf Area Index (LAI) mapping for Niassa Reserve, northern Mozambique. *Journal of Geophysical Research-Biogeosciences*, *113*.

Rignot, E. J. M., & Vanzyl, J. J. (1993). Change detection techniques for Ers-1 Sar Data. *IEEE Transactions on Geoscience and Remote Sensing*, *31*, 896–906.

Rosenqvist, A., Shimada, M., & Milne, A. K. (2007). *The ALOS Kyoto & Carbon Initiative* (pp. 3614–3617)..

Saatchi, S. S., Houghton, R. A., Alvala, R., Soares, J. V., & Yu, Y. (2007). Distribution of aboveground live biomass in the Amazon basin. *Global Change Biology*, *13*, 816–837.

Sankaran, M., Hanan, N. P., Scholes, R. J., Ratnam, J., Augustine, D. J., Cade, B. S., et al. (2005). Determinants of woody cover in African savannas. *Nature*, *438*, 846–849.

Sano, E. E., Ferreira, L. G., & Huete, A. R. (2005). Synthetic aperture radar (L band) and optical vegetation indices for discriminating the Brazilian savanna physiognomies: A comparative analysis. *Earth Interactions*, *9*.

Santos, J. R., Lacruz, M. S. P., Araujo, L. S., & Keil, M. (2002). Savanna and tropical rainforest biomass estimation and spatialization using JERS-1 data. *International Journal of Remote Sensing*, *23*, 1217–1229.

Shimada, M., Isoguchi, O., Tadono, T., & Isono, K. (2009). PALSAR radiometric calibration and geometric calibration. *IEEE Transactions on Geoscience and Remote Sensing*, *47*, 3915–3932.

Smith, T. B., Kark, S., Schneider, J., Wayne, R. K., & Moritz, C. (2001). Biodiversity hotspots and beyond: The need for preserving environmental transitions. *Trends in Ecology and Evolution*, *16*, 431.

Smith, T. B., Wayne, R. K., Girman, D. J., & Bruford, M. W. (1997). A role for ecotones in generating rainforest biodiversity. *Science*, *276*, 1855–1857.

Taiz, L., & Zeiger, E. (2006). *Plant physiology* (4th Edition). Sunderland, MA: Sinauer Associates.

Touzi, R., Lopes, A., Bruniquel, J., & Vachon, P. W. (1999). Coherence estimation for SAR imagery. *IEEE Transactions on Geoscience and Remote Sensing*, *37*, 135–149.

Ward (2005). Do we understand the causes of bush encroachment in African savannas? *African Journal of Range and Forage Science*, 101–105.

Williams, M., Ryan, C. M., Rees, R. M., Sarnbane, E., Femando, J., & Grace, J. (2008). Carbon sequestration and biodiversity of re-growing Miombo woodlands in Mozambique. *Forest Ecology and Management*, *254*, 145–155.

Woodhouse, I. H. (2005). *Introduction to microwave remote sensing.* CRC Press.

Woodhouse, I. H. (2006). Predicting backscatter-biomass and height-biomass trends using a macroecology model. *IEEE Transactions on Geoscience and Remote Sensing*, *44*, 871–877.

World Bank (2007, March). *World Bank Development Indicators Database.* Washington DC: World Bank Accessed online at http://www.worldbank.org/data/onlinedatabases/wdi.

Zanne, A. E., Lopez-Gonzalez, G., Coomes, D. A., Ilic, J., Jansen, S., Lewis, S. L., et al. (2009). *Global wood density database.* Dryad http://hdl.handle.net/10255/dryad.235.

Zar, J. H. (2007). *Biostatistical analysis* (5th Edition). USA: Prentice-Hall.

Zeng, N., & Neelin, J. D. (2000). The role of vegetation–climate interaction and interannual variability in shaping the African savanna. *Journal of Climate*, *13*, 2665–2670.

Zhang, Q. F., Justice, C. O., Jiang, M. X., Brunner, J., & Wilkie, D. S. (2006). A GIS-based assessment on the vulnerability and future extent of the tropical forests of the Congo Basin. *Environmental Monitoring and Assessment*, *114*, 107–121.

Appendix 3

Published version of Chapter 5

GEOPHYSICAL RESEARCH LETTERS, VOL. 36, L23401, doi:10.1029/2009GL040692, 2009

Using satellite radar backscatter to predict above-ground woody biomass: A consistent relationship across four different African landscapes

E. T. A. Mitchard,[1] S. S. Saatchi,[2] I. H. Woodhouse,[1] G. Nangendo,[3] N. S. Ribeiro,[4] M. Williams,[1] C. M. Ryan,[1] S. L. Lewis,[5] T. R. Feldpausch,[5] and P. Meir[1]

Received 16 September 2009; revised 26 October 2009; accepted 2 November 2009; published 2 December 2009.

[1] Regional-scale above-ground biomass (AGB) estimates of tropical savannas and woodlands are highly uncertain, despite their global importance for ecosystems services and as carbon stores. In response, we collated field inventory data from 253 plots at four study sites in Cameroon, Uganda and Mozambique, and examined the relationships between field-measured AGB and cross-polarized radar backscatter values derived from ALOS PALSAR, an L-band satellite sensor. The relationships were highly significant, similar among sites, and displayed high prediction accuracies up to 150 Mg ha^{-1} (±∼20%). AGB predictions for any given site obtained using equations derived from data from only the other three sites generated only small increases in error. The results suggest that a widely applicable general relationship exists between AGB and L-band backscatter for lower-biomass tropical woody vegetation. This relationship allows regional-scale AGB estimation, required for example by planned REDD (Reducing Emissions from Deforestation and Degradation) schemes.
Citation: Mitchard, E. T. A., S. S. Saatchi, I. H. Woodhouse, G. Nangendo, N. S. Ribeiro, M. Williams, C. M. Ryan, S. L. Lewis, T. R. Feldpausch, and P. Meir (2009), Using satellite radar backscatter to predict above-ground woody biomass: A consistent relationship across four different African landscapes, *Geophys. Res. Lett.*, *36*, L23401, doi:10.1029/2009GL040692.

1. Introduction

[2] There is no universally accepted methodology for assessing the above-ground biomass (AGB) of woody tropical landscapes. While there is a degree of consensus on the best methods of collecting ground-based inventory data [*Brown*, 1997; *Chave et al.*, 2009; *Phillips et al.*, 2009], and a general agreement that remote sensing data provides the best methodology for both scaling-up ground-based measurements and monitoring changes over large scales, there is a plethora of different sensors and analytical procedures available for scaling-up AGB estimates [*Lu*, 2006].

[3] Tropical savanna and woodland ecosystems provide substantial ecosystem services at local to global scales: the provision of timber, fuel and other products, the regulation of soil and water, biodiversity retention, atmospheric services and eco-tourism. However, attempts to mitigate rising atmospheric CO_2 levels have led to projects aiming to preserve these ecosystems based solely on their carbon stocks. To be successful, whether in voluntary carbon markets or via a post-Kyoto climate change agreement under one of the Reducing Emissions from Deforestation and Degradation (REDD) frameworks, a universal, low-cost and robust way to measure and monitor carbon stocks over large regions is needed [*Grassi et al.*, 2008].

[4] An ideal large-scale AGB measurement system would be one that could sense AGB directly, and as such would have no upper biomass limit, and do so independently of cloud cover. Currently no such system exists, although future satellite platforms which will combine fully polarimetric radar with measurements of vegetation height may come closer to this goal [*Donnellan et al.*, 2008; *Le Toan et al.*, 2008]. However, for areas with an AGB < ∼150 Mg ha^{-1}, which incorporates the savanna and woodland biomes, and drier tropical forest formations, the L-band radar sensor ALOS PALSAR may go some way towards providing a system for measuring AGB that meets observational requirements. In this paper we set out evidence supporting this claim.

[5] Synthetic Aperture Radar (SAR) sensors are active instruments, sending a pulse of microwave radiation and detecting the radiation scattered back (backscatter, referred to as sigma0 [σ^0]) by the surface and the 3-dimensional structures on it. When longer wavelength microwaves are used (>20 cm) the detected radiation is mostly due to backscattering from the branching elements and stems of the trees, and thus radar should respond in a characteristic way to forest volume and biomass [*Saatchi and Moghaddam*, 2000]. As a result, long wavelength SAR has a stronger and more universal relationship than optical or short wavelength microwave sensors which are sensitive to leaf characteristics, where relationships with the woody component of vegetation are indirect and thus highly site- and season- specific. The radar backscatter response saturates at higher biomass values in savanna ecosystems, at a variable point (>60 Mg ha^{-1} [*Santos et al.*, 2002], >80 Mg ha^{-1} [*Lucas et al.*, 2000], and >150 Mg ha^{-1} [*Mitchard et al.*, 2009], all using different L-band systems). This saturation point is due to the competing mechanisms of scattering and attenuation (absorption) of microwave energy in the canopy of the vegetation, and is highly dependent on the canopy density, stem density, tree species, and vegetation and soil moisture conditions, as well as the characteristics of the radar data used. Nevertheless, this point is high enough that useful biomass

[1]School of Geosciences, University of Edinburgh, Edinburgh, UK.
[2]Jet Propulsion Laboratory, California Institute of Technology, Pasadena, California, USA.
[3]Wildlife Conservation Society, Kampala, Uganda.
[4]Faculdade de Agronomia e Engenharia Florestal, Universidade Eduardo Mondlane, Maputo, Mozambique.
[5]Earth and Biosphere Institute, School of Geography, University of Leeds, Leeds, UK.

0094-8276/09/2009GL040692$05.00

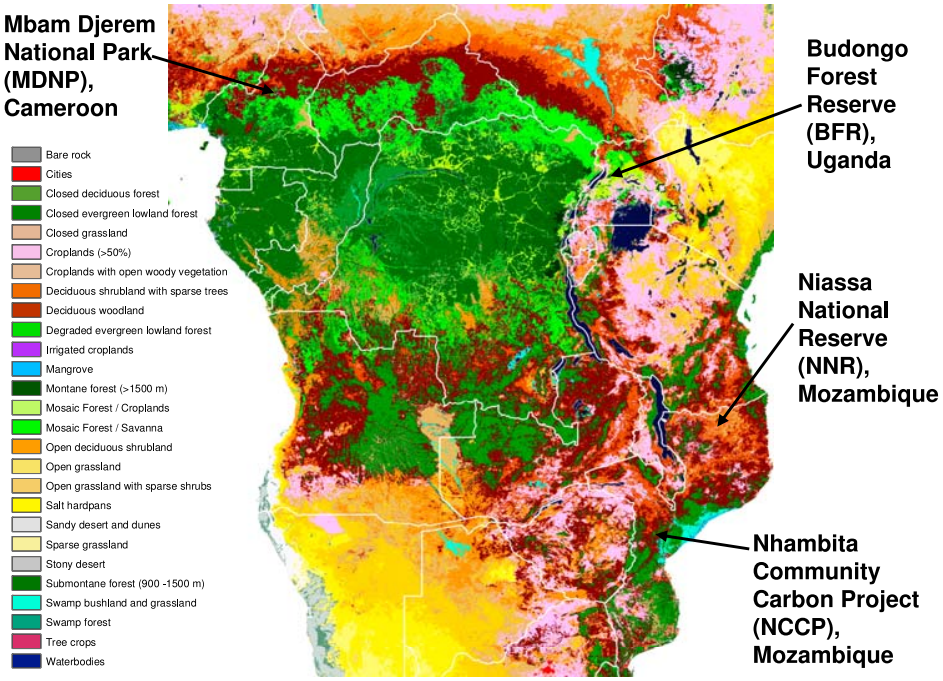

Figure 1. The location of the field sites is shown on a landcover map for the year 2000 produced by *Mayaux et al.* [2004].

estimates are possible for mixed tree-grass systems (savannas and woodlands), as these typically have maximum AGB values <100 Mg ha^{-1}, though higher values can exist in gallery forests [*Brown*, 1997].

[6] Advanced Land Observing Satellite (ALOS) Phased Array L-band Synthetic Aperture Radar (PALSAR) was launched in January 2006. It operates at a 23.6 cm wavelength in a number of modes, but the Fine-beam dual-polarization (FBD) mode, which provides HH (horizontal transmit and horizontal receive) and HV (horizontal transmit and vertical receive) data at a 34.3° incidence angle, shows the greatest potential for these purposes. This is because of its high signal:noise ratio, high resolution (~20 m), provision of cross-polarized data, and because it is being systematically collected across the tropics with the aim of forming a freely-available 50 m resolution mosaic (http://www.eorc.jaxa.jp/ALOS/en/kc_mosaic/kc_mosaic.htm).

[7] PALSAR, and other L-band systems, have previously been shown to respond to the AGB of tropical savannas and woodlands with varying degrees of accuracy [*Lucas et al.*, 2000; *Mitchard et al.*, 2009; *Podest and Saatchi*, 2002; *Santos et al.*, 2002]. However, in these studies the field datasets were small and from one geographic area. Here we examine the PALSAR response to AGB at four different intensively sampled locations across tropical Africa to test the consistency of the relationship between backscatter and AGB. We then examine the efficacy of models derived from three sites to predict the AGB of measured plots in a fourth site, thus providing a much better test of the utility of such data for assessing AGB than has previously been performed.

2. Data and Methods

2.1. Field Data

[8] The field sites were located in Cameroon, Uganda and Mozambique (Figure 1); in all cases standardized forestry methodologies were employed. Diameters of all stems >10 cm diameter at breast height (DBH) were measured and their species recorded; height was also measured for ~30% of stems in the Cameroon and Uganda sites using vertex hypsometers (Haglöf, Sweden). None of the study areas exhibit steeply dissected topography.

2.1.1. Mbam Djerem National Park (MDNP), Cameroon

[9] MDNP encompasses the transition between savanna and forest contiguous with the Congo Basin. Eight 1 ha square plots and ten 0.4 ha transects (8 × 20 m × 200 m & 2 × 40 m × 100 m) in forest and savanna regions in three areas of the park near 6°9′N, 12°50′E were sampled in 2007, with AGB ranging from 6 – 418 Mg ha^{-1} [*Mitchard et al.*, 2009]. Transects that covered both forest and savanna were split into two data-points, giving 24 points in total.

2.1.2. Budongo Forest Reserve (BFR), Uganda

[10] BFR is a remnant patch of tropical forest surrounded by farmland to the south and east, and savanna to the west and north. One 1.86 ha square plot and eleven 0.5 ha transects (20 m × 250 m) were measured in 2008 by E. Mitchard, and 261 × 0.04 ha & 335 × 0.05 ha circular plots in the savannas and woodlands to the north of the reserve were measured in 2001 [*Nangendo et al.*, 2005]; these latter plots are small and highly clustered, and as such were averaged in groups of 5–6 within 100 m × 100 m areas, giving a total of 118 data points (0.2 – 0.3 ha). AGB ranged from 6 – 876 Mg ha^{-1}, with the plots near 1°52′N, 31°39′E.

2.1.3. Niassa National Reserve (NNR), Mozambique

[11] NNR is a 23 000 km^2 protected area in the north of Mozambique, dominated by Miombo woodland, with the woody fraction of vegetation increasing in density from East to West due to a rainfall and disturbance gradient. Fifty 0.07 ha circular plots distributed across the park were

measured in 2004 [*Ribeiro et al.*, 2008] around 12°2′S, 37°15′E. ALOS PALSAR scenes were available for 42, ranging in AGB from 2–41 Mg ha^{-1}.

2.1.4. Nhambita Community Carbon Project (NCCP), Mozambique

[12] NCCP is an area of Miombo woodland in central Mozambique. It has more influence from humans and is more regularly burnt than NNR, and has different dominant species. Data were collected for thirteen 1 ha square plots, five 0.5 ha circular plots, and thirty-eight 0.25 ha square plots in 2004-7, with an AGB of 3–120 Mg ha^{-1}, near 18°57′S, 34°9′E [*Williams et al.*, 2008].

2.2. Conversion to AGB

[13] Field plot data were converted to AGB using the best available methods for each vegetation type. For MDNP and BFR no local allometry data exist, so the *Chave et al.* [2005] pan-tropical optimum allometric equations were used, using wood density, height and DBH. The moist tropical forest equation was used for forest species, and the dry forest equation for savanna species. Height was measured for ∼30% of the stems and used to develop site-specific height-DBH relationships to obtain AGB [*Mitchard et al.*, 2009]. Wood density data were taken from the Global Wood Density Database [*Chave et al.*, 2009]; where species-specific data was not present, the average value for African members of the same genus were used. For NNR an allometric equation involving DBH alone was used, derived from similar vegetation and climatic conditions nearby in Tanzania, taken from *Mugasha and Chamshama* [2002]. For NCCP destructive sampling was performed to produce a site-specific allometric relationship [*Ryan*, 2009]. All plot AGB values were then converted to Mg ha^{-1}; it should be noted that these values are dry AGB, not carbon content, and exclude woody stems < 10 cm, shrubs, grasses, below-ground sources and necromass. This exclusion of other above-ground vegetation will cause an underestimate of AGB of ∼5% for forest and dense woody savanna plots [*Mitchard et al.*, 2009], and the size of this error will increase for lower biomass plots (it is 12% for NCCP [*Ryan*, 2009]). However, the derivation from field data of a local correction factor should be sufficient to correct for this, as L-band radar will respond mostly to larger stems [*Collins et al.*, 2009].

2.3. SAR Data

[14] L-band dual-polarization (HH/HV) satellite radar data from the ALOS PALSAR sensor in the FBD mode were acquired over all field sites from 2007 (see Table S1 of the auxiliary material for scene IDs and dates)[1]. The data were provided at a 12.5 m pixel spacing (4 looks per pixel), and were converted from digital number to sigma0 using the revised calibration coefficients [*Shimada et al.*, 2009]. The scenes were warped to Landsat ETM+ data covering the areas of the field sites, using observable common features such as islands, road junctions, and permanent vegetation features, with a Root Mean Square Error (RMSE) always <0.6 Landsat pixels (18 m), and the backscatter values for pixels covering each field site extracted, with pixels averaged in the power domain so the arithmetic, not geometric, means were used. This type of warping is only possible because all the study areas have little significant topography, so the problem of layover (where topographic features are distorted, bending towards the sensor) is minimized. After averaging, power values were converted back to sigma0 before being regressed against AGB. All remote sensing analyses were performed using ENVI 4.6 (ITT, Boulder, USA), and all regression analyses with Sigmaplot 11.0 (Systat, Chicago, USA).

3. Results

3.1. Plot Level AGB-Backscatter Relationships

[15] Strong relationships between AGB and HV backscatter were found at each of the four landscapes (r^2 0.61 – 0.76, $p < 0.0001$), with a clear reduction in sensitivity (saturation) obvious between 150 and 200 Mg ha^{-1}; relationships with the HH polarization were less consistent, though significant positive relationships were still observable in all cases (Figure S1 and Table S2 of the auxiliary material).[1] The fitted models were of the form:

$$\sigma^0 = a + b.\ln(B_{AG}) \quad (1)$$

$$\sigma^0 = a + b.\ln(B_{AG}) + c.(\ln(B_{AG}))^2 \quad (2)$$

Where σ^0 is the sigma0 in decibels, B_{AG} is the AGB in Mg ha^{-1}, and a, b and c are constants. Both models were fitted to the observed data, with equation (2) being preferred if the log-squared term was significantly different from zero. These models were chosen as they produced the highest r^2 and lowest RMSE values of a number of simple models tested. Coefficients and uncertainties are shown in Table S2.

3.2. Combined AGB-Backscatter Relationships

[16] Combining the HV sigma0 and AGB values of all four datasets produced a strong relationship, with an r^2 of 0.73 and $p < 0.0001$ using equation (2), and with some sensitivity clearly still present in the data up to 150–200 Mg ha^{-1} (Figure 2b). There was also a significant relationship with HH ($r^2 = 0.56$, $p < 0.0001$), but this was less consistent, with saturation occurring at 50–100 Mg ha^{-1} (Figure 2a). The HV relationship fitted was:

$$\sigma^0_{HV} = -22 + 2.73\ln(AGB) - 0.156(\ln(AGB))^2 \quad (3)$$

which rearranged to:

$$AGB = EXP\left[\frac{-2.73 + \sqrt{7.45 - \left(0.623\left(22 + \sigma^0_{HV}\right)\right)}}{-0.311}\right] \quad (4)$$

allows the prediction of AGB from sigma0 values (Figure S2). Attempts were made to combine HH and HV data in a general linear model, but the HH terms were never significant once the HV terms had been taken into account.

3.3. Testing Consistency

[17] The consistency of the general relationship described above was tested using the four independent datasets. For each of the four sites, AGB predictions and resultant RMSE values were calculated using the site-specific HV equations

[1]Auxiliary materials are available in the HTML. doi:10.1029/2009GL040692.

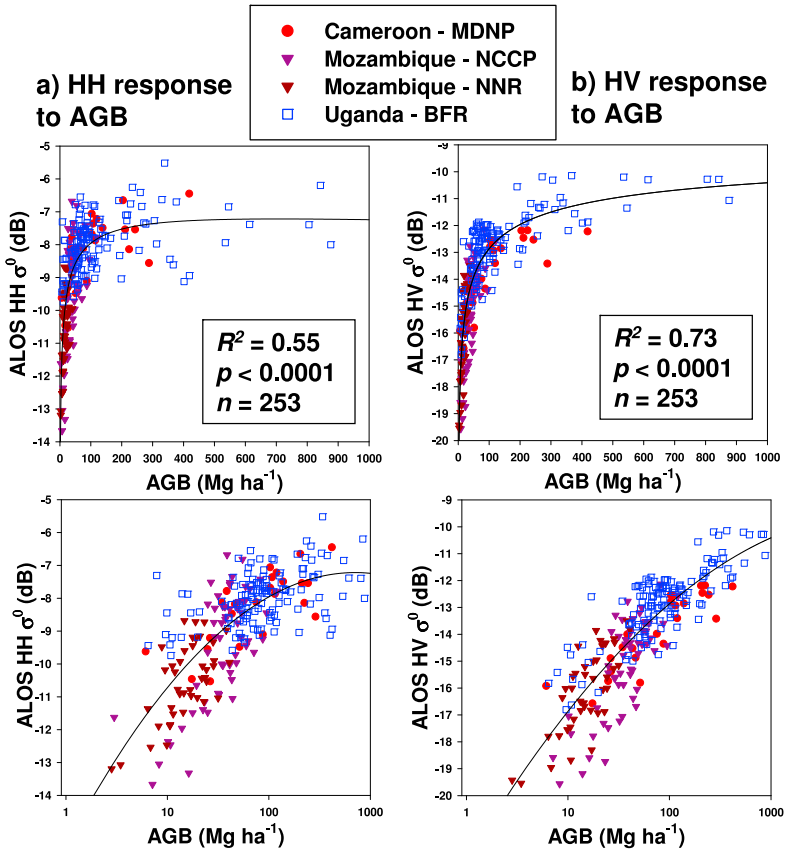

Figure 2. ALOS PALSAR (a) HH and (b) HV backscatter (σ^0) are plotted against field-measured AGB (Mg ha^{-1}) for all four sites combined, with the x-axes shown with conventional and $\log_{10}$ scales. Second order log regression lines are fitted.

(Figure S1 and Table S2). New equations were then calculated using equations derived from the other three datasets only, and predictions made again using the HV values. Both field and predicted values were limited at 400 Mg ha^{-1}, as all possible sensitivity to AGB will be lost by this point, and thus making predictions at such high AGB values has no validity. Predictions for each site obtained by using an equation developed from the three other sites increased the RMSE by only 12–30%, and particularly for data points with AGB < 150 Mg ha^{-1} the RMSE values remained low (Table 1). The average AGB predicted using site-specific equations was within 30% of the field-derived average AGB values, and this error increased negligibly when the equations derived from the other three sites were used (Table 1). However, as the biomass estimation error from radar depends on the errors associated with both radar and ground measurements, the true errors could be greater [*Mitchard et al.*, 2009].

4. Discussion

[18] We have found that PALSAR HV backscatter responds strongly to AGB in a consistent manner across four African sites widely separated in space and differing greatly in their vegetation structure. The relationship derived does contain significant prediction errors (±~20% for plots <150 Mg ha^{-1}). These are partly because L-band SAR does not respond directly to AGB, but to aspects of vegetation structure [*Saatchi and Moghaddam*, 2000], partially due to spatial variability in structure [*Saatchi et al.*, 2009], and partially due to radar calibration and orthorectification [*van Zyl*, 1990] and field estimation errors propagating through the analysis [*Chave et al.*, 2004]. In addition,

Table 1. Average AGB and RMSE for Field Plots Predicted From HV Data and a Site-Specific Model Versus a Model Derived From the Three Other Sites[a]

		Average AGB (Mg ha^{-1})			RMSE (Mg ha^{-1})		RMSE for Points < 150 Mg ha^{-1}	
Site	*n*	Ground Data	Site-Specific	Other-Three	Site-Specific	Other-Three	Site-Specific	Other-Three
MDNP Cameroon	24	114.7	115.5	82.1	61.5	67.5	37.4	22.3
BFR Uganda	129	137.2	176.8	174.0	67.1	74.9	48.8	69.42
NNR Mozambique	42	17.28	19.0	20.2	8.3	12.8	8.3	12.8
NCCP Mozambique	58	40.7	44.6	37.1	19.2	25.2	19.2	25.2

[a]All AGB values were limited at 400 Mg ha^{-1}

backscatter responds differently to differing soil and vegetation moisture conditions, and the surface topography, adding to observed prediction errors. For a detailed discussion of the errors and uncertainties involved in this type of analysis see *Mitchard et al.* [2009]. Despite these factors, our analysis shows that AGB can be predicted using radar data for large areas dominated by differing vegetation types with useful accuracy. Notably, errors do not increase dramatically when a continental PALSAR HV-AGB equation, rather than one based on local biomass plots, is used to estimate local AGB.

[19] The better relationship between AGB and the HV rather than HH polarization, and its higher congruence among sites, is to be expected, as this polarization is much less influenced by soil and vegetation moisture than HH [*Collins et al.*, 2009]. HV is also less influenced by topography [*van Zyl*, 1993], though in areas of substantial topographical change significant inaccuracies in estimation and geolocation will still arise.

[20] These results have a higher saturation point and less noise than found in previous studies using L-band HV data, [e.g., *Lucas et al.*, 2000; *Santos et al.*, 2002; *Viergever et al.*, 2007]. This could be due to structural features of African savannas, or that the data were acquired during the dry season where errors associated with moisture are minimized. Moreover, FBD data is collected at a low incidence angle (34.3°) compared to airborne radar sensors used by the above studies, allowing the radar signal to penetrate deeper into the vegetation canopy. This, in turn, improves the sensitivity of HV backscatter to AGB and reduces the sensitivity of HH backscatter to AGB because of impacts of soil moisture and roughness. The large number of good quality, well-geolocated field plots in relatively flat areas that were obtained for this study could also be a factor, producing more accurate results than other studies by increasing the signal-to-noise ratio.

[21] When applying equation (4) to any PALSAR scene over African woodlands and savannas errors of 20–30% are to be expected (Table 1), probably increasing by another 10% when uncertainties in allometries are included [*Chave et al.*, 2004; *Williams et al.*, 2008]. Local calibration with a network of field plots will remain essential at least for validation, and for estimating a 'correction factor' for adding the AGB of grasses and stems <10 cm. However, this finding of a consistent response to AGB in these widely separated and quite different ecosystems from an operational satellite SAR sensor offers the potential of rapid, accurate, high resolution, and low cost mapping of the lower biomass woody vegetation of Africa, and potentially other regions in the world. Moreover, the 46-day repeat cycle will allow sufficient images to be captured during the year to negate any effects of seasonality and soil moisture, and allow the monitoring of landscapes for any changes in AGB. This finding suggests that utilization of PALSAR data should be essential for projects involving the mapping and monitoring of woodland and savanna biomass, thus having important implications for carbon-credit projects, such as those under proposed REDD schemes.

[22] **Acknowledgments.** JAXA, ASF, and USGS provided remote sensing data. E Mitchard is funded by Gatsby Plants, and Cameroon fieldwork was also funded by TROBIT, a NERC-funded consortium, and assisted by WCS Cameroon and Bonaventure Sonké. Kirsty Laughlin assisted with data collection in BFR, where the Budongo Conservation Field Station provided local support. C Ryan was funded by NERC and data collection for NCCP was part-funded by the EU, and assisted by Envirotrade Ltd. N Ribeiro acknowledges the Eduardo Mondlane University – Department of forest engineering, IUCN-Mozambique and SGDRN (Sociedade para Gestao e Desenvolvimento da Reserva do Niassa). S Lewis is funded by a Royal Society Research Fellowship. Jon Lloyd provided help and expertise.

References

Brown, S. (1997), Estimating biomass and biomass change of tropical forests, *FAO For. Pap. 134*, Food and Agric. Organ. of the U. N., Rome.

Chave, J., R. Condit, S. Aguilar, A. Hernandez, S. Lao, and R. Perez (2004), Error propagation and scaling for tropical forest biomass estimates, *Philos. Trans. R. Soc. London, Ser. B*, *359*(1443), 409–420, doi:10.1098/rstb.2003.1425.

Chave, J., et al. (2005), Tree allometry and improved estimation of carbon stocks and balance in tropical forests, *Oecologia*, *145*(1), 87–99, doi:10.1007/s00442-005-0100-x.

Chave, J., D. Coomes, S. Jansen, S. L. Lewis, N. G. Swenson, and A. E. Zanne (2009), Towards a worldwide wood economics spectrum, *Ecol. Lett.*, *12*(4), 351–366, doi:10.1111/j.1461-0248.2009.01285.x.

Collins, J. N., L. B. Hutley, R. J. Williams, G. Boggs, D. Bell, and R. Bartolo (2009), Estimating landscape-scale vegetation carbon stocks using airborne multi-frequency polarimetric synthetic aperture radar (SAR) in the savannahs of north Australia, *Int. J. Remote Sens.*, *30*(5), 1141–1159, doi:10.1080/01431160802448935.

Donnellan, A., et al. (2008), Deformation, Ecosystem Structure, and Dynamics of Ice (DESDynI), in *Proceedings of the 2008 IEEE Aerospace Conference*, pp. 163–175, Inst. of Electr. and Electron. Eng., New York.

Grassi, G., S. Monni, S. Federici, F. Achard, and D. Mollicone (2008), Applying the conservativeness principle to REDD to deal with the uncertainties of the estimates, *Environ. Res. Lett.*, *3*(3), 035005, doi:10.1088/1748-9326/3/3/035005.

Le Toan, T., H. Baltzer, P. Paillou, K. Papathanassiou, S. Plummer, S. Quegan, F. Rocca, and L. Ulander (2008), Biomass, in *Candidate Earth Explorer Core Mission*, *Rep. Assess. SP-1313/2*, Eur. Space Agency, Noordwijk, Netherlands.

Lu, D. S. (2006), The potential and challenge of remote sensing-based biomass estimation, *Int. J. Remote Sens.*, *27*(7), 1297–1328, doi:10.1080/01431160500486732.

Lucas, R. M., A. K. Milne, N. Cronin, C. Witte, and R. Denham (2000), The potential of synthetic aperture radar (SAR) for quantifying the biomass of Australia's woodlands, *Rangeland J.*, *22*(1), 124–140, doi:10.1071/RJ0000124.

Mayaux, P., E. Bartholome, S. Fritz, and A. Belward (2004), A new land-cover map of Africa for the year 2000, *J. Biogeogr.*, *31*(6), 861–877, doi:10.1111/j.1365-2699.2004.01073.x.

Mitchard, E. T. A., S. S. Saatchi, I. H. Woodhouse, T. R. Feldpausch, S. L. Lewis, B. Sonké, C. Rowland, and P. Meir (2009), Measuring biomass changes due to woody encroachment and deforestation/degradation in a forest-savanna boundary region of central Africa using multi-temporal L-band radar backscatter, *Remote Sens. Environ.*, in press.

Mugasha, A. G., and S. A. O. Chamshama (2002), Tree biomass and volume estimation for miombo woodlands at Kitulangalo, Morogoro, Tanzania, in *Indicators and Tools for Restoration and Sustainable Management of Forests in East Africa*, *I-TOO Working Pap. 9*, Ethiopian Agric. Res. Cent., Addis Ababa.

Nangendo, G., O. van Straaten, and A. de Gier (2005), Biodiversity conservation through burning: A case study of woodlands in Budongo Forest Reserve, NW Uganda, in *African Forests Between Nature and Livelihood Resources: Interdisciplinary Studies in Conservation and Forest Management*, edited by M. A. Ros-Tonen and T. Dietz, pp. 113–128, Edin Mellen, New York.

Phillips, O. L., T. R. Baker, T. R. Feldpausch, and R. Brienen (2009), Field manual for plot establishment and remeasurement, RAINFOR, Univ. of Leeds, Leeds, U. K. (Available at http://www.geog.leeds.ac.uk/projects/rainfor/)

Podest, E., and S. Saatchi (2002), Application of multiscale texture in classifying JERS-1 radar data over tropical vegetation, *Int. J. Remote Sens.*, *23*(7), 1487–1506, doi:10.1080/01431160110093000.

Ribeiro, N. S., S. S. Saatchi, H. H. Shugart, and R. A. Washington-Allen (2008), Aboveground biomass and leaf area index (LAI) mapping for Niassa Reserve, northern Mozambique, *J. Geophys. Res.*, *113*, G02S02, doi:10.1029/2007JG000550.

Ryan, C. M. (2009), Carbon cycling, fire and phenology in a tropical savanna woodland in Nhambita, Mozambique, Ph.D. thesis, Univ. of Edinburgh, Edinburgh, U. K.

Saatchi, S., and M. Moghaddam (2000), Estimation of crown and stem water content and biomass of boreal forest using polarimetric SAR imagery,

IEEE Trans. Geosci. Remote Sens., *38*(2), 697–709, doi:10.1109/36.841999.

Saatchi, S., M. Marlier, D. Clark, R. Chazdon, and A. Russell (2009), Impact of spatial variability of forest structure on radar estimation of aboveground biomass in tropical forests, *Remote Sens. Environ.*, in press.

Santos, J. R., M. S. P. Lacruz, L. S. Araujo, and M. Keil (2002), Savanna and tropical rainforest biomass estimation and spatialization using JERS-1 data, *Int. J. Remote Sens.*, *23*(7), 1217–1229, doi:10.1080/01431160110092867.

Shimada, M., O. Isoguchi, T. Tadono, and K. Isono (2009), PALSAR radiometric calibration and geometric calibration, *IEEE Trans. Geosci. Remote Sens.*, in press.

van Zyl, J. (1990), Calibration of polarimetric radar images using only image parameters and trihedral corner reflector responses, *IEEE Trans. Geosci. Remote Sens.*, *28*(3), 337–348, doi:10.1109/36.54360.

van Zyl, J. (1993), The effect of topography on radar scattering from vegetated areas, *IEEE Trans. Geosci. Remote Sens.*, *31*(1), 153–160, doi:10.1109/36.210456.

Viergever, K. M., I. H. Woodhouse, and N. Stuart (2007), Backscatter and interferometry for estimating above-ground biomass in tropical savanna woodland, in *IGARSS 2007: IEEE International Geoscience and Remote Sensing Symposium—Sensing and Understanding Our Planet*, pp. 2346–2349, Inst. of Electr. and Electron. Eng., New York.

Williams, M., C. M. Ryan, R. M. Rees, E. Sarnbane, J. Femando, and J. Grace (2008), Carbon sequestration and biodiversity of re-growing miombo woodlands in Mozambique, *For. Ecol. Manage.*, *254*(2), 145–155, doi:10.1016/j.foreco.2007.07.033.

T. R. Feldpausch and S. L. Lewis, Earth and Biosphere Institute, School of Geography, University of Leeds, Leeds LS2 9JT, UK.

P. Meir, E. T. A. Mitchard, C. M. Ryan, M. Williams, and I. H. Woodhouse, School of Geosciences, University of Edinburgh, EH8 9XP, UK. (edward.mitchard@ed.ac.uk)

G. Nangendo, Wildlife Conservation Society, P.O. Box 7487, Kampala, Uganda.

N. S. Ribeiro, Faculdade de Agronomia e Engenharia Florestal, Universidade Eduardo Mondlane, P.O. Box 257, Maputo, Mozambique.

S. S. Saatchi, Jet Propulsion Laboratory, California Institute of Technology, Pasadena, CA 91109, USA.

Appendix 4 – Alternative methodology for Chapter 6

Introduction

It is clear that the backscatter values for the field plots vary markedly between 2007 and 2009. The differences for each plot average ~2 dB, and are fairly pronounced when the two datasets are plotted together (Figure 2 & 3). It is not clear why this is, though we suggest it could be due to calibration issues with the PALSAR datasets, or due to soil/vegetation moisture conditions differing between the two dates.

In the main paper (Chapter 6), this is solved by producing separate AGB-backscatter equations for 2007 and 2009, using the same field plots for each. We believe this is the most reliable method, as it uses known field plots from the same area and landcover type as the agroforestry/REDD/degraded areas. However, in order to remove the possibility that this process introduces bias, we present here the results of a different methodology.

The cross-calibration of multiple remote sensing datasets using unchanged targets is well established in the remote sensing literature (Lu, 2004; Mitchard *et al.*, 2009). As long as the invariant targets chosen cover the full range of the dataset, and truly are invariant, such targets allow one dataset to be accurately adjusted to conform to the range of another. Therefore we here follow this approach, choosing a number of suspected invariant targets to allow the adjustment of the 2009 PALSAR data to the 2007 imagery, and then applying the same AGB-backscatter relationship (derived from 2007) to both time-points.

Methods

Twenty-one suspected invariant areas were selected from across the image. These were for features such as lakes, grasslands, agricultural areas, and dense forest, and were selected to cover the whole range of backscatter values seen in the image. The two time-points were found to be well correlated, with an r^2 of 0.99 for an RMA linear regression (Figure S1). The fitted equation was:

$$\sigma^0_{HV09} = a + b(\sigma^0_{HV07}) \quad \text{(S1)}$$

Where coefficients (± standard errors) were $a = 4.62 \pm 0.4$, $b = 1.12 \pm 0.02$, $r^2 = 0.99$, $n = 21$, $p < 0.0001$.

Figure S1

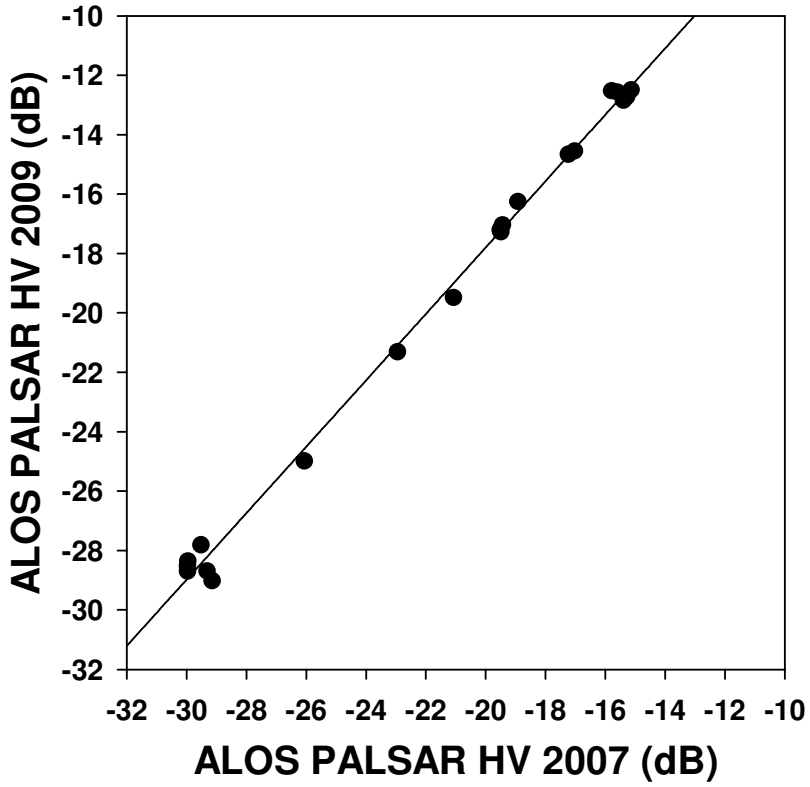

Sigma^0 values for 2009 plotted against 2007 for 21 suspected invariant targets.

Equation S1 was applied to the HV 2009 scene to create a new adjusted 2009 image, with values comparable to the 2007 scene. The AGB-backscatter relationship from 2007 was then applied to the adjusted 2009 image, and the analysis from then on proceeded as before.

Results

The results found were very similar to those using the method in Chapter 6. For a summary of the principle results, see Table S1.

Table S1 – comparison of average AGB change results

Landcover	ÀGB Change (Method from main paper)	AGB Change (Cross-calibration method)
Agroforestry	**+0.74**	**+0.56**
Deforestation	**-6.09**	**-6.76**
REDD	**+2.22**	**+1.79**

Uncertainty values, RMSE values and error spreads are also very similar to those found using the method presented in the main paper.

Discussion

From this analysis it appears that the choice of methodology is not that important: either directly producing AGB maps at each time-point using field data, or cross-calibrating the radar data and applying one AGB-backscatter relationship, produces very similar results. Given the uncertainties inherent in this analysis, the results are effectively identical.

We would recommend that projects calibrate radar data each individual year using field plots measured in that year. However, if such data are not available, and assuming the field plots have not changed is not a valid assumption, then this cross-calibration methodology should still produce useable results.

References

Lu, D.S., 2004. Change detection techniques. International Journal of Remote Sensing 25, 2365-2401.

Mitchard, E.T.A., Saatchi, S.S., Gerard, F.F., Lewis, S.L., Meir, P., 2009. Measuring Woody Encroachment along a Forest-Savanna Boundary in Central Africa. Earth Interactions 13, 1-29.

Appendix 5

Published version of Chapter 7

Biogeosciences Discuss., 8, 8781–8815, 2011
www.biogeosciences-discuss.net/8/8781/2011/
doi:10.5194/bgd-8-8781-2011

Biogeosciences Discussions

Mapping tropical forest biomass with radar and spaceborne LiDAR: overcoming problems of high biomass and persistent cloud

E. T. A. Mitchard[1], S. S. Saatchi[2], L. J. T. White[3,4,5], K. A. Abernethy[4,5], K. J. Jeffery[3,4,5], S. L. Lewis[6], M. Collins[7], M. A. Lefsky[8], M. E. Leal[9], I. H. Woodhouse[1], and P. Meir[1]

[1]School of GeoSciences, The University of Edinburgh, UK
[2]Jet Propulsion Laboratory, California Institute of Technology, Pasadena, California, USA
[3]Agence Nationale des Parcs Nationaux, Libreville, Gabon
[4]School of Natural Sciences, University of Stirling, Stirling, FK9 4LA, UK
[5]Institut de Recherche en Ecologie Tropicale, CENAREST, Libreville, Gabon
[6]Earth and Biosphere Institute, School of Geography, University of Leeds, UK
[7]Grantham Research Institute on Climate Change and the Environment, London School of Economics, London, UK

[8]Natural Resource Ecology Laboratory, Colorado State University, Fort Collins, Colorado, USA
[9]Missouri Botanical Garden, St. Louis, Missouri, USA

Received: 23 April 2011 – Accepted: 9 August 2011 – Published: 29 August 2011

Correspondence to: E. T. A. Mitchard (edward.mitchard@ed.ac.uk)

Published by Copernicus Publications on behalf of the European Geosciences Union.

Abstract

Spatially-explicit maps of aboveground biomass are essential for calculating the losses and gains in forest carbon at a regional to national level. The production of such maps across wide areas will become increasingly necessary as international efforts to protect primary forests, such as the REDD+ (Reducing Emissions from Deforestation and forest Degradation) mechanism, come into effect, alongside their use for management and research more generally. However, mapping biomass over high-biomass tropical forest is challenging as (1) direct regressions with optical and radar data saturate, (2) much of the tropics is persistently cloud-covered, reducing the availability of optical data, (3) many regions include steep topography, making the use of radar data complex, (4) while LiDAR data does not suffer from saturation, expensive aircraft-derived data are necessary for complete coverage.

We present a solution to the problems, using a combination of terrain-corrected L-band radar data (ALOS PALSAR), spaceborne LiDAR data (ICESat GLAS) and ground-based data. We map Gabon's Lopé National Park (5000 km^2) because it includes a range of vegetation types from savanna to closed-canopy tropical forest, is topographically complex, has no recent cloud-free high-resolution optical data, and the dense forest is above the saturation point for radar. Our 100 m resolution biomass map is derived from fusing spaceborne LiDAR (7142 ICESat GLAS footprints), 96 ground-based plots (average size 0.8 ha) and an unsupervised classification of terrain-corrected ALOS PALSAR radar data, from which we derive the aboveground biomass stocks of the park to be 78 Tg C (173 Mg C ha^{-1}). This value is consistent with our field data average of 181 Mg C ha^{-1}, from the field plots measured in 2009 covering a total of 78 ha, and which are independent as they were not used for the GLAS-biomass estimation. We estimate an uncertainty of ± 25 % on our carbon stock value for the park. This error term includes uncertainties resulting from the use of a generic tropical allometric equation, the use of GLAS data to estimate Lorey's height, and the necessity of separating the landscape into distinct classes.

As there is currently no spaceborne LiDAR satellite in operation (GLAS data is available for 2003–2007 only), this methodology is not suitable for change-detection. This research underlines the need for new satellite LiDAR data to provide the potential for biomass-change estimates, although this need will not be met before 2015.

1 Introduction

Tropical forest ecosystems have a variety of values, monetary and otherwise, that vary markedly with the scale considered. However, many of these, especially the more general benefits at a larger scale, are often not included in decisions relating to whether a forest area remains forest or is converted to another land-use (Stern, 2008;Engel et al., 2008). At a local scale the individual plants and animals have value, providing non-timber forest products, bushmeat, fuel, and timber (Ahrends et al., 2010); at a regional scale they can provide protection from extreme weather events and preserve water supplies (Kaiser and Roumasset, 2002; Swetnam et al., 2011); and at a global scale they influence global energy budgets through regulation of evapotranspiration, rainfall, and other climatic variables (Meir et al., 2006), also acting as a large store of carbon, and as a carbon sink (Phillips et al., 2008; Lewis et al., 2009b; Lewis et al., 2009a). The fate of an area of forest has tended to be controlled by the opportunity to liquidate its considerable timber value (Geist and Lambin, 2002) by destructively harvesting its trees, or clearing the land to convert it to a more productive land-use, e.g. agriculture (though in many cases local people derive no benefit from conversion (Rodrigues et al., 2009)). Further difficulties arise in the optimum allocation of land to differing uses due to ownership, sovereignty, governance, and the ability and will to monitor forests, particularly at larger scales (Chhatre and Agrawal, 2008, 2009).

One approach to preventing this loss of forests has been attempts to place a price on forests, based on the carbon they store, with the avoided emissions from deforestation producing carbon credits tradable on carbon markets. Carbon is only one element of the benefits provided by living forests, but it is one that is relatively tangible

and easy to quantify. Past international structures largely excluded pricing existing forest carbon, for example under the United Nations Clean Development Mechanism (CDM), which formed part of the Kyoto Treaty, carbon credits for forestry were given only for planting new forests or for reforestation, rather than for protecting threatened forests. However, the 2010 Cancun Agreement, agreed at the UNFCCC COP-16 Conference, has created an international framework for valuing forest carbon within the Reducing Emissions from Deforestation and forest Degradation (REDD+) scheme. The aim is to rapidly and radically reduce the rate of deforestation across the tropics, via performance-related payments to countries who reduce deforestation and degradation related carbon emissions (Clements, 2010). Though the details of REDD+ are yet to be finalised, its adoption was agreed at COP16 at Cancun, and considerable funds have already been committed (USD 28.3 billion have been committed by the developed world to developing world as fast-start finance for climate mitigation programs, including REDD+ (WRI, 2010)). Additionally, REDD+ transfers through government-government agreements and through the voluntary sector have already started, and are accelerating (Clements et al., 2010).

Whilst recognising the numerous limitations and problems associated with valuing forests for their carbon alone, a carbon price may establish a minimum value for forests, which may alter the decisions of land-owners in the future. Yet such a price associated with an area of forest can only be assessed if the carbon stocks of an area of forest can be accurately determined, with known uncertainties giving a minimum carbon stock at each time point, and then such a carbon map updated regularly in order to calculate deforestation rates, and therefore payments.

Scientific forest inventory plots are thought to provide the most accurate data on the aboveground biomass (AGB) of an area: these usually involve measuring the diameter at breast height (DBH), and ideally the height and species too, of every tree with a DBH $>$ 10 cm (Brown, 1997; Phillips et al., 2009). AGB is then estimated from these measurements using either locally-derived or standard allometric equations; there are thought to be significant errors associated with these equations, as destructive

harvesting data is not available for specific species and areas. Often for tropical forests a pantropical equation is used, derived from 2410 destructively harvested trees from 27 sites (Chave et al., 2005). It includes equations stratified by forest type, with DBH, height and wood density as parameters. The approach not only reduces the model error compared with using DBH alone, but also increases applicability to tree-types not used to define the original equations.

However, for reasons of resources, time and access, it is not possible to place a sufficient number of plots across a forested area, let alone a country, in order to be able to use such plots to estimate AGB for the whole area directly. Instead remote sensing data is used to extrapolate the plot data across the landscape, with the methods used split into two major categories:

1. Direct statistical relationship between AGB and a remote sensing variable (or variables, possibly including modelled variables and environmental data layers), allowing the production of a continuous AGB map for the area. With the notable exception of LiDAR (see below), such relationships are strong for lower AGB levels but tend to decrease in accuracy and eventually saturate as AGB increases, making higher biomass areas hard to map. This saturation point varies greatly depending both on the source data and vegetation type – ranging from 15–70 Mg ha^{-1} for visible/near-infrared vegetation indices (Lu, 2006), or from 40 to 150 Mg ha^{-1} for L-band radar data (Lu, 2006; Mitchard et al., 2009).

2. Classification into landcover type, usually using optical remote sensing data, with each forest type then given an AGB value and these classes then summed to estimate AGB over the whole site. Ideally the average AGB of each class is derived from field data, but often national or continental average values are used (GOFC-GOLD, 2009).

An exception to the above is LiDAR data, which by sending a short pulse of laser light either from an aircraft or from space can be used to elucidate the height and even vertical structure of a forest. Tree height, and other LiDAR-derived metrics, have been

shown to relate strongly to forest biomass, with no saturation at higher biomass values (Lefsky et al., 2005). Unfortunately aircraft LiDAR data acquisition is costly, and the capacity to collect annual data over whole countries does not exist currently. However, space-borne LiDAR data was collected by the ICESat sensor from 2003 to 2007 (Lefsky, 2010), and more such data will be collected by ICESat 2 (Abdalati et al., 2010), due for launch in 2015. Aircraft LiDAR tends to be imaging LiDAR, with small footprints collected at a very high density, leading to a detailed 3-dimensional image of the area of interest; however current spaceborne systems are profiling LiDARs, collecting isolated, widely separated footprints, thus sampling the landscape. As a result in order to create full-coverage spatial layers from spaceborne LiDAR the data must be fused with other datasets. It has been shown previously that satellite LiDAR data has great potential for estimating biomass over large areas when fused with radar data (Shugart et al., 2010).

Methods for estimating AGB using one or other of the two methods above are relatively well established, and are being employed with success as part of the monitoring schemes for many pilot REDD+ projects (CCBA, 2011). However, much of the tropics is suboptimal for the above methods in three respects. Firstly, many areas exhibit frequent cloud-cover, making classification using optical data next to impossible. Secondly, many areas include high biomass forest, at which most methods saturate. Third, many forest overlay areas of steep topography, making radar data less useful. Thus methods to overcome these obstacles are needed.

Here we use the mountainous and persistently cloud-covered Lopé National Park in Gabon to show how a novel AGB estimation method, involving terrain-corrected L-band radar data, field data and GLAS LiDAR data, can accurately determine AGB over a densely forested landscape with specified and relatively high accuracy. The use of high resolution optical data was not possible over this site, as there are no cloud-free SPOT, ASTER or Landsat scenes covering over 50 % of the study site from 2000 to the present day.

2 Study site

The study area is the Lopé National Park (LNP), which is situated in central Gabon (Fig. 1), and covers an area of 4948 km^2; it has been a wildlife reserve since 1946, and a National Park since 2002. Though surrounded by closed-canopy tropical rainforest typical of the Congo basin, the north of the park is characterised by savanna and a mosaic of low-biomass forest types (principally monodominant Okoumé (*Aucoumea klaineana*) forest, and distinctive open-canopy Marantaceae forest, so-called because the understory is dominated by a thick layer of herbaceous plants of the Marantaceae and Zingiberaceae families). The forest-savanna mosaic is a remnant of the landscape that dominated much of the Congo basin during the Last Glacial Maximum (LGM) (White, 2001). At the LGM savanna covered the majority of LNP, but the increase in precipitation has since caused an expansion of forest to cover nearly the whole area, with forest continuing to expand into the savannas today (White, 2001). Certain forests in the south of the study area may represent Pleistocene refuges that survived through successive glacial maxima that resulted in savanna expansion (Leal, 2001), but much of the northern half of LNP was dominated by savanna until an apparent large reduction in the human population ca. 1400 BP (Oslisly and White, 1995). In about 1920 the colonial administration moved all villages from the interior of the LNP, initiating large-scale forest regeneration in previously cultivated zones (Pourtier, 1989). The savanna that remains is maintained by a combination of now limited human burning and the rain-shadow of the Massif du Chaillu, which reduces rainfall to 1500 mm yr^{-1} in the north of the park (White and Abernethy, 1997); whereas rainfall in the south of the park is ~2500 mm yr^{-1} (Tropical Rainfall Measuring Mission (TRMM) 3B43 V6 data January 1998 to January 2010). The site features significant topographic variation and dissection: the altitude ranges from 72 to 980 m a.s.l., and 23.7 % of the study area has a slope great than 20 % (11.3°).

3 Methods

3.1 Field data

A wealth of forestry data has been collected in the LNP since 1983. However, in order to investigate the relationship between radar data and AGB we only used the plots that were re-measured in 2009, which include 3 transects of length 5 km, 20 plots of 20 m × 40 m, and one plot of 100 m × 100 m.

For the 20 × 40 m plots and the 100 m × 100 m plot all stems with a diameter at breast height (DBH) ≥10 cm had their DBH measured and were identified to the species level (or genus if species identification was not possible). The locations of all four corners of each plot were determined using a Garmin 60 CSx GPS. For the 5 km transects all stems > 10 cm DBH were only measured for a 5 m wide band, with stems > 70 cm DBH being measured for a 50 m band. We therefore split each transect into 25 sections of 200 m × 50 m, giving 25 plots of 1 ha size per transect. To calculate AGB values for each 1 ha section of the 50 m wide band, the AGB of the stems between 10 and 70 cm DBH (in the 5 m band) were multiplied by ten and added to the AGB for the > 70 cm stems.

Tree heights were measured in addition to DBH for 3673 stems along the 5 m band of the five transects in 1989. The tree heights were estimated to the nearest meter using a clinometer. These data were used to build a site-specific relationship between tree height and DBH.

AGB was estimated using the moist tropical forest equation from (Chave et al., 2005), involving DBH (D), height (H) and wood specific gravity (ρ):

$$\mathrm{AGB} = 0.0509 \left[\rho D^2 H\right] \quad (1)$$

This equation gives AGB in kg dry biomass; throughout this study AGB has been reported in Mg ha^{-1} dry biomass, but where appropriate this has been converted to carbon (Mg C) using the standard conversion factor of 0.5 (IPCC, 2003). Wood specific

gravity data were derived from the Global Wood Density database (Chave et al., 2009a, 2009b): species-specific data were available for 64 % of stems, for the rest the average density for members of the genus from tropical Africa were used.

3.2 Lorey's height to AGB relationships

The method used to process the LiDAR data gave an estimate of Lorey's height, a basal-area weighted measure of height (Sect. 3.4). In order to develop a relationship between Lorey's height and AGB, Lorey's height (L) was calculated for each plot using height in metres (H) and basal area in m^2 (A_B, calculated as $\pi(\mathrm{DBH}/2)^2$) for each stem using the following equation:

$$L = \frac{\sum(H \cdot A_\mathrm{B})}{\sum A_\mathrm{B}} \quad (2)$$

For calculating Lorey's height from the ground plots we preferred plots for which we had height measurements for every stem – using DBH-height relationships reduces the accuracy of height measurements, and also introduces a spurious correlation as both axes will scale directly with basal area, with only wood density providing the scatter. We therefore used the 5 m band data of the five LNP transects from 1989 (split into 0.25 ha sections, a similar size to the LiDAR footprints, giving 50 plots in total), but this did not give a sufficient number of plots, especially for lower AGB values, to enable us to build up a suitable relationship. To resolve this issue we added the 20 plots of 20 m × 40 m from LNP; though we had to use the DBH-height relationship for these, every stem that was broken off, damaged or deformed was noted in the field notes, reducing errors. We also added plots from nearby areas where DBH and height had been measured for every stem, adding four more 1 ha plots from Gabon (Lewis et al., 2009b), and 14 plots from Mbam Djerem National Park, on the forest-savanna transition zone in Cameroon, which has a similar vegetation type and rainfall to LNP (Mitchard et al., 2011). In total this gave 88 plots where field-measured Lorey's height and AGB could be compared.

3.3 Radar data

Six ALOS PALSAR (Advanced Land Observing Satellite Phased Array L-band SAR) scenes captured on the 25 June 2009 (3 scenes) and 24 July 2009 (3 scenes) were acquired through an ESA (European Space Agency) Category-1 Proposal. These were FBD (Fine-Beam Dual-polarisation) scenes, provided at the 1.1 processing level. We projected the scenes using the Alaska Satellite Facility's software package MapReady 2.3. Terrain slope has a significant impact on radar scenes, impacting both the projection of the slant-range image, and the backscatter values, which due to changes in the radar incidence angle are increased on slopes facing the sensor, and reduced on slopes facing away. To perform the terrain correction we needed a Digital Elevation Model (DEM): we used the 90 m resolution Shuttle Radar Topography Mission (SRTM) dataset, using the void-filled Version 4 product produced by CGIAR-CSI (http://srtm.csi.cgiar.org). We used MapReady to correct geolocation and radiometric problems due to terrain (including adjusting pixel areas due to incidence angle, adjusting backscatter values to account for radar incidence angle, and interpolating layover/shadow regions). The terrain correction was successful, with the topography not visible in the corrected HH and HV images, and there being no residual correlation between the corrected backscatter values and the radar incidence angle.

All processing, including the extraction of radar data values for the field plots, was performed at a 100 m (1 ha) spatial resolution: the same scale as the majority of the field plots (76 out of 96), and a scale at which the heterogeneity of forest structure is normally distributed (Chave et al., 2004), and at which we are confident in our geolocation.

3.4 LiDAR data

Space-borne LiDAR data were collected from 2003–2007 over LNP by the Geoscience Laser Altimeter System (GLAS) on the Ice Cloud and Land Elevation Satellite (IceSAT). These data are in the form of circular footprints, with each footprint ranging from

0.2–0.25 ha in size, depending on the terrain slope. In total data for 37 021 individual footprints overlapping with the PALSAR scenes were recorded. However, 26 747 of these footprints were removed through cloud filtering, with a further 3132 points removed as they fell on steep slopes (> 20 %), where accuracy decreases markedly (Lefsky et al., 2005). This left 7142 GLAS footprints coincident with our six radar scenes (Fig. 1b). Features of the waveforms were correlated with measured Lorey's height from 95 plots in three forest sites in the Amazon, with field plots coincident with GLAS data ($r^2 = 0.83$, RMSE = 3.3 m, $n = 95$), see Lefsky, (2010) for details.

3.5 Unsupervised classification

Due to saturation, direct regression between the field plots data and radar backscatter, as performed for example in (Mitchard et al., 2009), was thought to be poorly suited to estimating AGB for LNP, apart from in the small area of savanna in the north. Though we performed the analysis for comparison, it is the LiDAR data that has the potential to estimate the AGB of LNP above the saturation limit of the radar. Rather than averaging the heights of the LiDAR footprints to get an average value for the park, we pursued a solution that would include the spatial information on vegetation structure contained in the radar data.

The Radar Forest Degradation Index (RFDI) (Saatchi et al., 2011) is a ratio between the power of the HH and HV polarisations, designed to assess the strength of the double-bounce term. It is defined as:

$$\mathrm{RFDI} = \frac{\mathrm{HH} - \mathrm{HV}}{\mathrm{HH} + \mathrm{HV}} \quad (3)$$

and picks out this term because HH is sensitive to both volume scattering and double bounce, whereas HV is mostly sensitive to volume scattering. We therefore found it to be a useful layer in helping to differentiate different vegetation types, pulling out more information from the dual-polarisation radar data.

We therefore used the radar backscatter (in HH and HV polarisations), RFDI, and altitude (from the DEM) to develop an unsupervised classification of the park (Fig. 2).

We aimed to use as many classes as possible, to enable us to fully characterise the different vegetation structures, and after experimentation we chose 40 classes as this left each class with at least 100 LiDAR observations.

The classification was performed using ENVI 4.7 (ITT Systems), using both the K-means and IsoData unsupervised classification methods, with 40 classes and 100 iterations. All four bands (HH, HV, RFDI & DEM height) were scaled to have an identical mean and standard deviation. At this number of iterations both methodologies produced an identical classified map. We then extracted the derived AGB value from each GLAS footprint within each class, averaged these AGB values, and assigned these mean AGB values to each class in order to produce an AGB map.

4 Results

4.1 Stem heights to DBH

We required AGB estimates for the field plots, but though we had DBH and species data for every stem, no stem height data was collected in 2009. Therefore we wished to develop a site-specific relationship between DBH and stem height, based on 3673 stem DBH and heights measured over four transects in 1989. The stem heights (H) were strongly correlated with DBH (D) ($r^2 = 0.62$, $p < 0.0001$, standard error of estimate = 4.97 m, Fig. 3). The fitted equation was:

$$H = a + b\left[D^c\right] \tag{4}$$

with coefficients (± standard errors): $a = -4.25 \pm 1.20$, $b = 4.37 \pm 0.90$, $c = 0.472 \pm 0.037$. This relationship was applied to the stems measured in 2009, allowing AGB to be calculated from the Chave et al. (2005) equation involving DBH, wood density and height.

4.2 Lorey's height to field biomass

We had estimates of Lorey's height from the LiDAR data, but needed to use field plot data to convert these Lorey's height estimates into AGB. To do this we used Lorey's heights (H_L) from the 88 field sites (both from within and near Lopé, and from the Mbam Djerem National Park in Cameroon) where height had been measured for every stem (see Methods). We found that Lorey's height was strongly related to AGB of these plots ($r^2 = 0.81$, $p < 0.0001$, Fig. 4); we treated AGB as the dependent variable here, as it was this that we wished to predict from Lorey's height. The fitted equation was:

$$\mathrm{AGB} = a\left[(H_L)^b\right] \tag{5}$$

with coefficients (± standard errors): $a = 0.564 \pm 0.013$, $b = 1.945 \pm 0.096$.

4.3 Direct biomass estimation with radar

We then correlated the terrain-corrected radar data (in both the HH and HV polarisations) with the field data. We found a strong relationship with both polarisations, with a saturation point around 100 Mg ha^{-1} for HH, and around 150 Mg ha^{-1} for HV (Fig. 5). The best fit model was the same as that used in Mitchard et al. (2011), also identical in form to the Water Cloud Model (Attema and Ulaby, 1978) (for coefficients see Table 1):

$$\sigma^0_{dB} = a + b[1 - \mathrm{EXP}(c \cdot \mathrm{AGB})] \tag{6}$$

Equation 5 was rearranged as follows to allow the production of an AGB map over the study area using the HV PALSAR data:

$$\mathrm{AGB} = \frac{1}{c} \cdot \ln\left[1 - \frac{\sigma^0_{dB} - a}{b}\right] \tag{7}$$

The relationship between PALSAR HV and AGB saturates at ~150 Mg ha^{-1} (Fig. 5b, Mitchard et al., 2009, 2011), and thus the map produced was limited at this value

(Fig. 6a). Using this upper limit means that using radar data in this way to estimate the AGB of LNP will result in a large underestimation; however for comparison, and as an absolute lower limit, this methodology estimates the aboveground biomass of LNP to be 67.5 Tg, equivalent to 33.7 Tg C (Fig. 6a).

4.4 Classification and mapping by GLAS

A K-means and IsoData classification with 40 classes and 100 iterations were found to give identical results, and a classification that, based on our field knowledge, classified separately and accurately all the major vegetation types. No more than 40 classes were used, as experimentation showed that more would have resulted in fewer than 100 GLAS footprints falling within each class.

Each class was given an average AGB value by converting each GLAS footprint into an AGB estimate (Eq. 4), then averaging these AGB estimates within each class (Table S1). This gives a carbon stock estimate for LNP of 156 Tg biomass, 78 Tg C (Fig. 6b). It gives the average AGB as 315 Mg ha^{-1}, which compares much better to the field plots and LiDAR data-derived averages (390 and 251 Mg ha^{-1} respectively) than the 136 Mg ha^{-1} from the (limited at 150 Mg ha^{-1}) PALSAR HV-derived map.

4.5 Comparisons with independent data

The LiDAR data were not used in the creation of the radar-based AGB map, and similarly the field data were not used to create the classification-based map. This allows a test of the accuracy of both approaches using independent data.

4.5.1 Comparison of radar-derived AGB map to LiDAR data

Due to geolocation errors and differences in scale a direct comparison between the 100 m AGB pixels and the 0.2–0.25 ha GLAS footprints would not give an appropriate estimation of error; even with a perfect AGB map there would be a lot of scatter in the

result. Instead the HV-derived AGB map was divided into 6 classes (0–25, 25–50, 50–75, 75–100, 100–150, and > 150 Mg ha^{-1}), and the mean and standard deviation of the LiDAR-derived AGB values in each class compared (Table 2). The mean of the LiDAR-derived AGB values for each class fall within that class, suggesting the PALSAR HV-derived map is producing consistent, unbiased results throughout its sensitivity range.

4.5.2 Comparison of LiDAR and classification-derived AGB map to field data

We do not have access to a sufficient number of field plots to enable the use of these to confirm the accuracy of all 40 classes. However, ten of the classes, covering 34.7 % of LNP in total, had four or more field plots located within them. The mean of these field plots were an average of 9.5 % (range: 1 %–16 %) different from the mean AGB derived from the GLAS data (Table 3). These data provide evidence of a small bias, with the average AGB values for the field data being on average 4.5 % higher than the mean value for the class derived from LiDAR data.

5 Error estimation

When providing estimates of carbon stocks for REDD+ and other carbon forestry projects, an estimate is useless without an associated estimate of accuracy. Normally the number of carbon credits awarded is based on the most conservative estimate (e.g. the lower boundary of a 95 % confidence interval about the mean) (Grassi et al., 2008; GOFC-GOLD, 2009). The results in Sect. 4.5 provide some confidence in our methodologies, but due to the limited number and spatial distribution of the field plots, and the inaccuracies inherent in LiDAR-AGB estimation, these do not provide an estimate of the true error of the analysis.

The uncertainty of any measurement can be divided into two components: that of accuracy and precision (IPCC, 2000). Accuracy is the distance of the mean (of many observations) from the true value: it is thus influenced by biases (consistent errors) in

the estimation process. It is this parameter that we are principally interested in here. The other component, precision, relates to how close an individual measurement is to the mean value of many measurements of the same parameter: in other words it is related to random errors. These random errors are caused by spatial and structural heterogeneity, geolocation errors, changes in vegetation between observations, and measurement error, and are responsible for much of the noise observable in Figs. 3–5, and the differences between field plot averages and the GLAS-averages of their classes reported in Sect. 4.5.2 and Table 3. It is not as important to quantify the degree of precision for our purposes here (calculating carbon stocks over a large area), as these random errors will cancel out over the very large number of measurements. However, the precision is important when measuring changes at a pixel level: therefore for any methodology that wishes to assess change precision is very important (see Mitchard et al., 2011). But precision will be discussed no further in this section, as it does not affect the uncertainty of the AGB estimate for the whole park: we are interested here only in accuracy, and thus in trying to estimate the magnitude of potential degree of biases throughout the stages of our estimation process.

5.1 Uncertainties in the LiDAR-classification map

1. Allometric equations: the AGB values derived from both the field and LiDAR data are ultimately derived from measurements of the diameter, height and species of trees. These are converted to AGB for this study using the Chave et al. (2005) equations, which while believed to be the best available, have significant, but hard to estimate, uncertainties. They are not derived from African trees, which may be a problem as there are known to be differences in height-DBH relationships between the continents (Feldpausch et al., 2010); however our use of a locally-derived DBH-height relationship should correct for this, and Lewis et al. (2009) showed that locally-derived relationships did not dramatically alter their biomass estimates from African forests (Lewis et al., 2009b). We therefore estimate the potential bias due to the allometric equation at ± 10 % (at the 95 % confidence level),

which though twice the figure published in the original paper with this equation (Chave et al., 2005), is similar to that discovered by Lewis et al. (2009), who propagated estimated height and diameter errors in their biomass estimates, and by Djomo et al. (2010), who used destructive sampling of trees in Africa to estimate the accuracy of various pantropical equations.

2. LiDAR waveform to Lorey's height: the relationship used to derive Lorey's height from the LiDAR waveforms is based on field plots coincident with LiDAR footprints from three sites in the Brazilian Amazon (Lefsky, 2010). Unfortunately no LiDAR footprints intersected with our field plots from LNP, so we cannot discern the extent to which this could cause inaccuracies, though the results in Sect. 4.5 provide some confidence. There are structural differences between the two continents' forests (Djomo et al., 2010), so we add an uncertainty of ± 5 %, similar in magnitude to the detected potential bias in Sect. 4.5.2, to account for this.

3. Classification: classifying the image into forty different clusters, based on similar radar returns and altitude, is bound to introduce errors by both over-simplification (the resulting vegetation types will not necessarily have identical average AGB values in different spatial locations) and mis-classification. As the clusters are only covered by LiDAR data from a spatially-limited portion of the image (Fig. 1b), this is likely to introduce biases. To test this we ran four additional models, excluding LiDAR data from one quarter of the park each time, and comparing the biomass results produced from that quarter with the original biomass estimates. This resulted in changes in the biomass estimate for each quarter of 4.8 % (range 4–7 %). This procedure only estimates part of the potential error due to this source, so to be conservative we add an error of ± 10 %.

5.2 Summing uncertainties

As these errors are all independent, and in order to use the most conservative method, these errors should be summed to give an estimate of the most extreme error (Eq. A1.1,

Page A.16, IPCC, 2000): this is ± 25 %. This gives the total AGB stocks of LNP, using the LiDAR data and unsupervised classification methodology, to be between 58.5 and 97.5 Tg C, with the lower number being that recommended for carbon payment purposes.

6 Discussion

Despite the high biomass and persistent cloud-cover, we have produced a high resolution (100 m) map of AGB over Lopé National Park in Gabon. This estimate was made possible through a novel fusion of radar and spaceborne LiDAR data. Also, using a conservative error-estimation method optimised for carbon payments for REDD+, we have shown that these estimates at a park level have a ± 25 % uncertainty, due to potential biased errors in our input data and estimations. We have shown from our field data that there is a strong relationship between Lorey's height and field-derived AGB, and then used this to give us an additional 7042 point-based AGB estimates from spaceborne LiDAR waveforms, which can estimate Lorey's height with high confidence (Lefsky, 2010). Finally we used the information in our dual-polarisation radar data, along with a DEM, to classify the vegetation into units with distinct biophysical parameters, enabling the spatial extrapolation of the radar data. While none of these steps are novel or controversial, we believe this new combination of methodologies provides an excellent pathway for combining the strengths of GLAS and radar data to produce AGB maps of high biomass forest.

This methodology enables the production of carbon maps for a tropical region or country, a requirement for example in advance of a deforestation-reduction program such as REDD+. The high resolution and spatially-explicit nature of these maps goes beyond the requirements of the lower two assessment standards given by the International Panel on Climate Change (IPCC), which rely on maps giving changes in land-cover type and not on spatially-explicit AGB maps. Therefore using such a methodology could give data required for the highest tier, Tier 3 (GOFC-GOLD, 2009). Running

Tier 3 assessments may be advantageous, as the increased certainty may lead to a larger number of certified emissions reductions for a landscape. Additionally, Tier 3 monitoring may increase investor confidence leading to increased investments in REDD. Furthermore, such monitoring may lead to this carbon being trade at a price premium if the REDD scheme moves to become a market-based scheme. The method developed here shows that a large investment in a high density of field plots or airborne LiDAR data may not be necessary to reach the accuracy required by this tier: a high density of GLAS plots, combined with optical or radar data for vegetation classification, may suffice, as long as there are sufficient field plots for validation.

Our approach to the uncertainty analysis, using conservative estimates of potential biases from a wide variety of sources, and then summing them, is conservative, but appropriate to the problem in hand. For such a large area it will produce much wider confidence intervals than commonly used estimates based on standard errors of means, but this is appropriate as for the purposes of conserving carbon stocks we must find the minimum likely carbon stocks of the park, not a mean estimate. We believe such an approach is essential for the monitoring of deforestation, where the conservativeness principle outlined by Grassi et al. (2008), that for the purposes of forest conservation the most conservative estimate of any parameter must always be used, must apply. This conservative approach is essential for two reasons. Firstly, if avoided deforestation credits are to be used to offset actual fossil fuel carbon emissions, then any overestimate of carbon savings realised would result in REDD+ have a net negative impact on net CO_2 emissions, exactly the opposite of its original intentions. Secondly, the majority of the errors included in our analysis are very hard to quantify, that is these uncertainties are themselves very uncertain. Therefore our conservative approach assists in ensuring that the confidence bands presented span the full range of possible values.

GLAS-LiDAR is clearly not the ideal tool for mapping biomass: its footprints cover only a tiny percentage of the total land-area of the planet, and the footprints, at 0.2–0.25 ha, are too large for detailed mapping. It would always be preferable to use

airborne LiDAR, as for example Asner et al. (2010) have done in the Peruvian Amazon, using a similar approach as described here but with airborne-LiDAR, extrapolated to other areas using the classification of high-resolution optical rather than radar data. However, airborne LiDAR data is expensive to collect, thus whole country censuses, let alone with annual repeat, are unlikely in the near future. GLAS represents a spatially distributed set of footprints, with hundreds of thousands to millions of footprints freely available across every country (Lefsky, 2010), and as such is a useful resource to assist mapping forest biomass carbon stocks. The patchy coverage necessitates using another dataset to classify the landscape: here we use radar data and a DEM due to data availability, but if cloud-free optical data (or other high quality spatially-explicit datasets) were available they should be added into the classification procedure.

A limitation with the approach we set out here is that IceSAT GLAS is no longer operational: suitable data were only produced from 2003 until 2007. Two satellites are being planned, both with a higher laser-footprint density than GLAS: IceSAT II and DESDynI. However, IceSAT II will not be launched until 2015 at the earliest, and DESDynI, a system with both a spaceborne LiDAR and an L-band fully-polarimetric radar, will not be launched until 2017. Thus the system can currently be used to produce carbon maps for the mid- to late- 2000s, but unfortunately not for change detection or deforestation monitoring. However this is still a useful development: both optical and radar systems can easily be used to detect changes in forest *area*, and so having an accurate carbon map at one time-point will allow the emissions caused by deforestation to be better estimated from landcover-change results.

Acknowledgements. This work is dedicated to the memory of Fabiane Lima de Oliveira, who passed away in Gabon in 2009 after falling ill whilst on fieldwork for this project. Her deep knowledge and love of the forest was highly respected by all who she met. She is greatly missed by family, friends and the scientific community.

ESA provided the ALOS PALSAR radar data at cost price through a Category 1 Application. These data were ultimately collected and processed by JAXA. ICESat GLAS data were provided by NASA. SRTM data were provided by NASA and processed by CGIAR-CSI (http://srtm.csi.cgiar.org). Funding for this work was provided by a PhD Studentship to Edward Mitchard, with the fieldwork being funded by a grant from the Gordon and Betty Moore Foundation and the Packard Foundation. Simon Lewis is supported by a Royal Society University Research Fellowship. The Gabonese Agence Nationale des Parcs Nationaux, the Station d'Etudes des Gorilles et Chimpanzés, and Etienne Massard provided essential logistical support to the fieldwork effort.

References

Abdalati, W., Zwally, H. J., Bindschadler, R., Csatho, B., Farrell, S. L., Fricker, H. A., Harding, D., Kwok, R., Lefsky, M., Markus, T., Marshak, A., Neumann, T., Palm, S., Schutz, B., Smith, B., Spinhirne, J., and Webb, C.: The ICESat-2 Laser Altimetry Mission, Proc. IEEE, 98, 735–751, 2010.

Ahrends, A., Burgess, N. D., Milledge, S. A. H., Bulling, M. T., Fisher, B., Smart, J. C. R., Clarke, G. P., Mhoro, B. E., and Lewis, S. L.: Predictable waves of sequential forest degradation and biodiversity loss spreading from an African city, P. Natl. A. Sci. USA, 107, 14556–14561, 2010.

Asner, G. P., Powell, G. V. N., Mascaro, J., Knapp, D. E., Clark, J. K., Jacobson, J., Kennedy-Bowdoin, T., Balaji, A., Paez-Acosta, G., Victoria, E., Secada, L., Valqui, M., and Hughes, R. F.: High-resolution forest carbon stocks and emissions in the Amazon, P. Natl. A. Sci. USA, 107, 16738–16742, 2010.

Attema, E. P. W. and Ulaby, F. T.: Vegetation Modeled as a Water Cloud, Radio Science, 13, 357–364, 1978.

Brown, S.: Estimating Biomass and Biomass Change of Tropical Forests, FAO Forest Paper 134, Rome, 1997.

CCBA: List of accepted CCBA projects, http://www.climate-standards.org/projects/index.html, 2011.

Chave, J., Condit, R., Aguilar, S., Hernandez, A., Lao, S., and Perez, R.: Error propagation and scaling for tropical forest biomass estimates, Philos. T. Roy Soc. B, 359, 409–420, 2004.

Chave, J., Andalo, C., Brown, S., Cairns, M. A., Chambers, J. Q., Eamus, D., Folster, H., Fromard, F., Higuchi, N., Kira, T., Lescure, J. P., Nelson, B. W., Ogawa, H., Puig, H., Riera, B., and Yamakura, T.: Tree allometry and improved estimation of carbon stocks and balance in tropical forests, Oecologia, 145, 87–99, 2005.

Chave, J., Coomes, D., Jansen, S., Lewis, S. L., Swenson, N. G., and Zanne, A. E.: Towards a worldwide wood economics spectrum, Ecol. Lett., 12, 351–366, 2009b.

Chhatre, A. and Agrawal, A.: Forest commons and local enforcement, Proceedings of the National Academy of Sciences of the United States of America, 105, 13286–13291, 2008.

Chhatre, A. and Agrawal, A.: Trade-offs and synergies between carbon storage and livelihood benefits from forest commons, P. Natl. A. Sci. USA, 106, 17667–17670, 2009.

Clements, G. R., Sayer, J., Boedhihartono, A. K., Venter, O., Lovejoy, T., Koh, L. P., and Laurance, W. F.: Cautious Optimism over Norway-Indonesia REDD Pact, Conserv. Biol., 24, 1437–1438, 2010.

Clements, T.: Reduced Expectations: the political and institutional challenges of REDD, Oryx, 44, 309–310, 2010.

Djomo, A. N., Ibrahima, A., Saborowski, J., and Gravenhorst, G.: Allometric equations for biomass estimations in Cameroon and pan moist tropical equations including biomass data from Africa, Forest Ecol. Manage., 260, 1873–1885, 2010.

Donnellan, A., Rosen, P., Graf, J., Loverro, A., Freeman, A., Treuhaft, R., Oberto, R., Simard, M., Rignot, E., Kwok, R., Pi, X. P., Blair, J. B., Abdalati, W., Ranson, J., Zebker, H., Hager, B., Shugart, H., Fahnestock, M., and Dubayah, R.: Deformation, Ecosystem Structure, and Dynamics of Ice (DESDynI), 2008 IEEE Aerospace Conference, 163–175, 2008.

Engel, S., Pagiola, S., and Wunder, S.: Designing payments for environmental services in theory and practice: An overview of the issues, Payments for Environmental Services in Developing and Developed Countries, 65, 663–674, 2008.

Feldpausch, T. R., Banin, L., Phillips, O. L., Baker, T. R., Lewis, S. L., Quesada, C. A., Affum-Baffoe, K., Arets, E. J. M. M., Berry, N. J., Bird, M., Brondizio, E. S., de Camargo, P., Chave, J., Djagbletey, G., Domingues, T. F., Drescher, M., Fearnside, P. M., França, M. B., Fyllas, N. M., Lopez-Gonzalez, G., Hladik, A., Higuchi, N., Hunter, M. O., Iida, Y., Abu Silam, K., Kassim, A. R., Keller, M., Kemp, J., King, D. A., Lovett, J. C., Marimon, B. S., Marimon-Junior, B. H., Lenza, E., Marshall, A. R., Metcalfe, D. J., Mitchard, E. T. A., Moran, E. F., Nelson, B. W., Nilus, R., Nogueira, E. M., Palace, M., Patiño, S., Peh, K. S.-H., Raventos, M. T., Reitsma, J. M., Saiz, G., Schrodt, F., Sonké, B., Taedoumg, H. E., Tan, S., White, L.,

Wöll, H., and Lloyd, J.: Height-diameter allometry of tropical forest trees, Biogeosciences Discuss., 7, 7727–7793, doi:10.5194/bgd-7-7727-2010, 2010.

Geist, H. J. and Lambin, E. F.: Proximate causes and underlying driving forces of tropical deforestation, Bioscience, 52, 143–150, 2002.

GOFC-GOLD: A sourcebook of methods and procedures for monitoring and reporting anthropogenic greenhouse has emissions and removals caused by deforestation, gains and losses of carbon stocks in forests, remaining forests, and forestation, Alberta, Canada, 2009.

Grassi, G., Monni, S., Federici, S., Achard, F., and Mollicone, D.: Applying the conservativeness principle to REDD to deal with the uncertainties of the estimates, Environ. Res. Lett., 3, 1–12, 035005, doi:10.1088/1748-9326/3/3/035005, 2008.

IPCC: Good Practice Guidance and Uncertainty Management in National Greenhouse Gas Inventories, IPCC, 2000.

IPCC: Good practice guidance for land use, land-use change and forestry, IPCC, 2003.

Kaiser, B. and Roumasset, J.: Valuing indirect ecosystem services: the case of tropical watersheds, Environment Dev. Econ., 7, 701–714, 2002.

Leal, M. E.: Microrefugia, Small Scale Ice Age Forest Remnants, Systematics and Geography of Plants, 71, 1073–1077, 2001.

Lefsky, M.: A global forest canopy height map from the Moderate Resolution Imaging Spectroradiometer and the Geoscience Laser Altimeter System., Geophys. Res. Lett., 37, 1–5, L15401, doi:10.1029/2010GL043622, 2010.

Lefsky, M. A., Harding, D. J., Keller, M., Cohen, W. B., Carabajal, C. C., Espirito-Santo, F. D., Hunter, M. O., and de Oliveira, R.: Estimates of forest canopy height and aboveground biomass using ICESat, Geophys. Res. Lett., 32, 1–4, L22S02, doi:10.1029/2005GL023971, 2005.

Lewis, S. L., Lloyd, J., Sitch, S., Mitchard, E. T. A., and Laurance, W. F.: Changing Ecology of Tropical Forests: Evidence and Drivers, Annu. Rev. Ecol. Syst., 40, 529–549, 2009a.

Lewis, S. L., Lopez-Gonzalez, G., Sonke, B., Affum-Baffoe, K., Baker, T. R., Ojo, L. O., Phillips, O. L., Reitsma, J. M., White, L., Comiskey, J. A., Djuikouo, M. N., Ewango, C. E. N., Feldpausch, T. R., Hamilton, A. C., Gloor, M., Hart, T., Hladik, A., Lloyd, J., Lovett, J. C., Makana, J. R., Malhi, Y., Mbago, F. M., Ndangalasi, H. J., Peacock, J., Peh, K. S. H., Sheil, D., Sunderland, T., Swaine, M. D., Taplin, J., Taylor, D., Thomas, S. C., Votere, R., and Woll, H.: Increasing carbon storage in intact African tropical forests, Nature, 457, 1003–1006, 2009b.

Lu, D. S.: The potential and challenge of remote sensing-based biomass estimation, Int. J.

Remote Sens., 27, 1297–1328, 2006.
Mayaux, P., Bartholome, E., Fritz, S., and Belward, A.: A new land-cover map of Africa for the year 2000, J. Biogeogr., 31, 861–877, 2004.
Meir, P., Cox, P., and Grace, J.: The influence of terrestrial ecosystems on climate, Trends Ecol. Evol., 21, 254–260, 2006.
Mitchard, E. T. A., Saatchi, S. S., Woodhouse, I. H., Nangendo, G., Ribeiro, N. S., Williams, M., Ryan, C. M., Lewis, S. L., Feldpausch, T. R., and Meir, P.: Using satellite radar backscatter to predict above-ground woody biomass: A consistent relationship across four different African landscapes, Geophys. Res. Lett., 36, 1–6, L23401, doi:10.1029/2009GL040692, 2009.
Mitchard, E. T. A., Saatchi, S., Woodhouse, I., Feldpausch, T., Lewis, S., Sonké, B., Rowland, C., and Meir, P.: Measuring biomass changes due to woody encroachment and deforestation/degradation in a forest-savanna boundary region of central Africa using multi-temporal L-band radar backscatter, Remote Sens. Environ., in press., doi:10.1016/j.rse.2010.02.022, 2011.
Oslisly, R. and White, L. J. T.: La relation homme-milieu dans la reserve de la Lopé (Gabon) au cours de l'Holocène; les implications sur l'environnement., in: Dynamique à long terme des Ecosystèmes Forestiers Intertropicaux, edited by: Servant, M. and Servant-Vildary, S., ORSTOM, 241–250, 1995.
Phillips, O. L., Lewis, S. L., Baker, T. R., Chao, K. J., and Higuchi, N.: The changing Amazon forest, Philos. T. R. Soc. B, 363, 1819–1827, 2008.
Field manual for plot establishment and remeasurement, http://www.geog.leeds.ac.uk/projects/rainfor/, 2009.
Pourtier, R.: Le Gabon. Tome 2: Etat et Développement., Editions L'Harmattan, Paris, 1989.
Rodrigues, A. S. L., Ewers, R. M., Parry, L., Souza, C., Verissimo, A., and Balmford, A.: Boom-and-Bust Development Patterns Across the Amazon Deforestation Frontier, Science, 324, 1435–1437, 2009.
Shugart, H. H., Saatchi, S., and Hall, F. G.: Importance of structure and its measurement in quantifying function of forest ecosystems, J. Geophys. Res., 115, 1-16, G00E13, doi:10.1029/2009JG000993, 2010.
Stern, N. H.: The economics of climate change : the Stern review, Cambridge University Press, Cambridge, xix, 692 p., 2008.
Swetnam, T., Falk, D. A., Hessl, A. E., and Farris, C.: Reconstructing landscape patter of historical fires and fire regimes, in: The lanscape ecology of fire, edited by: McKenzie, D.,

Miller, C., and Falk, D. A., Springer. Ecological Studies, 213, 165–192, 2011.
White, L. J. T. and Abernethy, K.: A guide to the vegetation of the Lopé Reserve, Wildlife Conservation Society, New York, 1997.
White, L. J. T.: Forest-savanna dynamics and the origins of 'Marantaceae Forest' in the Lopé Reserve, Gabon, in: African Rain Forest Ecology and Conservation, edited by: Weber, B., White, L. J. T., and Vedder, A., Yale University Press, 165–192, 2001.
WRI: Summary of Developed Country "Fast-Start" Climate Finance Pledges, World Resources Institute, 2010.

Table 1. Coefficients in radar-biomass regressions (± standard errors).

Polaraisation	*a*	*b*	*c*	r^2	*p*	*n*
HH	−15.01 ± 1.82	6.85 ± 1.77	−0.012 ± 0.003	0.4	< 0.0001	96
HV	−23.40 ±2.79	10.00 ± 1.76	−0.017 ± 0.003	0.76	< 0.0001	96

Table 2. Mean LiDAR-derived AGB in broad radar-derived biomass classes.

AGB class from PALSAR HV ($Mg\,ha^{-1}$)	Mean AGB from LiDAR footprints within this class ($Mg\,ha^{-1}$)	Standard Deviation LiDAR-AGB ($Mg\,ha^{-1}$)	Number of LiDAR footprints
0–25	14.1	13.1	148
25–50	43.1	25.1	131
50–75	68.7	33.8	158
75–100	89.9	35.1	236
100–150	134.4	45.5	1847
> 150	297.2	102.9	4522

Table 3. Comparison of mean AGB for classes from LiDAR with mean AGB from field plots found within these classes.

Class number	Class mean AGB (from GLAS) (Mg ha^{-1})	Mean AGB field plots (Mg ha^{-1})	Standard Deviation of field plots (Mg ha^{-1})	Number field plots in class
14	296.1	305.2	44.6	5
5	313.0	310.0	82.1	5
9	314.5	271.6	109.0	13
15	325.6	359.9	74.5	8
12	337.3	370.0	163.8	16
23	338.5	405.3	52.4	6
28	347.7	363.9	111.2	11
18	366.1	320.7	90.7	5
11	393.0	453.6	152.7	8
20	421.1	458.9	95.0	4
Mean	345.3	361.9	97.6	8.1

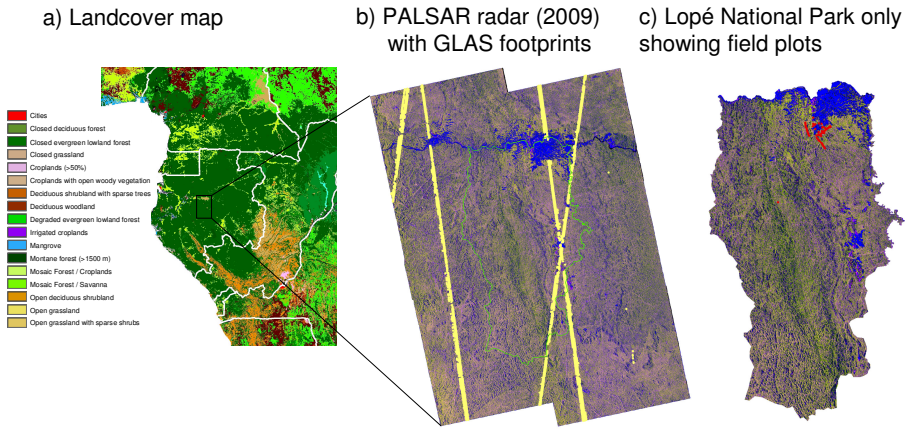

Fig. 1. (a) Map showing the location of the field site within a Landcover map for the year 2000 (Mayaux et al., 2004), **(b)** the ALOS PALSAR radar mosaic (HH in red, HV in green, and HH/HV in blue) shown with the location of the GLAS lidar footprints post-filtering, **(c)** the same radar image, but cut out around Lopé National Park, showing the location of the field plots.

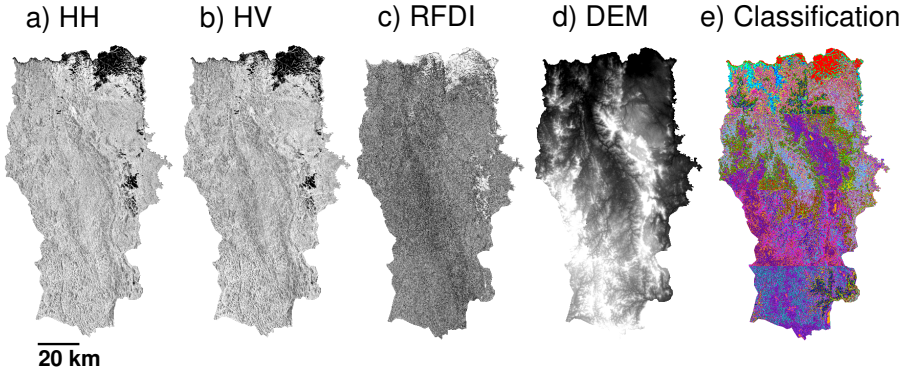

Fig. 2. Images of Lopé National Park using **(a)** PALSAR HH, **(b)** PALSAR HV, **(c)** Radar Forest Degradation Index (RFDI), **(d)** Digital Elevation Model (DEM), **(e)** Classified map, showing 40 classes with arbitrary colours.

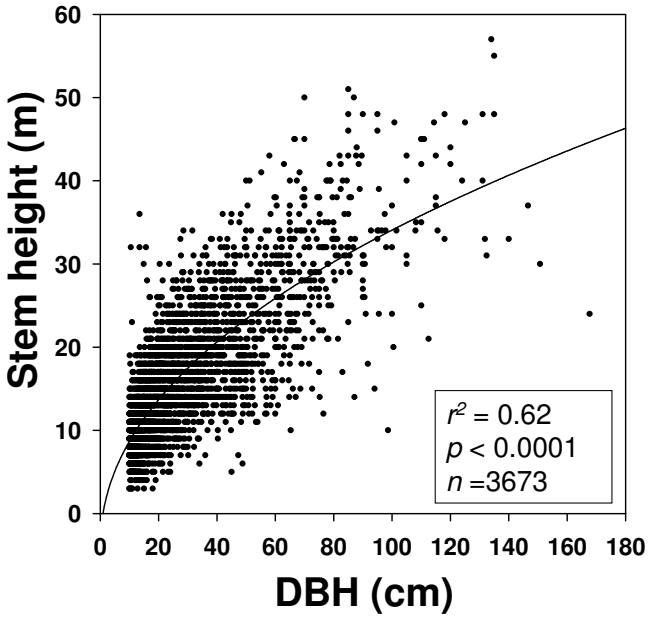

Fig. 3. The relationship between diameter (DBH, cm) and height (m) for 3673 trees measured in 1989 is shown.

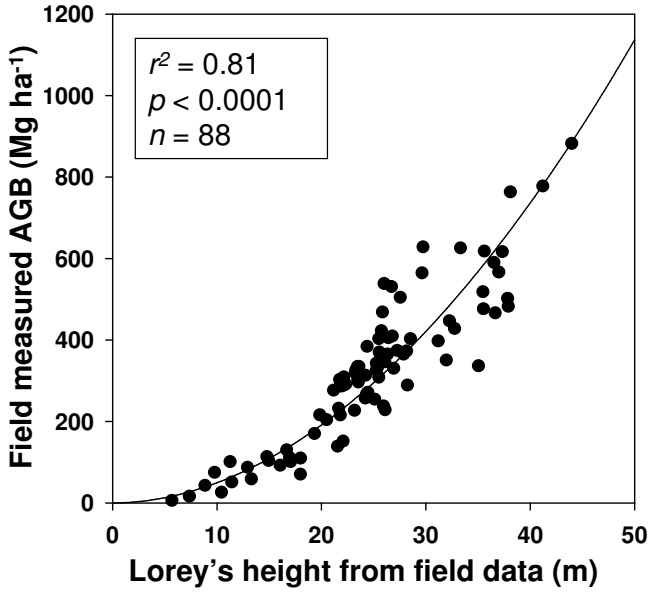

Fig. 4. Field measured AGB for 88 field plots from Lopé in Gabon, nearby plots in Gabon, and Mbam Djerem National Park in Cameroon, plotted against field-measured Lorey's height for these plots. This plot dataset is different to that used for the radar-biomass relationship, as the emphasis here was for plots from the same vegetation-type where every stem was measured, to produce an accurate regression relationship between Lorey's height and AGB.

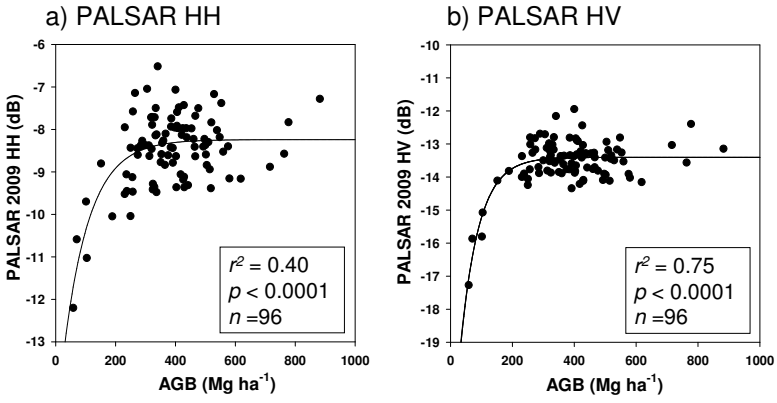

Fig. 5. ALOS PALSAR backscatter in **(a)** HH and **(b)** HV polarisations is plotted against AGB for 96 field plots (including 75 × 1 ha sections of long transects).

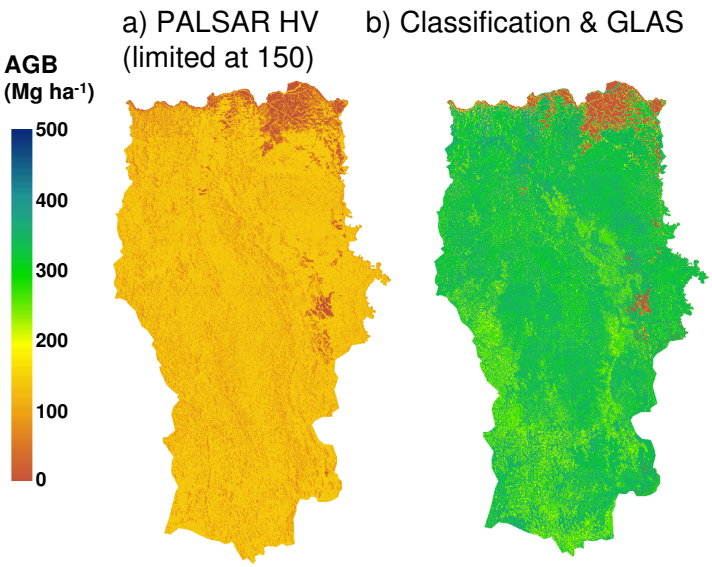

Fig. 6. Two different AGB maps for Lopé national park are displayed. **(a)** is for the regression with PALSAR HV, which is limited at 150 Mg ha^{-1} due to the saturation of these data; **(b)** is for the map produced by classifying PALSAR data and giving the 40 classes AGB values derived from GLAS footprints.

Appendix 6

Published version of Chapter 8

Comment on 'A first map of tropical Africa's above-ground biomass derived from satellite imagery'

2011 Environ. Res. Lett. 6 049001

(http://iopscience.iop.org/1748-9326/6/4/049001)

IOP Publishing Environmental Research Letters
Environ. Res. Lett. **6** (2011) 049001 (6pp) doi:10.1088/1748-9326/6/4/049001

COMMENT

Comment on 'A first map of tropical Africa's above-ground biomass derived from satellite imagery'

E T A Mitchard[1], S S Saatchi[2], S L Lewis[3], T R Feldpausch[3], F F Gerard[4], I H Woodhouse[1] and P Meir[1]

[1] School of GeoSciences, University of Edinburgh, Drummond Street, Edinburgh EH8 9XP, UK
[2] NASA Jet Propulsion Laboratory, California Institute of Technology, 4800 Oak Grove Drive, Pasadena, CA 91109, USA
[3] Earth and Biosphere Institute, School of Geography, University of Leeds, Leeds LS2 9JT, UK
[4] Centre for Ecology and Hydrology, Maclean Building, Benson Lane, Crowmarsh Gifford, Wallingford, Oxfordshire OX10 8BB, UK

E-mail: edward.mitchard@ed.ac.uk

Received 5 May 2011
Accepted for publication 27 September 2011
Published 4 November 2011
Online at stacks.iop.org/ERL/6/049001

Abstract
We present a critical evaluation of the above-ground biomass (AGB) map of Africa published in this journal by Baccini *et al* (2008 *Environ. Res. Lett.* **3** 045011). We first test their map against an independent dataset of 1154 scientific inventory plots from 16 African countries, and find only weak correspondence between our field plots and the AGB value given for the surrounding 1 km pixel by Baccini *et al*. Separating our field data using a continental landcover classification suggests that the Baccini *et al* map underestimates the AGB of forests and woodlands, while overestimating the AGB of savannas and grasslands. Secondly, we compare their map to 216 000 × 0.25 ha spaceborne LiDAR footprints. A comparison between Lorey's height (basal-area-weighted average height) derived from the LiDAR data for 1 km pixels containing at least five LiDAR footprints again does not support the hypothesis that the Baccini *et al* map is accurate, and suggests that it significantly underestimates the AGB of higher AGB areas. We conclude that this is due to the unsuitability of some of the field data used by Baccini *et al* to create their map, and overfitting in their model, resulting in low accuracies outside the small areas from which their field data are drawn.

Keywords: aboveground biomass, Africa, AGB, carbon, GLAS, LiDAR, MODIS, random forest, regression tree, remote sensing, savanna, tropical forest

S Online supplementary data available from stacks.iop.org/ERL/6/049001/mmedia

1. Introduction

The ERL paper by Baccini *et al* (2008), 'A first map of tropical Africa's above-ground biomass derived from satellite imagery', was a timely attempt to combine available field and remotely sensed data to produce the first above-ground biomass (AGB) map of a significant portion of sub-Saharan Africa. The authors used passive optical remote sensing data, which generally has not been found to be very sensitive to AGB at higher biomass values (Zheng *et al* 2004, Lu 2006,

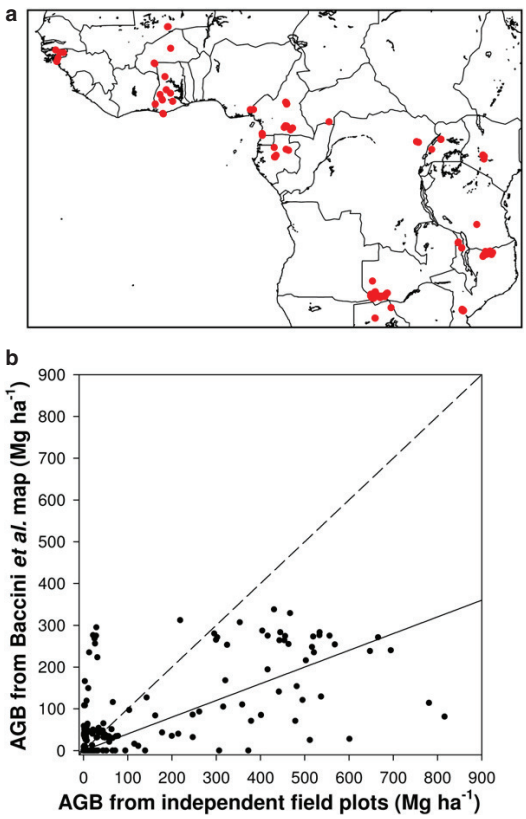

Figure 1. (a) Location of the 1154 scientific inventory plots used to compare to the Baccini *et al* AGB map; (b) AGB values from pixels of the Baccini *et al* map containing inventory plots plotted against the weighted average AGB of independent inventory plots; also shown is the best fit line (solid), and the 1:1 line (dotted).

GOFC-GOLD 2009, Mitchard *et al* 2009). Still, Baccini *et al* report a high accuracy, with the map explaining 82% of the variance in AGB for 10% of field plots held back for validation, with a root mean squared error (RMSE) of 50.5 Mg ha^{-1}. They then perform a test against spaceborne LiDAR height metrics from across the whole spatial extent of the map, and report an r^2 of 0.90 in a regression between mean LiDAR derived height and AGB (averaged over 10 Mg ha^{-1} AGB classes). We tested the Bacinni *et al* results against independent and spatially extensive field data, and newly calculated spaceborne LiDAR results, and found little support for the accuracy of the map (figures 1, 2, table 1). Our conclusion is that this is due to the low accuracy and limited spatial extent of the field data used to train and validate the Random Forest model used to produce the AGB map.

2. Test against field data

We first test the accuracy of the Baccini *et al* map directly using AGB derived from 1154 scientific inventory plots from 16 African countries, ranging in size from 0.1–10 ha (mean plot size 0.32 ha, mean 1.5 ha inventoried per 1 km pixel, figure 1; for plot details, see the supplementary material, available online at stacks.iop.org/ERL/6/049001/mmedia). In order to ensure sufficient sampling within each 1 km pixel, small plots (<0.5 ha) are included in this analysis only if the 1 km pixel in which they are located contains at least 0.5 ha of inventory plots. If multiple field plots occurred within one pixel, we calculated a mean AGB value, weighted by the square root of plot size. There are on average 4.8 field plots per 1 km pixel, so we compared field plots and the AGB map in a total of 239 pixels. The plots were collected from 1995 to 2010, with a mean julian date corresponding to July 2005 (compared to the remote sensing data in the Baccini *et al* map from 2000 to end 2003).

We find a significant, but very weak correlation, between our field plot AGB values and those in the Baccini *et al* map: a linear regression gave $r^2 = 0.28$, $p < 0.001$ (F-test), slope of 0.37, and RMSE of 145 Mg ha^{-1} (figure 1(b)). In this the best fit line had an intercept and slope significantly different from 0 and 1 respectively ($p < 0.01$). Errors range from an overestimate of 295 Mg ha^{-1} to an underestimate of −734 Mg ha^{-1}; the Baccini *et al* map has a much smaller range of AGB values than our field plots, with all higher AGB plots underestimated. When the plots are grouped by landcover type, using the Global Land Cover 2000 (GLC 2000) dataset (Mayaux *et al* 2004), the AGB of forest and woodland classes are underestimated by the Baccini *et al* map by ∼50%, while shrubland/grassland classes are mostly overestimated (table 1, only landcover classes where we had at least 10 ha of field plots covering at least ten 1 km pixels were considered).

There are five possible explanations for this discrepancy if the Baccini *et al* map is accurate; however regressions with subsets of our field data do not support any of these hypotheses. In all the following regressions the best fit lines are significant ($p < 0.01$), and intercepts and slopes are significantly different from 0 and 1 respectively ($p < 0.05$). First, this could be caused by our field plots having a larger AGB range than the AGB map. This is not the case, as excluding pixels with an average AGB > 338 Mg ha^{-1} (the maximum in the Baccini *et al* dataset) gives an r^2 of 0.12, slope of 0.36, and an RMSE of 79.6 Mg ha^{-1} ($n = 204$ pixels): as would be expected the RMSE is reduced by removing the high AGB plots, but the overall accuracy (based on the r^2 and slope) actually decreases. Second, the non-normal distribution of biomass for very small plots (Chave *et al* 2003) may drive the poor fit. This is not the case, as if we limit our field data to pixels that have a total plot area ⩾1 ha (1% coverage of the 1 km^2 pixel), although the r^2 increases to 0.32, the slope does not change at 0.38 ($n = 128$), and the RMSE of 169.5 Mg ha^{-1} is higher than for the whole dataset; additionally we have four plots of 10 ha in size from eastern Democratic Republic of Congo—these have an average AGB value of 463 Mg ha^{-1}, but the two Baccini *et al* pixels in which they fall (of which these plots sample 15%), are given AGB values of 273 and 283 Mg ha^{-1}. Third, our independent validation compares field-measured values from small plots to 1 km pixels (mean plot size = 0.3 ha, mean 4.8 plots per 1 km pixel); such plots may not sample the whole pixel sufficiently to accurately estimate its AGB. However, we do not think this third hypothesis can explain the extent of the poor correlation,

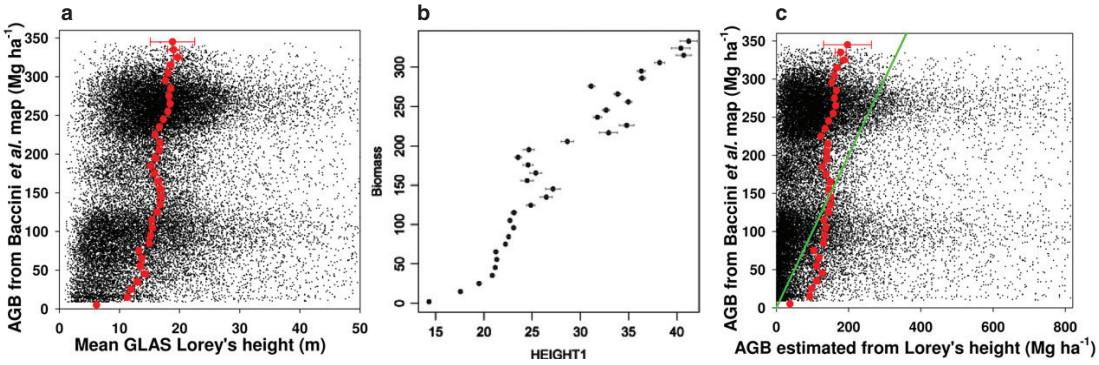

Figure 2. (a) AGB from 35 034 pixels from the Baccini *et al* map plotted against the mean Lorey's height from that pixel, each estimated from ⩾5 ICESat GLAS footprints; also shown in red is the mean height estimated for each 10 Mg ha^{-1}, with error bars showing standard errors; (b) reprint of figure 7(a) from Baccini *et al*, showing the mean maximum height for each pixel averaged into 10 Mg ha^{-1} biomass classes, with errors bars showing standard errors; (c) as for (a), but with Lorey's height values transformed into estimates of AGB (using an equation derived from African plot data), and with a 1:1 line shown in green.

Table 1. Difference between Baccini *et al* map and field plots by landcover class. (Note: the average AGB value from the Baccini *et al* map and field plots are displayed, separated by the class from the GLC 2000 land cover class Mayaux *et al* 2004.)

GLC 2000 land cover class	Number of pixels sampled	Total number of field plots within sampled pixels	Total area of field plots within sampled pixels (ha)	Mean AGB from Baccini *et al* (Mg ha^{-1})	Mean AGB from independent field plots (Mg ha^{-1})	Difference (Mg ha^{-1})
Closed evergreen lowland forest	29	38	75.1	202.5	445.1	−242.6
Submontane forest (900–1500 m)	11	16	20.2	210.0	438.1	−228.1
Deciduous woodland	66	308	76.7	20.2	36.5	−16.3
Deciduous shrubland with sparse trees	44	196	42.1	14.8	4.3	10.4
Open deciduous shrubland	28	371	46.0	0.2	4.1	−3.9
Closed grassland	16	99	32.5	27.0	3.9	23.0

as the error increases when we only consider the 70 pixels that have more than five field plots located within them (mean 13 plots per 1 km pixel for this reduced dataset): $r^2 = 0.14$, slope = 0.42, RMSE = 170.2 Mg ha^{-1}. Fourth, there is a potential for changes in the landcover of our field plots (which range from 1995 to 2010, compared to 2000 to 2003 for the remote sensing data of Baccini *et al*); however considering only field plots from 2000 to 2003 the results do not improve, with $r^2 = 0.36$, slope = 0.39, and RMSE = 291 Mg ha^{-1} ($n = 38$). Finally, our fifth hypothesis relates to differences in the choice of the allometric equations relating measured tree parameters to AGB. The allometrics chosen differ between our datasets and those of Baccini *et al*: Baccini *et al* use the Brown *et al* (2005) equation involving diameter alone for the majority of their field plots, whereas we use a combination of the Chave *et al* (2005) 'moist forest' equation involving diameter, height and wood density for our forest plots, and for savanna/woodland vegetation we used either the Chave *et al* (2005) 'dry forest' equation or locally derived area-specific equations (see the supplementary material, available online at stacks.iop.org/ERL/6/049001/mmedia). We tested the impact of equation choice for 87 of our field plots where we have access to the raw stem data (from savannas and tall forests in Cameroon, Gabon and Uganda, with similar characteristics to the field data used by Baccini *et al*): the plots had a mean AGB of 363 Mg ha^{-1} using a combination of the Chave *et al* (2005) dry and moist equations, and 376 Mg ha^{-1} using the Brown *et al* (2005) equation involving diameter alone. A direct comparison of individual plot values using both allometric equations provides little support for bias at low or high biomass values: linear RMA regression gave intercept = 3.2, slope = 0.98, $r^2 = 0.97$, $p < 0.0001$.

3. Test against LiDAR data

In our second test, we examine the spaceborne LiDAR verification as performed by Baccini *et al*. To do this we used a dataset of ICESat Geoscience Laser Altimeter System (GLAS) footprints collected between 2003 and 2007, which were processed to provide estimates of Lorey's height, a basal-area-weighted average height that can be estimated accurately from GLAS waveforms (Lefsky *et al* 2005, Lefsky 2010). We use Lorey's height, as opposed to maximum height and HOME as used by Baccini *et al*, because the evidence suggests it can more accurately be determined from GLAS data, and because it has a stronger relationship with AGB (Lefsky *et al* 2005, Lefsky 2010). After cloud- and terrain-filtering (Saatchi *et al* 2011), we selected pixels that contained ⩾5 GLAS footprints (Baccini *et al*'s used three; each footprint covers 0.20–0.25 ha), giving a total of 35 034 test pixels, using 215 733 GLAS footprints. We find only a very weak

relationship between Lorey's height and Baccini *et al*'s AGB values when considering individual pixel values (figure 2(a), linear regression: slope = 0.02, r^2 = 0.045). We also averaged Lorey's height values in 10 Mg ha^{-1} bins, replicating the display method used in figure 7 of the Baccini *et al* study, and reproduced here as figure 2(b). We could not replicate their strong relationship between mean height and AGB, instead finding just a weak trend towards increasing height with increasing AGB up to ∼80 Mg ha^{-1}, and no relationship thereafter. We extend this analysis further by using Lorey's height (H_L)–AGB relationship derived from plot data in Africa (AGB = 0.3542 ($H_L^{2.0528}$), n = 75, r^2 = 0.85, p < 0.001, Saatchi *et al* 2011); again this suggests the Baccini *et al* map underestimates AGB in higher AGB areas, and has a low accuracy throughout the range of AGB values (figure 2(c), linear regression: slope = 0.05, r^2 = 0.01, RMSE = 173 Mg ha^{-1}).

We are unable to explain this discrepancy between our GLAS analysis and that of Baccini *et al*, though one factor could be that the metric derived from the raw GLAS waveform that we used (Lorey's height) is different from the metric they used (an estimate of canopy height, and the ratio of HOME to height). As Lorey's height is an average height weighted by basal area, its value will always be lower than maximum height for the same forest. However, it should be more sensitive to AGB than any estimate of height alone, and yet it does not appear to increase with AGB here. The result we report here does appear to concur with the results of the field data comparison, that is, that the Baccini *et al* map appears to have a low accuracy, in contrast to those reported within the paper. The possible causes of this low accuracy are fourfold: (i) the quality of the field data, which were mostly not scientific plots; (ii) the field data were not collected at a similar time to the remote sensing data; (iii) some of the 'field data' points used by Baccini *et al* are derived from a landcover map, itself derived from remote sensing; (iv) the field data were from a very limited spatial distribution, and not from across the continent. These issues are discussed below.

4. Discussion of Baccini *et al*'s field data

We fully sympathize with the difficulties faced by Baccini *et al* in obtaining sufficient numbers of high quality field plots across a continent, as this is extremely challenging. However, the field data used by Baccini *et al* are unlikely to be suitable for developing an accurate AGB map, as in addition to likely high randomly distributed inaccuracies, they are also likely to have consistent biases. We shall specifically examine the three datasets Baccini *et al* used in detail in order to highlight the potential problems with these types of data.

(1) The commercial forest inventory plots in the Republic of Congo (collected 2001–3) relied on measuring the diameters of just 1% of stems >40 cm diameter, 0.5% of stems 20–40 cm, and 0.2% of 'commercial species only' 2–20 cm. This very low proportion of diameters measured is likely to lead to inaccurate AGB estimates and, unless the small proportion chosen for measurement is strictly random (with regards to both species and diameters), will lead to biased estimates. Additionally, logging companies, until very recently, have not collected data to estimate biomass stocks, but to assess the approximate density and size-class distribution of timber trees. Therefore: (i) the plot sizes and tree diameters may be inaccurate (indeed it is not specified whether or not the trees were measured here, often in such commercial inventories trees are placed in broad DBH classes rather than measured to the nearest mm); and (ii) the trees to be measured were unlikely to be a strict random subset of all the trees present. Though Réjou-Méchain *et al* (2011) did not find that commercial forestry inventories have a strong bias towards commercial species, as is often assumed, the above problems are still sufficient to result in large errors in AGB estimates. Baccini *et al* only used these data when at least three biomass plots were located within the same 1 km pixel. However, this averaging step will only reduce noise in the dataset; it will not correct for any systematic biases introduced by the methodology. This dataset makes up 65% of the pixels used by Baccini *et al* for training and validation.

(2) The dataset used by Baccini *et al* from Cameroon involved measuring the diameters of all stems greater than 10 cm DBH for 3 ha × 1 ha plots within each of 61 pixels. Unfortunately the diameters were only recorded as being within 10 cm bands rather than measured to the nearest millimetre, as is normal for scientific inventory plots: this will reduce accuracy. The biomass results for these plots appear very low for 'dense humid forest' from South-Central Cameroon (mean c. 100 Mg ha^{-1}, maximum 220 Mg ha^{-1}, based on Baccini *et al*'s figure 3). Other field plots published from within this area all have AGB values >400 Mg ha^{-1} (Djuikouo *et al* 2010, Lewis *et al* 2009). Furthermore the plots were measured in 1994, while the remote sensing dataset is from 2000 to 2003: Baccini *et al* use Landsat TM scenes from 1990 and 2000 to exclude plots that have undergone 'forest cover change' over this period, but quite significant changes will not necessarily be visible in TM data (GOFC-GOLD 2009). The accuracy of this dataset is therefore hard to assess, but it makes up only 4% of the pixels used in the Baccini *et al* study.

(3) Baccini *et al*'s dataset from Uganda is possibly the least accurate. Again, very little description of these plots is given in the paper, however the referenced Drichi (2003) 'National biomass study' from the Uganda Forest Department presents a landcover map of Uganda, with the country divided into vegetation classes using SPOT remote sensing data from 1990 to 1994, with data from a field campaign involving 4000 small forest inventory plots being used to give each vegetation class an average AGB value. However, the actual field plots were not used for this study, but instead Baccini *et al* interpolated AGB values for their pixels from this 'high resolution land cover type map', i.e. the proportion of each landcover class within each 1 km MODIS pixel was multiplied by its AGB value in order to give a weighted mean AGB value for that

pixel. Landsat TM data was then used to select <0.2% of the ∼236 000 pixel dataset (442 pixels are used, selected using undefined criteria). The use of optical remote sensing data to define the original landcover classes could explain the high accuracies reported by Baccini *et al*, as similar spectral information is used both to define and later separate biomass values; this will inevitably lead to higher accuracies than when truly independent field data is used. Equally, the use of a single average AGB value for each landcover class introduces pseudoreplication, as multiple pixels containing the same landcover class will be given identical AGB values (derived from the same plot data), but are treated as independent data points by the analysis. This dataset provides almost all the savanna and woodland training points used in the Baccini *et al* map, which is the landcover of 91% of the total area predicted (Mayaux *et al* 2004).

5. Discussion

Given the likely quality of the field data, it is surprising that the model Baccini *et al* develop appears to be so accurate against their test data. For example, it performs well against 10% of data held back for testing (training: 96% variance explained and RMSE 23.5 Mg ha^{-1} versus testing: 82% and 50.5 Mg ha^{-1}). This apparent contradiction, with the model performing well against the three datasets included in Baccini *et al*, but not in the field data we compiled, may be because of the circularity of using a landcover map partially derived from remote sensing data to derive the Uganda dataset, the pseudoreplication inherent in the Uganda dataset, and the small biomass range in the Baccini *et al* dataset compared to our dataset. However, an alternative explanation may be that the complex Random Forest model developed using a suite of MODIS variables to relate to AGB is not invariant across the continent. This is a significant danger: the Baccini field plots are located in three relatively small areas from approximately 1°N–4°N, and most vegetation types, or ecoregions, were not sampled. In general using Random Forest (or other non-parametric models) with limited and uneven spatial sampling of variables, results in overfitting the training data and produces large predictive errors outside the training regions (Genuer *et al* 2008). We suggest that their model may work relatively well for these three regions containing training data, while being poor in other regions, if, as is conceptually likely, the complex interactions of reflectance data that correspond to different AGB values within their model are not invariant across the full extent of the predicted AGB map.

6. Conclusion

In conclusion, we present evidence that the Baccini *et al* biomass map of Africa has large errors, with discrepancies between their map and independent scientific inventory plots resulting in an RMSE of 145 Mg ha^{-1}, and field data averaged by vegetation class suggesting that the AGB values for forest areas are underestimated, and for savanna areas mostly overestimated. Three major lessons should be taken from this analysis, to avoid these types of errors in the future: these apply equally to all studies that attempt to use point data to extrapolate an ecological variable across a landscape. The first lesson is that care must be taken to use good quality, unbiased field data: if there are sufficient plots then it is not necessary for the individual field data points to have a high accuracy, but if they have inherent biases then the resulting map will not be valid. The second lesson is that field data must be drawn from across the spatial extent and ecological variability of the prediction area; due to logistical constraints an even spatial distribution of plots is rarely possible. However, if plots are unevenly distributed then this must be considered in the analysis, and ideally a map showing an estimated distribution of accuracy should be included. Finally, accuracy assessments should be done against truly independent datasets, not a small random subset of the input data, which may suffer from the same biases or be related in other ways than just the parameter of interest.

Acknowledgments

We thank Alessandro Baccini and his coauthors for providing their AGB map for us to compare to our data. Michael Lefsky provided processed ICESat GLAS Lorey's height data. We thank the following people and institutions for providing help in collecting field data, or for permission to use their field data for this study: Tropical Biomes in Transition (TROBIT, NERC Consortium project, NE/D005590/1): Jon Lloyd, University of Queensland, Bonaventure Sonké, Université de Yaoundé I, Cameroon; CARBOVEG Guinea-Bissau (funded by the Ministry of Environment, Portugal (PA), the Ministry of Science and Technology, Portugal (FCT) & The Gulbenkian Foundation): João Carreiras, Tropical Research Institute (IICT), Lisbon, Portugal, Maria José Vasconcelos, IICT, Lisbon, Portugal; Nhambita Carbon & Communities Project (funded by the EU, NERC): Casey Ryan, University of Edinburgh, UK, Emily Woollen, University of Edinburgh, UK, Mathew Williams, University of Edinburgh, UK; Malawi data (funded by NERC, Moss Centenary Scholarship, Natural Resources International Foundation Travel Award): Gemma Cassells, University of Edinburgh, in-country support provided by the Department of Forestry and Department of Land Management at Mzuzu University, Bennet Mataya and Jarret Mhango; Zambia data: Ministry of Forestry, Zambia, Leon-Jaques Theron & Dr Solomon Tesfamichael, Peace Parks Foundation, Stellenbosch, South Africa; Lyndon Estes, University of Virginia, USA; Natascha Ribiero, Universidade Eduardo Mondlane, Mozambique; the Southern African Regional Science Initiative 2000 (SAFARI 2000) project; Biomass collection work in Lopé national park was funded by the Gordon and Betty Moore Foundation and the Packard Foundation, and supported by the Gabonese Agence Nationale des Parcs Nationaux, the Station d'Etudes des Gorilles et Chimpanzés, Murray Collins, Lee White, Kate Abernethy, Kath Jeffery, & Etienne Massard; Uganda data: Doug Sheil (ITFC), Kirsty Laughlin, and the Budongo Conservation Field Station (funded by the Royal Zoological Society of Scotland). Simon Lewis is supported by a Royal Society University Research Fellowship. Edward Mitchard is funded by Gatsby Plants.

References

Baccini A, Laporte N, Goetz S J, Sun M and Dong H 2008 A first map of tropical Africa's above-ground biomass derived from satellite imagery *Environ. Res. Lett.* **3** 045011

Brown S, Pearson T, Moore N, Parveen A, Ambagis S and Shoch D 2005 Impact of selective logging on the carbon stock of tropical forests: Republic of Congo as a case study *Technical Report 6* (Winrock International http://www.winrock.org)

Chave J, Condit R, Lao S, Caspersen J P, Foster R B and Hubbell S P 2003 Spatial and temporal variation of biomass in a tropical forest: results from a large census plot in Panama *J. Ecol.* **91** 240–52

Chave J *et al* 2005 Tree allometry and improved estimation of carbon stocks and balance in tropical forests *Oecologia* **145** 87–99

Djuikouo M N K, Doucet J-L, Nguembou C K, Lewis S L and Sonké B 2010 Diversity and aboveground biomass in three tropical forest types in the Dja Biosphere Reserve, Cameroon *Afr. J. Ecol.* **48** 1053–1063

Drichi P 2003 *National Biomass Study Technical Report* (Forest Department PO Box 1613, Kampala, Uganda)

Genuer R, Poggi J-M and Tuleau C 2008 Random Forests: some methodological insights *Research report INRIA Saclay, RR-6729* (http://hal.inria.fr/inria-00340725/fr/)

GOFC-GOLD 2009 Reducing greenhouse gas emissions from deforestation and degradation in developing countries: a sourcebook of methods and procedures for monitoring, measuring and reporting *GOFC-GOLD Report, Version COP14-2* (Alberta)

Lefsky M A 2010 A global forest canopy height map from the Moderate Resolution Imaging Spectroradiometer and the Geoscience Laser Altimeter System *Geophys. Res. Lett.* **37** 043622

Lefsky M A, Harding D J, Keller M, Cohen W B, Carabajal C C, Espirito-Santo F D B, Hunter M O and de Oliveira R 2005 Estimates of forest canopy height and aboveground biomass using ICESat *Geophys. Res. Lett.* **32** L22S02

Lewis S L *et al* 2009 Increasing carbon storage in intact African tropical forests *Nature* **457** 1003–6

Lu D 2006 The potential and challenge of remote sensing-based biomass estimation *Int. J. Remote Sens.* **27** 1297–32

Mayaux P, Bartholome E, Fritz S and Belward A 2004 A new land-cover map of Africa for the year 2000 *J. Biogeogr.* **31** 1–17

Mitchard E T A, Saatchi S S, Gerard F F, Lewis S L and Meir P 2009 Measuring woody encroachment from 1982–2006 along a forest-savanna boundary in central Africa *Earth Interact.* **18** 8

Réjou-Méchain M, Fayolle A, Nasi R, Gourlet-Fleury S, Doucet J-L, Gally M, Hubert D, Pasquier A and Billand A 2011 Detecting large-scale diversity patterns in tropical trees: Can we trust commercial forest inventories? *For. Ecol. Manage.* **261** 187–194

Saatchi S S *et al* 2011 Benchmark map of forest carbon stocks in tropical regions across three continents *Proc. Natl Acad. Sci. USA* at press (doi:10.1073/pnas.1019576108)

Zheng D, Rademacherb J, Chena J, Crowc T, Bresee M, Moined J L and Ryu S 2004 Estimating aboveground biomass using Landsat 7 ETM + data across a managed landscape in northern Wisconsin, USA *Remote Sens. Environ.* **93** 402–11